Modifications of Zein Biopolymer for Material Applications: Biopolymer Blends, Films, Bioactive Delivery Nanoparticles, and Nanofibers

By

Debela Tesfaye Tadele

A thesis
presented to the University of Waterloo
in fulfillment of the
thesis requirement for the degree of
Doctor of Philosophy
in
Chemical Engineering

Waterloo, Ontario, Canada, 2024

© Debela Tesfaye Tadele 2024

Examining Committee Membership

The following served on the examining committee for this thesis. The decision of the examination committee is by majority vote.

External Examiner: Loong-Tak Lim
Professor, Department of Food Science
University of Guelph

Supervisors: Tizazu H. Mekonnen
Associate Professor,
Department of Chemical Engineering
University of Waterloo

Internal Examiner: Hamed Shahsavan
Assistant Professor Department of Chemical Engineering,
University of Waterloo

Milad Kamkar
Assistant Professor, Department of Chemical Engineering,
University of Waterloo

Internal-External Examiner: Trevor Charles
Professor, Department of Biology,
University of Waterloo

Author's Declaration

I hereby declare that I am the sole author of this thesis. This is a true copy of the thesis, including any required final revisions, as accepted by my examiners. I understand that my thesis may be made electronically available to the public.

Abstract

The need for sustainable and high-performance materials is becoming increasingly urgent as society confronts escalating environmental challenges and pressing healthcare demands. Zein, a protein derived from corn, offers promising potential as a renewable, biodegradable, and biocompatible material for various applications. However, its utility is hindered by intrinsic limitations, such as poor processability, inadequate mechanical properties, and limited thermal stability. This research aims to address these challenges through chemical modifications of zein, blending with complementary polymers, and employing advanced fabrication techniques to develop nanoparticles and nanofibers for targeted applications. The first part of this study focused on chemically modifying zein via esterification using fatty acid chlorides of varying chain lengths (C6, C10, and C16). The findings revealed that fatty acid-modified zein exhibited significantly enhanced hydrophobicity, improved melt processability, and superior tensile properties compared to unmodified zein. The introduction of fatty acid chains also acted as internal plasticizers, facilitating the creation of a melt-processable biopolymer suitable for scalable production. In the second phase, the modified zein (mZein) was blended with poly(butylene adipate-co-terephthalate) (PBAT) via melt extrusion to fabricate biodegradable films. The study explored the effects of varying blending ratios on the compatibility, morphology, and physicomechanical properties of the films. It was observed that the esterification with decanoic acid (C10) significantly enhanced mZein's compatibility with PBAT, enabling the formation of films with balanced mechanical and barrier properties. A composition of mZein/PBAT at 30/70 wt% exhibited optimal performance, achieving a tensile strength of 10.88 MPa, elongation at break of 561.41%, and a modulus of 105.63 MPa. Furthermore, the blend demonstrated superior oxygen barrier properties, reduced water vapor permeability, and improved disintegration rates, making it suitable for food packaging and agricultural applications.

The third component of this research examined zein as a biopolymer matrix for nanoencapsulation of bioactive compounds, specifically quercetin and α-tocopherol. Zein nanoparticles (ZNPs) were fabricated using a green antisolvent co-precipitation method, achieving encapsulation efficiency of 96% with particle sizes ranging from 50 to 320 nm.

Co-encapsulation of quercetin and α-tocopherol in various formulations revealed distinct release dynamics, with the Zein/Que/Toc (20:1:1) formulation demonstrating controlled release rates over 8 hours. ATR-FTIR and fluorescence spectroscopy highlighted the hydrogen bonding and hydrophobic interactions critical to the encapsulation mechanism. In the final phase, α-tocopherol-encapsulated zein was integrated with polyvinyl alcohol (PVA) to produce nonwoven fiber mats via solution blow spinning. These mats exhibited uniform fiber morphology (diameter: 350–796 nm), excellent mechanical properties, and sustained release of α-tocopherol over 24 hours. Cytotoxicity assessments confirmed high cell viability (>90%) and enhanced cell spreading, suggesting the potential for biomedical applications such as wound dressings.

Overall, this research contributes significantly to the fields of biodegradable polymers and bioactive delivery systems. By overcoming the intrinsic limitations of zein through chemical modification and advanced processing techniques, this work offers a scalable framework for the development of high-performance sustainable materials. These findings have broad implications for applications in food packaging, agriculture, pharmaceuticals, nutraceuticals, and biomedical sciences, paving the way for more environmentally friendly and functional material solutions.

Acknowledgements

I would like to express my profound gratitude to my supervisor, Prof. Tizazu Mekonnen, for his consistent guidance, unwavering support, and the opportunity to explore the field of polymer science. His expertise, insightful discussions, and encouragement have been instrumental in the success of my doctoral research projects.

I am deeply grateful to my thesis examination committee Prof. Loong-Tak Lim, Prof. Hamed Shahsavan, Prof. Milad Kamkar, and Prof. Trevor Charles for their valuable time, effort, and constructive feedback, which have significantly enhanced the quality of my thesis.

I extend my heartfelt thanks to past and present members of Prof. Mekonnen's research group for their advice, support, collaboration, and camaraderie, which greatly enriched my research journey.

Special thanks to Prof. Evelyn Yim and her student, Dency David, for their collaboration and support on one of my doctoral research projects. Their willingness to assist made a substantial contribution to this work.

I am profoundly thankful for the unwavering love and support of my parents, siblings, and friends, whose encouragement and belief provided a constant source of strength. A special acknowledgment goes to my wife, Adi Girma, and my son, Liban Debela, for their incredible patience, understanding, and support throughout my studies. Their presence provided immense comfort and motivation during challenging times.

Lastly, I gratefully acknowledge the financial support from the Faculty of Engineering at the University of Waterloo, through the IBET Ph.D. Project, and Mitacs which made this research possible.

Dedication

I dedicate this work to my beloved mother, Workitu Eda, my father, Tesfaye Tadele.

Table of Contents

Examining Committee Membership ..... *ii*

Author's Declaration ..... *iii*

Abstract ..... *iv*

Acknowledgements ..... *vi*

Dedication ..... *vii*

List of Figures ..... *xii*

List of Tables ..... *xvi*

List of Schematics ..... *xvii*

Nomenclature ..... *xviii*

List of Publications from PhD ..... *xx*

Chapter 1: Introduction *1*

1.1. Overview and Motivation 1

1.2. Research objective 3

1.3. Thesis Outline 4

Chapter 2. Background and Literature Review *6*

2.1. Zein Protein 6

2.2. Fundamental Aspects of Zein 6

2.2.1. Zein composition and molecular structure 6

2.2. Co-encapsulation of zein nanocarriers 9

2.2.1. Synergistic effects of zein co-encapsulation 10

2.2.2. Stability and structural integrity in zein-based co-encapsulation systems 11

2.2.3.Controlled release mechanisms 11

2.3. Fabrication of zein nanoparticles for co-encapsulation 17

2.3.1. Desolvation 18

2.3.2. Dispersing 20

2.3.3. Micro-mixing 21

2.4.Fabrication of zein nanofibers 22

2.4.1. Electrospinning 23

2.4.2. Solution blow spinning 24

2.5. Modifications to enhance zein for co-encapsulation 26

2.5.1. Chemical modification 27

2.5.2. Physical modification 28

2.5.3. Enzymatic modification 28

2.5.4.Hybridization of zein with metal-organic frameworks (MOFs) 29

2.6. Techniques for characterizing co-encapsulation systems 30

2.7. Applications of zein nanoparticles and nanofibers 32

2.7.1. Zein nanofibers and nanoparticles in the food industry 32

2.7.2. Zein-based films for smart and edible packaging 33

2.8. Biomedical applications 35

2.9. Challenges and Future Outlook 38
2.10. Conclusions 39
Chapter 3. Fatty acid modified zein films: effect of fatty acid chain length on the processability and thermomechanical properties of modified zein films *41*
3.1. Introduction 41
3.2. Materials and methods 44
3.2.1. Materials 44
3.2.2. Modification of zein protein with fatty acid chlorides 44
3.3. Characterization of the unmodified and modified zein specimen 46
3.3.1. Attenuated total reflectance Fourier transform infrared (ATR-FTIR) spectroscopy 46
3.3.2. Carbon nuclear magnetic resonance (^{13}C-NMR) spectroscopy 47
3.3.3. Solubility test 47
3.3.4. Fabrication of films 47
3.4. Characterization of samples and films 48
3.4.1. Rheology 48
3.4.2. Microscopy 48
3.4.3. Light transmittance of films 48
3.4.4. Tensile property testing 48
3.4.5.Water absorption rate 49
3.4.6. Water contact angle 49
3.5. Statistical analysis 49
3.6. Results and discussion 49
3.6.1. Rheology of zein solution 49
3.6.2. ATR-FTIR and solid-state C-NMR spectra of modified zein 52
3.6.3. Solubility of modified zein in organic solvents 56
3.6.4.Morphology of modified zein films 57
3.6.5. Optical Clarity 60
3.6.6. Rheological properties of zein films 61
3.6.7. Mechanical properties 63
3.6.8. Water absorption and contact angle 66
3.7. Concluding Remarks 68
Chapter 4. PBAT/Corn Zein Ester Blends: Rheology, Morphology, and Physicochemical Properties 69
4.1. Introduction 69
4.2. Materials and methods 71
4.2.1. Materials 71
4.2.2. Esterification of zein protein with decanoic acid 72
4.2.3. Blend preparation 73
4.2.4. Film compression molding 74
4.2.5. Contact angle measurements 74
4.3. Characterization of mZein- PBAT blends 75
4.3.1. Attenuated total reflectance Fourier transform infrared (ATR-FTIR) spectroscopy 75
4.3.2. Mechanical properties 75
4.3.3. Dynamic mechanical analysis (DMA) 76
4.3.4. Rheological studies 76
4.3.5. Polarizing Optical Microscopy (POM) 76
4.3.6. Scanning electron microscopy (SEM) 76
4.3.7. Light transmittance of blends 77

4.3.8. Water absorption rate 77
4.3.9. Water barrier properties 77
4.3.10. Oxygen barrier properties 78
4.3.11. Disintegration test 78
4.4. Statistical analysis 79
4.5. Results and discussions 80
4.5.1. ATR-FTIR spectroscopy 80
4.5.2. Surface and Interfacial free energy 81
4.5.3. Morphology analysis 84
4.5.4. Mechanical Properties 87
4.5.5. Rheological Properties 90
4.5.6. Dynamic mechanical analysis (DMA) 94
4.5.7. Water absorption and Optical clarity 95
4.5.8. Water vapor and oxygen permeability 97
4.5.9. Disintegration test 98
4.6. Concluding Remarks 100
Chapter 5. Co-encapsulation of Quercetin and α-Tocopherol bioactives in Zein Nanoparticles: Synergistic interactions, stability, and controlled release 102
5.1. Introduction 102
5.2. Materials and methods 105
5.2.1. Materials 105
5.2.2. Fabrication of quercetin and α-Tocopherol loaded zein nanoparticle 106
5.2.3. Optimization of nanoparticles 106
5.3. Characterization of zein-Que-Toc nanoparticles 107
5.3.1. Particle size, polydispersity index (PDI), and ζ-potential (mV) 107
5.3.2. Encapsulation efficiency (EE) and Loading capacity (LC) 108
5.3.3. Rheology 109
5.3.4. Morphology 109
5.3.5. Attenuated Total Reflection Fourier transform infrared spectroscopy (ATR-FTIR) and Fluorescence Spectroscopy 109
5.4. Physicochemical stability nanoparticles 110
5.4.1. Storage stability 110
5.4.2. Light stability 110
5.4.3. pH stability 111
5.5. *In Vitro* gastrointestinal digestion 111
5.6. Statistical analysis 112
5.7. Results and discussion 112
5.7.1. Effect of co-encapsulation of quercetin and α-Tocopherol Physicochemical properties of zein/Que/Toc co-encapsulated particles 112
5.7.2. Effect of pH on zein-nanoparticles 114
5.7.3. Morphological analysis 116
5.7.4. ATR-FTIR Spectroscopy and Rheological/Fluorescence Analyses of Zein/Que/Toc Nanoparticles 118
5.7.5. Physicochemical stability analysis 120
5.7.6. *In-vitro* release 122
5.7.7. Optimization co-encapsulated zein nanoparticles 124
5.8. Concluding Remarks 125

Chapter 6. Development and Characterization of PVA-Zein/α-Tocopherol Nonwoven Mats for Functional Wound Dressing Applications *126*
6.1. Introduction 126
6.2. Materials and methods 129
6.2.1. Materials 129
6.2.2. Synthesis of α-tocopherol loaded zein nanoparticles 129
6.3. Characterization of zein-α-tocopherol nanoparticles 130
6.3.1. Particle size, polydispersity index (PDI), and ζ-potential (mV) 130
6.3.2. Encapsulation efficiency (EE) and Loading capacity (LC) 130
6.3.3. Fabrication of nanofibrous mats by solution blowing spinning 131
6.4. Characterization of the nonwoven nanofiber mats 133
6.4.1. Morphology 133
6.4.2. Attenuated total reflection Fourier transform infrared spectroscopy (ATR-FTIR) 133
6.4.3. Rheology 133
6.4.4. Differential scanning calorimetry (DSC) 133
6.4.5. Mechanical properties 134
6.4.6. Degradation behavior of PVA/Zein-Toc mats 134
6.5. *In vitro* drug release kinetics 135
6.6. Mathematical models for drug release kinetics 135
6.7. Cell culture studies 136
6.7.1. Cell viability and cytotoxicity test 136
6.8. Statistical analysis 137
6.9. Results and Discussion 138
6.9.1. Morphology analysis of tocopherol loaded PVA-Zein nonwoven fiber mats 138
6.9.2. ATR-FTIR and Rheology Analysis 140
6.9.3. Thermal properties, degradation behavior, and surface charge analysis of PVA-Zein/α-tocopherol nanofibrous mats 143
6.9.5. Tocopherol release kinetics from nonwoven fibrous mats 149
6.10. Concluding Remarks 155
Chapter 7. Conclusions and Future Work *156*
7.1. Conclusions 156
7.2. Recommendations and Future Work 158
References *161*
Appendix A *182*
Appendix B *186*
Appendix C *190*
Appendix D *194*

List of Figures

Figure 2.1. a) Displays various α-helical secondary structures. These structures include elongated, wheels, cylinders) Displays various α-helical secondary structures. These structures include elongated, wheels, cylinders, supercoiled, and hairpin models. The permission to reproduce these structures was obtained from the published ref[31]. Copyrighted in 2023 by Elsevier. b) Possible mechanism for zein self-assembly from individual molecules to nanospheres. Initially, α-helices in the zein solution transformed into β-sheet strands, which are then aligned side-by-side to form antiparallel β-sheets, creating a long ribbon driven by hydrophobic interactions. This ribbon curl into a toroid or ring, with center hole sealing to form core-shell and entrapment compounds, which are fundamental for zein-based NP production. Reproduced from ref [38] Copyright 2018 Elsevier. 9

Figure 2.2. Co-Encapsulation of bioactive in zein nanocarriers and nanofibers: Chemical structure and functional benefits. 13

Figure 2.3. Overview of zein nanoparticle preparation techniques for co-encapsulation of multiple bioactive compounds, permission from Elsevier, Copyright 2024[57]. 18

Figure 2.4. (i) Schematic representation of electrospinning and solution blowing spinning techniques for zein-based nanofiber fabrication; (ii) SEM and confocal microscopy images illustrating MSC adhesion, proliferation, and spreading on various zein/PLLA-based composite nanofiber scaffolds functionalized with Dexamethasone (DEX) and Bone Morphogenetic Protein-2 (BMP-2. This figure has been adapted/reproduced from ref, [90], with permission from Elsevier, Copyright 2018. 26

Figure 2.5. Schematic representation of the application of ZNP-based smart primary packaging with functionalities for sustainable food packaging. 35

Figure 2.6. Schematic illustration of the diverse applications of zein-based nanostructures in biomedicine, including their use in bone regeneration, wound dressing, nerve guide conduits, and tissue engineering. 38

Figure 3.1. Complex viscosity versus shear stress of zein solution with concentrations ranging from 2.5 to 30 wt.% at 30 °C. 50

Figure 3.2 . The effect of concentration on viscosity for zein solutions, a) dilute region when concentration is less than overlap concentration ($C < C*$), b) overlap region ($C = C*$), c) semi-dilute region ($C > C*$). 52

Figure 3.3. ATR-FTIR spectra of (a) zein modified with palmitoyl acid chloride (ZC16), (b) zein modified with decanoyl acid chloride (ZC10), c) zein modified with hexanoyl acid chloride (ZC6). 54

Figure 3.4 . ^{13}C-NMR spectra of zein: (a) modified with palmitoyl chloride (ZC16), (b) modified with decanoyl chloride (ZC10), and (c) modified with hexanoyl acid chloride (ZC6). 56

Figure 3.5. Solubility of zein samples modified in a) Acetone, b) DMSO, c) Ethanol, d) Toluene, and e) Water. 57

Figure 3.6 . Melting evaluation optical micrographs: unmodified zein film at: a) 27 °C, b) 120 °C, c) 150 °C, d) 180 °C, and e) 210 °C, modified zein film at: f) 27 °C, g) 120 °C, h) 150 °C, i) 180 °C, and j) 210 °C. 58

Figure 3.7. Optical microscopic surface morphologies , a) pristine zein b) zein/hexanoyl acid (ZC6-50) c) zein/decanoyl acid (ZC10-50), d) zein/palmitic acid (ZC16-50). 59

Figure 3.8. SEM surface morphologies of zein films a) baseline zein, b) zein modified with hexanoyl chloride (ZC6-50), c) zein modified with decanoyl chloride (ZC10-50), and d) zein modified with palmitoyl chloride (ZC16-50). 60

Figure 3.9. a) Light transmission measured with a UV-vis spectrometer, b) Photographs of representative films. 61
Figure 3.10. Storage modulus (G') and Loss modulus (G") of compression molded zein films: (a) Storage modulus (G′) vs. strain (%), (b) Loss modulus (G″) vs. strain (%) and (c) Complex viscosity vs. strain (%). 63
Figure 3.11. Mechanical properties of baseline and modified zein films: (a) tensile strength, (b) elongation at break, (c) elastic modulus, and (d) typical stress-strain plot. 66
Figure 3.12. Water absorption of pristine and fatty acid modified zein films 67

Figure 4.1 ATR-FTIR Spectra: a) Full spectra of Zein, mZein, PBAT, and PBAT/mZein; b) Magnified view at 1710 cm^{-1} and 1525cm^{-1} of mZein/PBAT blends 81
Figure 4.2 . Water contact angle and surface energy for mZein/PBAT blend films. 84
Figure 4.3. Optical microscope images of (a) neat mZein, (b) PBAT; scanning electron microscopy images of cross-sectional area of (c) neat mZein and (d) PBAT 85
Figure 4.4. SEM images of cross-sectional area of (a) mZein/PBAT (70/30 wt.%); (b) mZein/PBAT (50/50 wt.%) and (c) mZein/PBAT (30/70 wt.%). SEM images of modified zein and PBAT blends surface after etching with DMSO: (d) mZein/PBAT (70/30 wt.%); (e) mZein/PBAT (50/50 wt.%) and (f) mZein/PBAT (30/70 wt.%) 87
Figure 4.5. Mechanical properties neat modified zein, PBAT and mZein/PBAT blend films: 90
Figure 4.6. Complex viscosity vs generalized models of neat mZein, PBAT and mZein/PBAT as function of angular frequency at: a)180°C and b) 220°C; (c) Storage modulus (G') and (d) loss modulus (G") of the neat and blended polymers at 180 °C. 93
Figure 4.7. DMA analysis of neat mZein, neat PBAT and mZein/PBA; a) tan δ , b) Storage modulus and c) Cole-Cole plot of blend films 95
Figure 4.8. a) Water absorption b) Optical clarity of neat mZein, neat PBAT and mZein/PBA blend films. 96
Figure 4.9. (a) Water vapor and (b) Oxygen permeability of neat mZein, neat PBAT and mZein/PBA blend films. 98
Figure 4.10. a) Images of samples taken after biodegradation in soil, and b) the remaining weight percentage of samples. 100

Figure 5.1. Shows a) PDI, b) particle size distribution, c) zeta potential, and d) encapsulation efficiency and loading capacity of zein nanoparticles for various formulations 114
Figure 5.2. Effects of pH on a) PDI, b) particle size distribution, c) zeta potential, (d) encapsulation efficiency and loading capacity of Zein/Que/Toc nanoparticles. 116
Figure 5.3. SEM images of (a) zein nanoparticles, (b) Zein/Que, (c) Zein/Toc, and (d) Zein/Que/Toc (20:1:1) nanoparticles. TEM images of (e) zein nanoparticles, (f) Zein/Que, (g) Zein/Toc, and (h) Zein/Que/Toc (20:1:1) nanoparticles 117
Figure 5.4. ATR-FTIR, Rheological, and Fluorescence Spectroscopy analysis. 119
Figure 5.5. There are four crucial aspects regarding the storage of Zein/Que/Toc nanoparticles for a period of 60 days: a) retention and release mechanism, b) particle size distribution, c) zeta potential, and d) degradation kinetics 122
Figure 5.6. In vitro release patterns of polyphenols were influenced by varying quercetin-to-tocopherol ratios within a dual encapsulation system. The release profiles of quercetin (a) and α-tocopherol (b) are shown separately. 124

Figure 6.1 Demonstrates the morphology of the nanofibers, revealing uniform diameter distribution and smooth surface topography, which are critical for ensuring consistent drug release: (a) SEM image of control PVA-zein fibers without α-tocopherol; (b) SEM image of PZT-15 fibers with 15% α-tocopherol; (c) SEM image of PZT-30 fibers with

30% α-tocopherol showing a more pronounced and uniform distribution of particles on the fiber surface; and (d) SEM image of PZT-50 fibers loaded with 50% α-tocopherol, exhibiting the densest particle distribution, indicating a high loading level.(e-h) Fiber diameter distributions corresponding to images (a-d), respectively, with average diameters of 587.7 nm, 796.4 nm, 347.2 nm, and 354.8 nm. (i-l) depict pictures of fibrous mats.....140
Figure 6.2.ATR-FTIR and Rheological Analysis of PVA-Zein/α-tocopherol Fibrous Mats. (a) ATR-FTIR spectra of PVA-Zein and PVA-Zein/α-tocopherol fibrous mats with different α-tocopherol loadings (PZT-15, PZT-30, and PZT-50). The samples were analyzed over the wavenumber range of 500–4000 cm^{-1} using an ATR-FTIR spectrometer (Thermo Nicolet 6700), and 64 scans were collected for each sample with a resolution of 4 cm^{-1}. Key peaks at 3300 cm^{-1} (OH/NH stretching), 1735 cm^{-1} (C=O stretching), and 1590 cm^{-1} (N-H bending) are identified to confirm the presence of zein and PVA, while peaks at 1079 cm^{-1} and 690 cm^{-1} correspond to the C-O-C and CH bending vibrations of α-tocopherol.(b) Rheological profiles of PVA-Zein and PVA-Zein/α-tocopherol solutions (PZT-15, PZT-30, PZT-50) as a function of shear rate (0.01 to 100 s^{-1}), measured at 25 °C using a HAAKE Mars III rheometer with P20CSL parallel plates and a gap size of 0.46 mm. The solutions were prepared with 10 wt.% PVA in deionized water and varying concentrations of α-tocopherol-loaded zein nanoparticles (15%, 30%, and 50%).(c) Particle size distributions of α-tocopherol-loaded zein nanoparticles (ZT-15, ZT-30, ZT-50) showing unimodal distribution with increasing particle size at higher tocopherol concentrations.(d) Encapsulation efficiency (EE%) and Loading capacity (LC%) for α-tocopherol-loaded zein nanoparticles. ZT-50 exhibited the highest EE% (~92%) and LC%, with ZT-30 displaying (~10%) 142
Figure 6.3. Structural Characterization and Degradation Behavior of PVA/Zein-Tocopherol Nanofibrous Mats:(a) DSC Thermograms of PVA-Zein (control) and PZT-15, PZT-30, and PZT-50 fibrous mats were recorded using DSC (Discovery 2500, TA Instruments) over a temperature range of 26 to 260 °C at a heating rate of 10 °C/min under nitrogen atmosphere (50 mL/min). The thermograms depict the endothermic transitions corresponding to the glass transition temperature and thermal degradation.(b) Zeta Potential Measurements of zein nanoparticles and α-tocopherol-loaded samples (ZT-15, ZT-30, ZT-50) were determined in PBS solution (pH 7.4) at 25 °C using a Zetasizer Nano (Malvern Panalytical). The zeta potential values indicate surface charge changes with increasing α-tocopherol loading.(c) Weight Loss Profiles of PVA-Zein and PZT samples during immersion in PBS at pH 7.4 and 37 °C over 24 hours. Fiber mats were weighed at intervals of 0, 0.5, 1, 2, 4, 8, and 24 hours, and weight loss was calculated as a percentage of the initial mass.(d) FTIR Spectral Analysis of PVA-Zein, PZT-15, PZT-30, and PZT-50 over 24 hours of degradation in PBS. Key peaks were monitored for hydroxyl (–OH) stretching at 3200–3500 cm^{-1}, amide I (C=O stretching) and amide II (N-H bending) at 1600–1700 cm^{-1}, and C-H stretching bands at 2800–2900 cm^{-1} to evaluate chemical changes in the polymer backbone during degradation. 146
Figure 6.4. Mechanical properties of nonwoven fiber mats from PVA-Zein loaded with α-tocopherol:(a) Stress-strain curves of PVA-Zein (control), PZT-15, PZT-30, and PZT-50 fiber mats, obtained through tensile testing using a Mandel-Shimadzu (AGS-X) tensile tester with a 0.5 kN load cell. The gauge length was set to 15 mm, and the test speed was 1 mm/min. (b) Tensile strength of the nonwoven fiber mats measured under the same conditions. Five samples were tested per group, and the mean values are presented with standard deviations.(c) Elongation at break, calculated as the percentage of elongation relative to the original length of the mats under tensile loading.(d) Young's modulus, which represents the stiffness of the fiber mats, was calculated as the slope of the linear

portion of the stress-strain curve for each sample. PZT-15, PZT-30, and PZT-50 indicate fibers loaded with 15%, 30%, and 50% α-tocopherol, respectively. 148
Figure 6.5. Release Kinetics of α-tocopherol from PVA-Zein/α-tocopherol Fibrous Mats: (a) Cumulative release profiles of α-tocopherol from PZT-15, PZT-30, and PZT-50 fibrous mats over 24 hours. Samples were incubated in 2 mL of phosphate-buffered saline (0.01 M PBS) (pH 7.4) at 37°C with constant agitation (100 rpm) section 2.6. Tocopherol release was quantified using UV-visible spectrophotometry at 292 nm. Three replicates were analyzed for each sample, and the cumulative release was calculated as a percentage of the total tocopherol loaded in the mats. (b) Release kinetics of PZT-50 fitted to zero-order, first-order, Higuchi, and Korsmeyer-Peppas models. (c) Release kinetics of PZT-30 analyzed using the same models as in (b).(d) Release kinetics of PZT-15, also fitted to zero-order, first-order, Higuchi, and Korsmeyer-Peppas models. The best-fit model for each formulation was selected based on the highest correlation coefficient (R^2). The release was driven primarily by Fickian diffusion and polymer relaxation, with initial burst release followed by sustained release. This data supports the potential for controlled therapeutic delivery in wound healing applications.....151
Figure 6 .6. Cell Viability and Cytotoxicity Studies (a) Representative fluorescence microscopy images of Live/Dead staining of NIH3T3 cells cultured with extracts from PVA-Zein, PZT-15, PZT-30, and PZT-50 at 24 h. Ethanol-treated cells served as a negative control and cells on tissue culture polystyrene (TCPS) with culture media served as a positive control. Cells were stained with calcein-AM for live cells (green fluorescence) and ethidium homodimer-1 for dead cells (red fluorescence). Scale bar = 100 μm. (b) Average cell area (20 cells from 2 samples were counted for each group). n = 2, * and ** indicate a significant difference using one-way ANOVA with $p < 0.05$ and $p < 0.01$, respectively. Scale bar = 100 μm. (c) Percentage of live cells after 24 h (n = 2). (d) Percentage of cell viability at 24 h in cells treated with extracts from PZ, PZT-15, PZT-30, and PZT-50 samples and cells cultured on TCPS (positive control) with culture media (cell viability % of all the samples at 24 h were normalized to TCPS positive control). n = 3, 'ns' indicates no significant difference using ordinary one-way ANOVA with Tukey's multiple comparison test. 154

List of Tables

Table 2.1 Co-encapsulation of various bioactive components with zein nanocarriers and nanofibers. 14

Table 3.1 Composition of unmodified and esterified zein samples. 46

Table 4.1 Composition of the unmodified (Zein), modified zein (mZein), and PBAT blends 73
Table 4.2 mZein/PBAT blend interfacial tension values 83
Table 4.3. Fitting parameter, Carreau model, for all samples 92

Table 6.1. Details of polyvinyl alcohol/α-tocopherol loaded zein nanoparticle solution preparation 132

Table A 1 Summary of mechanical properties for zein films 185

Table B 1. Comparison of properties of mZein/PBAT blends with different studies on bio-based polymeric blends 188
Table B.2. Summary of mechanical properties for unmodified and modified zein/PBAT blend films 189

Table C.1. Experiment Factors and Levels 191
Table C.2. Box-Behnken Design Matrix 191

Table D 1 . Release kinetics of nonwoven fibrous mats from PVA-zein-loaded α-tocopherol. 195

List of Schematics

Scheme 3.1 Proposed reaction mechanism of fatty acid chlorides and zein protein. 45

Scheme 4.1 Schematics of zein protein modification with fatty acid chloride.....72

Schematic 5.1. Overview of Co-Encapsulation Process of Quercetin and α-Tocopherol in Zein Nanoparticles, Including Fabrication Steps, Characterization, Stability, and Controlled Release Profiles.....105

Schematic 6.1. Schematic showing the basic setup for fabricating α-tocopherol-loaded zein nanoparticles – PVA mats using a solution blowing process.....132

Nomenclature

Abbreviation	Definition
%	Percent
°C	Degree Celsius
13C-NMR	Carbon-13 nuclear magnetic resonance
α	Alpha
AFM	Atomic Force Microscopy
ANOVA	Analysis of Variance
ATR-FTIR	Attenuated Total Reflection Fourier Transform Infrared Spectroscopy
β	Beta
CGM	Corn gluten meal
CGF	Corn gluten feed
DDG	Distillers dried grains
DDGS	Distillers dried grains soluble
DLS	Dynamic Light Scattering
DI	Deionized Water
DMA	Dynamic Mechanical Analysis
DMSO	Dimethyl Sulfoxide
EE	Encapsulation Efficiency
ECM	Extracellular matrix
g	Gram
GRAS	Generally Recognized as Safe
G'	Storage Modulus
G''	Loss Modulus
h	Hour
Hz	Hertz
KBr	Potassium Bromide
LC	Loading Capacity
m	Meter
mg	Milligram
min	Minute

mL	Milliliter
mZein	Modified Zein
NaOH	Sodium Hydroxide
nm	Nanometer
NP	Nanoparticles
O-H	Hydroxyl Group
OP	Oxygen Permeability
PBT	Poly(butylene terephthalate)
PDI	Polydispersity Index
Pa	Pascal
PBAT	Poly(butylene adipate-co-terephthalate)
PLGA	Poly(lactic-co-glycolic acid)
POM	Polarizing Optical Microscopy
PVA	Polyvinyl Alcohol
PZT	PVA-Zein-Tocopherol
Que	Quercetin
rpm	Revolutions Per Minute
SBS	Solution Blow Spinning
SEM	Scanning Electron Microscopy
Tg	Glass Transition Temperature
THF	Tetrahydrofuran
Toc	α-Tocopherol
TEM	Transmission Electron Microscopy
w/v	Weight/Volume
wt.%	Weight Percent
WVTR	Water Vapor Transmission Rate
ZC6	Zein modified with hexanoyl chloride
ZC10	Zein modified with decanoyl chloride
ZC16	Zein modified with palmitoyl chloride
ZNPs	Zein Nanoparticles
ZPs	Zein Particles

List of Publications from PhD

1. Tadele, D., Mekonnen, T.H. "Co-encapsulation of Quercetin and α-Tocopherol Bioactives in Zein Nanoparticles: Synergistic Interactions, Stability, and Controlled Release," ACS Applied Polymer Materials (2024).

2. Tadele, D., Shorey, R., Mekonnen, T.H. "Fatty Acid Modified Zein Films: Effect of Fatty Acid Chain Length on the Processability and Thermomechanical Properties of Modified Zein Films," Industrial Crops and Products (2023), 192.

3. Tadele, D., Trinh, B.M., Mekonnen, T.H. "PBAT/Corn Zein Ester Blends: Rheology, Morphology, and Physicochemical Properties," Polymer 2023, 283.

4. Chang, B.P., **Tadele, D.,** Trinh, B.M., Bandara, N., Mekonnen, T.H. "Natural Antioxidant and Antimicrobial Agents and Processing Technologies for the Design of Active Food Packaging Polymers," Polymer Review (2023).

5.Trinh, B.M., **Tadele, D**., Mekonnen, T.H. "Robust and High Barrier Thermoplastic Starch – PLA Blend Films Using Starch-Graft-Poly(Lactic Acid) as a Compatibilizer," RSC Materials Advances (2022).

6.Tadele, D., Mekonnen, T.H. "Development and Characterization of PVA-Zein/α-Tocopherol Nonwoven Mats for Functional Wound Dressing Applications," Colloids and Surfaces B: Biointerfaces (2024),246.

7.Tadele, D., Muhammad Shahidul Islam, Mekonnen, T.H. "Zein-Based Nanoparticles and Nanofibers: Co-Encapsulation, Characterization, and Application in Food and Biomedicine," Trends in Food Science and Technology (2024), 104809.

8. Liena Zaidan **Debela T. Tadele** , Mustafa Yavuz, Michal Bajcsy ,Tizazu H. Mekonnen "Reusable TiO_2/rGO FET Biosensor for Ultra-Sensitive and Selective Detection of SARS-CoV-2: A One-Step Green Synthesis Approach"2024, (Under review).

Chapter 1: Introduction

1.1. Overview and Motivation

Plastics play a vital role in modern life, providing versatile, durable, and cost-effective solutions across a wide range of applications. However, their environmental impact has become a significant concern due to their reliance on non-renewable fossil fuels and their persistence in ecosystems as non-biodegradable waste [1,2]. With global plastic production exceeding 450 million tons annually, the resulting environmental degradation and waste management challenges have prompted a growing emphasis on developing sustainable alternative bioplastics that can fulfill functional requirements while mitigating environmental harm [3–5]. Bio-based polymers derived from natural sources such as plants, animals, and microorganisms have emerged as attractive alternatives, with the potential to reduce the environmental footprint and reliance on fossil fuels [6,7].

Among bio-based polymers, zein, a corn-derived prolamin protein, holds significant promise for applications in sustainable packaging, biomedical materials, and drug delivery systems due to its biodegradability, film-forming properties, and inherent biocompatibility [8–10]. Zein is abundantly available as a by-product of corn wet milling from bioethanol production [11]. However, the practical adoption of unmodified zein is hindered by its inherent weaknesses, including poor mechanical strength, limited thermal stability, and challenging processability due to strong intermolecular hydrogen bonds restricting its use in sectors where robustness and flexibility are required [12]. Therefore, to develop zein as a sustainable and functional biopolymer, it is essential to overcome these limitations. Various chemical, physical, and enzymatic modification strategies have been proposed to enhance zein mechanical and barrier properties, as well as its thermal processability for enhanced physicochemical

functionality [12,13]. Furthermore, the blending of modified zein with biopolymers has been reported with balanced compatibility, mechanical performance, and barrier properties suitable for practical applications [14–16].

Additionally, there is a growing demand for the utilization of zein protein for hydrophobic bioactives delivery, including curcumin, quercetin, and tocopherols, which exhibit low solubility and stability in aqueous media[17–19]. Zein's molecular structure makes it a promising candidate for encapsulating bioactive compounds due to its amphiphilic nature; however, its encapsulation efficiency and release control require substantial improvements to ensure practical viability [20]. The application of zein in nanofiber fabrication for bioactive delivery is still in its early stages; thus, advancements are required to optimize the release profiles, mechanical properties, and overall functionality for biomedical uses [21,22]. The motivation for this research is rooted in addressing these gaps by providing novel methodologies for enhancing zein through esterification with fatty acids of varying chain lengths; developing modified zein with biodegradable polymer like poly(butylene adipate-co-terephthalate) (PBAT) blends with balanced properties for sustainable packaging; and fabricating zein-based nanoparticles and nanofibers for bioactive delivery. Ultimately, this research seeks to contribute to the broader field of sustainable materials by improving the functional properties of zein and demonstrating its versatility across packaging, biomedical applications, and pharmaceuticals.

1.2.Research objective

The main objective of this study is to investigate the material attributes of corn derived zein, enhance its properties through chemical modifications, and expand its application potential via advanced fabrication approaches. Zein, in its natural state, has limited processability, mechanical properties, and thermal stability. This study aims to overcome zein's limitations and develop functional materials for packaging, bioactive delivery, and biomedical applications by improving the material characteristics through tailored modifications and advanced processing techniques.

Specific objectives include:

- To chemically modify zein through esterification using fatty acids of different chain lengths (C6, C10, C16). The aim is to evaluate the effects on zein's material properties, processability, thermal stability, and surface properties to design sustainable packaging films with improved performance.
- To develop and characterize blends of modified zein (mZein) with poly(butylene adipate-co-terephthalate) (PBAT) using melt extrusion with the aim of producing biodegradable films with balanced material properties.
- To fabricate zein-based nanoparticles for the co-delivery of bioactive compounds
- To produce functional fiber mats for biomedical applications by utilizing solution blow spinning.

1.3.Thesis Outline

The dissertation consists of seven chapters, each contributing to the overall objective of the research project.

Chapter 1: Introduction

Provides an overview of the study, motivation, and defines the core objectives. This chapter sets the foundation for the entire thesis by outlining the need for sustainable materials and identifying zein as a promising biopolymer for various applications.

Chapter 2: Literature Review

Reviews existing literature on zein, its properties, limitations, and potential applications. This chapter identifies key research gaps that subsequent chapters aim to address, providing context for the experimental work and highlighting the novelty of the research.

Chapter 3: Fatty Acid Modification of Zein

Presents a systematic study of zein esterification with fatty acids of varying chain lengths. This chapter directly addresses the core objective of improving zein's processability and material properties through chemical modification, laying the groundwork for subsequent studies.

Chapter 4 : mZein/PBAT Blends

Investigates melt blending of modified zein with PBAT. This chapter builds on the modifications from Chapter 3, exploring how the enhanced zein can be blended with other polymers to create materials with balanced properties suitable for packaging applications.

Chapter 5: Zein Nanoparticles for Bioactive Encapsulation

Develops zein-based nanoparticles for encapsulating bioactive compounds. This chapter addresses the objective of developing advanced delivery systems using zein, demonstrating its potential in pharmaceutical and nutraceutical applications.

Chapter 6: PVA-Zein/α-Tocopherol Nonwoven Mats

Fabricates functional nanofibers incorporating zein and bioactive compounds. This chapter further expands on zein's potential in biomedical applications, specifically addressing the objective of creating materials for wound dressing applications.

Chapter 7: Conclusions and Future Work

Summarizes key findings and contributions, tying together how each chapter has addressed the overall research objectives. This chapter also outlines future research directions, suggesting ways to further enhance zein's functionality and expand its applications

Chapter 2. Background and Literature Review

2.1. Zein Protein

Zein is a prolamin protein found exclusively in corn and is primarily located in the rough endoplasmic reticulum of corn kernels. The corn kernel comprises over 60 wt% starch and has a protein content between 7 and 12 wt%, with zein constituting approximately 44–79 wt% of the total protein content [23]. First discovered by Gorham in 1821[24,25], zein was historically used as cattle feed. Its commercial production for industrial applications began in 1939[24]. Corn gluten meal (CGM), distillers dried grains (DDG), distillers dried grains soluble (DDGS), and corn gluten feed (CGF) are protein-rich sources that can be used to extract zein from corn processing by-products [24]. Zein possesses beneficial properties, making it an ideal component for creating biodegradable films, bioplastics, fibers, and systems for delivering bioactive compounds across various applications [26].

2.2. Fundamental Aspects of Zein

2.2.1. Zein composition and molecular structure

Zein exists within corn seeds as protein aggregates linked by disulfide bonds, constituting a significant portion of maize protein. Zein is predominantly composed of hydrophobic and non-polar amino acids, with leucine (20%), proline (10%), and alanine (12%) and polar acidic (glutamic acid, 20%) [27,28]. Zein also contains low levels of tryptophan and lysine, resulting in limited nutritional value for human consumption [28]. [1]

[1] **Tadele, D.,** Muhammad Shahidul Islam, Mekonnen, T.H. "Zein-Based Nanoparticles and Nanofibers: Co-Encapsulation, Characterization, and Application in Food and Biomedicine," *Trends in Food Science and Technology* .https://doi.org/10.1016/j.tifs.2024.104809.2024, 104809

Zein comprises four types of prolamins based on differences in solubility and structural arrangement: α-, β-, γ-, and δ-zein prolamin, with α-zein prolamin (with molecular weights of 19 and 22 kDa) constituting 75–85% of the total fraction with alcohol-soluble dimers and oligomers [17,29]. The molecular weight of β-zein is estimated at 17 kDa, δ-zein at 10 kDa, and molecular weight of γ-zein fluctuates between 18 and 27 kDa [30]. The high hydrophobic content of α-zein prolamin and the presence of polar and non-polar amino acid sequences render it insoluble in both water and pure ethanol. However, it dissolves in hydroalcoholic solutions (65%–95% aqueous ethanol) and in highly alkaline solutions (pH ≥ 11.5), which disrupt hydrophobic interactions by transforming insoluble amines into soluble forms, thereby facilitating protein dissolution[31]. The solubility of zein is influenced by the concentration, pH, temperature, and ionic strength of the solution[32]. Adjusting solution parameters can further optimize its solubility. Furthermore, zein exhibits an amorphous structure with a glass transition temperature of 165 °C and demonstrates thermal stability up to 280 °C, offering high resistance to thermal degradation with an isoelectric point of pH 6.2 [31].

The properties of zein are dependent not only on the composition of amino acids, but also on their molecular structures. Self-assembling properties of zein are intricately linked to its molecular structure, which has led to the proposal of several structural models, each providing insight into its organization as shown in **Figure 2.1**. The cylinder model posits that α-zein comprises approximately 50-60% α-helices, interspersed with turns and random coils. This model describes zein's primary structure as a sequence of 20 amino acid residues repeated nine times, with helices flanked by turn regions rich in polar amino acids, such as glutamine [33]. In this structure, nine adjacent, antiparallel helices cluster to form a cylindrical surface stabilized by van der Waals forces and hydrogen bonding, allowing glutamine-rich regions to facilitate intermolecular connecting [31]. The ribbon-like model further explores zein conformation when dissolved in 70% ethanol [34]. This model highlights two-dimensional

hydrophobic aggregation, where side chains accumulate into a hydrophobic surface while maintaining hydrophilic ends, thus enhancing structural stability. This configuration further explains how zein molecules orient on surfaces with differing hydrophobicity and how they self-assemble into nanoparticles. The hairpin model, derived from nuclear magnetic resonance (NMR) and Fourier-transform infrared (FTIR) analyses, presents zein as a series of helices extended and connected into rings or loops [35]. The molecular structure of α-zein is comprised of linear stacks of rod-shaped helical repeat units. These units are connected by glutamine-rich bridges or loops which introduce hydrophilic regions that facilitate interactions with other bioactive macromolecules [36]. The superhelical model was introduced, describing α-zein as a structure consisting of three antiparallel helices connected by glutamine-rich turns. These turns provide additional structural stability through hydrogen bonding, enhancing the protein's aggregation capacity and intermolecular interactions in different environments [37]. However, the composition, properties, and molecular structure of α-zein render it a suitable material for biodegradable film formation and protein-based nanocarrier production. Zein-based nanocarriers are employed for the co-encapsulation of both hydrophobic and hydrophilic active compounds. Appropriate modifications of zein can facilitate advanced interactions with bioactive molecules, resulting in enhanced encapsulation efficiency, stability, bioavailability, and synergistic efficacy for various applications.

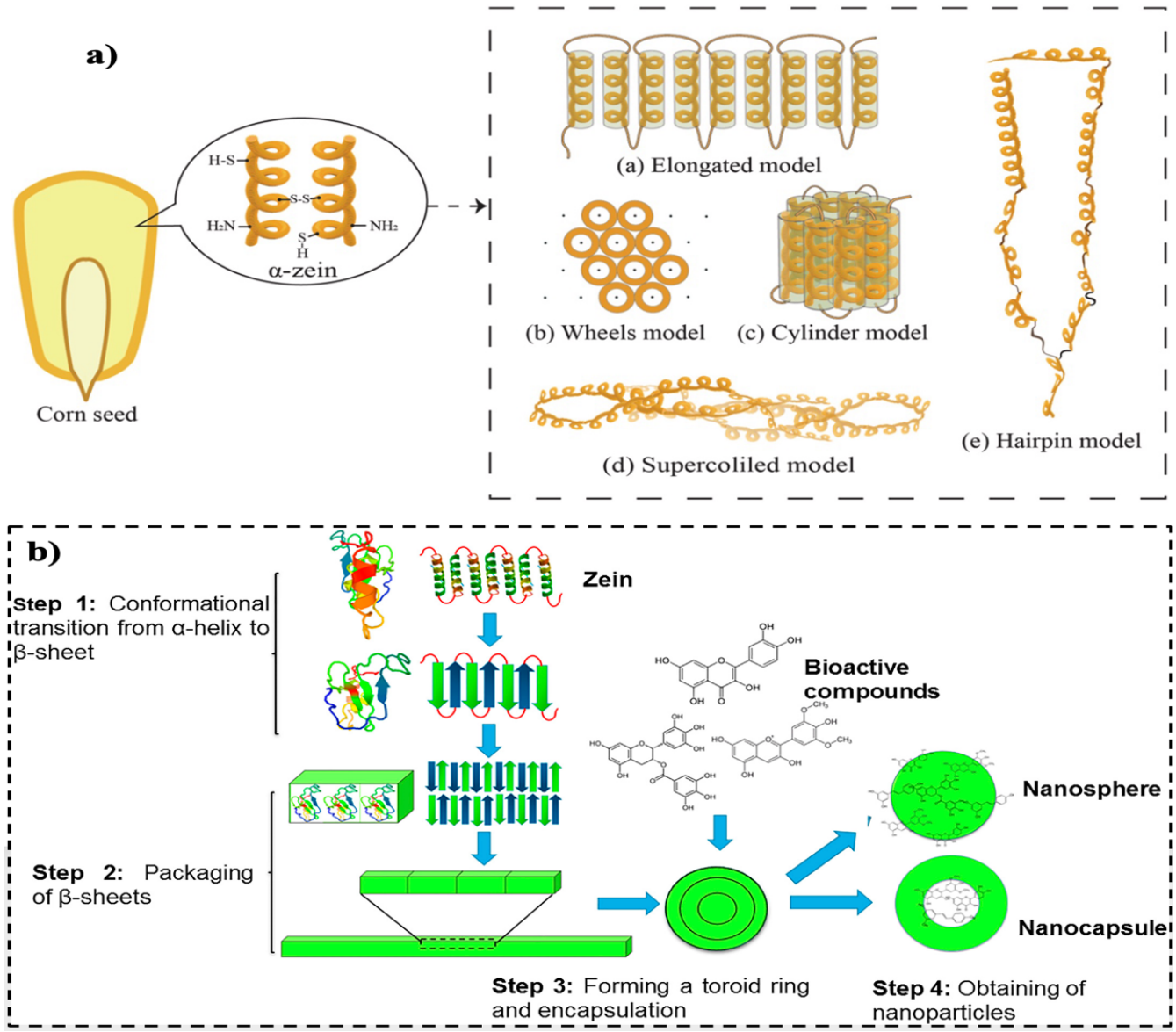


Figure 2.1. a) Displays various α-helical secondary structures. These structures include elongated, wheels, cylinders) Displays various α-helical secondary structures. These structures include elongated, wheels, cylinders, supercoiled, and hairpin models. The permission to reproduce these structures was obtained from the published ref[31]. Copyrighted in 2023 by Elsevier. b) Possible mechanism for zein self-assembly from individual molecules to nanospheres. Initially, α-helices in the zein solution transformed into β-sheet strands, which are then aligned side-by-side to form antiparallel β-sheets, creating a long ribbon driven by hydrophobic interactions. This ribbon curl into a toroid or ring, with center hole sealing to form core-shell and entrapment compounds, which are fundamental for zein-based NP production. Reproduced from ref [38] Copyright 2018 Elsevier.

2.2. Co-encapsulation of zein nanocarriers

Co-encapsulation has emerged as an effective strategy to improve the stability, bioavailability, and functionality of various bioactive compounds, particularly in applications requiring dual

or multi-component delivery. This approach is gaining traction in the development of nanofibers and nanoparticles due to their capacity to encapsulate and deliver multiple active ingredients within a single carrier, facilitating synergistic health benefits and enhanced therapeutic effects [39,40]. Zein-based nanoparticles and nanofibers, with their amphiphilic and biodegradable properties, serve as suitable platforms for co-encapsulating bioactive compounds like polyphenols, vitamins, and essential oils. By co-encapsulating these compounds, zein-based carriers stabilize sensitive ingredients, protect them from degradation, and extend their functional activity within food and biomedical contexts, often resulting in significantly improved bioavailability and synergistic effects [41]. Moreover, nanofibers and nanoparticles have garnered significant attention as delivery vehicles for encapsulating two or more bioactive compounds within a single carrier (**Figure 2.2**).

2.2.1. Synergistic effects of zein co-encapsulation

The co-encapsulation of multiple bioactive compounds within zein-based systems can lead to synergistic effects that enhance the functional efficacy of each component. The synergistic effects arise from combining multiple bioactives, allowing them to interact beneficially within a single delivery system. For instance, the combined encapsulation of antioxidants like resveratrol and quercetin in zein-based carriers has shown increased efficacy in therapeutic applications, including anti-inflammatory and anti-cancer effects [40]. This synergy supports the concept that whole food matrices with multiple bioactives often demonstrate superior health benefits compared to isolated compounds. Moreover, in co-encapsulated systems involving polyphenols or vitamins, the protective matrix formed by zein reduces the degradation of these compounds under adverse conditions, such as high temperatures or exposure to light, thereby preserving their bioactivity until they reach their target site in the body. This controlled release mechanism helps optimize the therapeutic efficacy and shelf life of bioactive compounds, providing long-term health benefits in nutraceutical and pharmaceutical formulations[42].

2.2.2. Stability and structural integrity in zein-based co-encapsulation systems

The stability and structural integrity of zein-based co-encapsulation systems are crucial for ensuring the functionality and efficacy of the encapsulated bioactives. Modifying zein nanocarriers through cross-linking or blending with other biopolymers, such as polysaccharides, can enhance the robustness of the encapsulation matrix. This approach improves encapsulation efficiency, enhances thermal stability, and protects bioactives from degradation under processing and storage conditions. For example, co-encapsulating bioactives in a zein-polysaccharide matrix creates a durable structure that prevents the premature release of bioactives, maintaining their functional properties over extended periods [38]. Studies have shown that co-encapsulation using nanoemulsions can achieve high encapsulation efficiencies for both hydrophilic and hydrophobic compounds, such as arbutin and coumaric acid, with efficiencies of 91% and 82%, respectively. These nanoemulsions demonstrate improved bioaccessibility and enable stable, controlled release under simulated gastrointestinal conditions, underscoring their potential for oral delivery applications in food and nutraceuticals [43].

2.2.3.Controlled release mechanisms

Zein-based co-encapsulation systems offer various release profiles to enhance the efficacy and stability of bioactive compounds. These profiles include burst release, which enables rapid, initial release of bioactives; sustained release, providing prolonged, steady delivery; delayed release, where bioactives are protected until reaching a specific site in the digestive tract; triggered release, which responds to internal or external stimuli; and targeted release, aimed at delivering bioactives to a precise location. These diverse mechanisms improve the functionality of zein nanocarriers in food and biomedical applications, addressing specific needs for controlled and site-specific bioactive delivery [44]. For instance, liposomal systems that co-encapsulate curcumin and resveratrol exhibit encapsulation efficiencies exceeding 80% and show enhanced stability and antioxidant properties when used in a 5:1 ratio. These co-

encapsulated liposomes release their contents over time, providing sustained therapeutic effects, which is particularly beneficial in pharmaceutical and functional food applications that require prolonged bioactive activity [42]. In addition to liposomal systems, microencapsulation techniques are used to achieve controlled release. Microencapsulation allows bioactives to be incorporated within tiny capsules that release their contents under specific conditions. For example, xylitol and menthol have been co-encapsulated in microcapsules for use in chewing gum, where the double-emulsion and complex coacervation methods were applied. This encapsulation strategy enhanced the stability and controlled release of the active compounds, improving the sensory properties of the gum [45]. Similarly, microcapsules containing coenzyme Q10 and vitamin E created via microfluidic jet spray drying demonstrated exceptionally high encapsulation efficiencies (98-99%), improved oxidative resistance, and greater retention rates of the bioactives, making them ideal for dietary supplement applications [46]. Furthermore, electrospinning is a widely used technique for producing nanofibers, providing a matrix that can encapsulate bioactive compounds within a fibrous structure. Zein-based nanofibers, particularly those blended with polyvinyl alcohol (PVA), offer significant potential as active packaging materials due to their ability to enhance food preservation. Recent research on ZN/PVA nanofibers infused with bioactive compounds such as thymoquinone (TQ) and resveratrol (RS) has shown that these nanofibers can effectively extend the shelf life and microbial safety of perishable foods. For instance, ZN/PVA-TQ-RS nanofibers used in packaging for refrigerated rainbow trout fillets reduced microbial counts and oxidative degradation, thereby extending the shelf life by at least three days [47]. The inclusion of TQ and RS provides natural antimicrobial and antioxidant protection, highlighting the potential of these nanofibers as bioactive packaging solutions for foods prone to spoilage. To efficiently fabricate and evaluate the efficacy of co-encapsulation systems, common synthesis techniques for zein protein-based co-encapsulation and advanced analytical techniques are employed to

assess the physicochemical properties, morphology, and functionality of the encapsulated compounds. These techniques were summarized in our review chapter below, respectively. Furthermore, **Table 2.2** provides a comprehensive summary of the benefits and structural characteristics of various bioactive compounds co-encapsulated in zein-based systems, elucidating their enhanced stability, bioavailability, and controlled release profiles under diverse environmental conditions.[45,55,56]

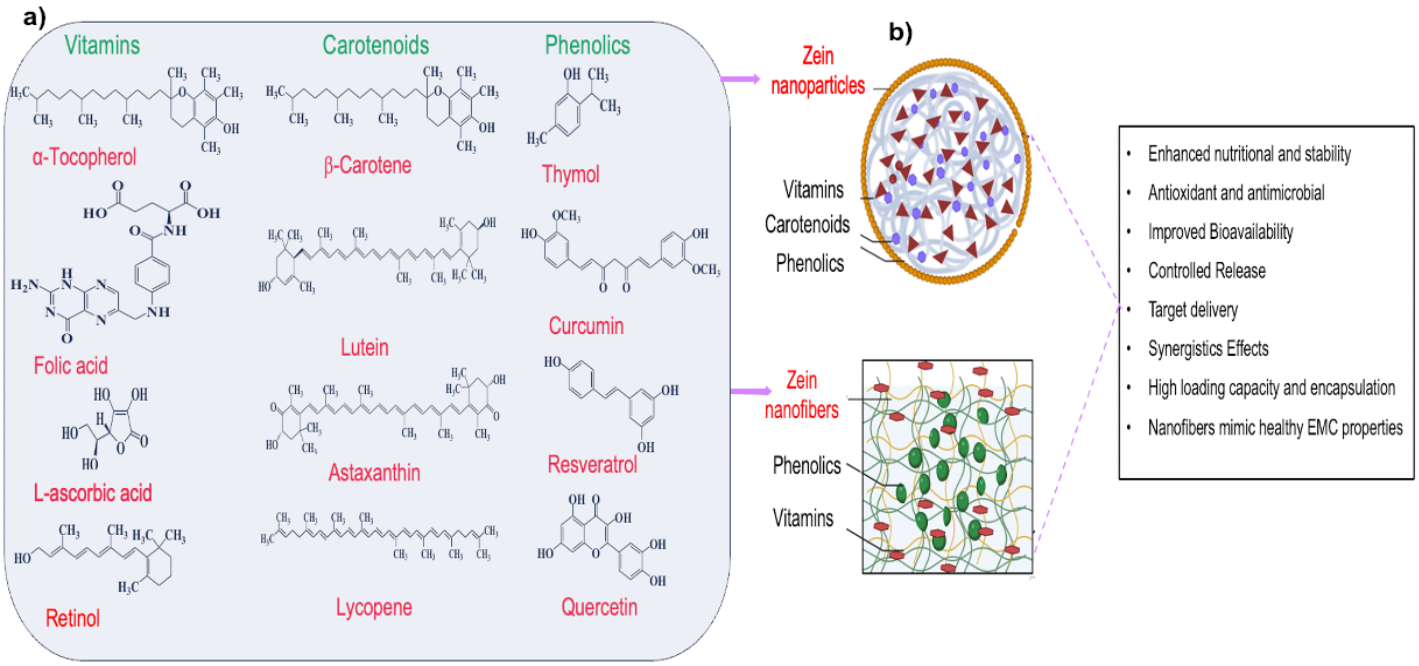


Figure 2.2. Co-Encapsulation of bioactive in zein nanocarriers and nanofibers: Chemical structure and functional benefits.

Table 2.1 Co-encapsulation of various bioactive components with zein nanocarriers and nanofibers.

Matrix	**Bioactive Ingredients**	**Encapsulation Method**	**Encapsulation Efficiency**	**Main Findings**	**Reference**
Zein, Caseinate	Curcumin, EGCG	Antisolvent Precipitation	Curcumin: 96.2%, EGCG: 77.9%	• Improved water solubility, antioxidant capacity, and bioavailability	[48]
Zein, Hyaluronic Acid	Curcumin, Quercetagetin	Layer-by-Layer Technology	Curcumin: 69.8%, Quercetagetin: 90.3%	• Improved stability against light and thermal degradation and controlled release	[49]
Zein, Chitosan	Tea Polyphenols, β-Carotene			• Excellent dispersibility and antioxidant activity	[50]

		Antisolvent Precipitation	Tea Polyphenols: 90.2%, β-Carotene: 88.5%		
Zein Propylene glycol alginate Tea saponin	Curcumin, β-Carotene	Freeze-drying	β-carotene: 97.58 % Curcumin: 96.49 0 %	• Synergistic improvement in β-carotene and curcumin chemical stability.	[51]
Zein, Casein	Eugenol, Thymol	Spray Drying	Eugenol: 21.49% Thymol: 16%,	• Stable dispersions, controlled release, and effective antimicrobial activity against Escherichia coli O157 and Listeria monocytogene	[52]
Zein, Polyvinyl Alcohol (PVA)	Thymoquinone (TQ), Resveratrol (RS)	Electrospinning	-	• Improved antimicrobial and antioxidant properties and enhanced microbial safety and sensory qualities of food	[47]

Zein Deoxyribonucleic acid (DNA)	Kaempferol, α-tocopherol	Anti-solvent dispersion	Kaempferol:92.90% α-tocopherol: 97.02%	• Improved stability and antioxidant protection , enhanced solubility and controlled release.	[53]
Zein, Chitosan	Curcumin Piperine	Electrospray	Curcumin:89% Piperine :87%	• Reduced neuroblastoma cell viability by 50% and enhanced solubility and bioavailability	[54]
Zein, Polyethylene Glycol (PEG) Ethyl cellulose	Curcumin, Resveratrol	Coaxial Electrospinning	Curcumin: 79%, Resveratrol: 82%	• Improved stability, controlled release, and bioavailability	[55]
Zein, propylene glycol alginate, and rhamnolipid	Resveratrol, Coenzyme Q10	Antisolvent Precipitation	Resveratrol: 91.80% Coenzyme Q10:87.64%	• Enhanced stability with sustained release	[56]

2.3. Fabrication of zein nanoparticles for co-encapsulation

The development of zein-based nanoparticles and nanofibers has attracted substantial interest in food, pharmaceutical, and biomedical fields due to their ability to co-encapsulate multiple bioactive compounds. Traditional fabrication methods, however, often encounter challenges such as inconsistent particle sizes, low encapsulation efficiency, and limited scalability. To address these limitations, recent advancements in fabrication techniques have been explored to enhance the functional capabilities, reproducibility, and commercial viability of zein-based nanostructures, specifically in co-encapsulation applications [31].

Recent advancements in the fabrication of zein nanocarriers have facilitated the development of innovative techniques that enhance both the efficiency and scalability of co-encapsulation systems, as illustrated in **Figure 2.3**. The fabrication of zein nanoparticles encompasses several key methods, including desolvation, dispersion, and micro-mixing, each employing distinct approaches. These fabrication techniques leverage the abundant hydroxyl, amino, and carboxyl groups on zein's side chains, which facilitate effective chemical coupling with a range of hydrophobic and hydrophilic bioactive compounds. This versatility results in high encapsulation efficiency, making these nanocarriers ideal for co-encapsulating multiple bioactives, thus enhancing their stability, bioavailability, and controlled release potential in food and biomedical applications.

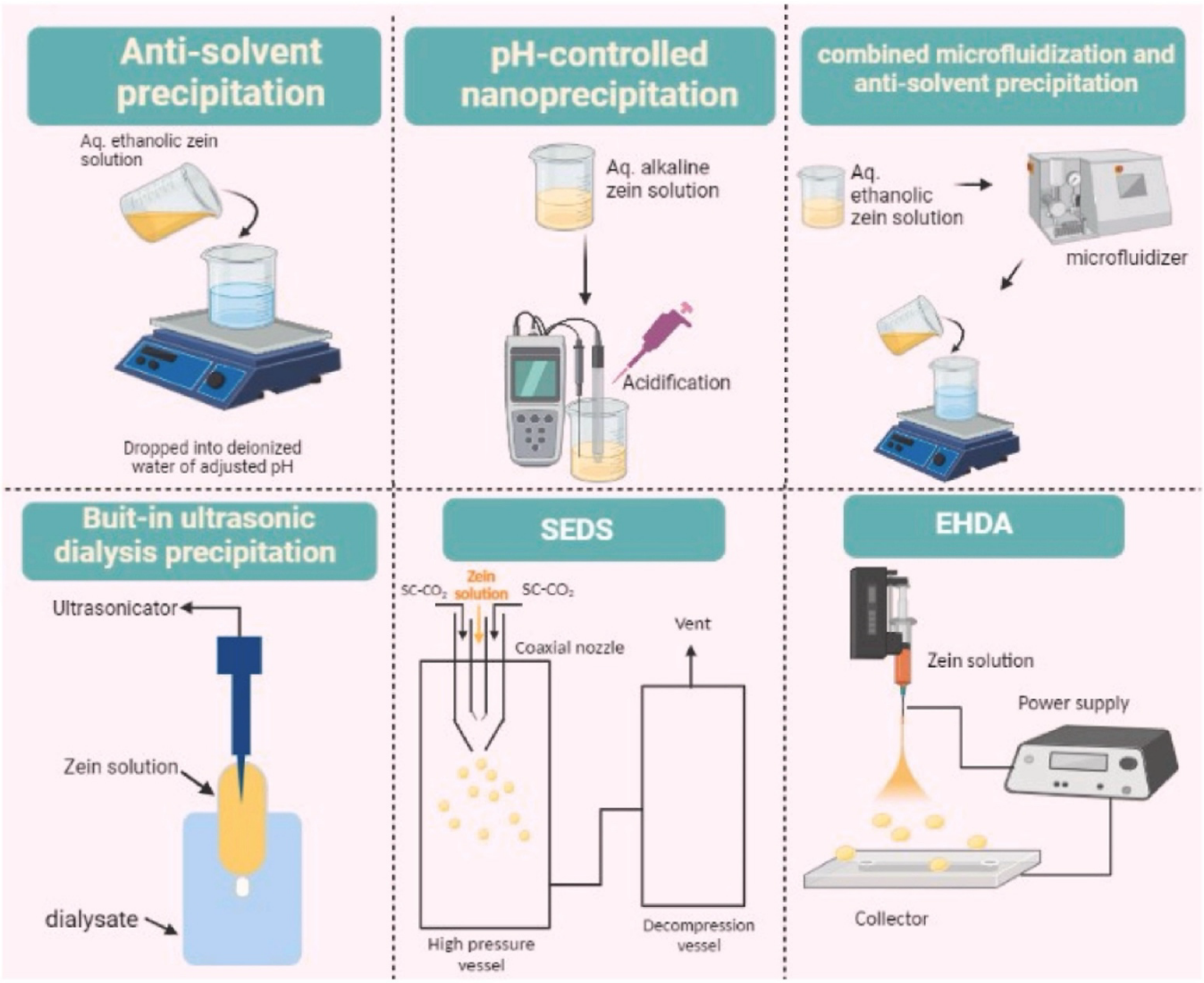


Figure 2.3. Overview of zein nanoparticle preparation techniques for co-encapsulation of multiple bioactive compounds, permission from Elsevier, Copyright 2024[57].

2.3.1. Desolvation

Desolvation techniques involve the incorporation of a reagent that diminishes zein solubility, resulting in the formation of nanoparticles. These techniques encompass solvent/nonsolvent, coacervation, pH-driven, and dialysis [58]. The antisolvent method, or nanoprecipitation, is commonly used for nanoparticle (NP) production due to its simplicity, low cost, and environmentally friendly nature. This approach involves dissolving a solute in a single solvent and then adding a miscible antisolvent, which induces precipitation through supersaturation. The process includes either dropwise addition or nanoprecipitation, where a shift in polarity

encourages the biopolymer to encapsulate the bioactive compound, forming a hydrophobic core with a protective outer layer. Nanoparticles solidify as the solvent is removed, typically via extraction, evaporation, centrifugation, washing, and drying after solvent removal [59]. The resulting zein nanoparticles typically exhibited smooth surfaces, small and uniform sizes, with higher encapsulation efficiency [60]. For instance, co-encapsulation of α-tocopherol and quercetin with zein NPs prepared using this method resulted in spherical and smooth surfaces with a particle size of 50-320 nm, and encapsulation efficiency (EE) and loading capacity (LC)of 96% and 13%, respectively [61]. Moreover, coacervation involves the dispersal of zein and the drug in an aqueous solution or anhydrous ethanol, followed by gradual addition of either ethanol or water [62]. This coacervation technique facilitates the encapsulation and controlled release of bioactive compounds; however, it also has some limitations [62]. The resultant particles typically exhibit micron-scale dimensions and relatively low encapsulation efficiencies (EE), ranging from 1.77% to 20.98% [63]. To address these constraints, other biopolymers and surfactant as a strategy for optimizing particle size and enhancing encapsulation efficiency are incorporated [64].

The pH-controlled method is a nanoencapsulation technique that involves adjusting the pH of a protein solution to extreme acidic or basic levels, prompting structural changes or unfolding in the protein. The pH is then brought back to neutral, leading the proteins to refold due to altered intermolecular interactions, which facilitates nanoparticle (NP) formation [17]. This technique has demonstrated efficacy in creating composite nanoparticles with a high encapsulation efficiency, such as carvacrol-loaded zein/sodium caseinate and curcumin-loaded zein/tea-saponin nanoparticles [65]. This approach has shown promising results, offering stability at elevated temperatures and protecting bioactives from degradation over extended periods. Dialysis is an alternative to the conventional solvent/nonsolvent methods. This approach employs a semipermeable membrane to facilitate solvent diffusion, alter the polar

environment, and promote the nanoparticle formation [66]. The dialysis method has the advantage of eliminating additional solvent removal steps. Recent innovations, such as the built-in ultrasonic dialysis process (BUDP), have further refined this technique, yielding particles with improved size distributions and encapsulation efficiency. For instance, BUDP has been successfully applied in the development of polydopamine-coated zein-indomethacin particles with a high encapsulation efficiency of 89.1% for targeted drug delivery applications [67]. Consequently, when nanoparticles were synthesized using any of the aforementioned methods, multiple factors influenced the size of the nanoparticles and encapsulation efficiency of bioactive compounds, including the polymer content, solvent and non-solvent types, solvent to non-solvent ratio, rate of solvent addition to non-solvent, stabilizer efficacy, and stirring speed.

2.3.2. Dispersing

Dispersing methods for zein nanoparticle formation encompass several techniques, including liquid-liquid dispersion, spray drying, electrospraying, supercritical antisolvent (SAS) processes, and atomizing/antisolvent precipitation (AAP). These approaches generally involve two critical steps: fragmentation of the stock solution into droplets followed by self-assembly and solidification into nanoparticles during solvent removal. The liquid-liquid dispersion technique uses a high-speed homogenizer to transform the zein stock solution (55-90% aqueous ethanol) into fine droplets, which are then introduced into deionized water. The rapid diffusion of ethanol into bulk water owing to its miscibility leads to solvent attrition. Nanoparticle formation occurs when the ethanol concentration in the droplets decreased below the zein solubilization limit. The particle size, typically ranging from 100-200 nm, can be modulated by adjusting the shear rate, ethanol concentration, and zein concentration [68]. Spray drying, another widely employed method that uses an electric field to create charged droplets from a liquid solution, enables the production of uniform zein nanoparticles (NPs) with high

encapsulation efficiency. This technique requires adjusting parameters such as voltage and collector distance to achieve optimal NP properties, impacting factors like particle size, density, and stability [69].

The supercritical antisolvent process is an advanced dispersion method that exploits the antisolvent effect of supercritical carbon dioxide ($scCO_2$). This technique involves dissolving the drug and zein in a CO_2-miscible solvent and spraying the solution into a precipitation vessel containing $scCO_2$. The rapid diffusion of the solvent into $scCO_2$ induces supersaturation, resulting in particle formation[70]. Although SAS offers advantages such as mild operating temperature, environmental benignity, and solvent-free products, it may produce irregular particles when solvents are poorly miscible with $scCO_2$ [71]. In addition, electrospraying has attracted considerable attention as a dispersion method. This technique uses an electric field to disperse the zein solution into finely charged droplets, thereby facilitating the efficient incorporation of therapeutic molecules [72]. Electrospraying generates particles of small size with high encapsulation efficiency without necessitating complex separation processes. Nevertheless, elevated zein concentrations can result in unfavorable particle morphology [73]. Coaxial electrospraying has been utilized to create zein-based microcapsules with core/shell structures, successfully encapsulating arachidonic acid, a polyunsaturated fatty acid. This method, verified through confocal laser scanning and electron microscopy, demonstrated enhanced oxidative stability and a reduction in unpleasant odor for the encapsulated acid. This approach shows promise for using zein as a fiber-forming plant protein to develop edible microcapsules suitable for food industry applications [74].

2.3.3. Micro-mixing

Micro-mixing techniques offer enhanced control and continuous operation for the fabrication of zein nanoparticles in confined spaces. Two prominent methods in this category are the flash nanoprecipitation (FNP) and microfluidic approaches. FNP involve the rapid mixing of two

solution streams in a confined chamber, leading to nanoparticle formation. This technique was successfully employed to create zein nanoparticles with controlled sizes and narrow distributions, as demonstrated by the production of the resveratrol-loaded zein nanoparticles [75]. Microfluidic methods are advanced techniques that facilitate rapid, adjustable, and reproducible nanoparticle production. The reduced turbulence resulting from smaller channel diameters ensures consistent mixing conditions and uniform particle formation. Studies have utilized microfluidic chips incorporating staggered herringbone micromixers or T-junction configurations to generate homogeneous zein -based nanocarriers that offers a comprehensive and in-depth elucidation of the functions and capacities for future uses in cancer therapy [76].

2.4.Fabrication of zein nanofibers

The production of zein nanofibers, primarily achieved through electrospinning, has gained significant attention due to the unique properties these materials offer for co-encapsulation. Nanofibers, with dimensions typically ranging from 0 to 1000 nm, provide a high surface-to-volume ratio and interconnected porosity, which enhance the encapsulation efficiency and controlled release capabilities for bioactive compounds. These characteristics make zein nanofibers an ideal medium for co-encapsulating multiple bioactives, promoting stability, bioavailability, and prolonged functionality in various food and biomedical applications [77,78]. These properties render them highly customizable and particularly advantageous for use in active food packaging and biomedical applications [79]. Zein nanofibers exhibit remarkable properties including mechanical strength, barrier functionality, superior thermal properties, and encapsulation efficiency [80]. Additionally, their ability to mimic the extracellular matrix (ECM) is attributed to their high inter-fiber porosity and interconnectivity, which are essential for supporting cell growth and tissue development [81]. Techniques such as electrospinning and solution blowing (**Figure 2.4)** are effective for fabricating zein nanofibers with tailored morphologies for enhanced food nutrient delivery and drug release

systems. These methods enable precise control over the nanofiber structure and composition, facilitating the development of advanced encapsulation systems with tunable release kinetics of nutrients and bioactive compounds for food and pharmaceutical applications.

2.4.1. Electrospinning

Electrospinning is a versatile technique for producing nonwoven nanofiber mats with tunable diameter, pore size, and orientation. This method can utilize a range of materials, including synthetic polymers, bio-based polymers, and their combinations. Post-processing techniques such as crosslinking and thermal curing, can further enhance the chemical and physical properties of the resultant nanofibers to enhance their encapsulation efficiency [82]. Electrospinning has recently emerged as a versatile technique for the fabrication of zein nanofibers, and its efficacy in food applications has been demonstrated. This method is particularly suitable for the encapsulation of bioactive compounds in food applications. Recent research has successfully fabricated composite nanofibers using a zein-acetic acid solution and carotenoid extract, achieving high encapsulation efficiency and bead-free fiber distribution for food coloring and supplementation applications [83]. A modified coaxial electrospinning technique was employed to fabricate drug-laden zein nanofiber structures. In this investigation, the researchers utilized a zein/ibuprofen (IBU) solution as the core and N,N-dimethylformamide (DMF) as the sheath material and produced fibers with average diameters of 0.94 ± 0.34 μm and 0.67 ± 0.21 μm for different sheath-to-core flowrate ratios. X-ray diffraction and differential scanning calorimetry (DSC) analyses confirmed the amorphous state of IBU post-electrospinning, facilitating efficient functionality and sustained drug release [82]. Furthermore, to enhance the mechanical properties of electrospun zein nanofibers, researchers have incorporated single-walled carbon nanotubes (SWCNTs) and ethyl cellulose (EC) into zein solutions. The result demonstrated that the addition of polyethylene oxide (PEO) to electrospun zein-EC nanocomposite scaffolds facilitates the simultaneous loading of

multiple drugs while maintaining optimal drug release characteristics, with average fiber diameters of 312 and 437 nm for the single and double drug-loaded variants, respectively, exhibited favorable water stability, mechanical strength, and in vitro drug release behavior [84]. Additionally, hybrid electrospinning of zein with other biopolymers, such as gelatin, effectively enhances the mechanical properties of zein nanofibers and good sustained release characteristics, making them suitable for delivering hydrophobic bioactives. For example, curcumin-loaded zein nanofibers also show significant antibacterial activity, with higher curcumin content increasing effectiveness against food-borne pathogens. When combined with konjac and glucomannan, these nanofibers exhibit enhanced hydrophobicity, water resistance, and antibacterial properties, indicating their potential in food packaging applications[85].

2.4.2. Solution blow spinning

Solution blowing spinning (SBS) is an advanced technique for nanofiber production that utilizes a high-velocity gas stream to shear liquid strands from a polymer solution, forming fibers as the solvent evaporates. The SBS setup comprises three main components: a solution feeding system, coaxial spinneret, and collection apparatus [86]. SBS offers several advantages over traditional electrospinning, including higher flux rates (typically 5–10 mL/h) and faster fiber formation. However, achieving optimal fiber production requires a careful balance between the solution flow rate, gas flow rate, and nozzle geometry [87].

Recent studies have demonstrated the efficacy of SBS in the fabrication of zein nanofibers. Liu et al. successfully produced zein fibers using acetic acid as a solvent and identified optimal fabrication conditions for the zein concentration (25% to 35% w/w), feed rate (0.04 to 0.1 mL/min), and air pressure (0.28 to 0.62 MPa). Under optimal conditions, they achieved an average fiber diameter (AFD) of 138 nm with a 23% (w/w) concentration, 0.04 mL/min feed rate, and 0.38 MPa air pressure[88].

Another study fabricates PVA/zein nanofibers using SBS in an aqueous solution containing 60% acetic acid, resulting in fibers with an average diameter of < 300 nm [89]. Moreover, recent study developed a biocompatible nonwoven fibrous mats composed of poly(vinyl alcohol) (PVA) and zein encapsulating α-tocopherol, specifically designed for wound dressing applications. By employing an antisolvent co-precipitation method for the nano-encapsulation of α-tocopherol in zein, followed by a scalable solution blow spinning (SBS) process, they successfully produced uniform nonwoven mats. These mats demonstrate promising structural integrity and biocompatibility, highlighting their potential for enhanced wound healing [44]. This demonstrates that solution blow spinning (SBS) is a viable technique for producing zein fibers with precisely controlled properties, which enhances the development of advanced nanofiber-based materials for applications in biomedical engineering and food science.

The solution blow spinning (SBS) process is designed to be scalable for large-scale production. Unlike traditional electrospinning, SBS does not require high-voltage equipment and can produce nanofibers at higher throughput rates. This scalability is achieved through the use of high-velocity air to shear fibers from a polymer solution, and it can be adapted for continuous manufacturing. While maintaining uniformity and consistent quality at scale is a key challenge, process parameters such as polymer concentration, air pressure, and nozzle design can be optimized to achieve the desired fiber morphology and mechanical properties across large batches.

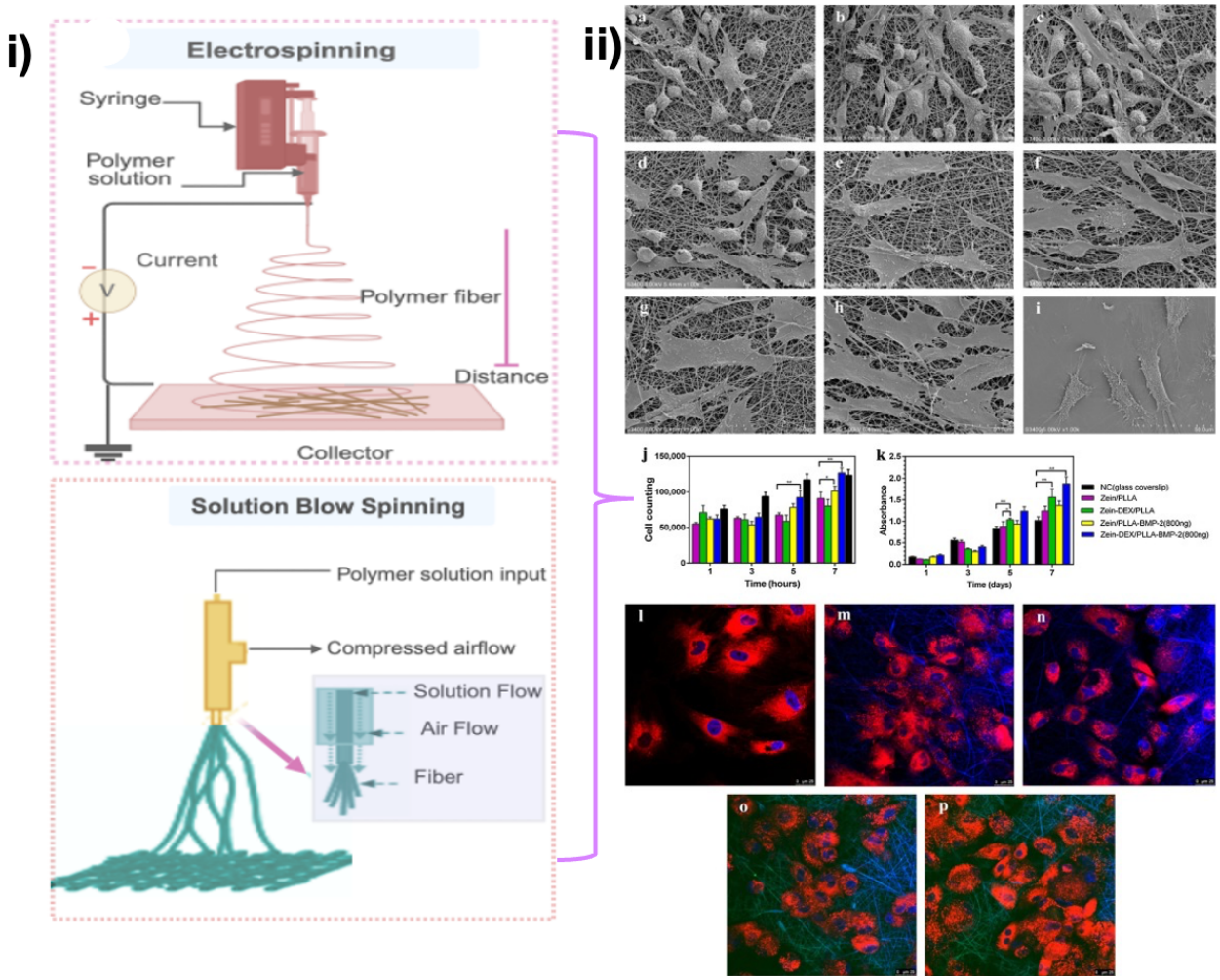


Figure 2.4. (i) Schematic representation of electrospinning and solution blowing spinning techniques for zein-based nanofiber fabrication; (ii) SEM and confocal microscopy images illustrating MSC adhesion, proliferation, and spreading on various zein/PLLA-based composite nanofiber scaffolds functionalized with Dexamethasone (DEX) and Bone Morphogenetic Protein-2 (BMP-2. This figure has been adapted/reproduced from ref, [90], with permission from Elsevier, Copyright 2018.

2.5. Modifications to enhance zein for co-encapsulation

While zein protein demonstrates promising properties for film formation, including high transparency, oxygen barrier capabilities, and humidity resistance, its application as a polymeric matrix faces certain limitations. These drawbacks impact its efficiency in co-encapsulating bioactive compounds. To overcome these limitations, modifications to zein interactions such as cross-linking, blending with other biopolymers, and structural adjustments are essential. These modifications not only enhance film properties but also improve the

stability, encapsulation efficiency, and controlled release of co-encapsulated compounds, making zein-based films more effective for food and biomedical applications [61,91,92]. These limitations include brittleness and poor flexibility, which restrict its widespread use [91]. To address these drawbacks, researchers have developed a range of modification strategies aimed at enhancing the mechanical properties, stability, and functional performance of zein-based materials through the addition of plasticizers, blending with biopolymers, and incorporation of nanoparticles and nanofibers [22,92–94]. One such approach involves blending zein with compatible biopolymers, such as poly(lactic acid) (PLA), with zein results in a composite with biodegradable films for practical applicability in food packaging [95]. Additionally, the incorporation of internal and external plasticizers during the film formation process is a common approach to increase the flexibility and mechanical properties of zein [91]. Furthermore, surface treatments, including coating and cross-linking techniques, are employed to enhance the stability, moisture resistance, mechanical strength, and barrier layers that protect zein-based films from environmental factors such as humidity and UV [96].These modifications implemented through chemical, physical, and enzymatic methods for broadening the application of zein, particularly for packaging materials and drug delivery systems [31].

2.5.1. Chemical modification

Zein is a promising carrier for bioactive compounds; however, it faces several challenges owing to its native form, including high hydrophobicity, near neutral isoelectric point (pH 6.3), and instability [31]. Chemical modification is a highly effective approach for altering the molecular structure of zein by introducing or removing specific functional groups leading to a high encapsulation efficiency [97]. This process utilizes reactive groups on the main peptide linkage or the amino acid side chains of zein, including the amino, carboxyl, and hydroxyl groups [98]. The primary chemical modification techniques include acylation reactions, Maillard reactions, deamidation and phosphorylation, polyphenol modifications, and cross-linking. Additionally,

the esterification of zein with long-chain fatty acids and its blending with compatible polymers such as PBA enhance the hydrophobicity of the modified zein, thereby improving the water resistance, processability, and mechanical stability of the resultant zein [92,93]

2.5.2. Physical modification

The physical modification of zein involves various techniques, including heating, high-pressure processing, ultrasonic waves, and plasma treatment [99]. According to studies on the effects of high-pressure treatment at different pressures on zein in an aqueous ethanol solution [100], it was observed that after treatment at 25 MPa, the α-helix and β-sheet content of the zein molecules increased. When the pressure was increased to 125 MPa, the size of the zein particles decreased and the fluorescence intensity reached its maximum. Further pressure increases resulted in partial denaturation of the zein molecules. Furthermore, plasma treatment has been shown to significantly reduce the particle size and enhance the solubility of zein by transforming β-turns and α-helices into β-sheets, thereby enhancing the barrier properties of zein nanocarriers [99]. The synergistic application of multiple physical treatments can enhance the properties of zein, thereby increasing its suitability for various applications, including the co-encapsulation of bioactive compounds for food packaging, drug delivery, and biomedical purposes.

2.5.3. Enzymatic modification

Enzymatic modification has emerged as a promising approach to tailor the molecular structure of zein nanocarriers for enhanced performance in food and biomedical applications. Enzymes, such as transglutaminase and proteases can be used to introduce functional groups that facilitate cross-linking or drug binding, thus improving the nanocarriers' stability, bioavailability, and controlled release properties [101]. The enzymatic process can increase the biocompatibility of zein by creating more biodegradable bonds, making the nanocarriers more suitable for biomedical applications like drug delivery and tissue scaffolding. However, despite these

advantages, enzymatic modification faces several challenges. One major drawback is the high cost of enzymes, which can limit scalability for industrial applications. Additionally, the process can sometimes compromise the mechanical strength of zein-based materials, making them less suitable for applications requiring durability [102].

2.5.4.Hybridization of zein with metal-organic frameworks (MOFs)

The hybridization of zein with Metal-Organic Frameworks (MOFs) presents a promising advancement in the utilization for advanced and funcational applications [103]. MOFs, particularly zinc-based variants, are emerging as multifunctional materials capable of enhancing food packaging performance due to their integration with polymer matrices like zein. The integration of zein with metal-organic frameworks (MOFs) and inorganic nanomaterials has emerged as a promising approach to enhance the functional attributes of zein-based films, opening new avenues for industry development [104]. MOFs, characterized by their high porosity, tunable structures, and multifunctionality, offer unique advantages when combined with biopolymers like zein. Zein-MOF composites have demonstrated enhanced mechanical strength, water resistance, and thermal stability, thereby improving the durability and performance of packaging films. Furthermore, MOFs contribute to active and intelligent packaging functionalities. For instance, they can act as carriers for bioactive compounds, allowing the controlled release of preservatives or antioxidants, thus extending food shelf life and enhancing safety [105].

In biomedical applications, MOFs demonstrate similar versatility. Zn-MOFs, for instance, are beneficial in cancer therapies due to their pH-responsive behavior, enabling targeted drug delivery to acidic tumor sites. Hybrid zein-MOF materials improve encapsulation efficiency and release kinetics of bioactive compounds, aided by the hydrophobicity of zein and the porosity of MOFs. Studies on the safety and/or toxicological concerns surrounding MOF fillers in food applications is emerging, highlighting the need for rigorous evaluation and mitigation

strategies to ensure consumer safety[103]. Overall, recent advancements in food packaging technology have introduced enhanced, active, and intelligent materials, with Metal-Organic Frameworks (MOFs) playing a pivotal role in co-encapsulation strategies. MOFs offer multifunctional benefits by enhancing mechanical strength, water resistance, thermal stability, UV-blocking, and barrier properties of biopolymer films, surpassing the limitations of traditional packaging materials. Additionally, their capacity to selectively regulate gases like oxygen, carbon dioxide, and ethylene within packaging creates controlled environments that extend food shelf life by slowing oxidation and reducing spoilage. As intelligent packaging indicators, MOFs can visually signal changes in pH, temperature, humidity, or gas composition, aiding consumers in assessing food freshness and contributing to food waste reduction. Furthermore, their ability to carry and release bioactive compounds in a controlled manner ensures sustained food quality and safety. However, challenges such as the high cost of MOF production, potential migration into food, and the need for comprehensive toxicological evaluations must be addressed for commercial viability. Future research should prioritize the development of affordable, stable MOFs with advanced sensing and adsorption capabilities, paving the way for their effective integration into intelligent food packaging systems that are safe and sustainable [103].

2.6. Techniques for characterizing co-encapsulation systems

Characterization of delivery nanoparticles and nanofibers is pivotal for optimizing their functionality, particularly when applied to sensitive bioactive compounds or targeted drug delivery systems. A range of sophisticated analytical techniques has been employed to accurately measure the size, shape, and surface charge of zein nanoparticles [61]. Photon Correlation Spectroscopy (PCS) and Dynamic Light Scattering (DLS) are commonly used to determine the hydrodynamic diameter and size distribution of particles and provides insights into their colloidal stability [106]. Field Emission Scanning Electron Microscopy (FE-SEM)

further corroborates these findings, offering insights into the surface morphology and particle size, with high-resolution images confirming the spherical and uniform nature of the nanoparticles[75]. Transmission Electron Microscopy (TEM) also offers high-resolution images, confirming the shape and size distribution of the nanoparticles (up to 50 nm and below), which are critical for their intended applications [61]. Atomic Force Microscopy (AFM) provides detailed topographical maps and can reveal primary particles that exhibit heights ranging from 15 to 50 nm, which contributes to their high surface area-to-volume ratio that is a key factor in enhancing the bioavailability and stability of encapsulated compounds [90].

Zeta potential measurements, which can be conducted using Zetasizer instrument, are essential for evaluating the stability of zein nanoparticles in suspensions. For example, zein-alginate particles have demonstrated a zeta potential of approximately -21 mV at pH 4.0, indicating good stability under these conditions. Stability is a critical parameter that is influenced by pH, ionic strength, and temperature [107]. Zein nanoparticles generally exhibit great stability at lower pH levels, where they maintain their structural integrity and resist aggregation [61,107]. At higher pH values, these nanoparticles tend to aggregate due to hydrophobic interactions between the non-polar groups on their surfaces. The stability of these particles can be enhanced by reducing the ionic strength, as higher ionic strengths can promote aggregation by decreasing the electrostatic repulsion. To prevent this, the addition of surfactants, such as Tween 80, can be used in addition to adjusting pH and ionic strength [107]. Moreover, Zein nanoparticles are generally more stable at lower temperatures, although they can tolerate moderate heating, which is advantageous for their use in various industrial applications [41].

Additionally, the presence of other materials, such as alginate, in core/shell structures can significantly alter the size, morphology, and stability of nanoparticles. For instance, core/shell zein-alginate nanoparticles have been reported to possess a core diameter of approximately 80

nm and shell thickness of 40 nm, yielding an overall particle size of approximately 160 nm [107]. These structures not only enhance the mechanical stability of the nanoparticles but also provide a controlled release profile, which is particularly advantageous for the delivery of sensitive bioactive compounds. Understanding and controlling these factors are crucial for optimizing the functionality and application of zein-based nanomaterials, particularly as they are integrated into innovative food delivery systems and other biomedical technologies.

2.7. Applications of zein nanoparticles and nanofibers

2.7.1. Zein nanofibers and nanoparticles in the food industry

Zein fibers and nanoparticles hold significant potential for the food industry, particularly in enhancing food preservation, extending shelf life, and offering innovative edible coating solutions. The biocompatibility, biodegradability, and film-forming properties of zein enable it to create protective barriers that can effectively slow down oxidation, moisture loss, and microbial growth. When incorporated with bioactive agents, such as antimicrobials or antioxidants, zein-based fibers and nanoparticles further improve food safety and quality by actively inhibiting spoilage-causing pathogens. These characteristics make zein a promising material for developing eco-friendly, functional food packaging and edible films, aligning with the industry's growing emphasis on sustainability and natural preservation methods [108]. These qualities make zein-based nanoparticles (ZNPs) particularly suited for active food packaging and edible coatings, which contribute functionalities like antimicrobial action, controlled degradation, thermal stability, and enhanced food safety [109].

Research indicates that co-encapsulated bioactive nutrients within zein matrices can synergistically enhance biological efficacy, offering sustained and controlled release in food environments [39]. Zein nanoparticles (ZNPs) can encapsulate a variety of active ingredients, including antimicrobial agents, antioxidants, and essential oils, thereby gradually releasing bioactive compounds, offering continuous protection against oxidation, microbial growth, and spoilage food environment to extend shelf life [108]. Zein-based nanofibers have shown

considerable promise in enhancing food packaging materials through improved mechanical properties, barrier effectiveness, and bioactivity. For instance, gelatin/zein nanofiber films loaded with bioactive compounds like perillaldehyde, thymol, or ε-polylysine demonstrated enhanced antibacterial properties and thermal stability, making them suitable for preserving chilled meat products [110]. The nanofiber structure not only provides a stable framework for encapsulating bioactive agents but also facilitates controlled release, which is crucial for extending the shelf life of perishable items. These findings support the potential of zein nanofibers as innovative, eco-friendly solutions in active food packaging, aligning with the industry's shift toward sustainable materials.

2.7.2. Zein-based films for smart and edible packaging

Zein's unique structural attributes allow it to form edible films and coatings that act as barriers against external factors, such as microorganisms, gases, and moisture, which are primary causes of food spoilage. The concept of using biopolymer-based films as a protective layer aligns with the industry's focus on sustainability, aiming to extend food shelf life naturally [80]. Zein-based films incorporate bioactive agents directly into the film matrix, functioning as both protective and active packaging by gradually releasing antimicrobial, antioxidant, or flavor-enhancing compounds over time [38]. This not only extends shelf life but also maintains product quality. The amphiphilic nature of zein, composed of both hydrophobic and hydrophilic domains, enables the encapsulation of diverse bioactive compounds, including essential oils, vitamins, and polyphenols, facilitating their controlled release. Advanced nanotechnology has further refined ZNP-based packaging, allowing for precise co-encapsulation and release mechanisms tailored to extend food stability, improve antimicrobial action, and maintain food quality over extended periods [39].

Studies highlight the versatility of zein in encapsulating hydrophobic and lipophilic food components, such as fat-soluble vitamins and natural antioxidants, effectively protecting these

compounds from degradation and improving their bioavailability [111,112]. For instance, zein-based encapsulation system for lutein, achieved an encapsulation efficiency of over 85% and enhancing its stability against oxidative degradation. This controlled release system is particularly valuable for maintaining nutrient integrity and extending food shelf life [112]. Other studies demonstrated that combining zein nanoparticles with bovine serum albumin (BSA) enhanced stability and provided optimal morphology for encapsulated compounds, underscoring the potential of zein-based nanocarriers for preserving food quality [111]. For example, a zein-chitosan bilayer system was developed that effectively protected polyphenols and probiotics, demonstrating stability throughout storage and resilience against digestive processes. Such systems, capable of withstanding processing conditions such as pasteurization, expand the potential applications of zein-based films in food preservation[113]. An innovative bio-nanocomposite of fish gelatin, carrageenan, and zein infused with turmeric essential oil (TEO) was reported to decrease bacterial colonies from 3.08 log CFU/g to 2.81 log CFU/g after 14 days against *Salmonella enterica*, demonstrating a significant improvement in shelf life for chicken meat through the sustained release of TEO [114]. These bio-nanocomposites exemplify sustainable and effective solutions for food preservation by enhancing food safety and quality through active, edible film applications.

The application of ZNP-based films and coatings as primary smart packaging materials with multifunctional properties (**Figure 2.5**) aligns with industry demands for reducing synthetic additives and promoting eco-friendly packaging alternatives. By leveraging zein's natural characteristics, these films serve as both active and edible packaging, supporting the development of sustainable food packaging solutions.

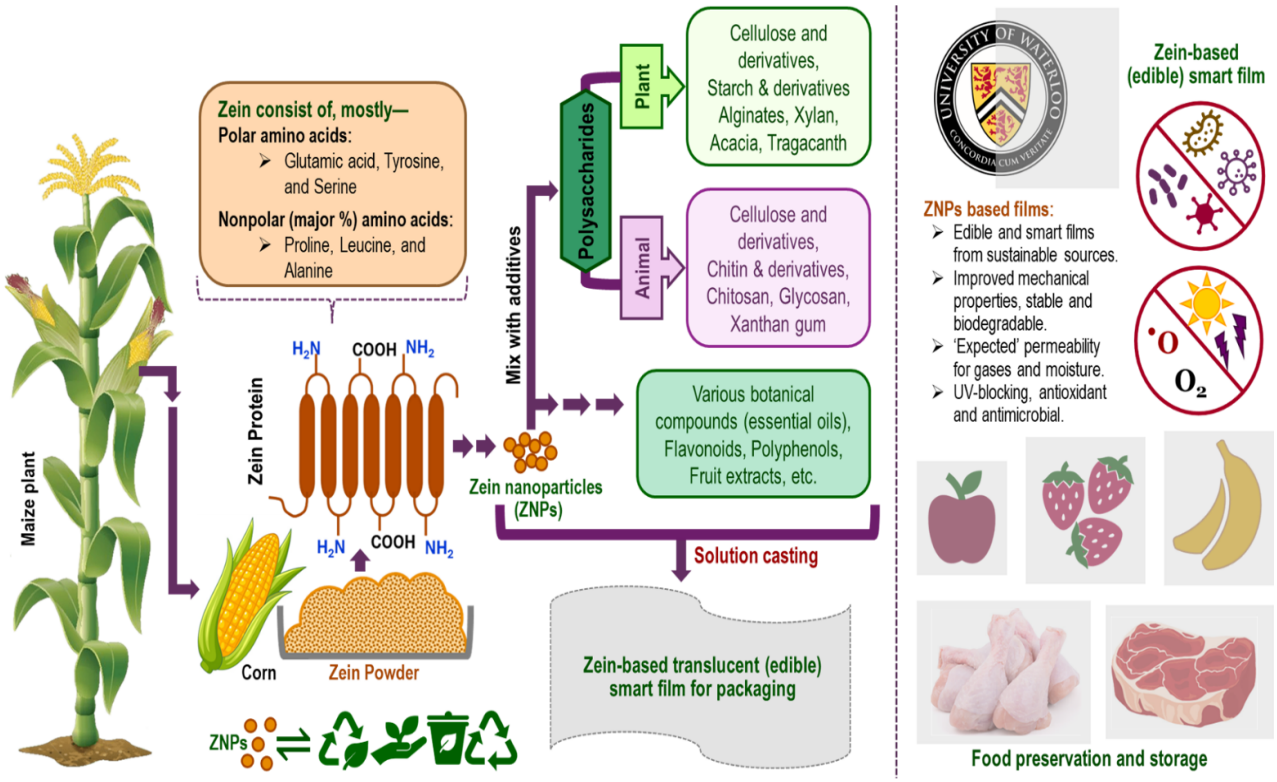


Figure 2.5. Schematic representation of the application of ZNP-based smart primary packaging with functionalities for sustainable food packaging.

2.8. Biomedical applications

In addition to the food industry, zein nanoparticles and nanofibers are gaining traction for biomedical applications, particularly in drug delivery, tissue engineering, and wound healing [115]. The biocompatibility and tunable properties of zein make it an ideal material for creating nanocarriers that can precisely deliver drugs to targeted sites within the body [116]. Zein nanoparticles have been used to co-encapsulate hydrophilic and hydrophobic drugs, offering controlled release profiles and enhanced therapeutic efficacy [115,116].

In tissue engineering, zein nanofibers, fabricated through electrospinning, provide a conducive environment for cell adhesion, proliferation, and differentiation [116,117]. These nanofibers have been used to develop scaffolds for bone tissue regeneration and nerve repair, in which the

controlled release of growth factors and other bioactive molecules supports tissue development [81,116]. Moreover, the unique properties of zein-based nanostructures make them suitable for wound dressings, where they not only protect the wound site, but also promote healing through the sustained release of therapeutic agents. For instance, zein nanofibers have been effectively used as scaffolds for tissue engineering owing to their excellent biocompatibility, which supports cell adhesion and proliferation [117]. The study demonstrated advancements in research on zein/poly(l-lactic acid) (PLLA) nanofiber scaffolds by incorporating bone morphogenetic protein 2 (BMP-2) and dexamethasone (DEX) into a coaxial electrospun scaffold to achieve dual controlled-release properties tailored for bone tissue engineering applications. The distinct release profiles of these bioactive molecules were significant: DEX exhibited a rapid release within the first three days, whereas BMP-2 was released over an extended period of 21 days. This differential release behavior was likely attributed to the localization of DEX in the shell layer, which resulted in an initial burst release. Importantly, 12 h post-inoculation with mesenchymal stem cells (MSCs), all the tested nanofiber scaffolds displayed excellent cell adhesion. Notably, the zein/PLLA scaffold with a dual controlled release of DEX and BMP-2 demonstrated superior cell viability, suggesting a synergistic effect between BMP-2 and DEX. This, combined with the inherent topographical features of the zein-DEX/PLLA-BMP-2 nanofibers, facilitated effective osteoinduction. These findings underscore the potential of zein/PLLA core–shell electrospun scaffolds with controlled dual release systems to not only enhance early cell adhesion but also promote osteogenic differentiation, making them highly suitable for bone tissue engineering applications [90]. Recently, a Zein/hyaluronic acid layer was developed on stainless steel for orthopedic applications, utilizing zein coating properties. This zein/hyaluronic acid coating significantly improved corrosion resistance, wettability, and biocompatibility in simulated biological environments. Furthermore, cross-linking techniques may further enhance the performance of electrospun

zein fibers for biomedical use [118]. The potential of a zein–polydopamine-based nanofibrous scaffold impregnated with titanium oxide (TiO_2) nanoparticles as a wound dressing material has been explored. In vitro studies revealed that the addition of metal oxide nanoparticles improved cell adhesion, proliferation, and migration, thereby enhancing the wound healing properties of the fibers [119]. Zein-based materials show promise in biomedical applications; however, their interactions with biological environments require careful consideration. Key challenges include managing immune responses, controlling biodegradation rates, and optimizing the influence of co-encapsulated bioactive compounds. Although zein is generally biocompatible, its proteinaceous nature may trigger immune reactions, necessitating research into surface modifications and anti-inflammatory strategies. Biodegradation rates must also be fine-tuned through factors, such as pH sensitivity, enzymatic activity, and polymer blending to match application-specific requirements. Furthermore, the encapsulation of bioactive compounds can significantly affect tissue response, therapeutic efficacy, and overall biocompatibility. Future research should focus on understanding and optimizing these interactions to enhance the performance of zein-based materials in drug delivery, tissue engineering, and wound healing applications. Zein-based materials, known for their excellent biocompatibility, hold significant promise in biomedical fields, particularly in drug delivery and tissue engineering. As biocompatible carriers, zein-based systems meet essential safety criteria, demonstrating non-toxicity, non-immunogenicity, and low cytotoxicity. Research has shown zein favorable interactions with cells, supporting attachment, morphology, and proliferation, as well as its non-hemolytic properties. These attributes make zein an ideal candidate for developing safe and effective bio-materials in medical applications and beyond, as illustrated in **Figure 2. 6.**

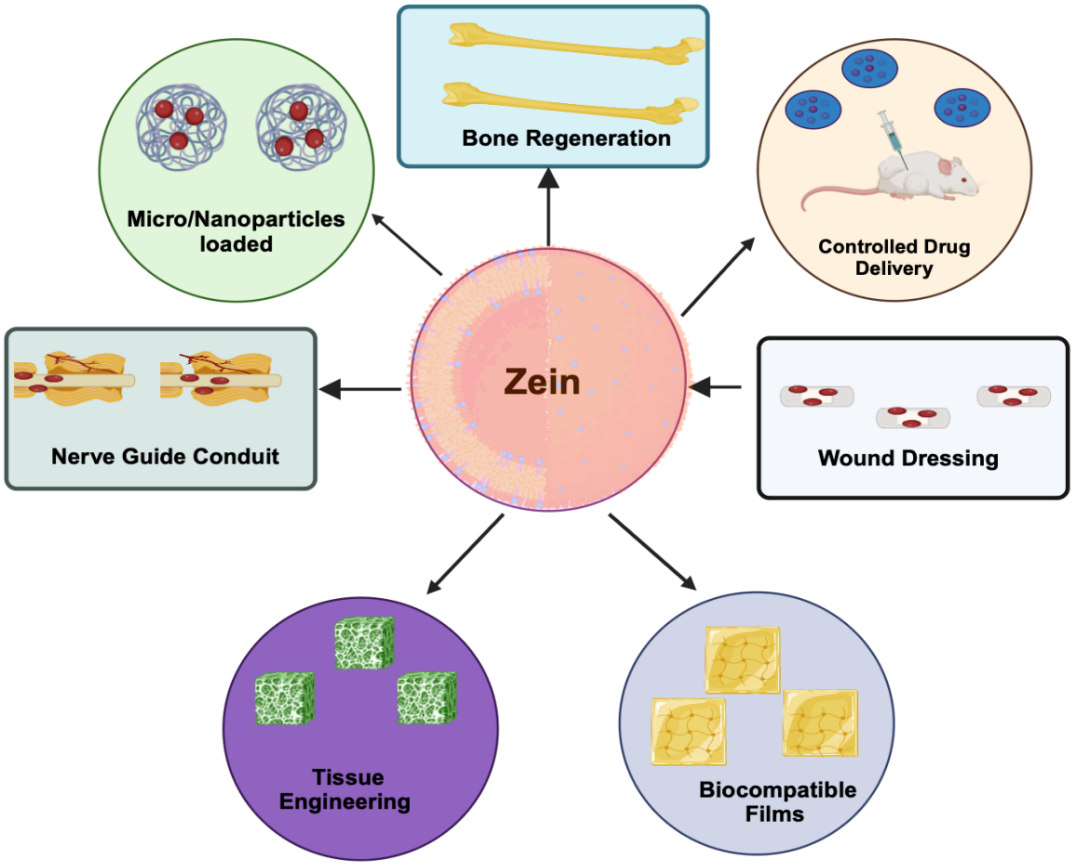


Figure 2.6. Schematic illustration of the diverse applications of zein-based nanostructures in biomedicine, including their use in bone regeneration, wound dressing, nerve guide conduits, and tissue engineering.

2.9. Challenges and Future Outlook

To fully harness the potential of zein-based nanoparticles and nanofibers in food and biomedical applications, it is crucial to focus on the synergistic effects that arise from co-encapsulation, as well as the associated challenges. A major advantage of co-encapsulation lies in the potential for synergistic interactions between bioactive compounds, which can enhance their bioavailability, stability, and controlled release profiles. However, these benefits often require complex, tailored co-encapsulation strategies that can accommodate the distinct properties of each compound, complicating scalability and limiting commercial viability.

For instance, co-encapsulating antioxidants like curcumin and resveratrol has shown enhanced bioavailability and stability through mutual protection from oxidative degradation [42]. Furthermore , the combination of hydrophobic and hydrophilic compounds within a single

carrier can enable multi-functional delivery systems that respond to specific physiological or environmental triggers, which is particularly valuable for applications in functional foods and therapeutic delivery [38]. However, developing such systems requires precision in encapsulation techniques to avoid degradation and ensure efficient release. One approach involves modification of zein through several mechanisms using agents like hydrolyzation to enhance surface properties Another set of modifications includes interactions with ionic reagents and specific pH conditions. Additionally, the incorporation of surfactants, ionic liquids and finding alternative route for interactions with other biological macromolecules has been explored to further improve zein functionality.

The development emerging as a promising material for co-encapsulation applications in edible food packaging and biomedical fields. Its stability, biocompatibility, and controlled degradation rate make zein-based nanoparticles (NPs) and nanofiber suitable for targeted drug delivery and functional food packaging. In edible packaging, zein's ability to encapsulate multiple bioactive compounds such as antioxidants, antimicrobials, and vitamins supports prolonged shelf life and enhanced food safety. In biomedical applications, zein NPs and nanofiber show potential in drug delivery, especially for cancer therapies, due to their compatibility and targeted delivery capabilities [57]. However, future research should address challenges related to optimizing the hydrophilic/hydrophobic balance, improving drug loading capacity, and understanding in vivo safety. Comprehensive studies on zein's bioavailability, toxicity, and efficacy in clinical settings are essential to unlock its full potential, paving the way for advanced, safe applications in food preservation and precision medicine.

2.10. Conclusions

Zein-based nanoparticles and nanofibers present substantial promise as co-encapsulation systems for bioactive compounds, driven by their unique nutritional value, stability, and biodegradability. These zein nanocarriers have versatile applications in both food and

biomedical sectors, facilitating the controlled, sustained release of bioactives like vitamins and antioxidants with high encapsulation efficiency. Recent advancements have expanded zein's role in functional foods and therapeutic solutions, with co-encapsulation systems providing precise delivery and enhanced stability in edible films. These films contribute to improved food safety, prolonged shelf life, and meet modern demands for targeted release in food preservation.

However, to fully realize the commercial potential of zein-based co-encapsulation systems, challenges such as high production costs, scalability, film standardization, and optimized controlled-release mechanisms must be addressed. Future research should prioritize scalable fabrication methods like microfluidics and solution blow spinning, as well as eco-friendly solvents and refined encapsulation processes to enhance safety and environmental sustainability. This review emphasizes the transformative potential of zein-based nanocarriers in advancing sustainable, functional edible films, laying a foundation for future research and commercial adoption in food science and pharmaceutical applications. Addressing these challenges will position zein-based materials as a standard in sustainable co-encapsulation technology.

Chapter 3. Fatty acid modified zein films: effect of fatty acid chain length on the processability and thermomechanical properties of modified zein films

3.1. Introduction

The extensive utilization of fossil resource-derived plastics for single-use applications, such as packaging and containment, has elicited environmental concerns. While these petrochemical-based conventional plastics exhibit desirable material properties, thus explaining their prevalence, they present a substantial environmental hazard due to their consumption in vast quantities, resistance to degradation, and accumulation in landfills that frequently disperse into the environment [120,121]. These challenges have led to an interest in the development of environmentally friendly, sustainable, biodegradable, and biocompatible polymers from natural resources[120]. In particular, the utilization of inexpensive and widely available natural macromolecules, such as plant-derived proteins and polysaccharides, has attracted considerable interest. Proteins are appealing natural macromolecules due to their inherently large molecular weight, film forming properties, and ease of chemical modification due to the presence of various functional groups [121]. Furthermore, proteins can be sourced from both animal (e.g., chicken feathers, hair, waste blood) and plant sources (e.g., wheat gluten, corn zein, soy protein, etc.)[122,123]. Some plant proteins, such as soy protein and wheat gluten, have been extensively investigated for bioplastic applications; however, limited commercial success has been observed due to their cost and performance. [2]

[2] ***Tadele, D.,*** *Shorey, R., Mekonnen, T.H. "Fatty Acid Modified Zein Films: Effect of Fatty Acid Chain Length on the Processability and Thermomechanical Properties of Modified Zein Films," Industrial Crops and Products ,192.10.1016/j.indcrop.2022.116028.2023, 116028*

Owing to inter- and intra-molecular hydrogen bonding and hydrophilicity exhibited by the majority of proteins, they lack inherent melt processability and exhibit high moisture absorption [117,124].

Zein is an alcohol-soluble prolamin storage protein extracted from corn. Being amphiphilic, it has nearly equal amounts of hydrophobic and hydrophilic amino acids [125]. Zein is recognized by the Food and Drug Administration (FDA) as generally safe[126] . Globally, corn is a major cash crop, and its extensive utilization for bioethanol production leaves behind enormous quantity of residue rich in zein protein [127]. The residue is typically used as an inexpensive animal feed, leaving the door open for value-added utilization of zein in sustainable polymers and other domains. Zein-based materials are recognized to be biodegradable, biocompatible, and have no allergenic ingredients for developing biopolymers [7]. Zein proteins are categorized based on their molecular weight, solubility, and amino acid content into four groups: α-zein (19 and 22 kDa), β-zein (14 kDa), γ-zein (16 and 27 kDa), and δ-zein (10 kDa) [11,12] The amino acid composition analysis of zein proteins revealed the presence of glutamine, leucine, proline, and alanine as the abundant amino acids, while the fractions of lysine and tryptophan were low. α-zein consists of about 80% of protein fractions and it is composed of alanine (10%), leucine (20%), proline (10%), and glutamine (21-26%) [35]. In addition, presence of amino acids with alcohol groups (such as serine and threonine) is lesser in α-zein than its other counterparts [128]. Furthermore, α-zein proteins have been observed to self-assemble into networks and thus, could easily be fabricated into films, fibers, and nanostructures [129,130].

The modification of zein protein is necessary to grant applicability in biopolymeric materials[131]. Among the various modification routes, successful incorporation of plasticizers to lubricate and improve chain movement has attracted substantial interest. This is because of the simplicity of the process, which can be carried out via a continuous extrusion process. For

instance, zein plasticized with oleic acid (OA) yielded a flexible and mouldable intermediate resin that was further molded into thin films possessing enhanced toughness and flexibility[132]. In another study, zein sheets added with palmitic acid (PA) or stearic acid (SA) exhibited more robust, waterproof, and viscoelastic properties. Due to better distribution throughout the resin, PA showed a better plasticization effect than SA[133]. However, most plasticizers being small molecules and sometimes moisture sensitive, leach out during use, causing further reduction in barrier and mechanical properties [10]. Alternative approaches to mitigate the plasticizer's limitations include chemical modification of zein proteins (such as esterification), grafting approaches, etc. [134]. The esterification of zein with organic acids, such as acid anhydrides and fatty acids, can offer hydrophobicity, ease of processibility, and enhanced physical and thermomechanical properties [135].

Acid chlorides that contain a polar carboxylic acid end and a nonpolar alkyl end can easily esterify proteins through a reaction with the protein's -NH_2 moiety [136]. The use of bases, such as pyridine or triethylamine, as a catalyst speeds up the reaction by deprotonating the positively charged intermediate [137]. Although the current research literature contains a little database on the esterification of zein proteins with fatty acid chloride to improve their film-forming ability, it is still a challenge to select the most practical and effective modification route [132,133]. There has been little work done to systematically compare the differential effect of fatty acid carbon chain length on the brittleness, barrier, and stability properties of the formed products.

This work aimed to investigate the effect of esterification of zein specimens employing various fatty acid chlorides on their respective physiochemical and film forming properties. The fatty acids used in this study (hexanoic, decanoic, and palmitic acid) were selected to represent a range of carbon chain lengths (C6, C10, and C16 respectively) commonly found in natural fats

and oils. This selection allows for a systematic investigation of how fatty acid chain length impacts the properties of modified zein. Using this range of fatty acids enables examination of how increasing hydrophobic chain length affects zein modification, processability, and film properties. The chosen fatty acids are also readily available, relatively inexpensive, and have been used in previous protein modification studies, allowing for comparisons to existing literature[133]. The success of modification reactions was confirmed and verified with infrared spectroscopy and other analysis. The changes in flow properties, dispersion homogeneity, mechanical properties and hydrophobicity were systematically evaluated. To the best of the authors' knowledge, no studies have been conducted on modifying zein protein with varying carbon chain length fatty acids to enhance the film forming, melt processibility, and physicochemical properties.

3.2. Materials and methods

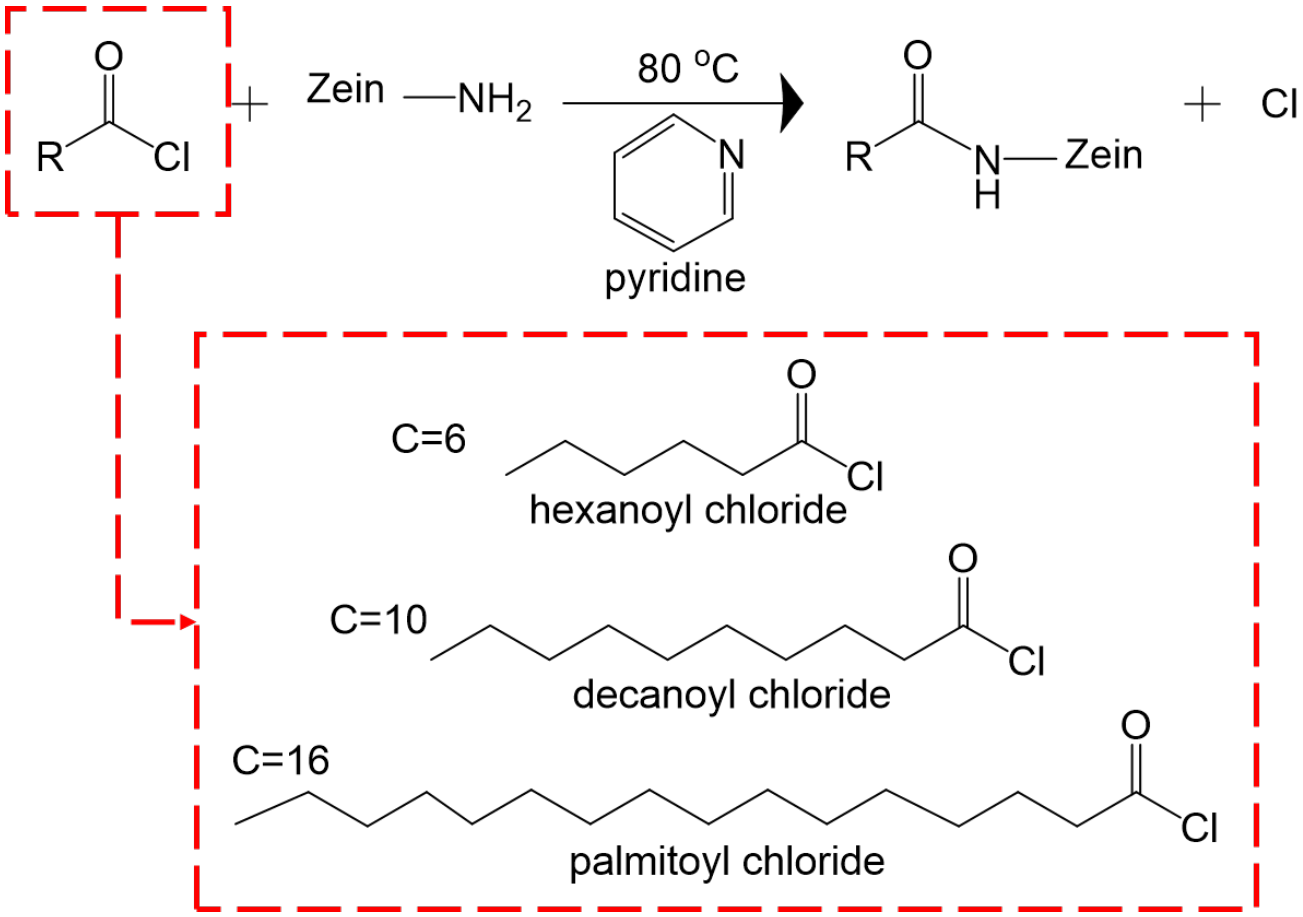
3.2.1. Materials

The α-Zein powder with a protein content of 95% (w/w) was purchased from Sigma-Aldrich. hexanoyl chloride (98%), hecanoyl chloride (98%), and palmitoyl chloride (>97%) were supplied by TCI chemicals. Pyridine (99.8%), chloroform (99%), toluene (99.9%), dimethyl sulfoxide (DMSO) (99.9%), tetrahydrofuran (THF) (≥99%, ACS grade), glycerol (≥ 98%), oleic acid (≥ 98%), acetone (≥99%), ethanol (≥99%), and glacial acetic acid (100%) were also purchased from Sigma-Aldrich (Oakville, ON, Canada).

3.2.2. Modification of zein protein with fatty acid chlorides

Hexanoyl, decanoyl, and palmitoyl chloride were employed to modify zein protein, as shown in **Scheme 3. 1**. For the modification, 10 wt.% of zein protein (10 g) was dissolved in 90 g of pyridine via sonication (30 min at room temperature). Pyridine served as a solvent and an acid

scavenger in the reaction. The prepared solution was then transferred to a round bottom flask (RBF) and heated to 85 ℃ in a silicone oil bath with constant stirring (300 rpm).



Scheme 3.1 Proposed reaction mechanism of fatty acid chlorides and zein protein.

As presented in **Table 3.1**, various reactions utilizing different concentrations of acid chlorides were conducted for 3 h each. The reaction temperature (85 ℃) and reaction time (1 h) were selected based on preliminary experimentations. The reaction mixtures, having attained a jelly-like consistency after 3 h of reaction, were cooled down to room temperature and washed with acetone (thrice). Complete removal of pyridine and unreacted acid chlorides was verified using an infrared spectrometer (ATR-FTIR) analysis. The washed products were subsequently dried overnight in a forced air oven at 70 ℃ and stored in zip lock plastic bags until further analysis.

Table 3.1 Composition of unmodified and esterified zein samples.

Sample identifier	Modifier	Moles of acid chlorides used(mmol)	Mass of acid chlorides used (g)
Zein (Z) control	-	-	-
ZC6-20	Hexanoyl chloride	20	2.7
ZC6-35	(C6)	35	4.7
ZC6-50		50	8.1
ZC10-20	Decanoyl chloride	20	3.8
ZC-10-35	(C10)	35	6.7
ZC10-50		50	9.5
ZC16-20	Palmitoyl chloride	20	5.5
ZC16-35	(C16)	35	9.6
ZC16-50		50	13.7

3.3. Characterization of the unmodified and modified zein specimen

3.3.1. Attenuated total reflectance Fourier transform infrared (ATR-FTIR) spectroscopy

The ATR-FTIR spectra of the modified and unmodified zein protein samples were acquired under ambient conditions using a Thermal Nicolet 6700 ATR-FTIR spectrometer (Thermo Electron Corp., Madison, WI). Approximately 2 mg of the zein protein and modified zein were dried overnight (70 °C), and the spectra were recorded in the transmission mode at 4 cm^{-1} resolution recording 64 scans in the frequency range of 4000 to 600 cm^{-1}.

3.3.2. Carbon nuclear magnetic resonance (^{13}C-NMR) spectroscopy

The solid-state ^{13}C-NMR spectra were recorded using a Bruker 500 MHz high-resolution NMR (Bruker-SpectroSpin 500 MHz Ultra shield, Bruker Corporation, MA). The C-NMR spectra were collected up to 200 ppm.

3.3.3. Solubility test

The effect of various modification reactions on the solubility of zein samples in different solvents was evaluated. A qualitative evaluation of the solubility of unmodified and modified zein samples in various solvents (five solvents with varying polarities) was made by visual inspection of the solid moieties dispersed in the solvent medium. The selected solvents were acetone, dimethyl sulfoxide (DMSO), ethanol, toluene, and water, with relative polarities of 0.355, 0.444, 0.654, 0.099, and 1.000, respectively. For this, 100 mg of the respective samples were added to 10 mL of each solvent and sonicated for 10 minutes. The dispersed samples were left undisturbed for 24 hours, and images were collected. Further, the dispersions were filtered, the filtered precipitate was dried at 50°C (1 h) and the dried precipitate was weighed.

3.3.4. Fabrication of films

The unmodified and modified zein solutions (5 wt.% in acetic acid) were mixed with 20 wt.% plasticizer with respect to the dry zein. The plasticizer consisted of an equal ratio of glycerol and oleic acid. The zein and plasticizer mixtures were dried (70 °C, overnight) to remove acetic acid. Further, 2.8 g of the dried specimens were pressed into films (with a 0.2 mm spacer) using a Carver press. The films measured 7.5 cm (length) x 7.5 cm (width) x 0.2 mm (thickness). The films were compressed for 3 min each at a temperature (90 °C) and pressure of 3,000 psi.

3.4. Characterization of samples and films

3.4.1. Rheology

The rheological properties of zein solutions in pyridine and molded films were evaluated on a HAAKE Mars III rheometer (Thermo Scientific, United States). An amplitude sweep analysis was carried out using a parallel plate geometry (PP35Ti and P20CSL) and spacing of 0.4 mm. The measurements were recorded at room temperature for the zein solutions and 150 °C for zein films.

3.4.2. Microscopy

A polarizing optical microscope (Olympus BX53M polarizing optical microscope, USA) was employed to investigate the surface morphologies of the unmodified and modified zein films at 50x magnification. Scanning electron microscopy (SEM) images of uncoated samples were acquired using Quantum FEG-SEM 250 at 20 kV under vacuum. The cross-sectional morphology of cryo-fractured films was also recorded.

3.4.3. Light transmittance of films

The baseline and modified zein films were cut into rectangular strips that fit into a cuvette (approximately 1 cm in width). The light transmittance of the films was then measured using a Cary 100 Bio UV-vis spectrophotometer between 380 and 780 nm.

3.4.4. Tensile property testing

The mechanical properties of the compression molded zein films were tested on a universal tensile testing machine (AGS-X series, Shimadzu, Japan) by employing a 500N load cell. Zein films were cut into tensile dog bones using an ASTM D638 Type V die with a gauge length and width of 27 cm and 3.12 cm, respectively. The tensile test was then conducted at a strain rate of 25 mm/min and at room temperature. Five samples for each formulation were tested, and their arithmetic mean was reported.

3.4.5.Water absorption rate

The water uptake rate of zein films was evaluated over the course of 72 h at room temperature (25±2 °C). Three strips of each zein film (50 mm × 50 mm) were cut for each formulation and dried in a forced air oven (70 °C, overnight). Specimens were immersed in 100 mL of water. Prior to weighing, the excess water was wiped off with Kimwipes™ to remove excess water, and their weight was recorded. Results were reported as the mean of three replicates

3.4.6. Water contact angle

Using a custom-built optical sessile drop system, the water contact angle (WCA) of the modified and unmodified zein films was evaluated. A syringe pump dispensed 5 µL of water onto each sample and contact angle images were captured at 24 °C using a high-magnification Basler scA 1000-30 fm camera after a 30-second contact time. This duration was chosen to reflect the material's inherent wettability, minimizing the influence of water absorption or evaporation. The recorded images were analyzed using the ImageJ program to ensure accurate and consistent measurements.

3.5. Statistical analysis

The data has been represented as mean ± standard deviation. The statistical differences in the data were verified by employing a one-way analysis of variance (ANOVA) Tukey test on the recorded data. The significance level for all analyses was set at $p < 0.05$.

3.6. Results and discussion

3.6.1. Rheology of zein solution

The rheological behavior of zein solutions was investigated to understand how concentration influences viscosity and flow properties (**Figure 3.1**). At concentrations up to 10 wt%, the viscosity remained constant with increasing shear strain, indicating Newtonian behavior. In

these solutions, zein chains in pyridine move freely, showing no significant resistance to flow. However, as the concentration exceeded 15 wt%, the solutions demonstrated a decrease in viscosity with increasing shear rate, characteristic of shear-thinning behavior. These findings align with the results reported by Wei et al. and Li et al., where similar changes in flow behavior were observed in zein solutions above 20 wt% and 15 wt%, respectively [32,138].

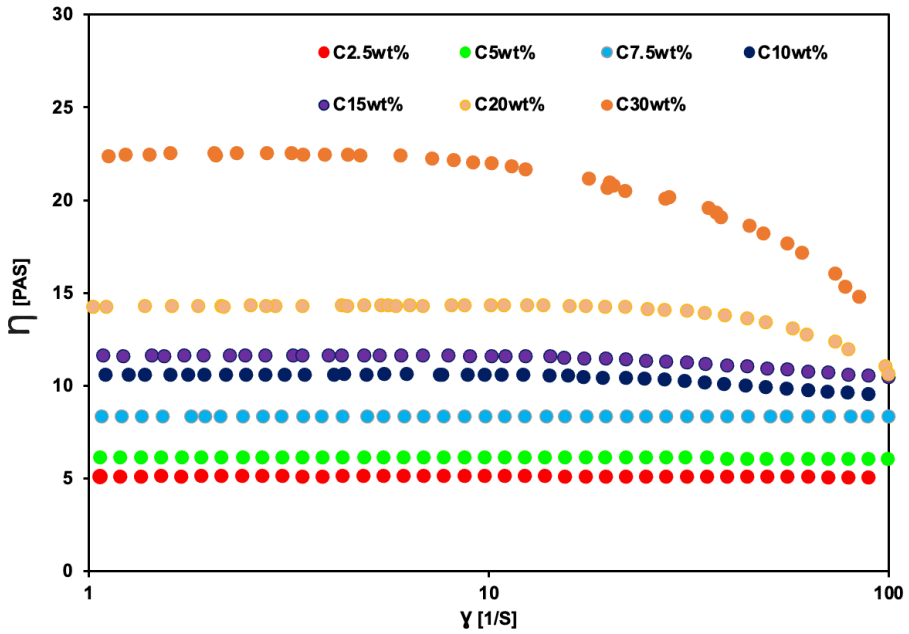


Figure 3.1. Complex viscosity versus shear stress of zein solution with concentrations ranging from 2.5 to 30 wt.% at 30 °C.

Further this transition is attributed to the onset of polymer chain entanglements, as indicated by the critical concentration (C*) . The concentration-dependent zero-shear viscosity showed distinct behavior across two regions, with slopes of 0.5 and 2.5, corresponding to the dilute and semi-dilute regions, respectively. The critical overlap concentration (C*) was determined to be approximately 4.9 wt%. Below this critical concentration, zein chains exist primarily as isolated entities (**Figure 3.2a**), allowing independent movement. As the concentration approaches and exceeds C*, the chains begin to entangle (**Figure 3.2b**), eventually behaving like a polymer melt at even higher concentrations (**Figure 3.2c**) leading to pronounced viscoelasticity.

Intrinsic viscosity ([η]) is another key parameter that offers insights into the contribution of zein to the overall solution viscosity and the suitability of pyridine as a solvent. It is calculated from the intercept of the Mark-Huggins equation fitted to specific viscosity and concentration data. The intrinsic viscosity of zein solution was determined to be approximately 54 mL/g as an extrapolated value of η_{sp}/C when zein concentration (C) approaches zero from equation (3.2).

$$\eta_{\text{specific viscosity}}\ (\eta_{sp}) = \frac{(\eta_{solution} - \eta_{solvent})}{\eta_{\text{solution}}} \tag{3.1}$$

$$[\eta] = \lim_{C \to 0}\left(\frac{\eta_{sp}}{C}\right) \tag{3.2}$$

Furthermore, the Huggins equation could also be expressed as

$$\eta_{red} = \frac{\eta_{SP}}{C} = [\eta] + K_H[\eta]^2 C \tag{3.3}$$

where η_{red} is the reduced viscosity, K_H is the Huggins coefficient, C is the concentration of the solution, and a linear relationship is presented

$$\eta_{sp} = [\eta]C + K_H([\eta]C^2) \tag{3.4}$$

In a double logarithmic coordinate, the plot of η_{sp} against $C[\eta]$ resulted in a linear relationship in the larger $C[\eta]$ range, which can be fitted using eq (3.4) [139]. Huggin's coefficient K_H was estimated as 0.24. Since the thermodynamic meaning of Huggins constant is still rather ambiguous, we were not interested in its quantitative analysis and discussion in this study, and it has been used rather empirically as a criterion for evaluating the solubility of a solute in a solvent [32,139]. It is generally accepted that $K_H < 0.5$ (zein) dissolves well in the solvent (pyridine). Pyridine, therefore, acts as a suitable solvent for zein, and also plays a role as a reaction medium, scavenging the HCl by-product during zein protein esterification.

The relationship between zein concentration to zero-shear viscosity, specific viscosity, and intrinsic viscosity to evaluate whether pyridine is a suitable solvent for zein was correlated

with a fitting curve using equations (3.1) to (3.4).These observations provide insights into the processing behavior of zein solutions, particularly for applications requiring controlled viscosity, such as film casting and nanoencapsulation processes.

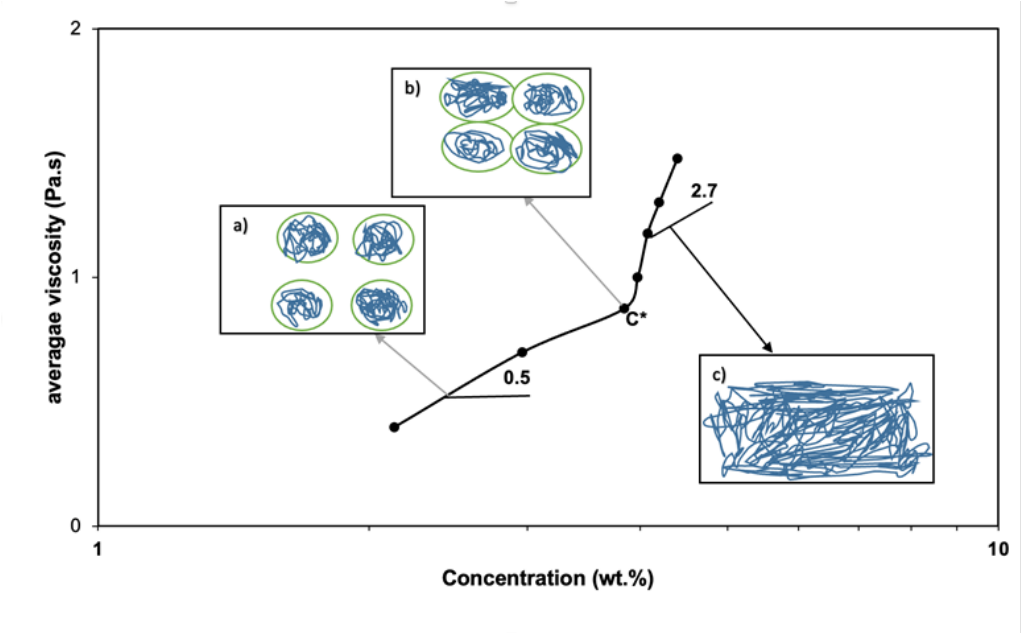


Figure 3.2 . The effect of concentration on viscosity for zein solutions, a) dilute region when concentration is less than overlap concentration ($C < C^*$), b) overlap region ($C = C^*$), c) semi-dilute region ($C > C^*$).

3.6.2. ATR-FTIR and solid-state C-NMR spectra of modified zein

AT*R-FTIR* spectra of the zein samples were collected to verify the proposed zein modification reactions. As shown in **Figure 3.3**, the spectra of the unmodified zein sample and its modified counterparts were compared. The broad peaks at 3400 cm^{-1} and 3100 cm^{-1} on the pristine zein correspond to the stretching vibrations of -OH and the $-NH_2$ moieties from amide A [140,141]. The vibrations related to hydroxyl moieties (-OH) could be explained by the presence of hydroxyl sidechains in serine and threonine amino acids of the α-zein[128]. A gradual decrease in the hydroxyl (-OH) peak intensity of the modified zein with the increase in the acid chlorides concentration was observed (**Figure 3.3(a-c)**). This was associated with the higher substitution of hydroxyl moieties due to more acid chlorides in the respective reactions[142]. Moreover, an

increase in the band at 1750 cm^{-1} associated with the acid chlorides' carbonyl groups (C=O) was observed. The decrease of the hydroxyl peak and the increase of the carbonyl peak have further verified the modification reaction of zein proteins with the fatty acid chlorides[121,143].

The peaks representing methylene ($-CH_2$) and methyl ($-CH_3$) groups were also observed at 2920 cm^{-1} and 2850 cm^{-1}, respectively. The progressive increase in the methylene and methyl peak intensities was attributed to the addition of fatty acid chloride chains to the zein molecular structure. The absence of -COCl characteristic peak at 1800 cm^{-1} confirmed and verified the effective removal of the unreacted acid chlorides from the modified zein specimens [143,144]. The above characteristic peaks showed the distinct functional groups of zein and confirmed the occurrence of successful reactions between baseline zein and the respective acid chlorides. The recorded observations were consistent with other studies [143,145]. The absence of characteristic pyridine signals between 1200-1025 cm^{-1} (C-N) and 860-480 cm^{-1} (C-H) in the ATR-FTIR spectra of the modified zein sample verified the removal of pyridine from the modified zein sample.

In addition, the ATR-FTIR spectra recorded for the zein films (Figure 3a) showed a similar trend to its powder counterpart. The IR spectra of the modified films displayed a peak at 3400 cm^{-1}, corresponding to the -OH and $-NH_2$ moieties of the samples. A decrease in its intensity was correlated to the successful reaction of the unmodified zein with the various acid chlorides, in accordance with **Scheme 3.1**. The changes in the peak intensity at 2920 cm^{-1} and 2850 cm^{-1} were attributed to the methylene and methyl moieties of the esterified zein. The appearance of carbonyl (C=O) stretching at 1750 cm^{-1} in the modified samples and its absence in the unmodified specimen verified the esterification reaction.

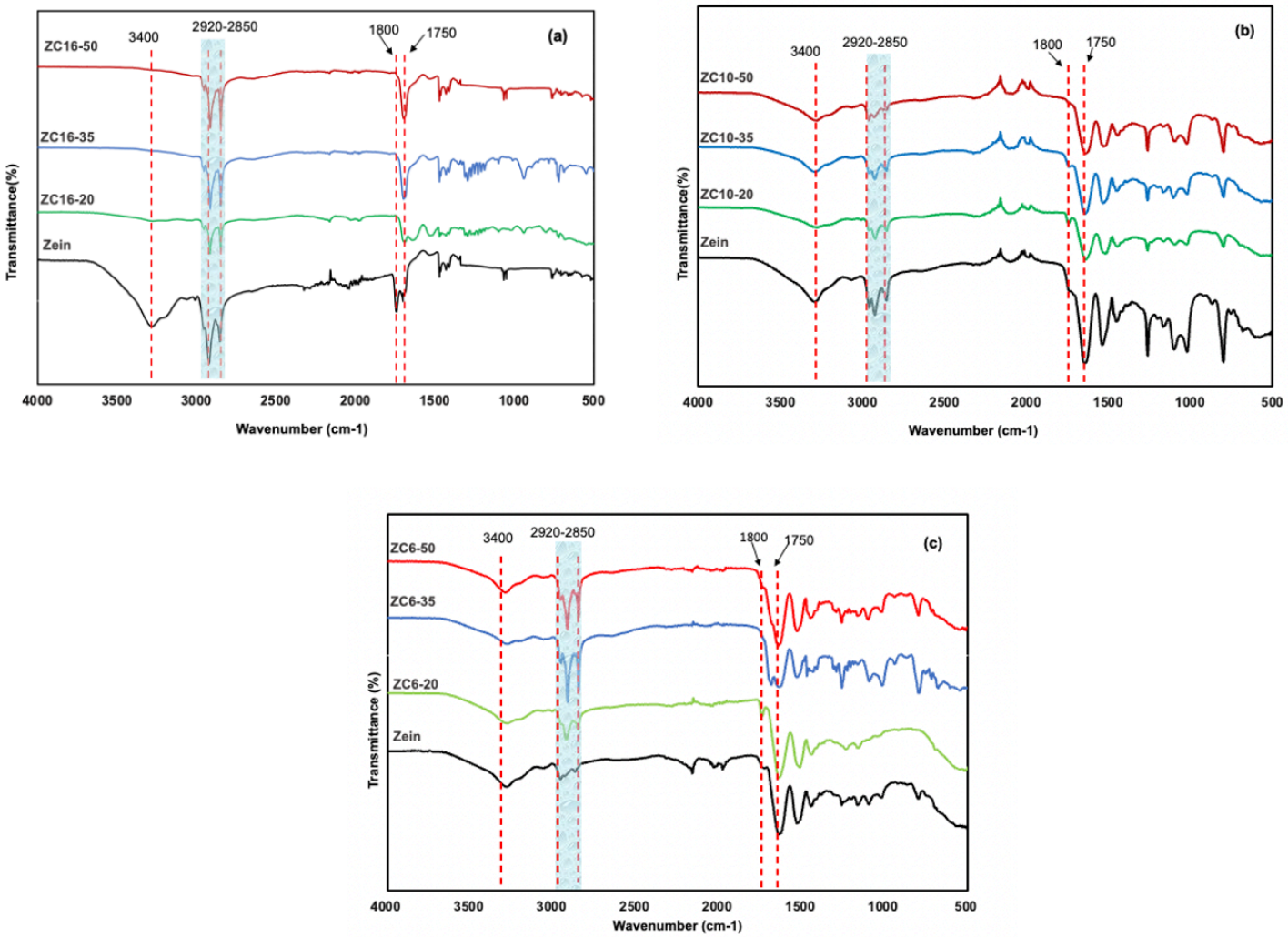


Figure 3.3. ATR-FTIR spectra of (a) zein modified with palmitoyl acid chloride (ZC16), (b) zein modified with decanoyl acid chloride (ZC10), c) zein modified with hexanoyl acid chloride (ZC6).

Figure 3.4 illustrates the solid-state *C-NMR* spectra of the baseline and acid-chloride-modified zein protein samples. The characteristic signals representing the long aliphatic chains from acid-chlorides were essential in verifying the proposed reaction (**Scheme 3.1**). The peaks between 35.1 and 23.3 ppm represented the methylene (-CH_2-) moieties of the long aliphatic carbon side chains, and the signal at 14.4 ppm corresponded to the methyl (-CH_3) groups[146]. As evident from **Figure 3.4 (a-c)**, the samples modified with medium (decanoyl chloride) and long (palmitoyl chloride) aliphatic carbon chains exhibited more pronounced carbon chain characteristic peaks. Moreover, a direct correlation was observed between the aliphatic carbon peak intensity and the number of acid chloride loadings. The 50 mmol samples displayed the highest intensity peaks, as evident from the samples (ZC6-50, ZC10-50, and ZC16-50). In agreement with the *ATR-FTIR* results, the characteristic signal at 175 ppm was associated with the carbonyl group (-C=O-), and the peaks at 140.2 ppm and 100.6 ppm represent the aromatic side chains associated with the amino acids (tyrosine and phenylalanine) in α- zein protein specimens [128,147]. In addition, the signal at 55.4 ppm represented the presence of α-carbon atoms, and the decrease in its intensity (as recorded in the reacted specimen spectra) verified the occurrence of the proposed reaction (Scheme 1). The results agreed with the literature on ^{13}CNMR analysis of zein protein specimens [148]. Herein, the spectral analysis confirmed and verified the proposed reaction mechanism.

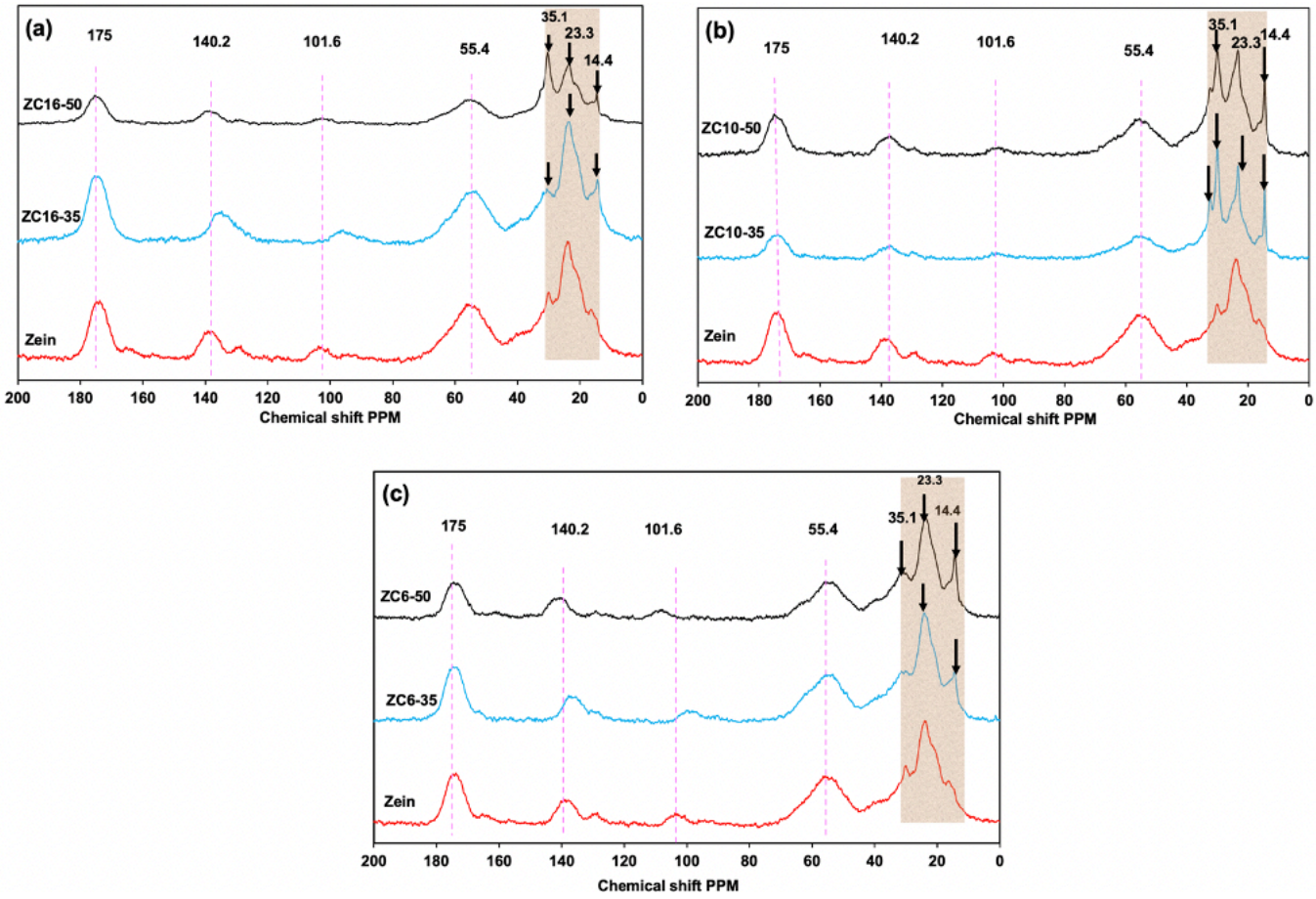


Figure 3.4 **.** ^{13}C-NMR spectra of zein: (a) modified with palmitoyl chloride (ZC16), (b) modified with decanoyl chloride (ZC10), and (c) modified with hexanoyl acid chloride (ZC6).

3.6.3. Solubility of modified zein in organic solvents

The solubility of the pristine and modified zein samples in various organic solvents was tested. The knowledge of solubility properties is important not only to evaluate the level of modification, but also to understand the solvent tolerance of bioplastics and to carry out structural characterization [149]. For this, the solubility of the highly modified zein samples (ZC6-50, ZC10-50, and ZC16-50) was investigated in acetone, dimethyl sulfoxide (DMSO), ethanol, toluene, and water. As evident from **Figure 3.5**, the esterification and grafting of the fatty acids on zein proteins alters its polarity. As anticipated, the modified specimens exhibited poor interaction with water, as noted from the rapid sedimentation.

On the contrary, the unmodified zein remained suspended in water. The enhanced hydrophobicity demonstrated by the modified zein over its unmodified counterparts was attributed to the grafting of the long-aliphatic carbon chains onto the zein molecules. Similar observations were noted for unmodified and modified zein samples in ethanol, acetone, and toluene (**Figure 3.5**), ascribed to the reduction in polarity of the modified zein samples. The modified specimens formed a stable dispersion in DMSO. This was attributed to the aprotic nature of DMSO. Further, a quantitate measurement of the amount of solute dispersed in the solvents (acetone, DMSO, ethanol, and toluene) was conducted. The filtered and dried precipitate did not result in significant losses in the amount recovered, owing to negligible dispersion in the solvent media. This further confirmed the hydrophobicity of the modified zein.

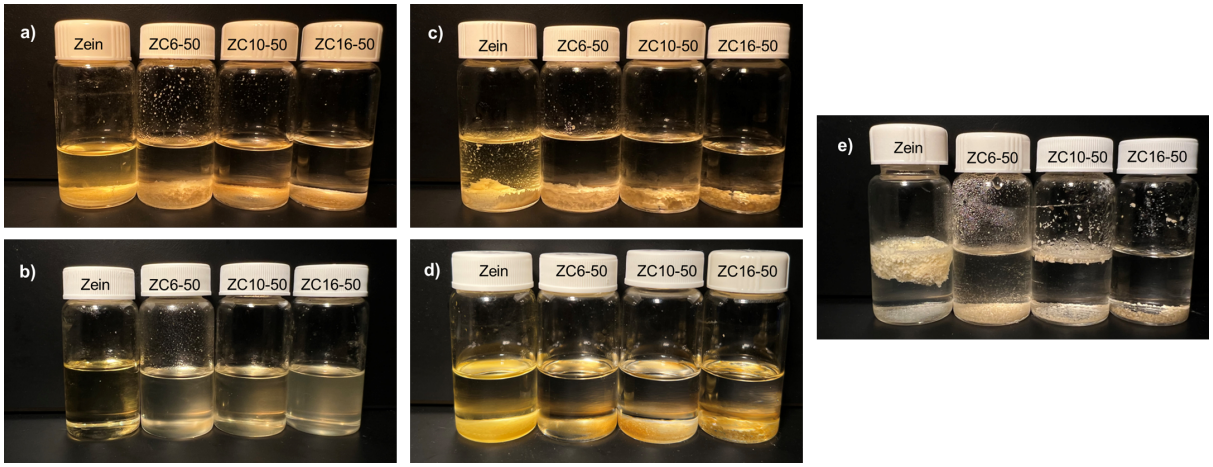


Figure 3.5. Solubility of zein samples modified in a) Acetone, b) DMSO, c) Ethanol, d) Toluene, and e) Water.

3.6.4.Morphology of modified zein films

The melt flowability of the plasticized zein (pristine) and modified zein with decanoyl chloride (ZC10-50) was evaluated using a hot stage microscopy. For this, the compression molding cast films were heated from room temperature (25 °C) to 120 °C and further exposing it to elevated temperatures (150 °C, 180 °C, and 210 °C). Significant differences in the melting

characteristics of unmodified and modified zein films were recorded with the increasing temperature. **Figure 3.6** shows no changes in the surface morphology were observed for the unmodified zein film at 120 °C. Heating the unmodified film further up to 210 °C did not significantly change surface morphology.

On the contrary, pronounced changes in the surface morphology of the modified specimen (at 120 °C) were recorded. With a further rise in temperature (150 °C), the modified zein film exhibited viscous behavior as evident from free-moving spherical moieties, and the disappearance of surface deformation incurred during the compression molding operation. The smooth surface exhibited by the modified zein specimen at 210 °C showed the effective melting behavior of the modified zein protein films resulting from grafting the fatty acid chains. These observations were synchronous to the initial hypothesis.

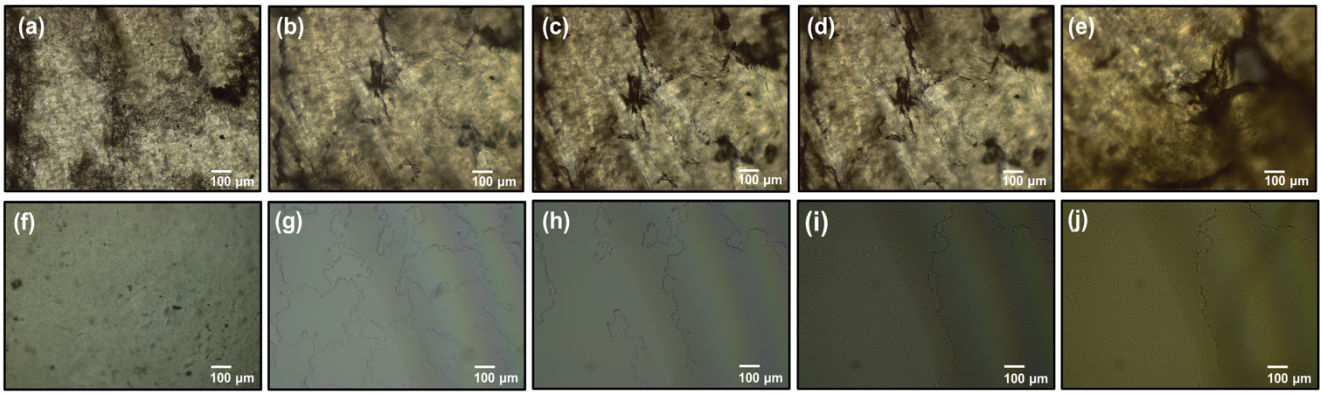


Figure 3.6 **.** Melting evaluation optical micrographs: unmodified zein film at: a) 27 °C, b) 120 °C, c) 150 °C, d) 180 °C, and e) 210 °C, modified zein film at: f) 27 °C, g) 120 °C, h) 150 °C, i) 180 °C, and j) 210 °C.

Furthermore, optical microscope evaluations were performed to study the surface morphology of unmodified and modified zein films. A significant difference between the baseline and modified zein films was observed, as illustrated in **Figure 3.7**. The pristine zein films exhibited a nonhomogeneous surface morphology, as presented in **Figure 3.7a**. This was attributed to the poor interaction between the unmodified zein and the plasticizer. In contrast, the modified zein

samples demonstrated a well-distributed surface morphology, owing to its better interaction with the plasticizer. The enhanced nonpolar behavior and better dispersibility of modified zein moieties in the moulded films could contribute to better physical properties. Wang. et al. reported enhanced homogeneity in the films fabricated with modified zein proteins [150].

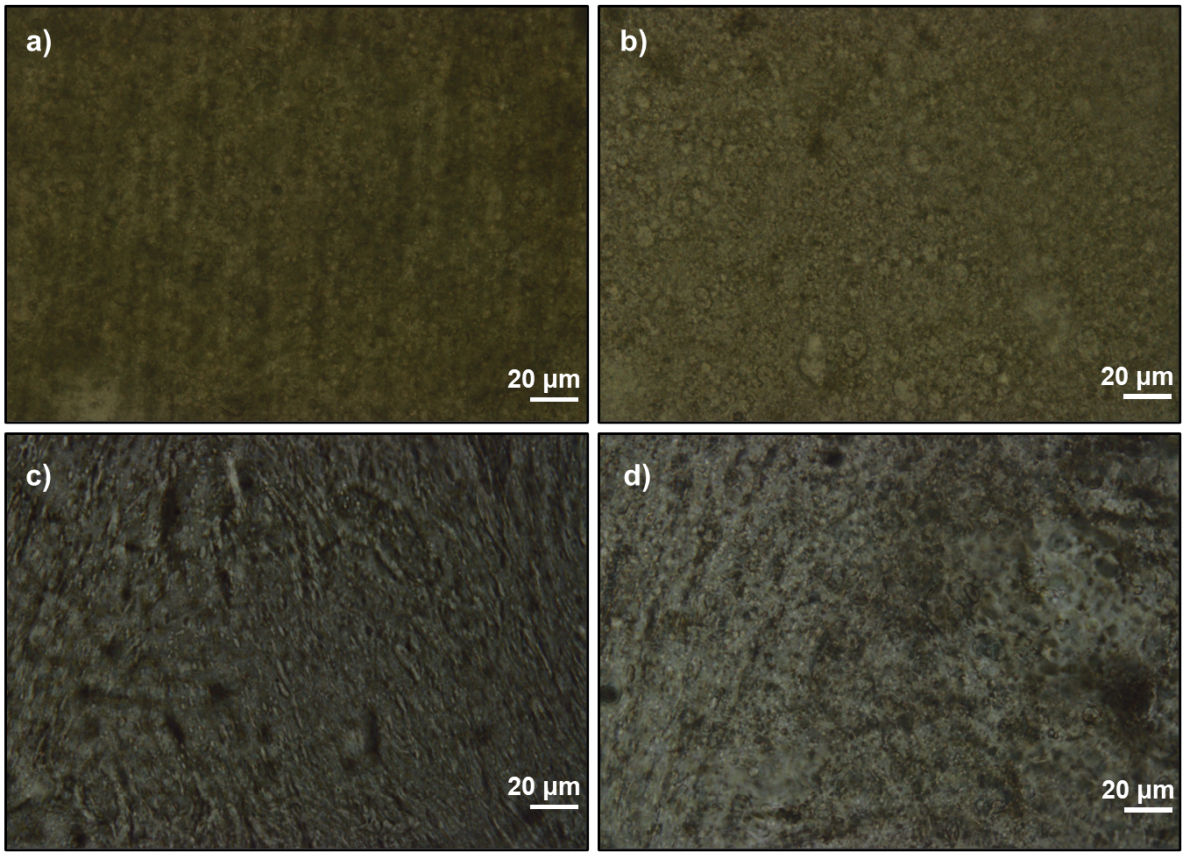


Figure 3.7*.* Optical microscopic surface morphologies , a) pristine zein b) zein/hexanoyl acid (ZC6-50) c) zein/decanoyl acid (ZC10-50), d) zein/palmitic acid (ZC16-50).

SEM images of the unmodified and modified zein films are shown in **Figure 3.8**. Significant changes in the morphology of modified zein films compared to their unmodified counterparts were observed. As evident from Figure 8, the modified zein films exhibited higher uniformity and minor deformations. These observations were synchronous with the optical microgram results (**Figure 3.7**) and were attributed to the better compatibility of the modified specimen with the plasticizers. The cross-sectional SEM micrograms of zein films are presented in **Figure A2**. It was noted that the cross-sectional homogeneity of the tested specimens differs

with the variations in the aliphatic carbon chain length used as the modifier. Overall, the modified zein films displayed minor surface deformities compared to their unmodified counterparts.

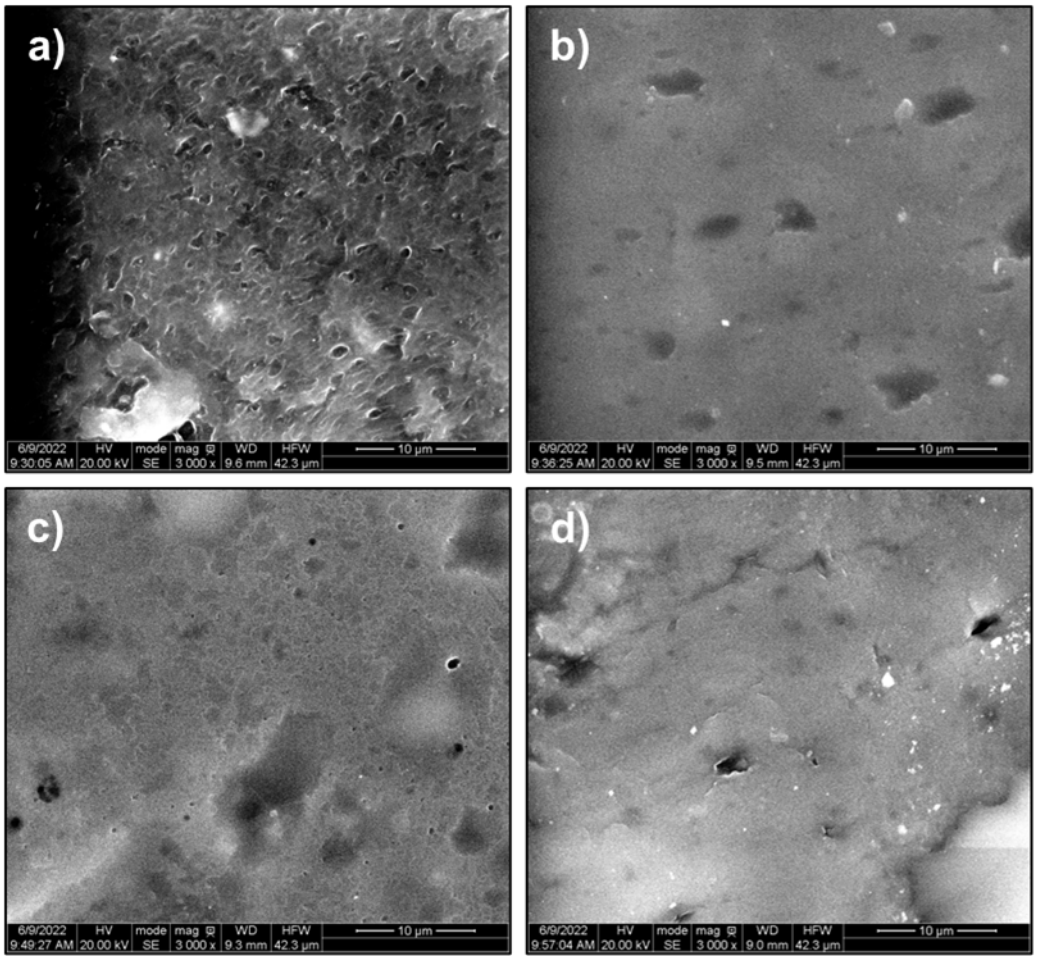


Figure 3.8. SEM surface morphologies of zein films a) baseline zein, b) zein modified with hexanoyl chloride (ZC6-50), c) zein modified with decanoyl chloride (ZC10-50), and d) zein modified with palmitoyl chloride (ZC16-50).

3.6.5. Optical Clarity

Among the desirable properties of a film, its transparency is one of the most important characteristics to consider for practical applications. The fatty acid modified zein films were smoother, shinier, more transparent and possessed a more prominent light-yellow tone in comparison to the baseline zein film, as illustrated in **Figure 3.9b**. The effects of the chemical modification of zein specimen on its transparency was evaluated using a UV-VIS

spectrophotometer via light transmission through the samples in the visible light range (400-800 nm). **Figure 3.9a** shows that modified zein films with medium carbon chain (ZC10-50) have the highest light transmittance of 40% at 580 nm. The light transmittance of the modified zein films with long carbon chains (ZC16-50) and short carbon chains (ZC6-50) also shows an increasing trend in optical clarity compared to the unmodified zein films. The factors contributing to this trend are improved grafting of fatty acid chlorides onto zein protein through reducing the potential formation of aggregates due to hydrophobic and electrostatic interactions[151]. Overall, these results indicate that modification of zein protein with fatty acid carbon chains produces films with good transparency.

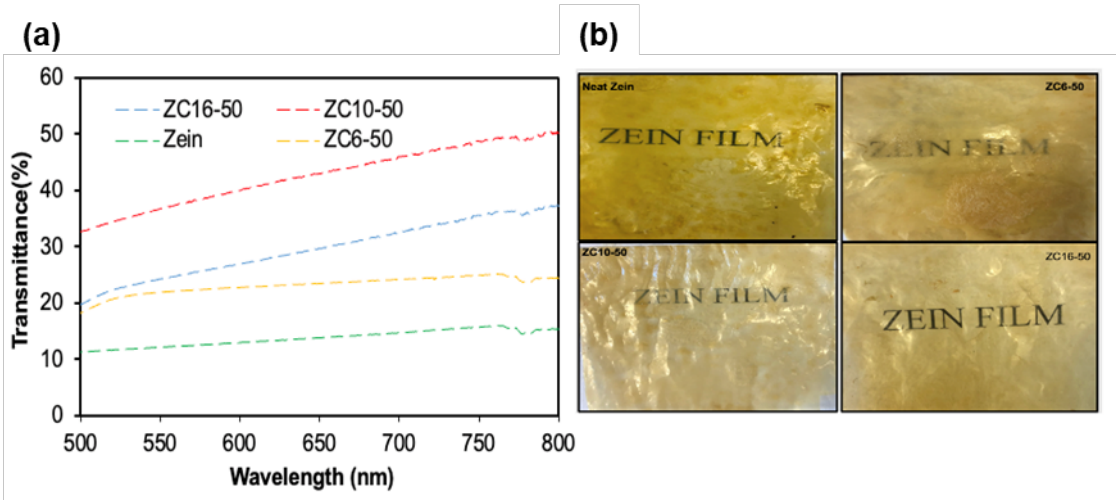


Figure 3.9. a) Light transmission measured with a UV-vis spectrometer, b) Photographs of representative films.

3.6.6. Rheological properties of zein films

The viscoelastic properties of the zein films were studied at 150℃ using amplitude sweep analysis based on preliminary tests. This analysis aimed to understand the solid-like and liquid-like behaviors of the films, characterized by the storage modulus (G') and loss modulus (G"), respectively [152]. G' is indicative of the elastic (solid-like) behavior, while G" represents the viscous (liquid-like) response. The examination of G' and G" is essential to predict the processability of these films in various manufacturing processes, including extrusion, injection

molding, and compression molding [144]. The results, as shown in **Figure 3.10**, demonstrate that all modified zein samples exhibited higher G' and G" values compared to the unmodified (baseline) zein film within the linear viscoelastic region. A clear plateau of constant moduli was observed, indicating the stability of the films' viscoelastic behavior within this region. This stability is crucial for determining the processing parameters for zein-based films. In **Figure 3.10(a-b),** zein films modified with ZC16-50 and ZC10-50 display slightly higher G" than G' in the linear viscoelastic range, suggesting a dominant viscous behavior. Notably, ZC16-50, which is modified with palmitoyl chloride, demonstrated the highest G" value among all formulations. This can be attributed to the increased hydrophobic interactions and restricted molecular mobility introduced by the long fatty acid chains, which enhances the viscous behavior and results in higher overall viscosity. These findings align with previous studies indicating that unmodified zein forms strong hydrogen bonds between its hydrophilic groups, contributing to its distinct rheological behavior compared to modified zein films [153]. The intersection of G' values between unmodified zein and short-chain modified zein (ZC6-50) may indicate a gelation point, where the viscoelastic behavior shifts from being primarily viscous to more elastic. This transition provides critical insight into the gelation behavior and network formation in zein samples modified with acid chlorides.

The dynamic viscosity analysis of zein films modified with fatty acid chains provided significant insights into the flow behavior and surface uniformity of the films. The incorporation of fatty acids into the modified zein films enhanced their viscoelastic flow behavior by balancing the rigidity and flexibility of the polymer chains, as demonstrated in **Figure 3.10(c)**. The results indicate that the presence of fatty acids induces a shear-thinning effect, which is more pronounced in films modified with ZC10-50 and ZC16-50. The extent of this behavior is influenced by the length and concentration of the fatty acid chains. The observed shear-thinning behavior arises from newly formed hydrophobic interactions and

altered hydrogen bonding patterns, which occur due to the chemical modification of zein with fatty acid chlorides [154]. These structural modifications decrease intermolecular friction during shear, thus enhancing the flow and processability of zein films, which is particularly beneficial for applications in film extrusion and coating processes.

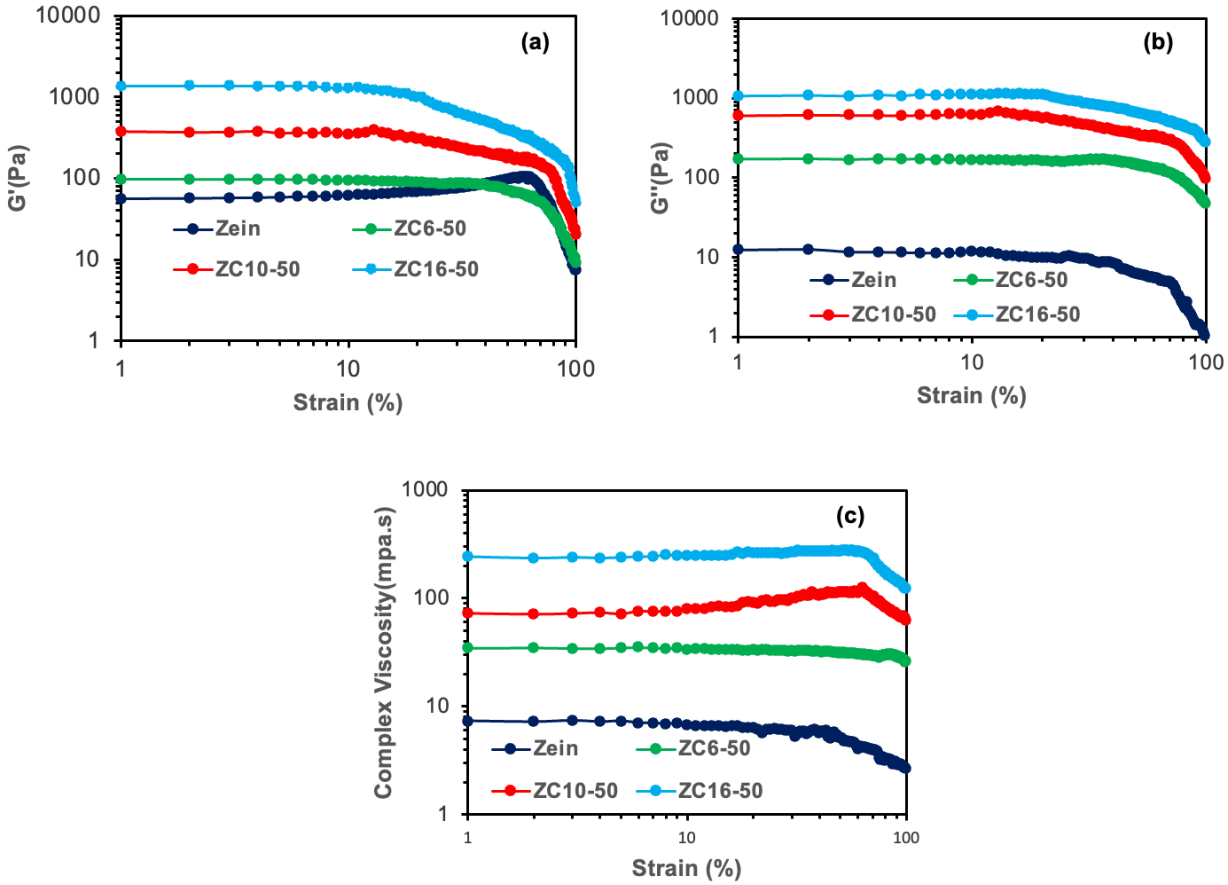


Figure 3.10. Storage modulus (G') and Loss modulus (G") of compression molded zein films: (a) Storage modulus (G′) vs. strain (%), (b) Loss modulus (G″) vs. strain (%) and (c) Complex viscosity vs. strain (%).

3.6.7. Mechanical properties

The mechanical properties of zein films were analyzed to assess the impact of fatty acid chloride modifications, with tensile tests conducted on compression-molded films as shown in Figure 3.11(a-d). The highest degree of modification was achieved using 50 mmol of acid chloride, verified through ATR-FTIR (**Figure 3.1**) and 13C-NMR (**Figure 3.2**). Consequently,

the mechanical properties of the extensively modified samples (ZC6-50, ZC10-50, and ZC16-50) were evaluated.

Unmodified zein films exhibited low tensile strength (1.70 MPa) due to poor film-forming capabilities and lack of molecular integration, as seen in the morphology analysis. In contrast, films modified with various fatty acid chlorides displayed significantly enhanced tensile properties. Zein films modified with hexanoyl chloride (ZC6-50) showed an improved tensile strength of 3.25 MPa, representing a 91% increase. More notably, films modified with decanoyl chloride (ZC10-50) exhibited the highest tensile strength of 8.3 MPa, a remarkable 388% improvement over the unmodified zein. ZC16-50, modified with palmitoyl chloride, also showed substantial enhancement with a tensile strength of 6.61 MPa, corresponding to a 288% increase. This significant improvement in tensile strength is attributed to the enhanced film-forming properties and increased interaction between zein chains and plasticizers, facilitated by the incorporation of aliphatic carbon chains of varying lengths. The observed trend suggests that medium-chain fatty acid chlorides (C10) may provide optimal mechanical enhancement, balancing chain length with molecular mobility and integration. These findings align with previous studies on zein modified with fatty acid chlorides, such as lauryl chloride (C12), which also reported substantial improvements in mechanical properties [12]. The elongation at break, indicative of the films' flexibility, was significantly enhanced in the modified samples. Compared to the unmodified zein film (38.41%), ZC6-50, ZC10-50, and ZC16-50 exhibited increases of 25.54%, 71.83%, and 77.04%, respectively, with values of 48.22%, 66%, and 68%. This trend demonstrates a positive correlation between the fatty acid chain length and the improvement in film flexibility. This improvement is attributed to the plasticization effect of the long aliphatic chains introduced by the acid chloride modification. The elastic modulus, calculated from the linear region of the stress-strain curve, showed an increasing trend with the elongation of fatty acid chain lengths in the modified films. This trend implies that the longer

aliphatic chains not only act as plasticizers but also enhance molecular mobility within the zein matrix, promoting better stress distribution and contributing to improved rigidity. However, contrasting findings in previous studies reported a decreasing modulus with oleic and palmitic acid chloride modifications [12,155]. This discrepancy may stem from differences in experimental conditions, such as the degree of modification, chain packing, and the specific matrix-filler interactions within the zein structure. Additionally, the plasticization mechanism could vary depending on the chain length and the compatibility between the fatty acid chains and the zein matrix, potentially influencing the resulting mechanical properties. The stress-strain curves in **Figure 3.11(d**) confirm these findings, where ZC16-50 demonstrates greater extensibility before failure, indicating enhanced flexibility.

The toughness, calculated as the energy required to break a specimen (area under the stress-strain curve), showed that modified zein films were at least 30 times tougher than the unmodified counterpart (**Table A1**).

Statistical analysis confirmed that all mechanical properties (tensile strength, elongation at break, toughness, and elastic modulus) were significantly different ($p < 0.05$) among the tested samples, as verified by ANOVA (**Table A1**).

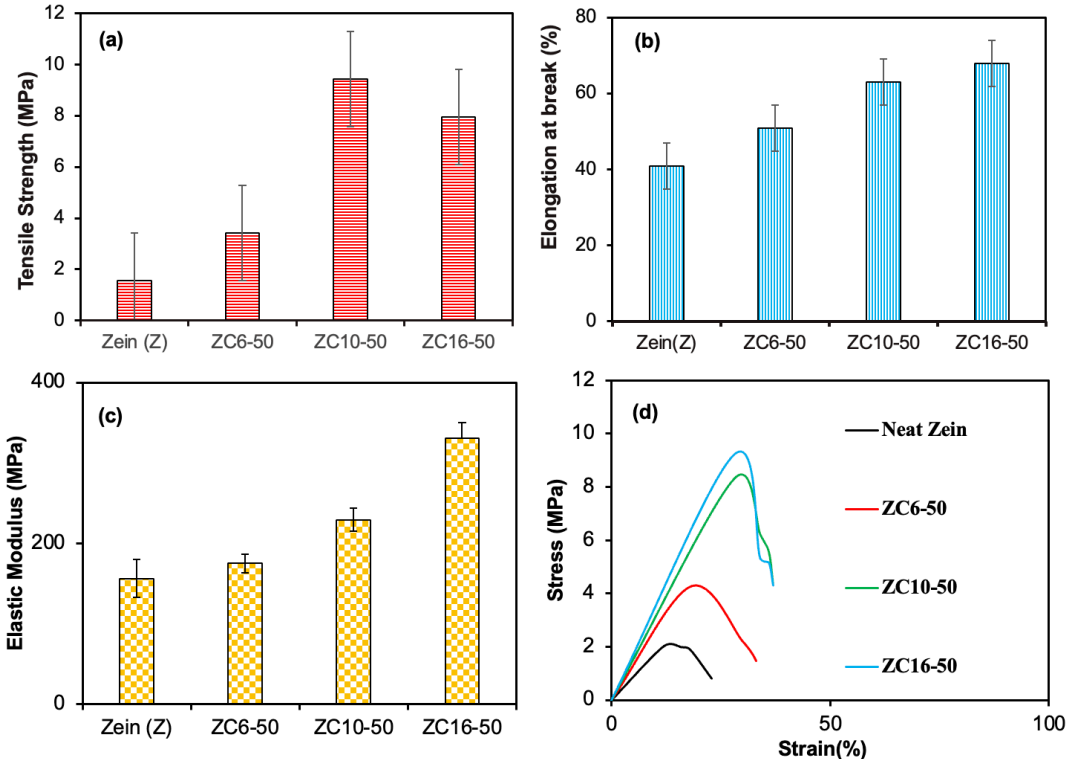


Figure 3.11. Mechanical properties of baseline and modified zein films: (a) tensile strength, (b) elongation at break, (c) elastic modulus, and (d) typical stress-strain plot.

3.6.8. Water absorption and contact angle

The effect of fatty acid modification on the water absorption rate of zein films was recorded for 72 hours, and the results are illustrated in **Figure 3.12**. In comparison to ZC10-50 and ZC16-50, unmodified zein film and hexanoyl chloride modification (ZC6-50) showed the highest water absorption. This was associated with the highest amount of water uptake (92%) by baseline zein samples. The baseline zein specimen constitutes two-thirds α-zein and 1/3 β-zein. The presence of intermolecular hydrogen bonds (due to the high helix ratio of the structure) has a positive effect on the osmotic swelling by water molecules. Furthermore, the glycerol plasticizer being a polar molecule, causes a significant drawback and contributes to the water absorption of the films[150,156]. The modification of zein with fatty acid chloride modifiers was expected to reduce the water absorption rate of zein films as it replaces the hydroxyl and amine polar moieties of pure zein with long aliphatic carbon chains, thus, enhancing the hydrophobicity of the zein film [133].

The zein films fabricated with decanoyl and palmitoyl chlorides (ZC10-50 and ZC16-50) retained their color and transparency. This could be attributed to the nonpolar characteristics (hydrophobicity) of modified zein specimens, thus, dramatically decreasing the water uptake. The recorded water absorption of zein film was accounted to be baseline zein (92%), ZC6-50 (71%), ZC10-50 (67%), and ZC16-50 (46%), respectively. In the literature, zein modified with glycerol and glutaraldehyde has water absorption of 50.73% and 24.08%, respectively[150]. Water contact angle (WCA) measurements were conducted to evaluate the hydrophobicity of esterified zein films, as shown in Figure A3. The esterified zein sample, ZC16-50, exhibited a significantly higher WCA of 84.75°, compared to 42.2° for unmodified zein. The unmodified zein films had the lowest WCA due to the relative hydrophilicity of the zein protein chain. In contrast, the highest WCA was observed in palmitoyl chloride-modified zein, showing a value nearly double that of unmodified zein. This increase in WCA aligns with the proposed mechanism in Scheme 1, where the substitution of hydroxyl and amine groups with nonpolar long aliphatic chains during esterification reduces hydrophilicity. Similar trends have been reported in other studies, further supporting these findings [144].

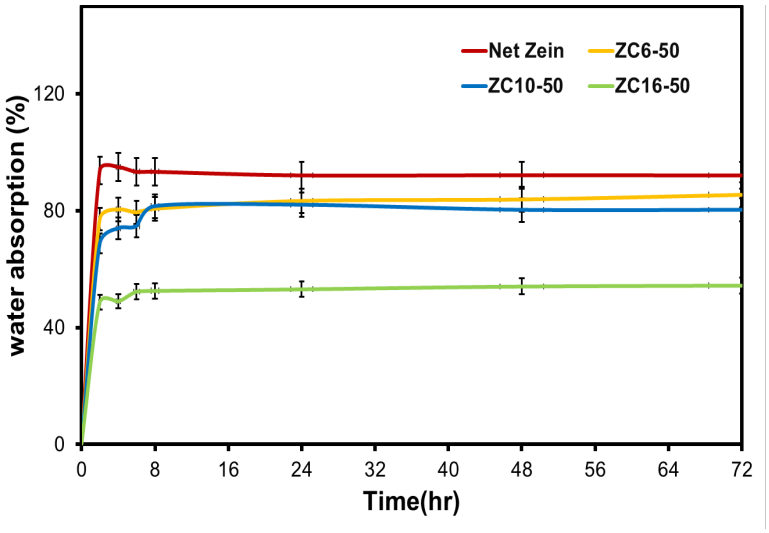


Figure 3.12. Water absorption of pristine and fatty acid modified zein films

3.7. Concluding Remarks

This study successfully demonstrated the modification of zein protein through the grafting of fatty acids hexanoic (C6), decanoic (C10), and palmitic (C16) via an acylation reaction. By varying the mole ratio of the activated fatty acids to zein protein, zein esters with varying substitution levels were synthesized. The fatty acid grafting altered the melting behavior, film-forming properties, and polarity of the zein at different degrees depending on the level of modification. These modifications were confirmed through ATR-FTIR, NMR, solubility analysis, and rheological studies.

The mechanical properties of both unmodified and modified zein were assessed by fabricating films and performing extensive characterization. Films with higher modification levels (ZC6-50, ZC10-50, and ZC16-50) exhibited significantly improved film-forming capabilities, tensile strength, surface morphology, and barrier properties compared to the unmodified zein films. Specifically, enhancements in tensile strength were noted as 91%, 388%, and 288% for ZC6-50, ZC10-50, and ZC16-50, respectively. The modified films maintained their uniformity and smooth surfaces, without any visible phase separation. Moreover, the alkyl chains attached to the modified zein films enhanced their hydrophobicity, contributing to improved water barrier properties. Overall, this study highlights the benefits of protein structural modifications in the development of sustainable materials from bio-sourced feedstock.

Chapter 4. PBAT/Corn Zein Ester Blends: Rheology, Morphology, and Physicochemical Properties

4.1. Introduction

The production of plastics from non-renewable petrochemicals, the poor management of plastic waste, the safety of plastics and their degradation residues are all major contributing factors that pose serious environmental issues to humankind. Researchers have been putting substantial efforts into developing renewable, biodegradable, and eco-friendly materials as alternatives to petrochemical-derived plastics. While extensive scientific progress has been made, there is still a long way until sustainable bioplastics can play a tangible role by complementing or displacing the more competitive petrochemical plastics as packaging and other single-use materials [157]. The development of bio-based and biodegradable materials can contribute towards achieving sustainable development goals and bioeconomy strategies, as well as acting as alternatives to comply with the ban on non-biodegradable plastic use in global jurisdictions that are continuously growing [158,159]. Biodegradable polymers, such as poly(lactic acid) (PLA), polyhydroxyalkanoates (PHAs), and poly(butylene adipate-co-terephthalate (PBAT) [160–162] received a great deal of attention as premier candidates of sustainable materials that can help relieve environmental concerns. [3] PBAT, which can partially be derived from bio-monomers, is also among the most appealing bioplastic candidates to replace non-biodegradable polymers derived from fossil fuels, such as polyethylene (PE) and polypropylene (PP), in packaging and agricultural film applications due to its biodegradability, inherent toughness, and commercial availability [163]. However, the high cost, as well as the relatively poor oxygen barrier properties of PBAT compared to traditional plastics, limit its

[3]
D.T. **Tadele,** B.M. Trinh, T.H. Mekonnen
PBAT/corn zein ester blends: Rheology, morphology, and physicochemical properties
Polymer, 283 .10.1016/j.polymer.2023.126258.2023, 126258

widespread application despite its excellent biodegradability and thermo-mechanical properties [163].

Currently, several approaches are being researched to produce biodegradable polymers with tailored properties that may relieve the mechanical, thermal, and barrier limitations of the currently marketed materials. Techniques such as chemical modifications, polymer blending, multilayer assembly, and the incorporation of fillers/nanofillers are extensively employed to help develop material systems that can satisfy thermomechanical property requirements, production cost, and biodegradability demand. Many studies have revealed melt blending of binary polymer systems, in which the blending materials that can complement each other's properties can potentially be an effective method to develop novel materials that can match with the incumbent polyolefin-dominated packaging plastics [164–166]. The possibility of blending PBAT with nature-derived biodegradable polymers, such as starch and soy protein, has been previously investigated, which could offer the benefit of balancing cost and properties [167,168].

Zein is one of the few known hydrophobic proteins derived from corn, which appears as an attractive alternative with rapid biodegradability and appealing physicochemical properties, including water insolubility, non-toxicity, versatility, and film forming ability [169]. Zein protein can be induced to fold into higher molecular structure polymers when plasticizers are added to the system. Plasticizers are typically small organic molecules that increase the flexibility of polymers with improved molecular structure and mechanical properties that enable various applications [170]. The grafting of fatty acids onto zein protein can be a suitable approach to further improve its hydrophobicity and thermoplastic properties, as suggested in multiple works [1,91].

This work builds upon previous research that has demonstrated the promising film-forming and melt-processing properties of modified zein films with medium and long fatty acid carbon

chains [91]. However, further investigation into the modification, processing, and film fabrication of zein is necessary to fully exploit its potential for practical applications. In this study, we explore the melt extrusion blending of fatty acid grafted zein with PBAT, focusing on their compatibility, morphology development, thermomechanical properties, and structure-property correlations. Additionally, we conduct targeted application studies to assess the oxygen and water barrier properties, optical properties, and disintegration behavior in a composting environment, thus evaluating its suitability as a packaging material. Notably, our work also investigates the influence of blending ratios of modified zein and PBAT on compatibility, morphology, and physicomechanical properties of the resulting blend, providing valuable insights for industrial applications. By addressing these research gaps, our study offers a novel and comprehensive approach to leveraging the potential of modified zein films and their compatibility with PBAT for packaging applications.

Comparing to previous studies, our work presented in **Table B1** showcases the enhanced characteristics of our modified Zein/PBAT blend, even without the use of any compatibilizing agents. This blend demonstrated enhanced barrier properties, disintegration behavior in a composting environment, and robust thermomechanical attributes, outperforming blends from earlier research that utilized compatibilizers. These advancements underscore the potential of our approach in the development of high-performance, environmentally friendly packaging material [14,171]. These findings underscore the novelty and significance of our research, positioning it as a valuable contribution to the field.

4.2. Materials and methods

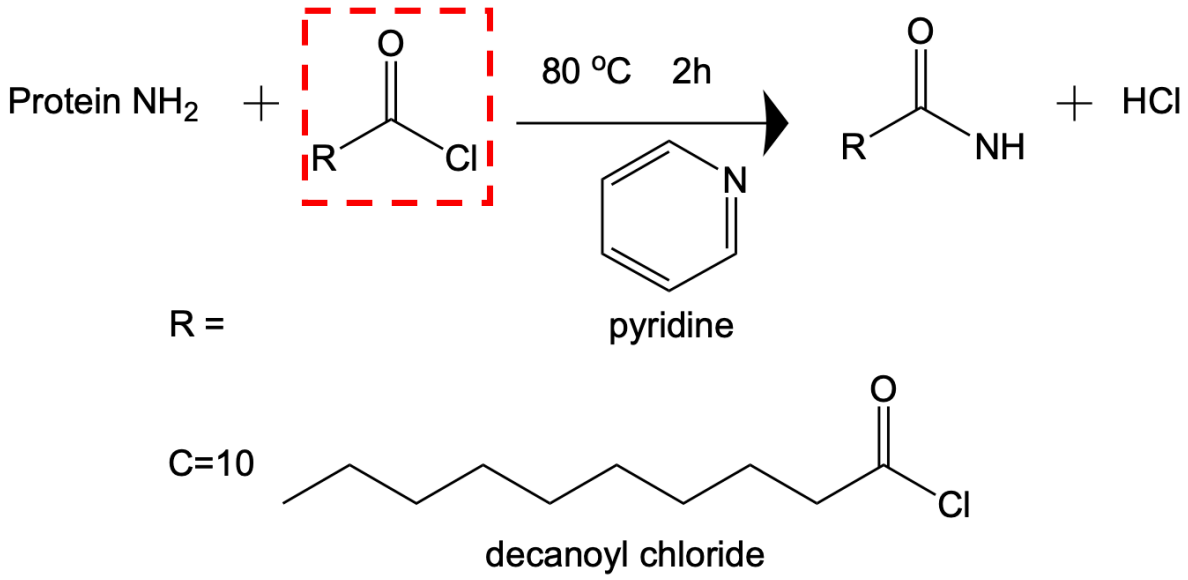
4.2.1. Materials

α-Zein powder with a protein content of 95% (w/w) was purchased from Sigma-Aldrich. TCI chemicals supplied decanoyl chloride (98 %). Pyridine (99.8 %), dimethyl sulfoxide (DMSO) (99.9 %), glycerol (≥ 98%), diiodomethane (>98%), and oleic acid (≥ 98 %) were also

purchased from Sigma-Aldrich (Oakville, ON, Canada). Poly(butylene adipate-co-terephthalate) (PBAT) pellets were provided by T&T Industry Group Ltd. (Shenzhen, China).

4.2.2. Esterification of zein protein with decanoic acid

The zein protein was modified by esterification reaction with decanoyl chloride using the method outlined in the previously published paper (**Scheme 1**)[91]. For this, approximately 10 wt.% of zein was dissolved in pyridine and transferred to a round bottom flask (RBF) while constantly stirring at 300 rpm. Next, the optimized amount of fatty acid (20 mmol of decanoyl chloride based on the previous study) was added to the zein solution using a burette. The esterification reaction was then conducted for 2h at 80 °C. The product was recovered as a yellowish soft solid mass, then rinsed with water, followed by three washes with acetone to remove excess unreacted pyridine and decanoyl chloride and dried in an oven at 70°C overnight - subsequently, 20 wt.% oleic acid plasticizer was added and stored in a zip lock bag until further use.



Scheme 4.1 Schematics of zein protein modification with fatty acid chloride.

4.2.3. Blend preparation

The pre-dried PBAT and modified zein (mZein/PBAT) were initially mixed in a Ziplock bag and fed into the extruder at a weight ratio of 30/70, 50/50, and 70/30, as shown in **Table 4.1**. The mixed blends were then extruded using a twin-screw extruder (Process 11 Parallel Twin-Screw Extruder, Thermo Fisher Scientific) with a specification of 440 mm in length, L/D of 40:1, and 11 mm in diameter. An extrusion temperature profile of 130/135/140/150/150/140/135/130 °C from die to feed with a screw speed and feed rate of 100 rpm and about 2g/min, respectively, was used. Preliminary experiments based on compression film casting, morphology, and tensile testing were used to determine extrusion parameters. The extruded and pelletized granules were cooled and stored in a sealed container (4 °C) until further use.

Table 4.1 Composition of the unmodified (Zein), modified zein (mZein), and PBAT blends

Samples	Zein (g)	mZein (g)	PBAT (g)
Zein	100	-	-
Zein/PBAT	70	-	30
Zein/PBAT	50	-	50
Zein/PBAT	30	-	70
mZein	-	100	-
mZein/PBAT	-	70	30
mZein/PBAT	-	50	50
mZein/PBAT	-	30	70
PBAT	-	-	100

4.2.4. Film compression molding

For the fabrication of the bioplastic films, approximately 3g of the modified zein (mZein/PBAT) pellets from each blend were compressed-moulded between two stainless steel metal plates with 200 µm mould spacers using a Carver press. Films were compressed for five minutes at a temperature and pressure of 115 °C and 5000 psi, respectively. Films with dimensions of 7.5 cm (length) × 7.5 cm (width) × 0.2 mm (thickness) were generated. The films were then conditioned at room temperature and 50% relative humidity for at least 48 h prior to the physicomechanical testing.

4.2.5. Contact angle measurements

The water contact angle (WCA) of the unmodified zein, modified zein, and PBAT blend films were determined at ambient temperature using a custom-built optical angle analyzer using a sessile drop method. In a typical procedure, the needle position was first adjusted to minimize the fall distance of the drop onto the polymer surface. Next, the pump was started, and the liquid water (polar) and diiodomethane (non-polar) was automatically pumped at 3 µL. Imaging was triggered with a high magnification camera (Basler scA 1000-30 fm) with a fixed focal length after a 30-second contact time. Each image was automatically analyzed, and the average contact angle was used to determine the total surface energy. To obtain the surface free energies of polymer blends, the water and diiodomethane contact angle measurements were collected on the specimen surfaces. Equations (4.1) and (4.2) were then used to calculate the solid surface tension for each sample from the contact angles.

$$\frac{1}{2}\gamma_w(1+cos\theta_w) = [\,(\gamma_s^d\gamma_w^d)^{\frac{1}{2}} + (\gamma_s^p\gamma_w^p)^{\frac{1}{2}}\,] \qquad (4.1)$$

$$\frac{1}{2}\gamma_{dm}(1+\ cos\theta_{dm}) = [\,(\gamma_s^d\gamma_{dm}^d)^{\frac{1}{2}} + (\gamma_s^p\gamma_{dm}^p)^{\frac{1}{2}}\,] \qquad (4.2)$$

where θ_w and θ_{dm} are the contact angles of water and diiodomethane on the sample, respectively. γ_w , γ_{dm} and γ_s are the solid surface energy of water, diiodomethane, and the sample, respectively. The superscript d represents the dispersive (non-polar) and p represents the polar components of surface tension, respectively.

Measuring and inserting the known values for water $\gamma_w = 72.8 \frac{mJ}{m^2}$, $\gamma_w^d = 21.8 \frac{mJ}{m^2}$ and $\gamma_w^p = 51.0 \frac{mJ}{m^2}$) and for diiodomethane ($\gamma_{dm} = 50.8 \frac{mJ}{m^2}$, $\gamma_{dm}^d = 49 \frac{mJ}{m^2}$and $\gamma_{dm}^p = 1.8 \frac{mJ}{m^2}$) and the solution of the two equations yields γ_s^p and γ_s^d. The surface energy tension is given by ($\gamma_s^d + \gamma_s^p$)[172].

4.3. Characterization of mZein- PBAT blends

4.3.1. Attenuated total reflectance Fourier transform infrared (ATR-FTIR) spectroscopy

The ATR-FTIR spectra of the mZein/PBAT blends samples were performed under ambient conditions using a Thermal Nicolet 6700 ATR-FTIR spectrometer (Thermo Electron Corp., Madison, WI). Approximately 1 mg of mZein, PBAT, and mZein/PBAT blends were dried overnight at 70 °C, and the spectra were recorded in the transmission mode at 4 cm^{-1} resolution, in the range of 4000–500 cm^{-1} with 32 scans.

4.3.2. Mechanical properties

According to ASTM D882 test method, the tensile strength, elastic modulus, and elongation at break were determined for neat polymers and their blends using a Mandel-Shimadzu (AGS-X) tensile testing unit equipped with a 500 N load cell (Shimadzu Corp., Kyoto, Japan). The crosshead speed was set at 5 mm/min, and the gauge length was 25 mm across each sample. The average and standard deviation of five specimens were calculated for each formulation at room temperature.

4.3.3. Dynamic mechanical analysis (DMA)

Tan delta (δ) analysis of the neat polymers and their blends was carried out by (Q800 DMA, TA Instruments). The damping factor (tan δ) was measured as a function of temperature from −90 °C to 20 °C. A film tension clamp was used at a constant heating rate, frequency, and strain of 3 °C/min, 1 Hz, and 0.2%, respectively. The glass transition temperature (T_g) was determined as the temperature corresponding to the maximum tan δ peak for the main transition displayed in the tan δ versus temperature curves.

4.3.4. Rheological studies

Rheological measurements were performed using a parallel plate rheometer (HAAKE MARS III, Thermo Fisher Scientific), with samples having a thickness of 0.30 mm and a diameter of 20 mm, respectively. An applied strain of 0.1% (in the linear viscoelastic region) and a plate gap of 0.2 mm were used for the analysis, with a frequency sweep from 0.01 to 100 Hz at 180 °C.

4.3.5. Polarizing Optical Microscopy (POM)

PBAT and mZein blend structure morphology was studied using a polarizing optical microscope (Olympus BX53M, USA). The mZein and PBAT blends of about 0.03 mm thick films were prepared by compression moulding at 120 °C. Images were collected at 50X magnification.

4.3.6. Scanning electron microscopy (SEM)

The cross-sectional morphology of the modified zein/PBAT blends was recorded using Quantum FEG-SEM 250 at 20 kV under vacuum without any sputter coating to examine the fracture. In addition, the cross-sectional morphology of the cryo-fractured films was also recorded after they were immersed in dimethyl sulfoxide (DMSO) for 8h to understand the blend phases better.

4.3.7. Light transmittance of blends

The neat polymers and their blend films were cut into rectangular strips that fit into a cuvette (approximately 1 cm in width). The light transmittance of the films was then measured using a Cary 100 Bio UV–vis spectrophotometer between 480 and 780 nm.

4.3.8. Water absorption rate

The water uptake rate of the neat polymers and their blend films were evaluated over the course of 168 h at room temperature (25 ± 2 °C). Three strips of each film (50 mm × 50 mm) were cut for each formulation and dried in a forced air oven (70 °C, overnight). Three specimens of each sample were first weighed and then completely submerged in distilled water in a glass container (100 mL). The weight of the specimens was recorded every 24 h, and prior to weighing, the excess water was wiped off with blotting paper to remove water. Results were reported as the mean and standard deviation of three replicates.

4.3.9. Water barrier properties

The water vapour transmission rates were measured using ASTM E96/E96M-16. The measurement was conducted using a barrier cup with an exposed area of 8.04 cm^2 to measure water vapor transmission rates (WVTR). A circular film is then placed over the opening of the barrier cup filled with 7 mL distilled water (relative humidity 100%). The cups were placed in a desiccator chamber with a temperature of 23 °C and a relative humidity of approximately 50%. Water permeation through the film was measured over time for 168 h. The WVTR values ($g/m^2 \cdot h$) were then calculated as follows:

$$WVTR = \frac{\Delta G}{t} \times \frac{1}{A} \quad (4.3)$$

The water vapour permeability (WVP) is calculated based on the following equation with two variables: G/t (g/h) represents the linear slope of the best fit of the weight loss vs. time graph, and A (m^2) represents the exposed area of the water barrier cup.

$$WVP = \frac{WVT \times l}{S(RH_1 - RH_2)} \quad (4.4)$$

The thickness of the films was *l* (m), the ambient temperature was 23 °C, S represent saturation vapour pressure and RH_1 and RH_2 were the relative humidity inside and outside the test cup. Each sample was tested with three specimens, and the averages were used as the final value.

4.3.10. Oxygen barrier properties

The oxygen permeability (OP) test was carried out using a custom bubble flow rate system. Two chamber cassettes, one attached to the oxygen source, and one to a bubble, were used to seal sample films with a surface area of 18.10 cm^2. The oxygen permeation barrier was set at 5 psig between the two chambers to ensure oxygen permeation.

The sample was measured by measuring the time it takes for bubbles to travel from the start of the experiment to the end of it using a volumetric unit of 100 mL. The OP values were calculated based on equation (4.5) in units of (cc·m/(m^2·day·Pa)).

$$OP = \left(\frac{V}{t.A}\right) \times \frac{l}{\Delta P} \quad (4.5)$$

Where V/(t·A) (cc/m2-day) is the oxygen flux, *l* (m) is the thickness of the films, and ΔP (Pa) is the pressure difference between the two sides of the film. Each sample was tested in triplicate at room temperature and in dry conditions.

4.3.11. Disintegration test

Modified zein/ PBAT blend biodegradability was evaluated by burying the samples in natural soil following GBT 19275-2003 (evaluation of the biodegradability of plastics under the action of specific microorganisms). To perform the analysis, a mixture of 2580g soil, 120g compost, 300g perlite, and 5.3 mL bloom was utilized. Initially, all blend sheets measuring 2.5 cm x 2.5 cm were dehydrated in vacuum ovens at 40°C for 24 h or until a stable weight was reached. Subsequently, three blend films were placed 20 cm below the soil surface. The compost's

moisture content was maintained at 55-56%, and its temperature was kept at 58 ± 2 °C. The weight difference between the degraded samples was measured after 7, 15, 30, and 45 d. A remaining weight was calculated for each film to calculate its degree of disintegration:

$$Remaining\ weight\ (\%) = \frac{m_{i\_}m_f}{m_i} \qquad (4.6)$$

Where m_i is the initial dry weight of the film sample, and m_f is the final dry weight of the residual film material recovered. The average remaining weight of the triplicate samples was calculated and reported.

4.4. Statistical analysis

Analysis of variance (ANOVA) was employed to identify statistical differences in data using Tukey's HSD mean comparison test with a 95% confidence level ($P < 0.05$).

4.5.Results and discussions

4.5.1. ATR-FTIR spectroscopy

The chemical interactions between neat and blended polymeric films were determined through attenuated total reflectance Fourier transform infrared (ATR-FTIR) analysis. ATR-FTIR results for mZein, PBAT, and mZein/PBAT blend films are shown in the **(Figure 4.1).** The characteristic peaks at 1525 cm^{-1} exhibit peaks corresponding to amide I and 1630 cm^{-1} amide II of modified zein proteins [14]. In addition, the characteristic peak of mZein/PBAT (70/30, 50/50, and 30/70) blends showed a reduction in intensity compared to neat PBAT, indicating the incorporation of modified zein into the PBAT matrix. Moreover, the carbonyl groups stretching peak of the ester bond (-COO-) at 1710 cm^{-1} remained unchanged for neat PBAT and mZein/PBAT blends [173]. The unchanged carbonyl group stretching peak at 1710 cm^{-1} in neat PBAT, mZein, and their blends indicates that the ester bonds in these materials undergo minimal chemical changes during the melting process. However, in the mZein/PBAT blends, the higher peak intensity suggests stronger chemical interactions compared to neat PBAT and mZein. This indicates that the blending of mZein and PBAT exhibited enhanced intermolecular interactions, such as hydrogen bonding or covalent bonding, resulting in more stable chemical structures and stronger bonding between the polymer chains[14].

Moreover, the spectrum of mZein/PBAT exhibited a disappearance of a wide peak in the range of 3100-3400 cm^{-1}, which could be ascribed to the incorporation of decanoyl chloride and oleic acid plasticizers. The peak at 2800 cm-1 in the FTIR analysis of neat mZein, PBAT, and blends of mZein/PBAT corresponds to the -CH2- and -CH3- functional groups present in both the fatty acid chain of modified zein and PBAT. The $-CH_2-$ and $-CH_3-$ groups on the modified zein and PBAT can form hydrogen bonds with the carbonyl groups on PBAT. This can result in enhanced interactions between the two materials, potentially leading to improved mechanical, barrier, and interfacial properties of the blended films. Furthermore, the chemical

modification of the zein protein with fatty acid chlorides can introduce new functional groups, such as carbonyl and hydrophobic groups, which can interact with the ester groups and alkyl chains of the PBAT polymer through hydrogen bonding and van der Waals interactions. These interactions enhance the interfacial adhesion between the two materials, improving compatibility and properties in the resulting blends. Additionally, the plasticizing effect of the fatty acid chlorides may improve the flexibility and processability of the blend, leading to more homogeneous mixing and distribution of the two materials.

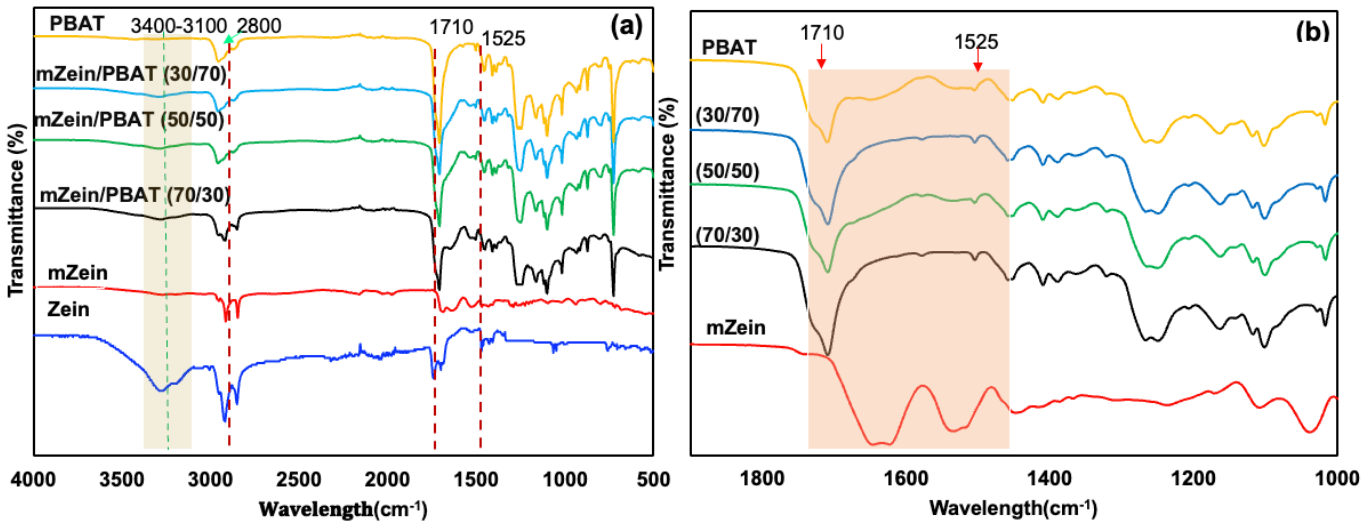


Figure 4.1 ATR-FTIR Spectra: a) Full spectra of Zein, mZein, PBAT, and PBAT/mZein; b) Magnified view at 1710 cm^{-1} and 1525cm^{-1} of mZein/PBAT blends

4.5.2. Surface and Interfacial free energy

Compatibility and miscibility can be evaluated based on the data obtained from water contact angle (WCA), surface tension, and interfacial properties of mZein, PBAT, and mZein/PBAT blends. Owens-Wendt-Kaelble (OWK) and Wu's models give a better insight into phase dispersion within a polymer blend [172,174]. Interfacial properties of a mZein and PBAT blend were studied by measuring water contact angles and surface free energy with polar (water) and nonpolar (diiodomethane) liquids. **Figure 4.2** shows the average contact angle values, as well as the surface free energy of mZein, PBAT, and mZein/ PBAT blends. The

modified zein (mZein) was shown to exhibit a higher contact angle than the neat PBAT, which contributes to the hydrophobicity of the modified zein from the reaction with decanoyl chloride, which has been shown to increase the hydrophobicity of the surface, and thus, the contact angle value[91,175]. The average water contact angle of modified zein (mZein) and neat PBAT was approximately 67.9° and 44.12°, respectively. As anticipated, blending PBAT with mZein showed an improvement in hydrophobicity, as there was an increase in water contact angle as the content of mZein went up, which peaked at 64.3° at mZein concentration of 70 wt.%. The increase in surface hydrophobicity is one of the promising properties of modified zein that can be utilized with PBAT to improve water resistance[175]. Another important parameter for estimating the intermolecular interaction, as well as determining the miscibility and compatibility of the blends, is surface energy[176]. The neat mZein and PBAT surface energies were calculated and found to be 42.68 and 60.9 mJ/m^2, respectively, by analyzing the dispersive and polar components of the average water content angle surface using equations (1) and (2). Tavares et al. also found similar results for the surface energy of PBAT[177]. Lower surface tension between modified zein and PBAT blends can indicate improved compatibility between the two polymers, leading to better mixing and reduced phase separation (**Figure 4.2)**. In contrast, unmodified zein and PBAT blends exhibit higher surface tension, which suggests that they have lower compatibility and less uniform blends. This observation is supported by supplementary information (**Figure B1)**, which shows a clear difference in surface tension between the modified and unmodified blends.

The surface tension reduction also suggests inadequate bonding between the polymer surface and liquid, reducing surface energy[178]. The interfacial tension of the mZein and PBAT blend can be determined by analyzing their dispersive and polar components from total surface energy at room temperature. Interfacial tensions of unmodified and modified zein and PBAT blends were calculated using the OWK's model (Equation 4.7), and Wu's model

(Equation 4.8) to determine the miscibility and compatibility of the blends, and the average values are presented in **Table 4.2**. Adding mZein to the PBAT blends resulted in a significant decrease in interfacial tension, as compared to the unmodified blends. The interfacial tensions of the modified blends were measured to be 2.015 mN/m, 1.524 mN/m, and 2.012 mN/m, considerably lower than the interfacial tensions of the unmodified blends, which were measured to be 9.734 mN/m, 7.244 mN/m, and 4.918 mN/m. This decrease in interfacial tension suggests that adding mZein improved the compatibility between the two polymers, leading to better mixing and reduced phase separation in the blend. The lower interfacial tension also indicates that the blend's mechanical properties, such as its tensile strength and impact resistance, may be improved, as the reduced interfacial tension allows for better stress transfer between the polymers[179].

$$\gamma_{12} = \gamma_1 + \gamma_2 - 2\left[(\gamma_1^d \gamma_2^d)^{\frac{1}{2}} + (\gamma_1^p \gamma_2^p)^{\frac{1}{2}} \right] \quad (4.7)$$

$$\gamma_{12} = \gamma_1 + \gamma_2 - 4\left(\frac{\gamma_1^d \gamma_2^d}{\gamma_1^d + \gamma_2^d} + \frac{\gamma_1^p \gamma_2^p}{\gamma_1^p + \gamma_2^p} \right) \quad (4.8)$$

Where, γ_{12} represents interfacial surface energy of mZein and PBAT blend, γ_1 surface energy of mZein, and γ_2 is surface energy of PBAT. γ_1^d and γ_1^p are the dispersive and the polar components of surface energy, respectively.

Table 4.2 mZein/PBAT blend interfacial tension values.

Sample	Zein (wt.%)	mZein (wt.%)	PBAT (wt.%)	OWK equation (mN/m)	Wu equation (mN/m)
Zein/PBAT (70/30)	70	-	30	6.120	3.614
Zein/PBAT (50/50)	50	-	50	5.571	1.673
Zein/PBAT (30/70)	30	-	70	1.896	3.022
mZein/PBAT (70/30)	-	70	30	0.352	1.663

mZein/PBAT (50/50)	-	50	50	1.029	0.495
mZein/PBAT (30/70)	-	30	70	1.975	0.037

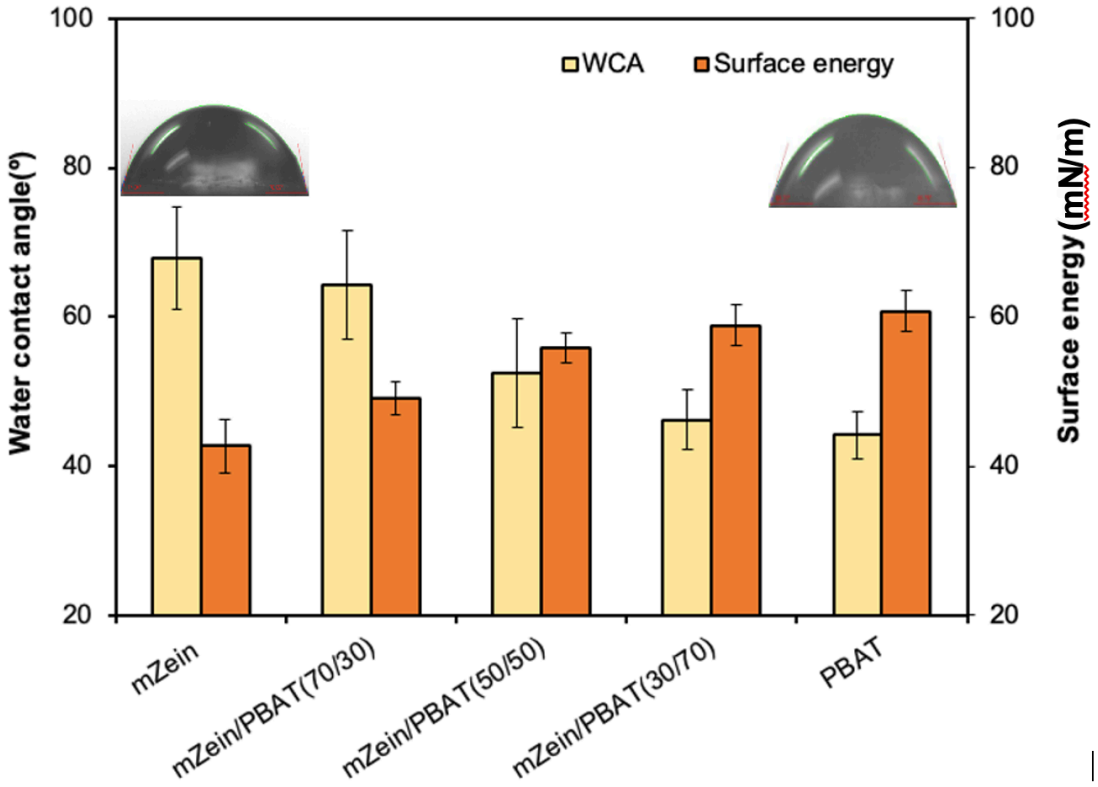


Figure 4.2 . Water contact angle and surface energy for mZein/PBAT blend films.

4.5.3. Morphology analysis

The morphology of polymer blends plays a crucial role in understanding the material's features, such as compatibility, mechanical, thermal, and permeability properties [180]. Therefore, the morphology of neat mZein, PBAT, and mZein/PBAT blends was evaluated by employing optical microscopy and SEM on the cross-sectional areas of the samples, as shown in **Figure 4.3**. **Figure 4.3(a-b)** shows that the neat mZein and PBAT samples show homogenous phases with light yellow and brown colours, respectively. The SEM image in **Figure 4.3(c)** reveals a rough surface morphology of neat mZein with significant surface defects, which was attributed to the low degree of plasticization of mZein. On the other hand,

the PBAT displays a much smoother and uniform morphology, indicating the excellent film-forming properties of PBAT as compared to mZein, as shown in **Figure 4.3(d)**.

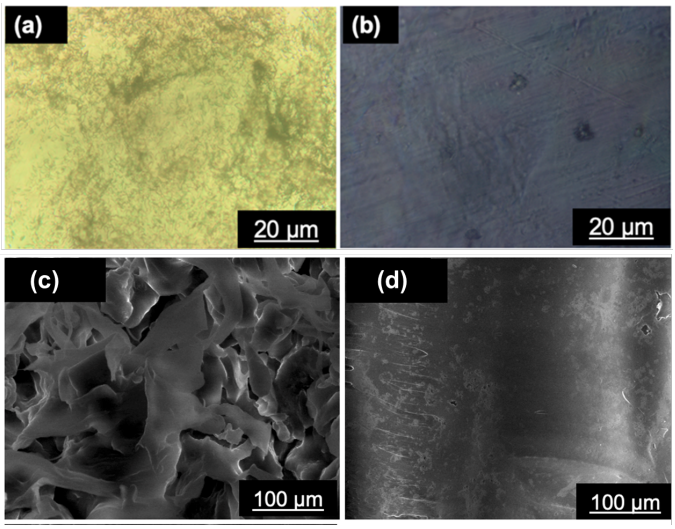


Figure 4.3. Optical microscope images of (a) neat mZein, (b) PBAT; scanning electron microscopy images of cross-sectional area of (c) neat mZein and (d) PBAT

In the case of the mZein/PBAT (70/30) blend, it contained rough surface morphology, with mZein constituting the continuous phase **Figure (4.4a)**. As the concentration of PBAT increases, the morphologies of the blends look more homogenous, especially at higher mZein/PBAT blend ratios (50/50) and (30/70), as depicted in **Figure 4.4(b-c)**. Similar observations were also reported by Fourati et al., that reported a similar trend for PBAT and starch blends [181]. Overall, the PBAT and mZein are fairly uniform and homogeneous in most blend formulations, indicating excellent compatibility and interactions at higher PBAT concentrations.

Additionally, the fractured blend sheets were immersed in dimethyl sulfoxide (DMSO) to etch out for 8 h, optimized based on the solubility of mZein in DMSO, to further investigate the phase distribution of the mZein and PBAT. DMSO was utilized for etching because can selectively dissolve mZein, while maintaining the PBAT phase, thus making DMSO a suitable solvent to remove mZein phase from the blend without affecting PBAT [91]. **Figure 4.4 (d-f)**

presents the morphology of PBAT after etching, revealing the microstructure of the blends. It was observed that the fraction of pores increased with the higher mZein loading in the blend composition. This indicates that the presence of mZein affects the morphology of the PBAT matrix. However, it is important to note that even at the highest mZein loading (mZein (70)/PBAT(30)), the etched blend maintained its integrity. This finding suggests that mZein was not completely etched out from the blend. The limited presence of pores in the etched blend despite the increased mZein loading points towards the existence of strong interactions between mZein and PBAT. One possible explanation for this observation is the formation of hydrogen bonds between the amino acid residues of mZein and the ester backbone of PBAT. These hydrogen bonds can contribute to the excellent compatibility between the blend components. Additionally, hydrophobic interactions between the hydrophobic regions of mZein and PBAT could also play a role in enhancing the blend's compatibility. The combination of hydrogen bonding and hydrophobic interactions within the mZein/PBAT blends contributes to the maintenance of the blend's microstructure even after etching. These interactions act as bridging forces that stabilize the blend and prevent the complete extraction of mZein from the PBAT matrix. Consequently, the etched blend retains its integrity and exhibits limited pore formation, indicating a strong attraction between the blend components. This strong interaction between mZein and PBAT polymer chains, facilitated by hydrogen bonding and hydrophobic interactions, plays a crucial role in implying the enhanced compatibility and integrity of the materials within the blend. These findings highlight the potential of mZein/PBAT blends for various applications that benefit from a well-preserved microstructure and enhanced material properties.

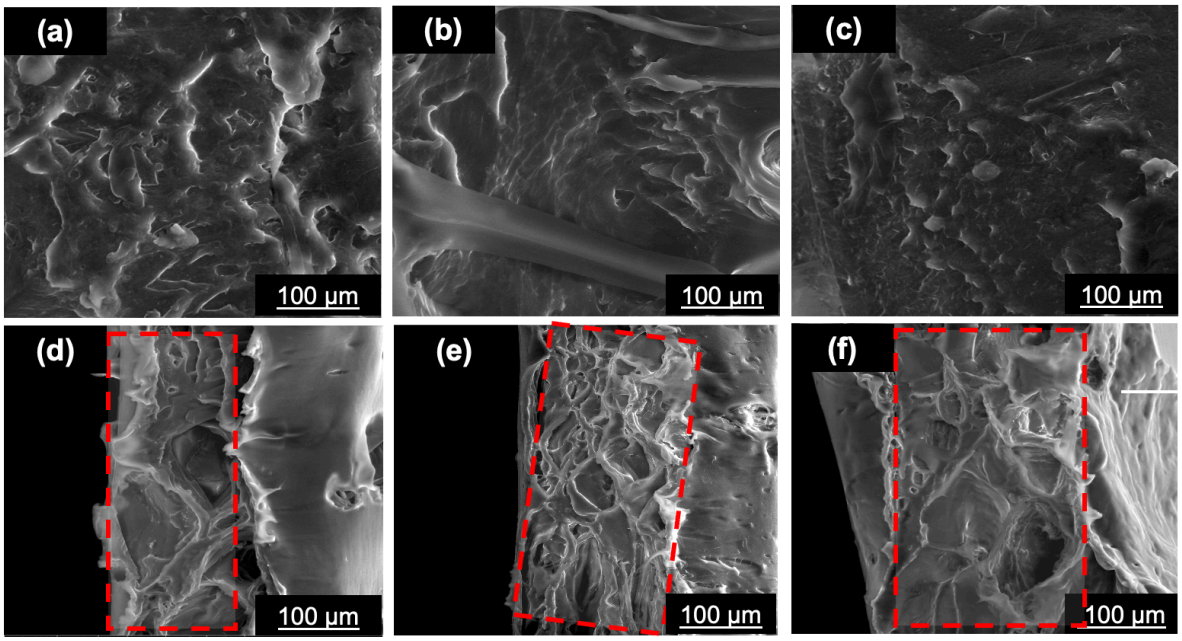


Figure 4.4. SEM images of cross-sectional area of (a) mZein/PBAT (70/30 wt.%); (b) mZein/PBAT (50/50 wt.%) and (c) mZein/PBAT (30/70 wt.%). SEM images of modified zein and PBAT blends surface after etching with DMSO: (d) mZein/PBAT (70/30 wt.%); (e) mZein/PBAT (50/50 wt.%) and (f) mZein/PBAT (30/70 wt.%)

4.5.4. Mechanical Properties

Figure 4.5 depicts the tensile strength, elastic modulus, and elongation at break of the mZein, PBAT, and mZein/PBAT blend films, which were shown to vary based on the composition of mZein and the blending conditions[182]. To provide a more comprehensive understanding of the mechanical behaviour of mZein, PBAT, and mZein/PBAT blends under stretch, the tensile properties of the films were investigated, and the stress-strain curves are presented in **Figure 4.5a**. Notably, the mZein and mZein/PBAT blend exhibits a linear elastic region followed by a slight plastic region, which can be attributed to the grafting of decanoic acid that acts as the internal plasticizer. **Figure 4.5b** presents the tensile strength of mZein, PBAT, and mZein/PBAT blends. It was noted that when the content of mZein in the blend compositions increased from 30 wt.% to 70wt.%, the resulting tensile strength shows a decreasing trend.

The tensile strength for the blends exhibited 3.25 MPa, 5.39 MPa, and 10.88 MPa, for the blend ratio of 70/30, 50/50, and 30/70, respectively. It was interesting to note that the tensile strength of the mZein/PBAT with (70/30) and (50/50) blend ratios has reduced from the mZein ($p < 0.05$). This could be attributed to the interference of intra and intermolecular interaction of zein with the PBAT chain that led to reduced entanglement and reduced tensile strength. However, when the blend is dominated by PBAT (mZein/PBAT 30/70), high tensile strength was noted (10.88 MPa), close to the tensile strength of PBAT. A study by Guo et al. investigated the blend of soy protein with PBAT matrices and reported that incorporating up to 20 wt.% of soy protein resulted in a maximum tensile strength of 9 MPa. However, incorporating more than 20% soy protein did not improve the tensile strength. This finding is similar to the observations for the mZein/PBAT blend [183].

The elastic modulus results (**Figure 4.5c)** demonstrated that the esterified zein (mZein) has a high modulus, and its blending with PBAT results in films with a high modulus that varies with its loading level in the blend. The high modulus of zein accompanied by low elasticity, is an inherent property of most proteinaceous macromolecules, attributed to strong intra – and intermolecular interaction [134]. For applications that require high stiffness, such as injection molded or thermoformed sheets, the mZein can bestow its stiffness to PBAT in the blends. This is appealing considering that PBAT has an inherent shortcoming of having low tensile modulus [184]. The elongation at break of mZein/PBAT blend films displayed a similar trend as tensile strength, with the maximum elongation at break obtained for formulations with a higher proportion of PBAT (561.41% for 30/70 ratio), as shown in **Figure 4.5d.**

Overall, the elongation at the break of the blends decreased with an increase in the modified zein content, which was in tandem with the tensile strength and modulus trends. The blend films containing 30% modified zein also exhibited a much better elongation at break than those containing 50 and 70 wt.% of mZein, indicating that the optimum mZein loading in the PBAT

should be about 30 wt.% for better mechanical properties. This result is comparable with those reported by Wei et al., which studied the incorporation of 20 wt.% unmodified zein into PBAT via reactive blending process with the employment of poly(ethylene glycol diglyceryl ether) compatibilizer and crosslinker, leading to elongation at break of 860%[14]. Despite the improved tensile strength and elongation at break of the mZein/PBAT blends compared to mZein, it is important to acknowledge these mechanical property of the blends are still lower than neat PBAT. While these limitations in high-tensile-strength applications of mZein/PBAT might limit the usage of the materials as highly functional packaging bags and agricultural mulching films, they may find usages in other suitable application scopes in areas where moderate tensile strength is sufficient, such as disposable packaging, non-load-bearing films, and non-structural components.

In addition, this tensile analysis took into account of the tensile strength, elastic modulus, and elongation at break of both unmodified zein and mZein/PBAT blend films, as depicted in **Table B2**. The results revealed a significant difference compared to the modified zein/PBAT blend ($p < 0.05$), which exhibited substantially enhanced mechanical properties. It is important to note that this work did not involve a compatibilizer to improve the blend compatibility but utilized modification of zein protein with fatty acid chlorides that can act as compatibilizer itself, which resulted in a net positive improvement on the mechanical properties, as long as the mZein ratio is maintained at a limited level in the blends.

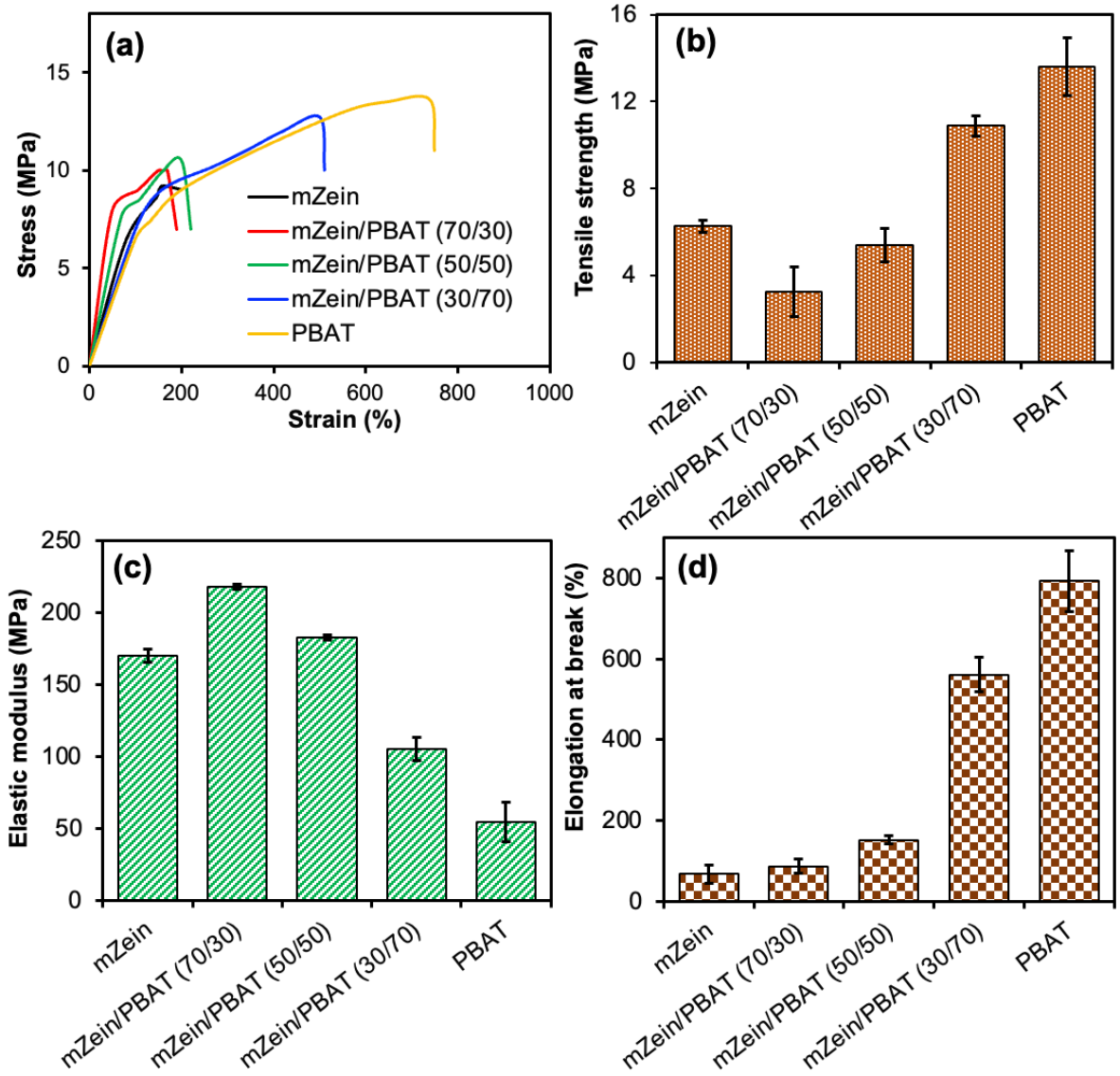


Figure 4.5. Mechanical properties neat modified zein, PBAT and mZein/PBAT blend films: (a) stress-strain curve, (b) tensile strength, (c) elastic modulus, and (d) elongation at break.

4.5.5. Rheological Properties

The rheology properties, such as complex viscosity, storage modulus, and loss modulus, can provide information about the molecular interactions, structures, and phase transition under the shear of the blend samples. Complex viscosity, which is a measure of the resistance of a polymer sample to flow under deformation, was analyzed for mZein, PBAT, and the

corresponding mZein/PBAT blend films as a function of frequencies using a parallel plate rheometer at 180°C and 220°C and results are shown in **Figure 4.6(a & b)**. As anticipated, the neat mZein exhibited the highest complex viscosity from the studied samples due to the high intra- and intermolecular chain interactions attributed to the amino acid residual functional groups on the zein structure. On the other hand, PBAT possesses lower complex viscosity, and the shear thinning slope was much steeper than mZein viscosity profile, showing that the viscosity of PBAT decreases drastically under high shear. This high shear-thinning behaviour of PBAT is more desirable for polymer processing as smooth melt flow of blended polymers would be preferable in the melt extrusion process at higher shear, as well as to improve the end-use performance of the sample.

The mZein/PBAT at (30/70) wt.% blend showed promising melt viscosity than mZein/PBAT at (50/50) and (70/30) wt.%, as the slope of (30/70) wt.% is similar to that of neat PBAT. The lower amount of mZein in the blends led to a decreased complex viscosity. The observed decrease in viscosity from a higher to lower modulus in the mZein/PBAT blends may primarily be due to changes in molecular dynamics, such as enhanced chain mobility and reduced entanglement. The plasticizing effect of blending PBAT with mZein likely reduces chain entanglement, thus promoting molecular mobility and decreasing viscosity. Additionally, the compatibility between mZein and PBAT can influence the viscosity profile, as improved phase interactions facilitate flow without significant polymer degradation [185]. Additionally, a gradual shift from Newtonian behavior at low frequency and deviations from shear thinning behavior at higher frequency was noted as the temperature increased from 180°C to 220°C. Carreau model was applied to predict the flow curve of the neat mZein, PBAT, mZein/PBAT samples using Equation 4.9, and the model was compared to the experimental data from the rheological study at 180 °C and 220 °C.

$$\eta(\omega) = \eta_0 * [1 + (\omega\lambda)^2]^{\left(\frac{n-1}{2}\right)} \quad (4.9)$$

Where η is the shear viscosity ; η_0 (Pa s) is the zero-shear viscosity ; λ (s) is the characteristic or relaxation time; n is a dimensionless parameter which determines the slope of shear viscosity versus shear rate in the shear-thinning (power law) and (ω) angular frequency (rad/sec). Higher value of power index (n) and relaxation time (λ) indicates a stronger shear thinning and slower recovery time behavior of the polymer blends, respectively [186,187]. The average values of zero-shear viscosity, power index, and relaxation time for the blends of mZein/PBAT obtained from the Carreau model curve are summarized in **Table 4.3**. **Figure 4.6(a-b)** shows the experimental findings and the Carreau model fit, presented with solid lines and markers, respectively. Despite some deviations at higher frequencies, the model fits the experimental data well for the samples, especially at 220°C.

Table 4.3. Fitting parameter, Carreau model, for all samples

Blends (mZein/PBAT)	**Zero Shear viscosity (η)**		**Power index (n)**		**Relaxation time (λ)**	
	180 °C	**200 °C**	**180 °C**	**200 °C**	**180 °C**	**200 °C**
mZein (100/0)	6009	1578	0.624	0.764	0.897	0.784
mZein/PBAT (70/30)	2122	1198	0.423	0.483	2.940	0.404
mZein/PBAT (50/50)	1415	945	0.454	0.592	1.12	0.197
mZein/PBAT (30/70)	778	684	0.321	0.568	0.895	0.127
PBAT (0/100)	598	498	0.147	0.470	0.458	0.0424

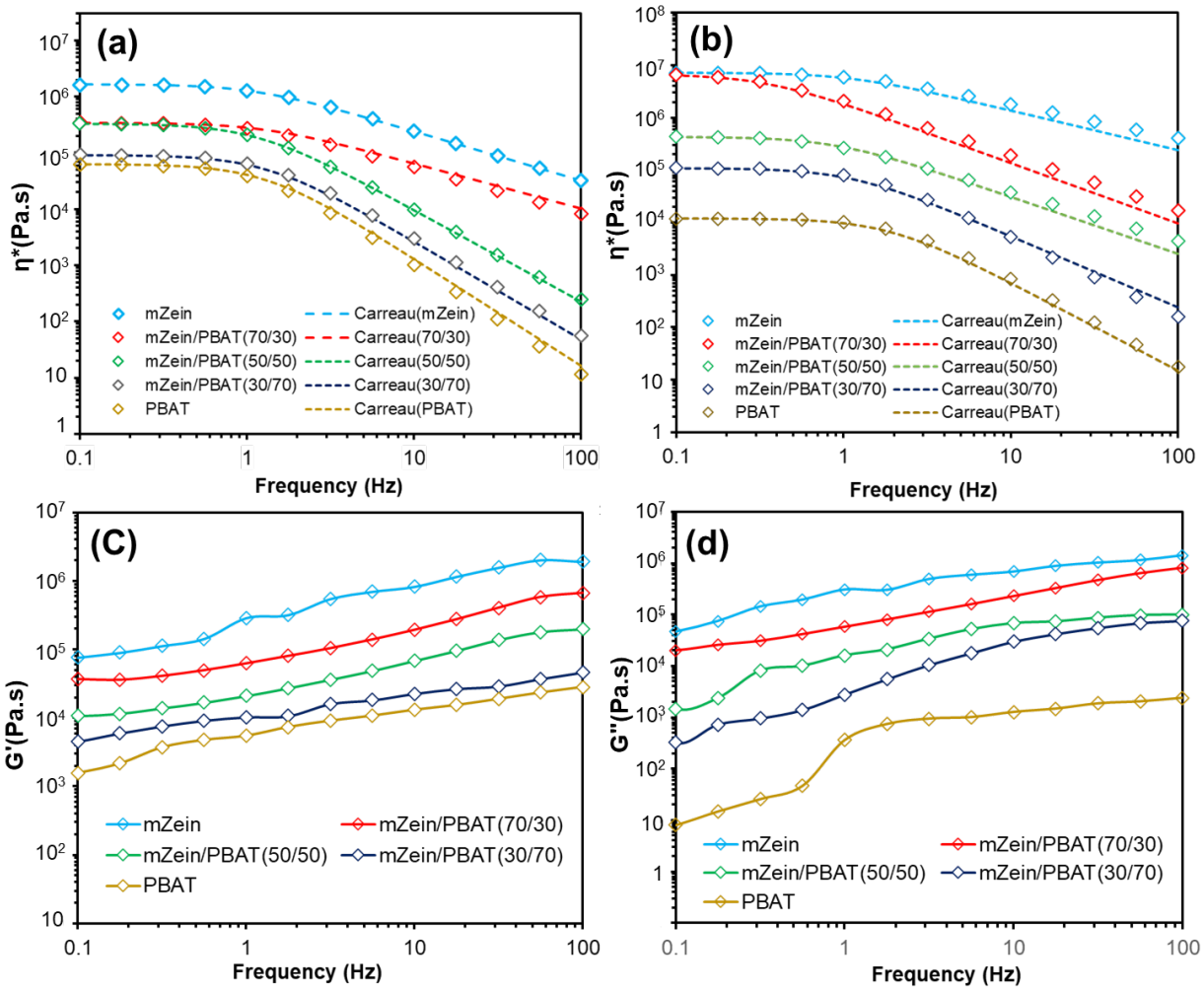


Figure 4.6. Complex viscosity vs generalized models of neat mZein, PBAT and mZein/PBAT as function of angular frequency at: a)180°C and b) 220°C; (c) Storage modulus (G') and (d) loss modulus (G") of the neat and blended polymers at 180 °C.

Figure 6(c-d) presents the storage (G′) and loss modulus (G″) of mZein, PBAT and mZein/PBAT blend samples as a function of angular frequency at 180 °C. The storage and loss modulus refers to the material's ability to store and dissipate energy during deformation, also used to characterize the viscoelastic properties of the samples. Blending mZein into PBAT substantially changed the storage (G′) and loss modulus (G″). It was demonstrated that the mZein and PBAT exhibited the highest (G' and G") and lowest moduli (G' and G"), respectively similar to the complex viscosity trend. Furthermore, incorporating mZein in PBAT increased the moduli with a magnitude proportional to the mZein loading levels. This result agrees with

the reduction in the ductility of the blends with the incorporation of mZein observed in the tensile property study (**Figure 4.5d**).

4.5.6. Dynamic mechanical analysis (DMA)

The effects of blending modified zein (mZein) with (PBAT) on the thermomechanical properties were further investigated with a dynamic mechanical analysis (DMA). Both the storage modulus and tan δ results as a function of temperature (**Figure 4.7(a &b**)) showed that the thermomechanical properties of mZein/PBAT blend films were significantly affected by the blend ratio. As illustrated in **Figure 4.7a,** the mZein has a tan δ peak at -55 °C attributed to the glass transition temperature. The observed low glass transition temperature of mZein is attributed to the effective plasticization via the grafted fatty acids. On the other hand, the PBAT displayed a tan δ peak at ~ -18 °C. Blending mZein with PBAT resulted in glass transition temperatures that are very close to that of the PBAT. It was also noted that no separate tan δ peaks were noted for mZein in any of the blends, including the 70/30 wt.% blend ratio. These observations indicate the high compatibility of PBAT with mZein, resulting in near homogeneous material with uniform distribution of mZein in the PBAT and vice vera. Moreover, the tan δ peak intensity gradually reduced with increasing mZein loading compositions of (70/30) wt.%, (50/50) wt.%, and (30/70) wt.%. This reduction in the tan δ may be attributed to the blend's restricted molecular motion due to the blending with the stiffer mZein [188,189].

Figure 4.7b displays the storage modulus (G′) of mZein, PBAT, and mZein/PBAT blends as a function of temperature. Generally, all curves, except for mZein, exhibit two typical plateaus in the temperature ranges of −90 to −20 °C and 15 to 20 °C, which are attributed to the glassy and rubbery states of PBAT chains, respectively[190]. The storage modulus (G') of the mZein and mZein/PBAT blend samples in the rubbery plateau region is higher than that of neat PBAT

due to the inherent stiffness of mZein (**Figure 4.5c**) incorporated in the blend formulations. On the other hand, the storage modulus curve of mZein shows the gradual transition of the material from a glassy state to rubber-elastic plateau to viscous flow region, indicating that the material is slowly approaching its melting point. Due to the internal plasticization of mZein, the material exhibited lower T_g and T_m, which was reflected on both the tan δ and storage modulus curves. However, it should be noted that the overall storage modulus of mZein is higher than PBAT and the mZein/PBAT blends, which agrees with the elastic modulus results obtained from tensile testing (**Figure 4.5c**). The analysis of Cole-Cole plots for modified zein and PBAT is another solid confirmation to indicate that the decanoic surface modification of zein leads to better intermolecular interaction between mZein and PBAT, as illustrated in **(Figure 4.7c)**. The plot reveals the shapes of semi-circle getting bigger as concentration of PBAT increase, which indicate the increase in uniformity and reduction in phase segregation between two polymeric between mZein and PBAT systems, an observation that aligns with the results obtained from SEM analysis.

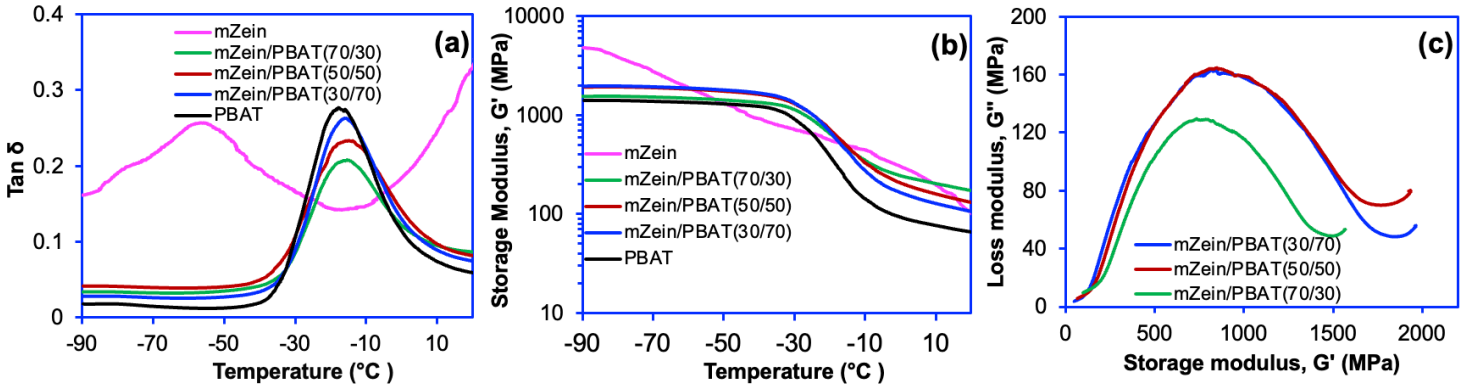


Figure 4.7. DMA analysis of neat mZein, neat PBAT and mZein/PBA; a) tan δ , b) Storage modulus and c) Cole-Cole plot of blend films

4.5.7. Water absorption and Optical clarity

The results of water absorption for neat mZein, PBAT, and mZein/PBAT blend samples were shown through immersion of films in distilled water for 168 hours, are shown in **Figure 4.8a**. Neat mZein absorbs about 25% water, while neat PBAT absorbs only about 7.85%, which is

in agreement with other studies[161]. This might be due to the porous structure of modified zein, as shown in the SEM results in conjuncture with the presence of residual polar functional groups in zein (e.g., amide, carboxyl, hydroxyl, secondary amine, etc.), which allows the binding of water molecules on the structure and subsequent diffusion through the film despite the hydrophobic modification of mZein. The water absorption rate of the mZein/PBAT blend formulations at (30/70), (50/50), and 70/30 wt.% were 19.32, 15, and 11.89%, respectively, indicating that the water absorption correlates with the mZein concentration in the blend. This is again attributed to the higher magnitude molecular interactions of water with mZein and the inhomogeneity of the blend morphology in the blends [191].

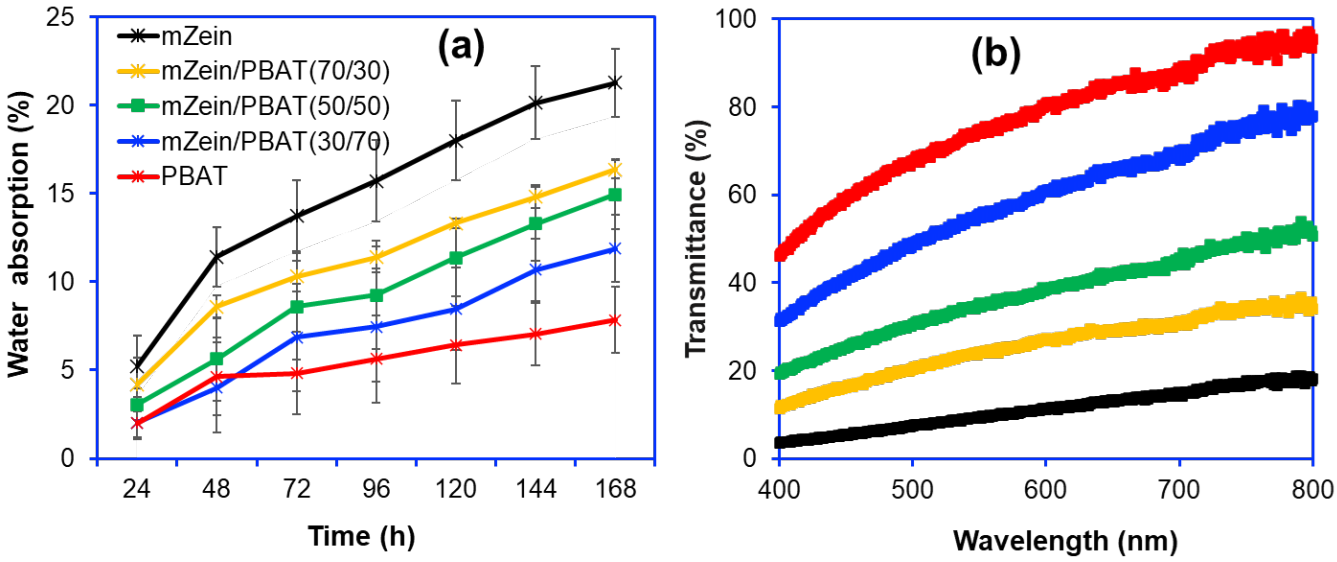


Figure 4.8. a) Water absorption b) Optical clarity of neat mZein, neat PBAT and mZein/PBA blend films.

Optical transparency/opacity is important in practical applications of films and sheets, such as food packaging and containment applications. The changes in the optical transparency of the neat mZein, PBAT and mZein/PBAT blend films were measured in the ultraviolet and visible regions (280–800 nm). As presented in **Figure 4.8b**, the neat mZein film showed lower transparency than the neat PBAT. This is due to the presence of pigments in zein that is responsible for reducing the film's transparency[192,193]. The blend of mZein/PBAT provided

transparency values that were in between the neat mZein and PBAT from the blending and colour dilution effect.

4.5.8. Water vapor and oxygen permeability

The water vapour permeability is another critical parameter in characterizing the barrier properties of films, which could also determine the film's moisture absorption and dehydration uptake based on diffusivity and solubility [194]. The mZein films have high water vapor permeability, which means water vapor passes through the films easily. This is due to a combination of the residual hydrophilic groups on the zein polymer's chain, such as secondary amine and carboxyl groups, as well as the porous structure as observed in the morphology evaluations. Zein's hydrophilic side chains can be blocked by esterification and grafting fatty acids, as demonstrated in the previous investigation[91] though the reactions may not be effective against all the diverse hydrophilic functional groups of zein protein, which makes mZein still slightly hydrophilic. On the other hand, PBAT was shown to generate uniform films with smooth morphology, as noted from SEM, which leaves fewer pathways for moisture molecules to diffuse through the film[7,163]. Thus, incorporating mZein into PBAT matrix at 70/30, 50/50, and 30/70 wt.% blend ratios increased the WVP by 68%, 59.8%, and 39.07%, respectively, compared to neat PBAT films, as shown in **Figure 4.9a**.

As shown in **Figure 4.9b**, mZein exhibited excellent oxygen barrier properties, having the lowest oxygen permeability (OP), which is attributed to the molecular structure of zein, which still contains many polar groups such as secondary amine and carboxyl groups that restrict the diffusion of oxygen molecules through the samples despite the grafting of fatty acids. PBAT, on the other hand, typically has high oxygen permeability due to the lack of polar groups on its butanediol and terephthalic co-polyester chains. This allows the non-polar oxygen molecules to pass through by enhanced absorption and diffusion[195]. The results in **Figure 4.9b** also

revealed that the blending of 30wt.%, 50 wt.% and 70 wt.% mZein with PBAT provides oxygen permeability improvement of 22%, 51%, and 59%, respectively.

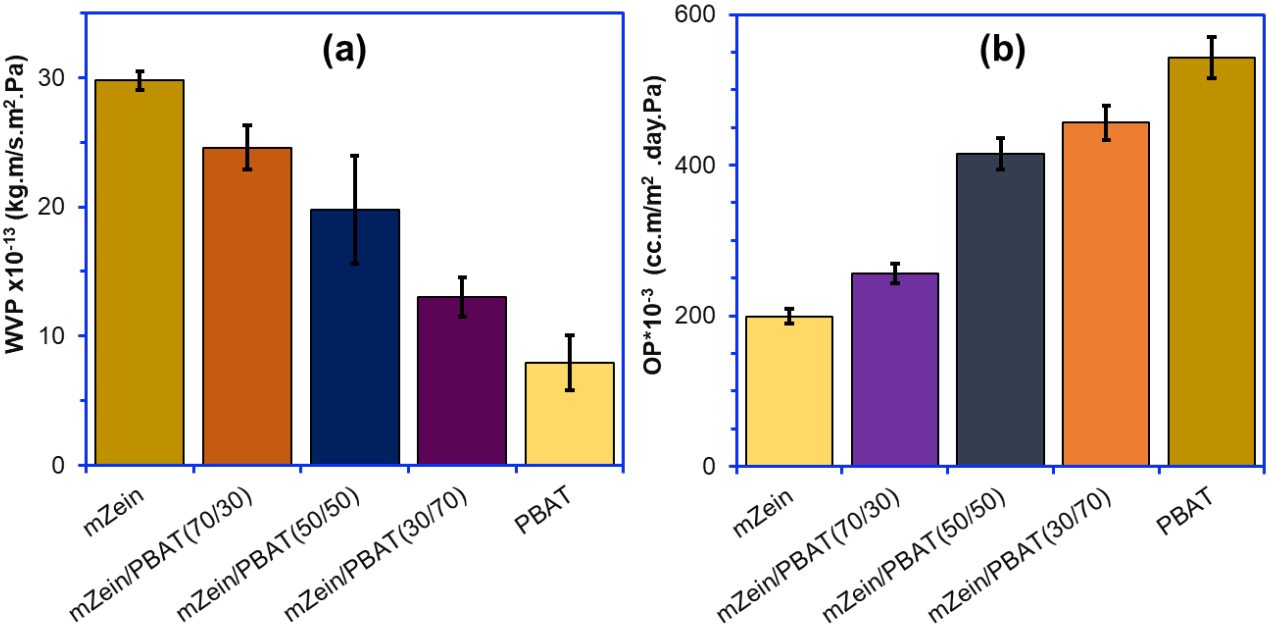


Figure 4.9. (a) Water vapor and (b) Oxygen permeability of neat mZein, neat PBAT and mZein/PBA blend films.

4.5.9. Disintegration test

The disintegration of neat mZein, PBAT, and mZein/PBAT blends in compost soil is presented in **Figure 4.10**. As shown in **Figure 4.10a**, the control and blend films displayed substantial disintegration and weight loss over 45 days study period employed in this investigation. Specifically, the mZein completely disintegrated and assimilated with the compost in only 30 days. In contrast, the neat PBAT film showed limited change, displaying minor surface cracks after 30 days of evaluation, indicating that PBAT does not disintegrate rapidly in compost soil. The weight loss data for neat PBAT film (**Figure 4.10b**) indicated that after 45 days of evaluation, it had lost approximately 36% of its weight, which suggests that it degrades at a significantly slower rate compared to neat mZein that assimilated in the compost soil within 30 days. The slightly longer time it takes for PBAT to become compostable compared to mZein could be attributed to the chemical composition of PBAT in addition to its compact

morphology. PBAT is composed of three monomers, namely, 1,4-butanediol, adipic acid, and terephthalic acid. These monomers are known to be more resistant to microbial degradation compared to the amino acid-based structure of mZein[196]. Incorporating mZein into the PBAT matrix have thus resulted in the enhancement of disintegration noted from the increased weight loss of the resulting mZein/PBAT blends. After 45 days of composting, the mZein/PBAT blends with the 70/30 blend has wholly assimilated with the compost and the 50/50 blend displayed 81% weight loss. The 30/70 blend also exhibited a 75% weight loss after 45 days, as depicted in **Figure 4.10b**. These observations suggest that incorporating mZein into the PBAT matrix can significantly enhance the biodegradability of the resulting blend films in composting environments. While the preliminary compost disintegration study showed promising results for the biodegradability of the mZein/PBAT blends, it is essential to conduct more comprehensive studies to obtain more conclusive results. Monitoring carbon dioxide generation and other relevant parameters can provide a more comprehensive picture of the biodegradability of these materials and help assess their environmental impact.

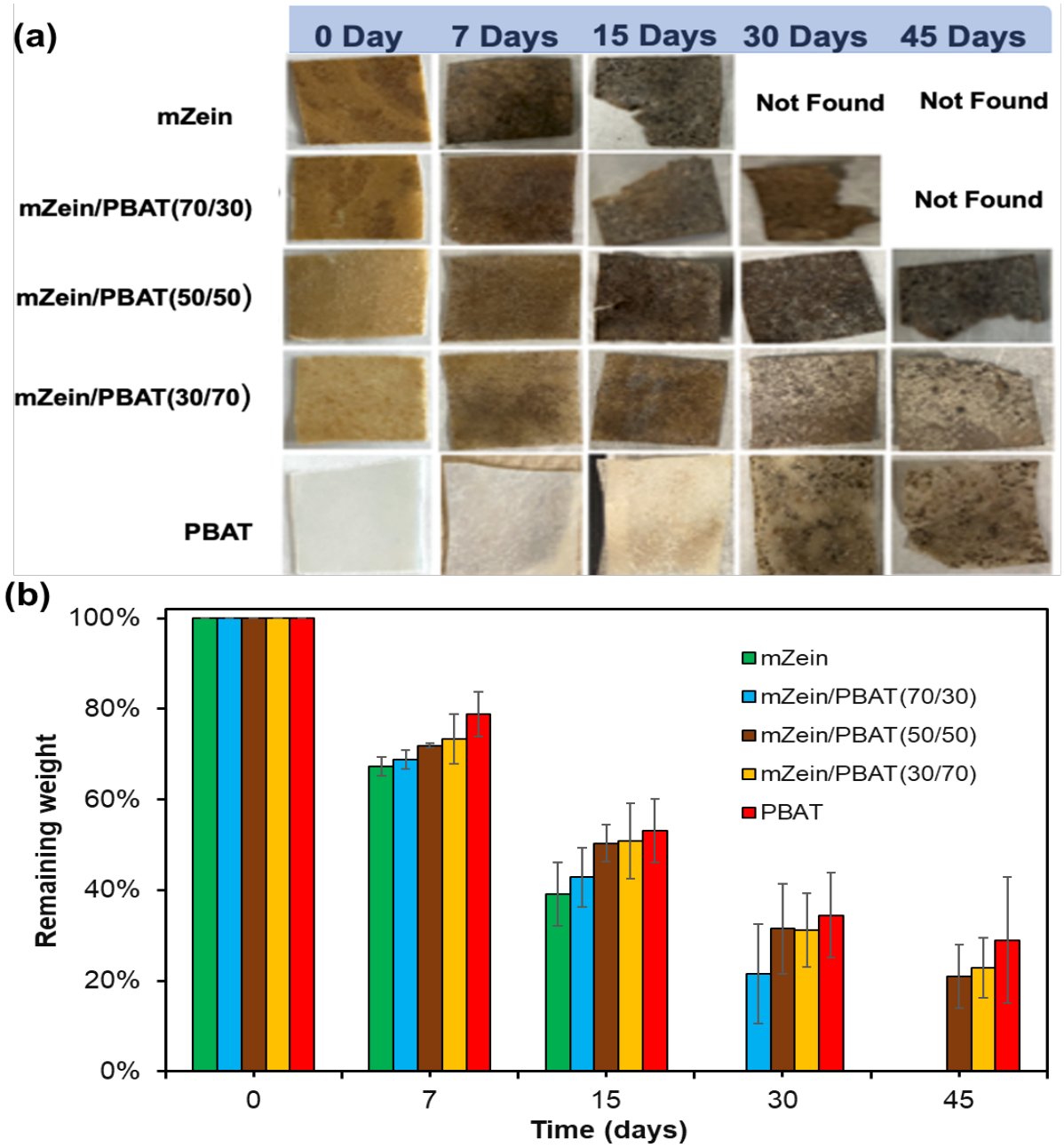


Figure 4.10. a) Images of samples taken after biodegradation in soil, and b) the remaining weight percentage of samples.

4.6. Concluding Remarks

This study investigated the blending of polybutylene adipate-co-terephthalate (PBAT) with modified zein proteins (mZein) to understand the surface energy mediated compatibility, phase morphology development, and physicomechanical properties. Considering that corn zein is an inexpensive and renewable macromolecule with appealing oxygen barrier and film-forming

properties, its employability as a complementary additive in PBAT could have practical significance for applications that benefit from cost efficiency, biodegradability, and oxygen barrier properties, such as food packaging films. It has been shown that the esterification modification of zein with decanoic acid led to enhanced compatibility with PBAT. Furthermore, the fatty acid chains acted as an internal plasticizer to improve the film-forming properties of the mZein. Incorporating mZein into PBAT has enhanced the oxygen barrier properties and disintegration with magnitudes dependent on the concentration of the blending partners. Adding 30 wt.% of mZein into PBAT provided appealing tensile properties, including sufficiently high tensile strength while also displaying high elongation at break and improved modulus. Moreover, this formulation (mZein/PBAT 30/70) provided balanced oxygen and moisture barrier properties between the mZein and PBAT and substantially improved disintegration attributes compared to PBAT. These findings suggest that appropriate compositions of mZein/PBAT blends have the potential to be used in practical applications, such as food packaging films, due to their enhanced thermomechanical and barrier properties. Further studies are needed to fully evaluate the performance and suitability of these blends for real-life applications.

Chapter 5. Co-encapsulation of Quercetin and α-Tocopherol bioactives in Zein Nanoparticles: Synergistic interactions, stability, and controlled release

5.1. Introduction

Chronic diseases, such as cancer, diabetes, and cardiovascular and respiratory conditions, currently account for approximately 71% of global death rates [197]. The increasing prevalence of chronic diseases has generated heightened interest in nutraceuticals and functional food ingredients, which are believed to offer health benefits beyond basic nutrition and may aid in the prevention and management of various health conditions [198,199]. Nutraceuticals and functional food ingredients are becoming increasingly popular because of their potential to support overall well-being and address specific health concerns [198]. The nutraceutical market is expected to experience significant growth, reaching an estimated value of USD 228.0 billion by 2025, with a projected compound annual growth rate (CAGR) of 7% from 2019 to 2025 [198,199]. This growth reflects an increasing consumer interest in natural health-promoting ingredients as part of a holistic approach to health and wellness. Quercetin and α-tocopherol are two bioactive nutraceuticals that have garnered attention owing to their potential health benefits. Quercetin, a flavonoid with antioxidant, antimicrobial, and anti-inflammatory properties, is known for its ability to prevent chronic diseases such as cardiovascular issues and tumors [41,200].

A-Tocopherol, also known as vitamin E, is a fat-soluble vitamin with antioxidant properties that protect cells from damage caused by free radicals [201–203]. The synergy between quercetin and α-tocopherol has promising implications in future multifunctional medicines. [4]

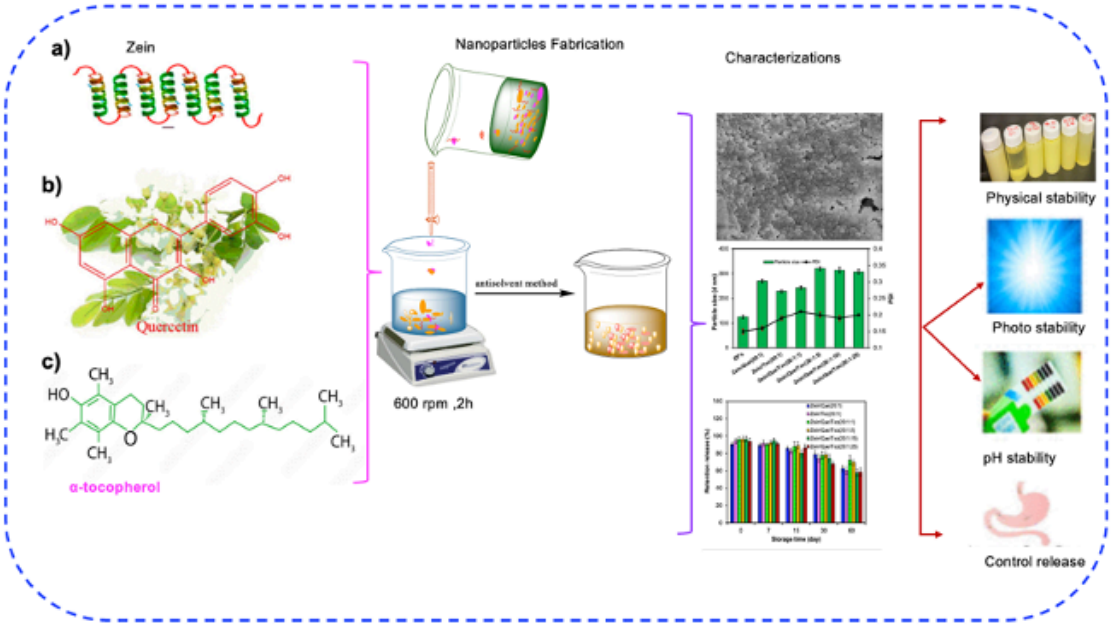
[4]D.T. **Tadele,** T.H. Mekonnen. Co-encapsulation of quercetin and α-tocopherol bioactives in zein nanoparticles: synergistic interactions, stability, and controlled release ,ACS Applied. Polymer. Material., (2024),6,7, 3767-3777 10.1021/acsapm.3c03000

However, their poor aqueous solubility, sensitivity to light and heat, and low bioavailability present challenges for their utilization in functional foods [204,205]. Addressing these obstacles is essential for realizing the full potential of nutraceuticals and for maximizing their health benefits. Research has shown interest in the combined encapsulation approach that overcomes these challenges and enhances the synergistic effects of these nutraceuticals, resulting in benefits greater than their individual effects against chronic diseases [55,62,205]. One effective method for achieving this is through the use of nanoparticles, which offer optimal particle size, high encapsulation efficiency, slow degradation rate, remarkable targetability, and penetration capabilities [55,62,206]. A recent evaluation of various colloidal delivery systems demonstrated the remarkable efficacy of zein-based nanoparticles, which can be attributed to the non-polarity of zein, simple fabrication process, exceptional loading capacity, and impressive physical and chemical stability [207]. In this study, we explored the possibility of improving the functional properties of zein-based nanoparticles by co-encapsulating them with quercetin and α-tocopherol. Zein, a protein derived from corn, is Generally Recognized as Safe (GRAS) for use in the food industry, making it a suitable candidate for such applications [92,93,208]. Zein is predominantly hydrophobic and insoluble in water but can be soluble in concentrated aqueous ethanol solutions (60-90%) or alkaline solutions (pH > 11) owing to its high proportion of non-polar amino acids. [24,91,92]. Zein proteins possess inherent qualities, including non-toxicity, biodegradability, and biocompatibility, which make them desirable materials for various applications [169,209]. The non-polar nature of zein and its unique solubility properties allow for effective nanoparticle formation through antisolvent precipitation methods [210,211]. The antisolvent precipitation method uses a solution of zein and a solvent that is subsequently introduced into an antisolvent, resulting in spontaneous self-assembly of zein molecules into nanoparticles or microparticles [211]. This method has been

employed to generate zein nanoparticles encapsulating diverse bioactive compounds such as β-carotene [73], curcumin [55], quercetin [62], and α-Tocopherol [205]. The incorporation of bioactive compounds into zein nanoparticles has been demonstrated to increase their stability with respect to light, pH fluctuations, and heating, as well as to enhance their oral bioavailability [18,59,212].

The utilization of zein nanoparticles in functional foods is frequently constrained because of their tendency to aggregate near their isoelectric point (6.2) under high ionic strengths, elevated temperatures, and in specific regions of the gastrointestinal tract [213,214]. Several strategies have been proposed to increase the chemical stability of zein nanoparticles and broaden the scope of bioactive compounds, such as surface modification [215], coating with polysaccharides [213,216], incorporation of emulsifiers[217], and utilization of surfactants. In this study, Tween 80 was employed to enhance the physicochemical properties of zein nanoparticles. Tween 80 was selected for its improved photostability, enhanced bioaccessibility, safety, and prolonged storage capacity, which provides a steric barrier that ensures optimal dispersion and stability of the encapsulated bioactive compounds [38,116,210].

The primary aim of this study was to develop a co-delivery system for unstable delivery of bioactive substances with high encapsulation efficiency and controlled release. In this regard, we synthesized zein nanoparticles as carriers for co-encapsulating quercetin and α-tocopherol, leveraging the unique properties of zein to create an innovative co-delivery system that enhances the synergistic health benefits of these compounds. The nanoparticles were thoroughly evaluated for their morphological structure, physicochemical and intermolecular interactions, stability, and controlled-release properties **schematic 5.1**. Our findings highlight the potential of this nano-delivery system for co-encapsulation and effective transport of unstable bioactive compounds.



Schematic 5.1. Overview of Co-Encapsulation Process of Quercetin and α-Tocopherol in Zein Nanoparticles, Including Fabrication Steps, Characterization, Stability, and Controlled Release Profiles.

5.2. Materials and methods

5.2.1. Materials

Zein powder (95 wt. %), quercetin (95 wt.%), and α-tocopherol (97 wt. %) were obtained from Sigma-Aldrich. Tween 80, hydrochloric acid (HCl) of ACS reagent grade (37%), sodium hydroxide (NaOH), and ethanol (EtOH) of 99.99% purity were purchased from Sigma-Aldrich (Oakville, ON, Canada). Pepsin from porcine gastric mucosa (600 U/mg , Sigma 77160) and pancreatic with 8 x UPS (Sigma P7545) and bile salts (Sigma B8756) were purchased from Sigma-Aldrich (Oakville, ON, Canada).

5.2.2. Fabrication of quercetin and α-Tocopherol loaded zein nanoparticle

In this study, we utilized the antisolvent co-precipitation (ASCP) method to fabricate zein nanoparticles loaded with quercetin and α-tocopherol. Deionized water was used, as previously described by Ma et al. [62]. The purpose of this approach was to create a stable nanoparticle formulation for co-drug delivery applications. For each formulation, 0.4g of zein was dissolved in 40 mL of 80:20 ethanol aqueous solution to achieve a concentration of 1% (w/v). A consistent 0.02 g of quercetin was added to all formulations based on the zein-to-quercetin ratio established from the preliminary experimental design. Varying amounts of α-tocopherol were then added, specifically 0.02 g, 0.1 g, 0.3 g, and 0.5 g. After complete dissolution, the resulting 40 mL solution was added dropwise to 100 mL of the antisolvent and stirred continuously (600 rpm) for 2h. To obtain zein/Que/Toc aqueous dispersions, ethanol was removed by rotary evaporation (45 °C for 20 min). After ethanol was removed via rotary evaporation, the volume of the concentrated zein/Que/Toc solution was reduced to approximately 80 mL. To compensate for the volume lost during evaporation and reach the intended concentration for effective nanoparticle formation, the volume was adjusted to 100 mL with deionized water. The solution was subsequently diluted to 200 mL to attain the optimal concentration range of the nanoparticles. The pH of the diluted dispersions was adjusted to a range of 3–9 using 1M HCl or 1M NaOH. The resulting samples were designated as zein/Que, zein/Toc, and zein/Que/Toc, respectively, based on predetermined weight ratios: zein/Que/Toc(20:1:1), zein/Que/Toc(20:1:5), zein/Que/Toc(20:1:15), and zein/Que/Toc(20:1:25). The samples were stored at 4 °C for further analysis.

5.2.3. Optimization of nanoparticles

To optimize the formulation of zein/Que/Toc nanoparticles, we employed a Box-Behnken design (BBD) to assess the influence of zein/Que/Toc concentration, pH, and Tween 80 on the nanoparticle formulation. This design was chosen for its superior predictability, particularly at

factor extremes, and ability to reduce the necessary number of experimental runs while ensuring robust data acquisition, as described by Sánchez-López et al.[218]. The interactions between the independent variables (pH, concentrations of zein/Que/Toc, and Tween 80) and dependent variables (mean size, polydispersity index, zeta potential, and encapsulation efficiency) were investigated using a central composite factorial design using Minitab®14.12.0. The resulting data were subjected to rigorous statistical analysis of variance (ANOVA), and the influence of the independent variables on the dependent variables was described using the polynomial quadratic equation (1).

$$Y_\mu = \beta_0 + \beta_1 X_1 + \beta_2 X_2 + \beta_3 X_3 + \beta_{11} X_1^2 + \beta_{22} X_2^2 + \beta_{33} X_3^2 + \beta_{12} X_1 X_2 + \beta_{13} X_1 X_3 + \beta_{23} X_2 X_3 + \varepsilon \quad (5.1)$$

where Y_μ is the observed response variable, β_0 to $\beta_{2,3}$ are the regression coefficients, ε the error, and X_1, X_2, and X_3 are the independent variables.

Details of the factors and their response parameters are provided in the Supporting Information (**Table C1 and C2)**, with the design replicated twice and with three center-point repetitions.

5.3. Characterization of zein-Que-Toc nanoparticles

5.3.1. Particle size, polydispersity index (PDI), and ζ-potential (mV)

The particle size, polydispersity index (PDI), and zeta potential (ζ-potential) of the formulated zein/Que/Toc nanoparticles were examined using a Malvern Zetasizer Nano series instrument (Westborough, MA, United States), which employs dynamic light scattering (DLS) and electrophoretic light scattering (Zetasizer Nano Series, DTS 1061) to measure these properties. To minimize the impact of multiple scattering effects, the nanoparticles were first diluted with deionized (DI) water and sonicated for 10 min to achieve a concentration of 1 mg/mL. All measurements were consistently conducted at 25 °C, and each sample was analyzed in triplicate, with the averages reported as standard deviations.

5.3.2. Encapsulation efficiency (EE) and Loading capacity (LC)

To measure the encapsulation efficiency (EE%) and loading capacity (LC%) of quercetin and α-tocopherol, we followed procedures from previous studies [62,206]. The nanoparticles were first diluted with deionized water and then sonicated for 10 min to achieve a range of concentrations. Ethyl acetate was used to remove unencapsulated quercetin and α-tocopherol, followed by centrifugation at 5000 rpm for 5 min. The supernatant collected after centrifugation was subjected to UV-visible spectroscopic analysis using a Cary 300 Bio UV-visible spectrophotometer.

A critical aspect of our analysis was the selection of distinct measurement wavelengths for quercetin and α-tocopherol to minimize potential spectral interference. Quercetin's concentration was determined at 369 nm, while α-tocopherol was measured at 295 nm. To ensure the accuracy of our measurements, particularly considering the close absorption maxima of these compounds, we established standard curves for both quercetin (R^2 = 0.9992) and α-tocopherol (R^2 = 0.9995) at their respective wavelengths. In addition, acknowledging the potential effect of quercetin on the absorbance of α-tocopherol, we generated an auxiliary standard curve for α-tocopherol at a wavelength of 369 nm (R^2 = 0.9993). This step was crucial for accurately discerning the contribution of each compound in the co-embedded system, ensuring reliable and interference-free measurements. The calibration curves are presented in the Supporting Information (**Figures C1**). Finally, the EE% values for quercetin and α-tocopherol were derived using equations (5.2) and (5.4), respectively, whereas their respective LC% values were obtained from equations (5.3) and (5. 5).

$$\text{EE}\ (\%) = \left(1 - \left(\frac{\text{free quercetin}}{\text{total quercetin}}\right)\right) \times 100 \qquad (5.2)$$

$$\text{LC}\ (\%) = \left(1 - \left(\frac{\text{free quercetin}}{\text{total mass of nanoparticles}}\right)\right) \times 100 \qquad (5.3)$$

$$\text{EE}\ (\%) = \left(1 - \left(\frac{\text{free tocopherol}}{\text{total tocopherol}}\right)\right) \times 100 \quad (5.4)$$

$$\text{LC}\ (\%) = \left(1 - \left(\frac{\text{free tocopherl}}{\text{total mass of nanoparticles}}\right)\right) \times 100 \quad (5.5)$$

5.3.3. Rheology

The rheological properties of the freshly prepared zein/Que, zein/Toc, and Zein/Que/Toc nanoparticles were evaluated using a rheometer (HAAKE Mars III, Thermo Scientific, United States). A parallel plate geometry with P20CSL plates and 0.46 mm spacing was employed for the analysis. Amplitude sweep analysis was conducted on the samples, which were tested over a shear rate range of 0.01 to 100 s^{-1} at 25 °C (in the linear viscoelastic region).

5.3.4. Morphology

The microstructure of freeze-dried zein, zein/Que, zein/Toc, and zein/Que/Toc nanoparticles was examined by field-emission scanning electron microscopy (SEM) using a Zeiss Ultra Plus microscope. The gold layer was applied to the samples using sputtering with an accelerating voltage of 5.0 kV. Transmission electron microscopy (TEM) was used to analyze a solution containing 5 mL of nanoparticles. The solution was placed on a 200-mesh grid and air-dried at room temperature before being loaded into a microscope. Images of the nanoparticles were captured using a Tecnai F20 G2 instrument operated at a voltage of 200 kV.

5.3.5. Attenuated Total Reflection Fourier transform infrared spectroscopy (ATR-FTIR) and Fluorescence Spectroscopy

ATR-FTIR spectroscopy was used to characterize the nanoparticles in various formulations, including zein, Que, Toc, zein/Que, zein/Toc, and zein/Que/Toc. The analysis was conducted over the wavenumber range of 500-4000 cm^{-1}, using a Thermo Nicolet 6700 ATR-FTIR

spectrometer (Thermo Scientific, United States). Each sample underwent 64 scans at a resolution of 4 cm^{-1}.

To analyze zein/Que/Toc nanoparticles, fluorescence spectroscopy was performed according to the method described by Ye et al. [203]. The nanoparticles were first diluted to a concentration of 0.2 mg/mL using DI water with a pH adjusted to 4.0. A BioTek fluorimeter was used to record the emission spectra of the samples, ranging from 280 nm to 450 nm, upon exposure to a light beam at an excitation wavelength of 280 nm. Synchronous fluorescence spectra were captured at wavelength shifts (Δλ) of 15 and 100 nm.

5.4. Physicochemical stability nanoparticles

5.4.1. Storage stability

Colloidal dispersions of zein/Que/Toc nanoparticles were stored under refrigerated conditions at 4 °C and monitored over a period of two months. The size of the nanoparticles was determined using DLS as outlined in section 3.5.1. The retention rates of α-tocopherol and quercetin were calculated using equation 6.

$$\text{Retention rate (\%)} = \frac{\text{Amount of } \alpha - \text{Tocopherol and quercetin in the nanoparicles}}{\text{Initila amount of } \alpha - \text{Tocopherol and quercetin}} \times 100 \quad (5.6)$$

5.4.2. Light stability

The light stability of colloidal dispersions consisting of free quercetin, free α-tocopherol, zein/Que, zein/Toc, and zein/Que/Toc nanoparticle formulations was evaluated utilizing the method outlined by Chen et al. [41]. The samples were extracted at intervals of 0, 30, 60, 90, 120, and 150 min. Flavonoid degradation typically follows first-order kinetics, and accordingly, the half-life ($t_{1/2}$) and degradation rate constant (k) were determined using the following equations:

$$ln\frac{C}{C_o} = -kt \quad (5.7)$$

$$t_{1/2} = \frac{\ln 2}{k} \quad (5.8)$$

where, (t) is the time (min), C_0 is the initial concentration, and C is the concentration at time (t).

5.4.3. pH stability

The pH of the freshly prepared nanoparticle solutions was adjusted using 1 M NaOH or HCl, thereby encompassing a range of 3–9, and the particle size (d nm), polydispersity index (PDI), zeta potential (mV), encapsulation efficiency (EE%), and loading capacity (LC%) were evaluated. Particle size, PDI, and zeta potential were determined using DLS (Section **5.3.1)**, whereas encapsulation efficiency and loading capacity were calculated according to the procedures outlined in **Section 5.3.2.**

5.5. *In Vitro* gastrointestinal digestion

In vitro gastrointestinal digestion of the nanoparticle samples was conducted according to the method described by Chen et al. [206]. In the gastric phase, 30 mL of particle dispersion was mixed with 60 mL of simulated gastric fluid (SGF) containing 3.2 g/mL pepsin. The pH was adjusted to 2.0, and the mixture was incubated at 37 °C on a shaker MaxQ 4450 (150 rpm for 1 h). For the intestinal phase, 40 mL of the gastric digesta was transferred to a 100 mL beaker, and the pH was adjusted to 7.0. Then, 40 mL of simulated intestinal fluid (SIF) enriched with 5 mg/mL bile salt and 0.4 mg/mL pancreatin was added. The pH was adjusted to 7.0, and the mixture was incubated at 37 °C under shaking (150 rpm) for an additional 1 h. Following digestion, samples were taken every 30 min to assess the zein/Que/Toc nanoparticle release profile, which was measured using the method described in section **5.3.2** and the following equation:

$$Release(\%) = \frac{Amount\ of\ Zein/Que/Toc\ released}{Total\ amout\ of\ encapsualted\ in\ the\ sample} \times 100 \qquad (5.9)$$

5.6. Statistical analysis

All measurements were conducted in triplicate, and the data are presented as mean ± standard deviation. To determine the significance of the results, one-way analysis of variance (ANOVA) with Tukey's test was performed. Statistical significance was considered at a p-value less than 0.05, indicating a significant difference between the mean values.

5.7. Results and discussion

5.7.1. Effect of co-encapsulation of quercetin and α-Tocopherol Physicochemical properties of zein/Que/Toc co-encapsulated particles

The physicochemical properties of the Zein/Que/Toc nanoparticles were investigated, and the average particle size distribution, polydispersity index (PDI), zeta potential, encapsulation efficiency (EE), and loading capacity (LC) of different compositions were evaluated (**Figure 5.1**). Uniformity of the nanoparticle size was indicated by the consistency of the PDI values, which were all less than 0.21 across all samples, as shown in **Figure 5.1a**. The average particle size of pure zein nanoparticles (ZPs) was 125.7 nm. Upon incorporation of quercetin and α-tocopherol, there was a notable increase in particle size, with the Zein/Que/Toc (20:1:25) formulation reaching a maximum of 320.83 nm. However, in the formulation of Zein/Que/Toc (20:1:5), a minimum particle size of 223.7 nm was observed, which was significantly smaller than that of the zein/que encapsulation alone (270 nm). Notably, Zein/Que/Toc nanoparticles **(Figure 5.1b)** exhibited a bimodal distribution across all formulations, with the majority of particles clustered around the average particle size and a small fraction of particles appearing at larger sizes, possibly resulting from particle aggregation [214]. This increase in size can be attributed to the variation in the precipitation efficiency of the combined bioactive compounds during the fabrication process, resulting from differences in polarity [201,204]. The zeta potential values, which are crucial for determining the surface charge of the nanoparticles, were

also investigated, and are shown in **Figure 5.1c.** The surface charge of the pure zein nanoparticles was found to be positive, as evidenced by the measured zeta potential of 18.5 mV. In contrast, quercetin and tocopherol exhibited negative surface charges, with measured zeta potentials of -9.7 mV and -0.5 mV, respectively. However, the Zein/Que, Zein/Toc, and Zein/Que/Toc complexes exhibited a significant reduction in zeta potential, to -27.81 mV, -23.5 mV, and -33.12 mV, respectively. This reduction is likely attributed to electrostatic adsorption occurring between the negatively charged quercetin and zein particles, with α-tocopherol being incorporated into the complex. Previous studies have indicated that electrostatic interactions between zein nanoparticles and other bioactive compounds, such as quercetin and curcumin, can alter zeta potential [204,219]. The observed zeta potential for the Zein/Que/Toc nanoparticles not only aligns with the widely accepted notion of adequate electrostatic stabilization (zeta-potential absolute value exceeding 30 mV), but also underscores the effectiveness of incorporating α-tocopherol and quercetin into zein nanoparticles in maintaining nanoparticle stability. Additionally, the observed zeta potential of the Zein/Que/Toc nanoparticles aligns with the effectiveness of co-encapsulation in biological environments, validating the maintenance of colloidal stability [220].

Figure 5.1d illustrates that Zein/Que/Toc nanoparticles exhibited the highest encapsulation efficiency (EE%) of 96% and loading capacity (LC%) of 13% among all formulations, highlighting the outstanding encapsulation and bioactive co-delivery potential of zein. The high EE% and LC% can also be attributed to the synergistic interaction of zein with quercetin and α-tocopherol, which facilitated efficient entrapment of the bioactive compounds within the zein nanoparticles. The significant encapsulation and loading capacities of Zein/Que/Toc nanoparticles make them promising candidates for the controlled release, therapeutic efficacy, and protection of encapsulated agents against biological and environmental stressors. These findings are supported by previous research on zein-based nanoparticles by Chen et al. [206],

demonstrated that zein nanoparticles loaded with curcumin exhibit high encapsulation efficiency and loading capacity, leading to enhanced stability and sustained release of the encapsulated compound. Similarly, Zhang et al. [205] showed that zein nanoparticles loaded with resveratrol had high encapsulation efficiency and loading capacity, resulting in improved stability and controlled release of bioactive compounds. Therefore, the combination of these two bioactive compounds with zein in Zein/Que/Toc nanoparticles may result in a synergistic effect, leading to enhanced controlled release and therapeutic efficacy.

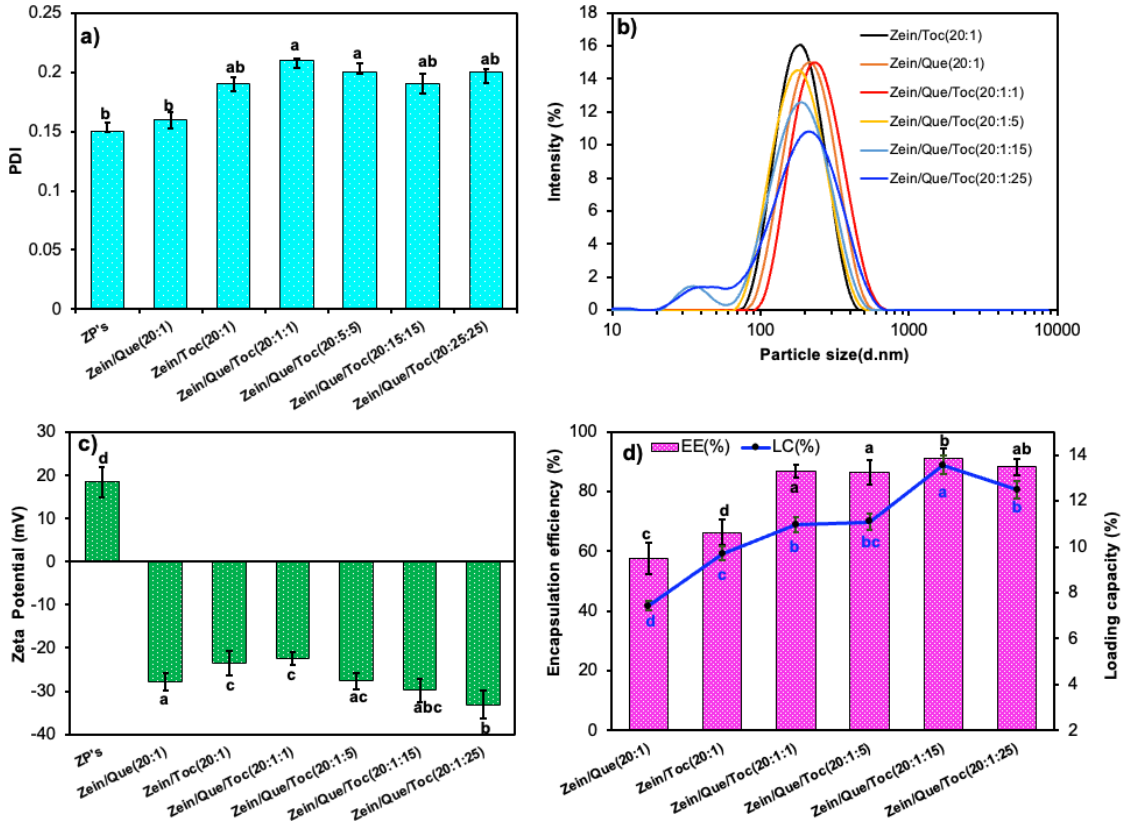


Figure 5.1. Shows a) PDI, b) particle size distribution, c) zeta potential, and d) encapsulation efficiency and loading capacity of zein nanoparticles for various formulations

5.7.2. Effect of pH on zein-nanoparticles

In the investigation of the properties of the nanoparticles at various pH levels, several intriguing findings were observed, as illustrated in **Figure 5.2**. The correlation between PDI and particle size is depicted in **Figure 5.2 (a-b)**, exhibiting a notable variation in the distribution throughout the pH spectrum in terms of size. This pH-mediated modulation of particle size underscores

the pivotal role of pH in influencing the colloidal stability [41]. This illustrates noticeable variations in particle uniformity and the possibility of aggregation in response to pH fluctuations, indicating the pivotal role of pH in governing the behavior and stability of nanoparticles [221]. Moreover, the electrostatic stability presented in **Figure 5.2c** elucidates the zeta potential across the spectrum of pH values. The Zein/Que/Toc formulations exhibited a notable zeta potential of -33 mV at pH 4, indicating a stable formulation due to electrostatic repulsion, minimizing aggregation. However, the zeta potentials at other pH values were relatively similar, regardless of the changes in the proportions of quercetin and α-tocopherol across each sample formulation. The variation in the encapsulation efficiency (EE%) and loading capacity (LC%) of zein nanoparticles across a range of pH values is shown in **Figure 5.2d**. At pH 4, the EE reached 94% owing to the positive charge on zein below its isoelectric point, enhancing compound encapsulation. At pH 7, which is close to the zein isoelectric point, EE was slightly lower at 86%, but LC peaked at 10.5%. This suggests that near-neutral charge conditions at pH 7 favor optimal packing within the nanoparticles, allowing for an increased loading of bioactive compounds. These results emphasize the significance of pH in the formulation of zein nanoparticles for efficient bioactive delivery [205,216].

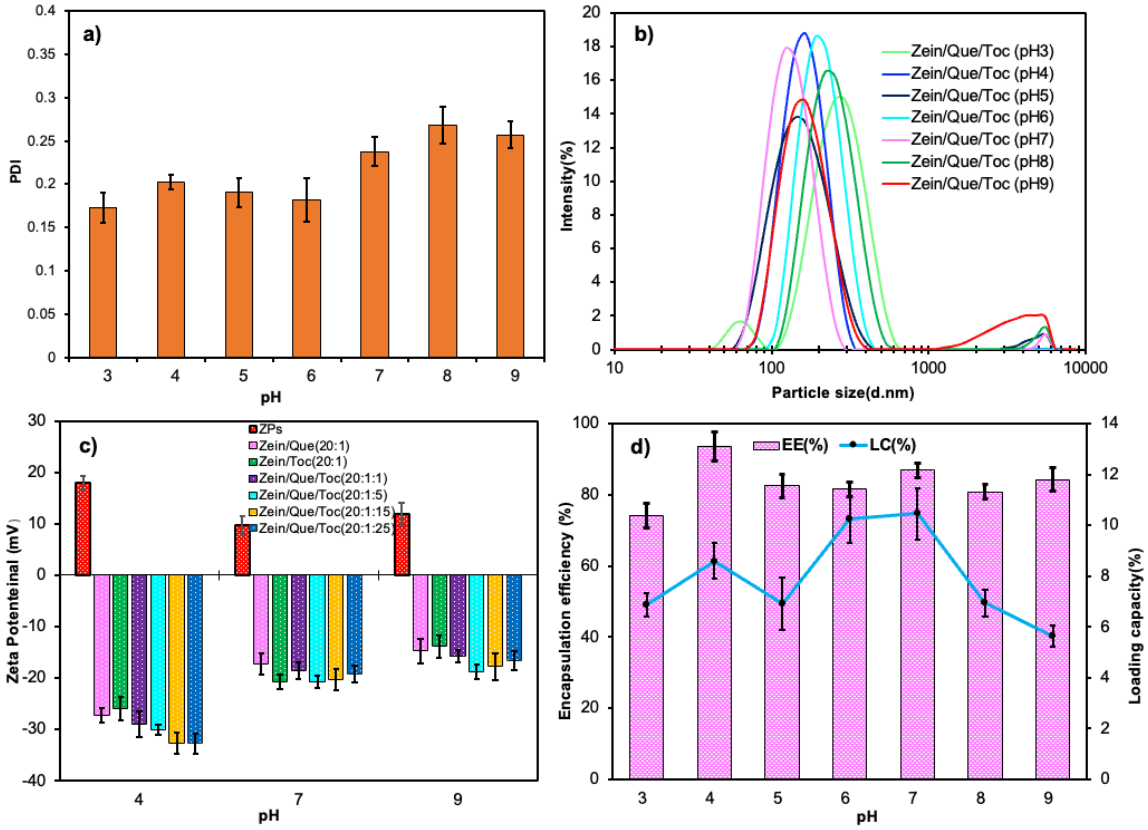


Figure 5.2. Effects of pH on a) PDI, b) particle size distribution, c) zeta potential, (d) encapsulation efficiency and loading capacity of Zein/Que/Toc nanoparticles.

5.7.3. Morphological analysis

Figure 3 illustrates scanning electron microscopy (SEM) and Transmission electron microscopy images that offer invaluable insights into the morphological features of co-encapsulated Zein/Que/Toc nanoparticle. Zein nanoparticles, depicted in **Figure 5.3a**, generally exhibited a spherical and uniform particle distribution, devoid of mass aggregation. This characteristic is attributed to the mutual surface charge [41]. The incorporation of quercetin and α-tocopherol into zein nanoparticles is evidenced by the distinct morphological alterations depicted in **Figure 5.3(b-c)**. This alteration may be attributed to the interaction between these compounds and zein nanoparticles. In addition, the combined effect of Zein/Que/Toc nanoparticles has demonstrated the phenomenon which has led to an enhancement in particle size and minor aggregation while simultaneously maintaining a uniform surface, as depicted in **Figure 5.3d**. The morphological characteristics of these zein

nanoparticles were aligned with the size distribution data obtained through dynamic light scattering. This finding highlights the significant influence of α-tocopherol and quercetin on the structural properties of nanoparticles. This observation is in line with prior studies, such as that by Ma et al., where the co-delivery of curcumin and quercetin with zein nanoparticles led to complex morphological changes as the concentrations of the bioactive compounds increased [62].

Additionally, the TEM images in **Figure 5.3(e-h)** reveal the morphology of zein nanoparticles that contain both quercetin and tocopherol. The particles were spherical in shape and exhibited a high level of stability against aggregation, as evidenced by the fact that only three particles adhered to one another. The particles' size distribution was observed within the range of 50 to 200 nm, which corresponded to the results obtained from the dynamic light-scattering instrument. The differences in the surface size of the particles suggest potential variations in the molecular arrangements within the particle structure and the surface charge of the nanoparticles[211].

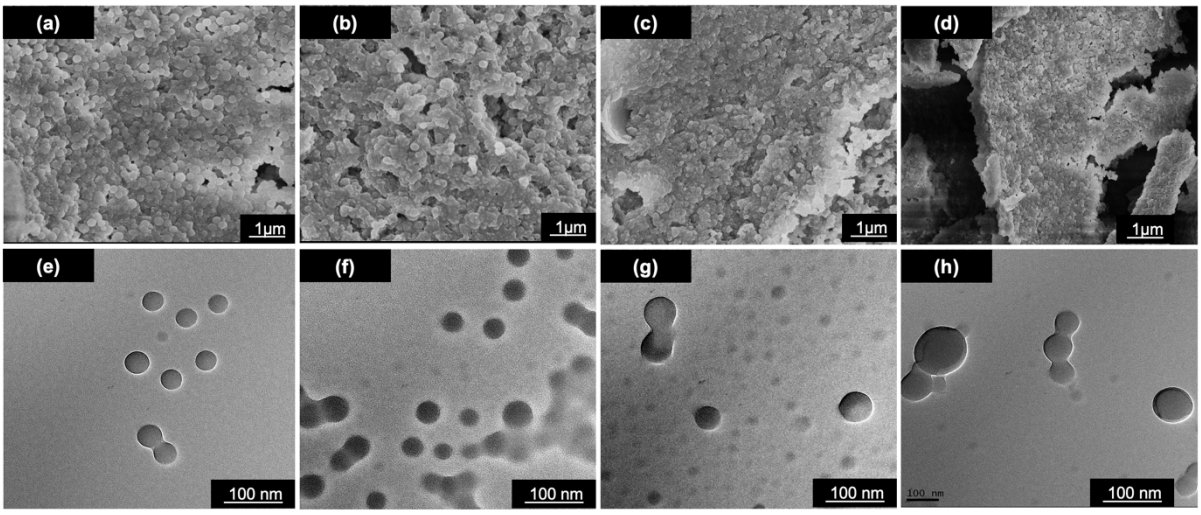


Figure 5.3. SEM images of (a) zein nanoparticles, (b) Zein/Que, (c) Zein/Toc, and (d) Zein/Que/Toc (20:1:1) nanoparticles. TEM images of (e) zein nanoparticles, (f) Zein/Que, (g) Zein/Toc, and (h) Zein/Que/Toc (20:1:1) nanoparticles.

5.7.4. ATR-FTIR Spectroscopy and Rheological/Fluorescence Analyses of Zein/Que/Toc Nanoparticles

The ATR-FTIR spectra depicted in **Figure 5.4a** provide a comprehensive and detailed analysis of the molecular structure of the zein/quercetin/tocopherol nanoparticles. The spectrum demonstrates a broad absorption band from 3408 to 3280 cm^{-1}, which corresponds to O-H stretching vibrations, suggesting the presence of essential hydrogen bonding that significantly contributes to the stability of the nanoparticles [62,205,208].The incorporation of tocopherol and quercetin into zein/Que/Toc nanoparticle frameworks has been confirmed through the identification of distinct C-H stretching peaks in the range of 2920-2850 cm^{-1}, which indicates the successful incorporation of these bioactive molecules [222]. These peaks were more pronounced than those observed for pure zein nanoparticles [223]. Furthermore, a sharp and distinct peak at approximately 1735 cm^{-1} signifies the presence of carbonyl (C=O) stretching vibrations. These vibrations are often associated with ester or carboxylic acid functional groups.

Notably, the band corresponds to the C-O stretching (amide I), and the C-N stretching coupled with N-H bending (amide II) further corroborating the presence of zein. These amide bands, compared to individual zein, have shifted to 1645 and 1515 cm^{-1} in the Zein/Que/Toc nanoparticles, with an increased peak intensity. Alterations in peak intensities and positions, particularly in the regions associated with aromatic C=C stretching and O-H bending, suggest structural modifications in quercetin and tocopherol upon interaction with zein [10,29].

Moreover, a discrete peak at 1095 cm^{-1}, corresponding to α-tocopherol's phenyl ring bending, exhibits a shift from its original 950 cm^{-1} position in pure tocopherol. This shift, coupled with the disappearance of a peak at 3408 cm^{-1}, implies a relaxation of the aromatic ring and hydrogen bond interactions with zein carbonyl groups. Such interactions are instrumental in altering the macromolecular chain conformation within the zein/Que/Toc complex, thereby impacting its flexibility and mobility [41]. These spectral changes are indicative of molecular

interactions critical for optimizing the delivery and release mechanisms of bioactive compounds [8,10].

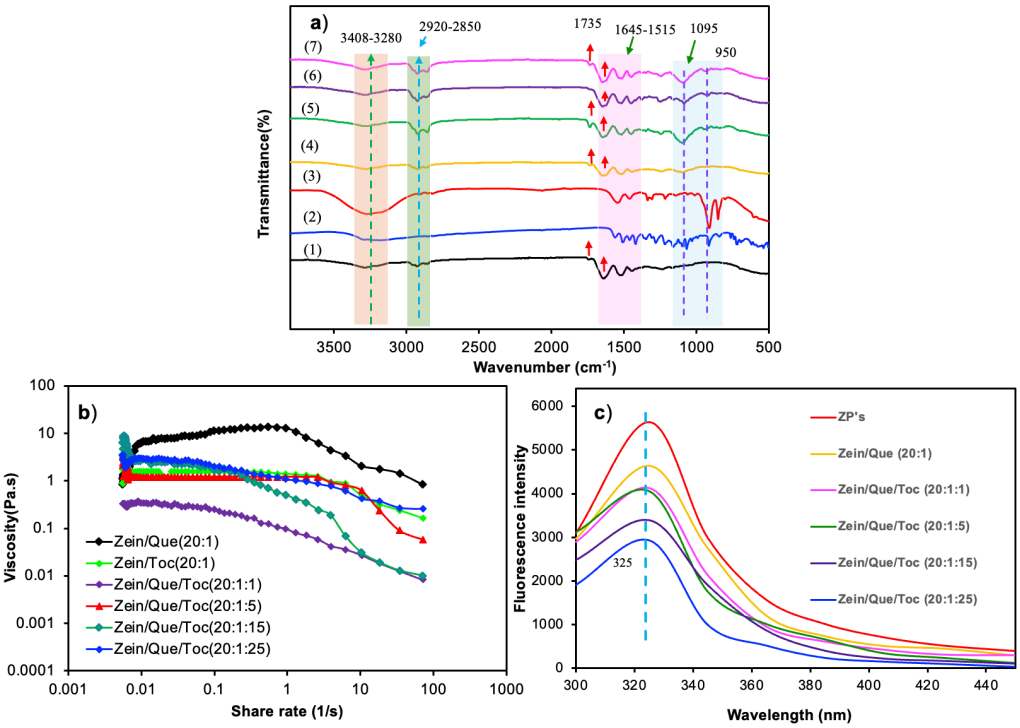


Figure 5.4. ATR-FTIR, Rheological, and Fluorescence Spectroscopy analysis.
Subsection (a) presents the ATR-FTIR spectral analysis of (1) Pure Zein, (2) Quercetin, (3) Tocopherol, (4) Zein nanoparticles (ZPs), (5) Zein/Que (20:1), (6) Zein/Toc (20:1), and (7) Zein/Que/Toc (20:1:25), (b) shows a rheological properties, (c) depicted the fluorescence spectroscopy for Zein/Que (20:1), Zein/Toc (20:1), and Zein/Que/Toc at various ratios of (20:1:1), (20:1:5), (20:1:15), and (20:1:25) nanoparticle formulations.

The rheological properties of the co-encapsulated quercetin and α-tocopherol in zein nanoparticles are shown in **Figure 5.4b**. The shear-thinning, non-Newtonian, pseudoplastic nature of the zein/Que combination suggests that the inherent structures become less viscous under shear. This property could be beneficial for bioactive encapsulation and for maintaining nanoparticle stability during storage [18]. Interestingly, the viscosity of zein/Toc was lower than that of zein/Que, possibly because of intermolecular hydrogen bonding initiated by α-tocopherol, resulting in a more viscous solution [202]. The tri-component system Zein/Que/Toc integrates the characteristics of both Zein/Que and Zein/Toc. The co-delivery of α-tocopherol and quercetin appears to enhance the network structure of the system. Notably,

the Zein/Que/Toc samples demonstrated a unique rheological pattern: a higher shear stress at low shear rates transitioning to a plateau as shear increases. This behavior could significantly affect bioactive encapsulation, release dynamics, and overall nanoparticle performance in drug/nutraceutical delivery.

The fluorescence spectroscopy data illustrated in **Figure 5.4c** explain the inherent behavior of zein nanoparticles, especially those with quercetin and α-tocopherol. For instance, Zein/Que/Toc (20:1:25) nanoparticles at a wavelength of 300 nm showed an emission intensity of 1909, which was lower than that of their counterparts, hinting at possible quenching or molecular adjustments within the nanoparticles at varying component ratios [221]. A marked increase in the emission intensity across all formulations was observed at 325 nm. The consistently high intensities of Zein/Que/Toc (20:1:5) between 345 nm and 450 nm suggest a strong fluorescence emission, which is potentially useful for tracking nanoparticles in biological systems. Overall, fluorescence data underscore the potential of zein-based nanoparticles in fluorescence-guided tracking and monitoring within bioactive delivery systems [203,204].

5.7.5. Physicochemical stability analysis

In the exploration of the co-encapsulation of quercetin and α-tocopherol within zein nanoparticles, we noted a controlled yet decreasing retention release of various Zein/Que/Toc formulations over a span of 60 days, as shown in **Figure 5.5a**. The Zein/Que (20:1) formulation began with a robust retention release of 90.45% on day 0, which decreased to 62.8% by day 60. Similarly, Zein/Toc (20:1) showed a decreasing trend from 94.23% to 60.56%. Intriguingly, the combined Zein/Que/Toc (20:1:1) and Zein/Que/Toc (20:1:25) formulations started with the release of 96.31% and 93.67%, respectively, tapering to 72.52% and 58.78%, respectively, on day 60. These patterns indicate that the combined encapsulation of quercetin and α-tocopherol within zein nanoparticles creates distinct release dynamics. This requires a deeper examination

to tailor the optimal bioactive release. Zhang et al. highlighted the sustained curcumin release from zein nanoparticles, which varied with formulation and encapsulation efficiency [217].

Particle size is pivotal in understanding the release behavior. As shown in **Figure 5.5b,** the size of the Zein/Que(20:1) nanoparticles ranged between 178.5-249.41 nm in size. This contrasted with Zein/Toc(20:1), which was 142.61-201.45 nm range. The combined formulations, Zein/Que/Toc(20:1:1), Zein/Que/Toc(20:1:5), Zein/Que/Toc(20:1:15), and Zein/Que/Toc(20:1:25), spanned in sizes of 189.36-239.84 nm, 201.47-248.1 nm, 217.9-262.48 nm, and 218.32-277.78 nm, respectively. These variations are anticipated to be instrumental in the observed differences in bioactive release across formulations.

The zeta potential, which is indicative of the surface charge of a nanoparticle and affects its interaction dynamics, also offers insights into its release behavior, as shown in **Figure 5.5c**. The ranges for Zein/Que(20:1), Zein/Toc(20:1), Zein/Que/Toc(20:1:1), Zein/Que/Toc(20:1:5), Zein/Que/Toc(20:1:15), and Zein/Que/Toc(20:1:25) were -27.54 to -17.3 mV, -29.2 to -18 mV, -32.5 to -12.4 mV, -33.2 to -27.1 mV, -33.7 to -22.8 mV, and -36.7 to -28.9 mV, respectively. In the context of bioactive compound co-delivery, zeta potential can significantly affect encapsulation efficiency, release speed, and overall therapeutic potential. A study by Leena et al. on zein nanoparticles for curcumin and resveratrol co-delivery found that zeta potential plays a crucial role in determining encapsulation efficiency and release dynamics [55].

Furthermore, it is imperative to understand the kinetic degradation. **Figure 5.5d** shows a decline in light stability across different time intervals, hinting at potential molecular structural changes or degradation of the nanoparticles. Specifically, the Zein/Que/Toc (20:1:25) formulation began to wane after 150 min, indicating a possible susceptibility to light-induced changes. Such degradation insights underscore the importance of ensuring nanoparticle stability to retain the efficacy of encapsulated compounds. Chen et al. noted that curcumin-

encapsulated zein nanoparticles exhibit heightened photothermal stability and antioxidant activity [206].

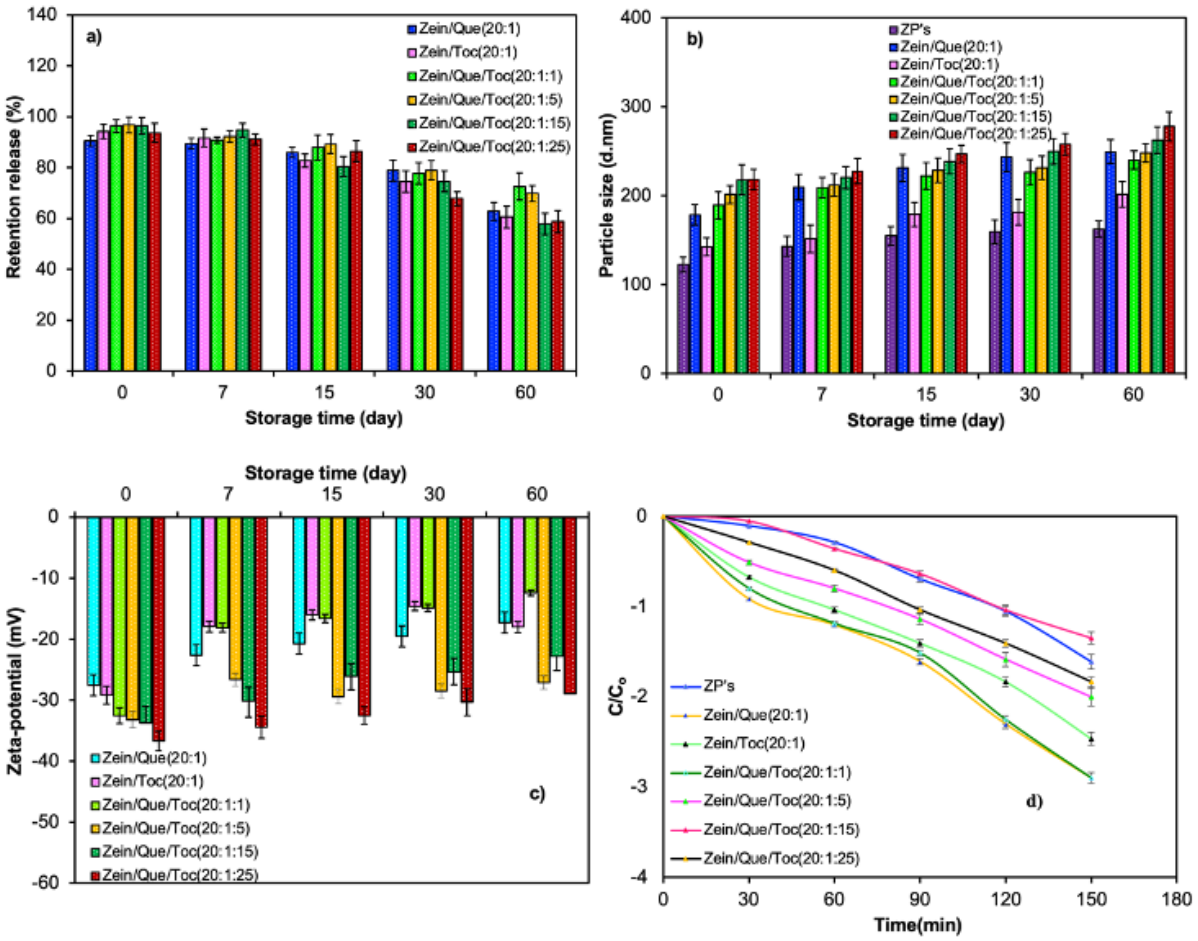


Figure 5.5. There are four crucial aspects regarding the storage of Zein/Que/Toc nanoparticles for a period of 60 days: a) retention and release mechanism, b) particle size distribution, c) zeta potential, and d) degradation kinetics.

5.7.6. *In-vitro* release

The *in vitro* release profiles of quercetin and α-tocopherol encapsulated in zein nanoparticles were analyzed, as illustrated in **Figure 5.6(a-b).** Quercetin consistently displayed a more pronounced release than α-tocopherol, with independent release peaking at 79.7% after 8 h. Interestingly, when incorporated into the Zein/Que (20:1) matrix, the release was marginally passive, settling at 74.9% within the same duration. This modulation by zein tip-offs at the

potential for controlled release is beneficial for practical applications [55,62]. α-Tocopherol exhibited a systematic release profile, culminating at 60.4% at 8-hour interval. However, upon encapsulation in the Zein/Toc (20:1) formulation, bioactive release increased to 72.1%, suggesting enhanced bioavailability. The release dynamics of the tri-component Zein/Que/Toc formulations were intricate. The Zein/Que/Toc (20:1:5) composition showed a release of 73.11% after 8 h, indicating a potential synergistic interplay between quercetin and α-tocopherol. In contrast, the Zein/Que/Toc (20:1:15) and Zein/Que/Toc (20:1:25) compositions showed slightly decreased release of 66.9% and 63.2%, respectively. These variations underscore the profound influence of the component ratios in shaping the encapsulation and release paths during gastrointestinal digestion. Moreover, co-encapsulated quercetin may also modulate the release rate by altering the zein matrix structure or by affecting the interaction of tocopherol with zein, potentially contributing to a more sustained release. The encapsulation of tocopherols within zein nanoparticles enhances their stability, solubility, and bioavailability, leading to a more rapid release than that of unencapsulated tocopherols. This controlled-release mechanism and protection against degradation are attributed to the encapsulation process, which modifies the physicochemical properties of tocopherols, such as their zeta potential. These changes were responsible for the observed differences in the release rates, as shown in **Figure 5.6b**.

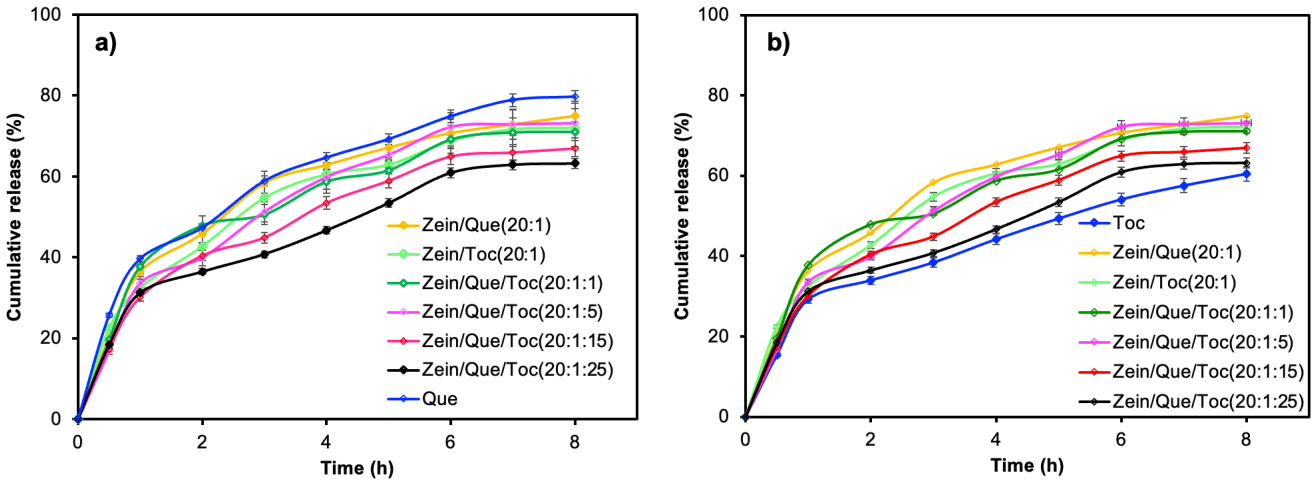


Figure 5.6. In vitro release patterns of polyphenols were influenced by varying quercetin-to-tocopherol ratios within a dual encapsulation system. The release profiles of quercetin (a) and α-tocopherol (b) are shown separately.

5.7.7. Optimization co-encapsulated zein nanoparticles

The optimization of the Zein/Que/Toc nanoparticle formulation was carried out by utilizing the Box-Behnken design methodology and building upon the previously identified optimal formulation of 20:1:5. The size of the nanoparticles was predominantly influenced by pH, with concentrations of quercetin and α-tocopherol falling within the range of 120-270 nm. The polydispersity index (PDI) exhibited a spectrum between 0.14-0.35, indicating the importance of pH and nanoparticle concentrations. Notably, an encapsulation efficiency (EE) surpassing 95% was achieved at the optimal pH and formulation ratio. The observed zeta potential ranged from -18.7 mV to -39.2 mV, and pH, in conjunction with zein, quercetin, and α-tocopherol concentrations, were found to be the most influential factors. This finding is consistent with those of previous studies, which support the validity and reliability of our findings [224–226]. The average particle size, PDI, EE (%), and zeta potential of the optimized zein/quercetin/tocopherol Zein/Que/Toc nanoparticles, as well as the normal probability plots of the supporting information, are shown in Figures S2 and S3, respectively.

5.8. Concluding Remarks

In this study, quercetin and α-tocopherol were successfully co-encapsulated in zein nanoparticles using an antisolvent co-precipitation technique. The integration of these bioactive compounds was confirmed by SEM and TEM analyses, which revealed distinct morphological shifts upon encapsulation. The ATR-FTIR spectra further demonstrated significant molecular interactions, highlighting the combined roles of α-tocopherol and quercetin. The *in vitro* release profiles of quercetin and α-tocopherol indicated that quercetin consistently exhibited a more pronounced release than α-tocopherol, which was associated with its enhanced interaction with zein. When incorporated into the zein/Que (20:1) matrix, the release of quercetin was slightly passive, suggesting a controlled release potential. In contrast, α-tocopherol demonstrated a systematic release profile that was enhanced when encapsulated in the Zein/Toc (20:1) formulation, potentially increasing its bioavailability. The tri-component Zein/Que/Toc formulations exhibited intricate release dynamics. The Zein/Que/Toc (20:1:5) composition achieved a moderate yet substantial release of 73.11% at the 8-hour mark, indicating a potential synergistic or stabilizing interaction between quercetin and α-tocopherol. The Zein/Que/Toc (20:1:15) and Zein/Que/Toc (20:1:25) compositions exhibited slightly attenuated releases of 66.87% and 63.19%, respectively, highlighting the influence of component ratios on encapsulation and release during gastrointestinal digestion. Overall, this study provides valuable insights into the co-encapsulation of quercetin and α-tocopherol within zein nanoparticles, showing their potential for advanced bioactive delivery applications.

Chapter 6. Development and Characterization of PVA-Zein/α-Tocopherol Nonwoven Mats for Functional Wound Dressing Applications

6.1. Introduction

The disposal of non-renewable petrochemical polymers has become a growing environmental concern due to their slow degradability and in some cases toxicity concerns [227]. To mitigate this issue, there has been a significant shift towards the development and utilization of biodegradable and biopolymer-derived plastics [228,229]. Biopolymers obtained from plant, animal, and microbial sources hold considerable promise for minimizing environmental impacts and enhancing sustainability, owing to their renewable nature and biodegradability [230,231]. In particular, biopolymers are of interest for applications in which bacterial infections are a primary concern, such as single-use medical products [232]. In contrast, the use of traditional petroleum-based polymers in these applications poses sustainability challenges, leading to increased interest in biopolymers as viable substitutes for petroleum-based plastics, particularly for short-term use products [233–235].

Wound healing remains a critical challenge in healthcare due to complications such as bacterial infections, oxidative stress, and chronic inflammation, which can delay or prevent the natural healing process [236–239]. Conventional wound dressings often fail to address these complex needs, underscoring the need for multifunctional materials capable of enhancing healing and controlling infections through sustained bioactive release[240,241]. [5]

[5] D.T. **Tadele,** D. David, E. Yim, T.H. Mekonnen
Development and characterization of PVA-zein/α-tocopherol nonwoven mats for functional wound dressing applications. Colloids and Surfaces B: Biointerfaces , 246 ,, 10.1016/j.colsurfb.2024.114355.2025,114355

Recent advancements in nanocarrier-based drug delivery systems have significantly improved wound healing outcomes by providing controlled and sustained release of therapeutic agents. Nanocarriers, such as polymeric nanoparticles and liposomes, loaded with bioactive compounds like antimicrobial peptides and [iii]antioxidants, have demonstrated the ability to enhance tissue regeneration, reduce infection, and accelerate wound closure [242–244]. These innovations highlight the need for advanced materials that not only protect wounds but also actively facilitate the healing process.

Polymer nanofibers, typically produced via electrospinning, have gained considerable attention for their application in drug delivery due to their high specific surface area, porosity, and tunable fiber diameter [245–247]. However, electrospinning suffers from low throughput, which typically range from 0.4 to 1 mL/, thus limiting its scalability for industrial applications [248–251].

Solution blow spinning (SBS) has emerged as a high-throughput nanofiber fabrication alternative. SBS uses high-velocity air to shear fibers from a polymer solution, achieving significantly higher production rates approximately 160 g/h for poly(ethylene oxide) making it suitable for large-scale manufacturing[87]. The SBS technique offers an energy-efficient and scalable process, producing fibers with comparable properties to those obtained via electrospinning[252]. This method has been successfully applied in the fabrication of nanofibers from biodegradable polymers, such as poly(hydroxybutyrate) (PHB) and ε-poly-L-lysine (ε-PLL),which exhibit both biocompatibility and antibacterial properties, making them promising candidates for multifunctional wound dressing [253].

Polyvinyl alcohol (PVA) is widely recognized for its spinnability, biocompatibility, non-toxicity, and biodegradability, making it an excellent matrix for wound healing applications

[254–258]. Research demonstrates the incorporation of PVA with zein, a biodegradable and amphiphilic protein extracted from corn, to produce nanofibrous mats utilizing the SBS technique[89]. Zein plays a crucial role in this system due to its encapsulation capabilities, particularly for hydrophobic bioactive agents like α-tocopherol (vitamin E), which is known for its antioxidant properties and ability to protect cells from oxidative damage[202,205,259]. The novelty of this work lies the combined use of antisolvent co-precipitation for synthesis of α-tocopherol-loaded zein nanoparticle and SBS for mat fabrication highlights a cost-effective, scalable approach to developing biodegradable wound dressings. This innovative approach presents a scalable and cost-effective alternative to traditional electrospinning for producing advanced wound dressings [24,170]. Our previous research demonstrated that zein nanoparticles could encapsulate bioactive compounds such as α-tocopherol, protecting them from degradation and sustained controlled release[61]. The sustained release of α-tocopherol from these mats not only facilitates the antioxidant activity necessary to manage chronic wounds but also enhances the wound healing environment by reducing the risk of infection. The structural, mechanical, and *in vitro* biological properties of these nanofibrous mats were systematically analyzed to assess their potential as advanced wound dressings. The results provide a promising platform for applications beyond wound care, including in biomedical devices, hygiene products, and environmentally friendly healthcare solutions, potentially leading to improved patient outcomes and more scalable sustainable clinical practices. Future research will focus on optimizing fiber composition, incorporating antimicrobial agents, and conducting in vivo studies to validate the efficacy of these mats in real biological environments.

6.2. Materials and methods

6.2.1. Materials

Zein powder (95 wt.%), α-tocopherol (97 wt.%), and Tween 80 were procured from Sigma-Aldrich. PVA with a molecular weight of 72,000 g/mol (99% hydrolyzed) was obtained from Sigma-Aldrich (Canada). NIH3T3 mouse fibroblast cells, Dulbecco's modified eagle medium (DMEM), 10% fetal bovine serum (FBS), and 1% penicillin-streptomycin (PS) were obtained from the American Type Culture Collection (ATCC, US). The LIVE/DEAD™ Viability/Cytotoxicity Kit for mammalian cells and alamarBlue™ Cell Viability assay reagent were procured from Invitrogen™ (Thermo Fisher Scientific, Eugene, OR, USA) and (DAL1025, Thermo Fisher Scientific, Mississauga, ON, Canada), respectively. Phosphate-buffered saline (PBS) was obtained from Fisher (Fisher Scientific, Mississauga, ON, Canada).

6.2.2. Synthesis of α-tocopherol loaded zein nanoparticles

In our previous work [61], we reported the antisolvent co-precipitation (ASCP) method for synthesizing α-tocopherol-loaded zein nanoparticles. The antisolvent co-precipitation technique was employed for the synthesis of α-tocopherol-loaded zein nanoparticles due to its simplicity, efficiency, and cost-effectiveness. This method allows for high encapsulation efficiency and controlled particle size, crucial for the sustained release of bioactive compounds in wound healing. In this study, a solution was prepared by dissolving 1.5 g zein in 50 mL of an 80:20 mixture of ethanol and water at room temperature. Subsequently, varying amounts of α-tocopherol were added to this solution to encapsulate zein nanoparticles. To be specific, 0.225 g, 0.45 g, and 0.75 g of α-tocopherol were added to achieve 15%, 30%, and 50% weight ratios, respectively. The resulting solution was added dropwise to 100 mL of the deionized water antisolvent while stirring continuously at 600 rpm for 2 h. Ethanol was removed by rotary evaporation (45 °C for 20 min) to obtain zein/α-tocopherol aqueous dispersions. The resulting

samples were designated as ZT-15, ZT-30, and ZT-50, respectively, and stored at 4 °C until further analysis.

6.3. Characterization of zein-α-tocopherol nanoparticles

6.3.1. Particle size, polydispersity index (PDI), and ζ-potential (mV)

The particle size, polydispersity index (PDI), and zeta potential (ζ-potential) of ZT-15, ZT-30, and ZT-50 nanoparticles were determined using a Zetasizer Nano series instrument (Malvern Panalytical, Westborough, MA, United States). Aliquots of freshly prepared dispersions (0.1 mg/mL) were pipetted into disposable folded capillary cells (DTS1070). Measurements for each sample were conducted in triplicate, with 10-100 runs performed per sample, at a temperature of 25 °C and an equilibration time of 60s.

6.3.2. Encapsulation efficiency (EE) and Loading capacity (LC)

To measure the encapsulation efficiency (EE%) and loading capacity (LC%) of α-tocopherol, a methodology adapted from previous studies [59,61]. The nanoparticles were first diluted with deionized water and then sonicated for 10 min to obtain a range of concentrations suitable for analysis. Ethyl acetate was used to separate unencapsulated α-tocopherol, followed by centrifugation at 5000 rpm for 5 min. The supernatant, collected after centrifugation, was subjected to UV-visible spectroscopic analysis using a Cary 300 Bio UV-visible spectrophotometer. The α-tocopherol concentration was measured at 294 nm and standard curves for α-tocopherol ($R^2 = 0.99$) wavelengths were generated. Detailed calibration curves at the specified wavelengths are presented in the Supporting Information **Figure D1.** The EE (%) and LC (%) values of α-tocopherol were calculated using equations (6.1) and (6.2), respectively:

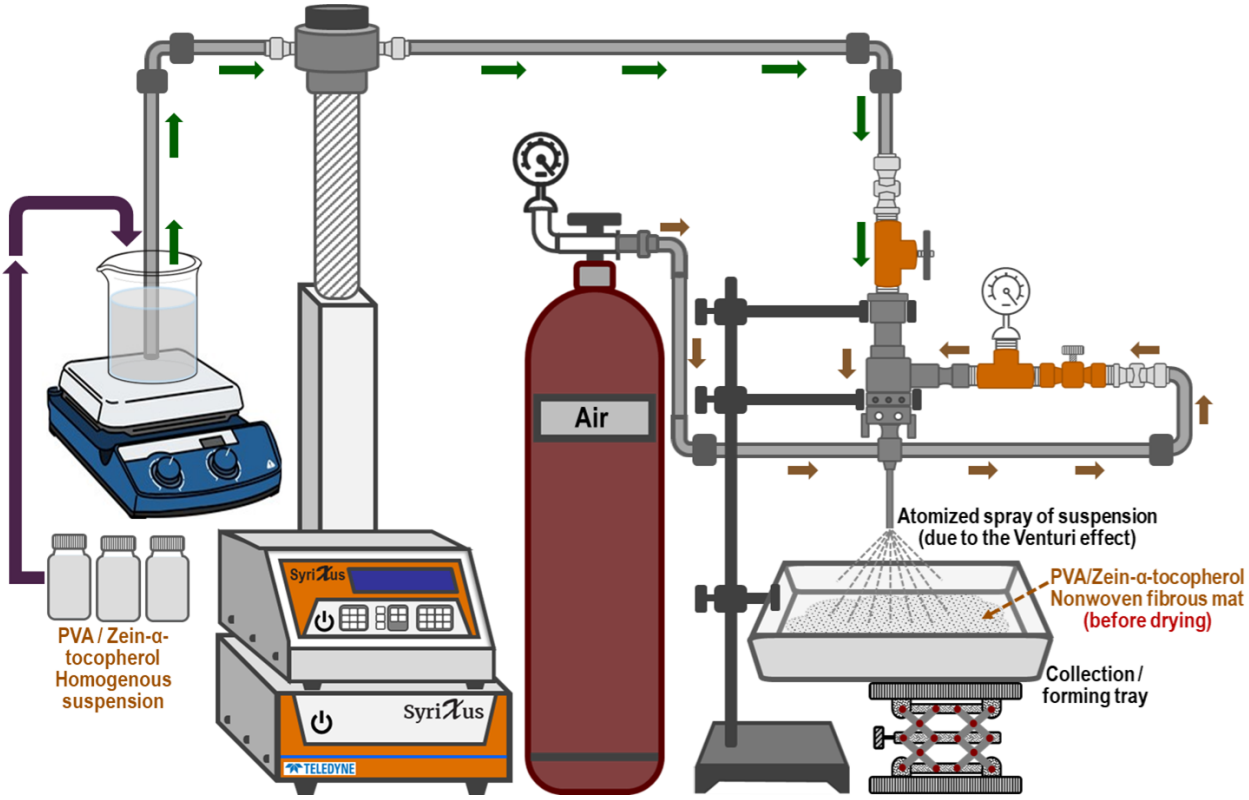
$$\text{EE (\%)} = \left(1 - \left(\frac{\text{free tocopherol}}{\text{total tocopherol}}\right)\right) \times 100 \qquad (6.1)$$

$$\text{LC}\ (\%) = \left(1 - \left(\frac{\text{free tocopherl}}{\text{total mass of nanoparticles}}\right)\right) \times 100 \qquad (6.2)$$

6.3.3. Fabrication of nanofibrous mats by solution blowing spinning

A 10 wt.% solution of PVA was prepared by dissolving PVA in distilled water at 90 °C on a hot plate with magnetic stirring at 250 rpm for 2 h. Following complete dissolution, the α-tocopherol-loaded zein nanoparticles were added to the PVA solution to generate a composite polymer dispersion. Specifically, dispersions of ZT-15, ZT-30, and ZT-50, corresponding to α-tocopherol to zein weight ratios of 15%, 30%, and 50%, respectively, were dispersed into the PVA solution.

The resulting polymer composite dispersions were then subjected to a solution blowing process to fabricate nonwoven nanofiber mats. The solution blow spinning process was performed using a coaxial needle procured from Rame-Hart Instrument Co., featuring an inner needle gauge of 14 and an outer needle gauge of 10. The inner needle had an internal diameter of 1.60 mm and an external diameter of 2.11 mm, whereas the outer needle had an internal diameter of 2.69 mm and an external diameter of 3.40 mm. The polymer dispersion was pumped at a flow rate of 6 mL/h using a Teledyne ISCO 500D syringe pump. High-velocity air at 100 psi was used to shear the fibers from the polymer dispersion cone. The coaxial needle setup ensured precise control over fiber formation, leading to uniform and consistent nonwoven mats. A schematic of the experimental setup of the coaxial needle assembled with a syringe pump is shown in **Fig.1**. The distance between the needle tip and the collector was maintained at 60 cm. Polytetrafluoroethylene (PTFE) nonstick Teflon sheets were used as collection substrates for the nanofibers. Detailed specifications and formulations of the blend compositions are listed in **Table 6.1.** A schematic of the experimental setup of the coaxial needle assembled with a syringe pump is shown in **schematic 6.1**.



Schematic 6.1. Schematic showing the basic setup for fabricating α-tocopherol-loaded zein nanoparticles – PVA mats using a solution blowing process.

Table 6.1. Details of polyvinyl alcohol/α-tocopherol loaded zein nanoparticle solution preparation

Sample code	Sample description	Zein (w t%)	α-tocopherol (wt.%)	PVA (wt.%)
PVA-Zein	PVA-Zein (control)	1.5	-	10
PZT-15	PVA-Zein- 15% of α-tocopherol	1.5	0.225	10
PZT-30	PVA-Zein- 30% of α-tocopherol	1.5	0.450	10
PZT-50	PVA-Zein- 50% of α-tocopherol	1.5	0.750	10

6.4.Characterization of the nonwoven nanofiber mats

6.4.1. Morphology

Morphology analysis of the nonwoven fiber mats was conducted using field emission scanning electron microscopy (FESEM, Quanta FEG 250 model, Abingdon, UK) operated at an accelerating voltage of 10 kV. Prior to observation, the double-sided fiber mats were mounted on metal stubs covered with carbon tape adhesive and subsequently sputter-coated with a thin layer of gold (10 nm) under high vacuum conditions. The diameters of arbitrarily selected fibers in the SEM micrographs were measured using NIH ImageJ software, and a histogram was plotted to display the frequency distribution of the fiber diameters, with a minimum of 100 individual fibers analyzed per sample.

6.4.2. Attenuated total reflection Fourier transform infrared spectroscopy (ATR-FTIR)

The FTIR spectra of the nanofibrous mats were analyzed using a Thermo Nicolet 6700 ATR–FTIR spectrometer. The spectra were obtained over a wavelength range of 500-4000 cm^{-1} with a resolution of 4 cm^{-1}, and 64 scans were collected for each sample.

6.4.3. Rheology

The rheological characteristics of the PVA-Zein, PZT-15, PZT-30, and PZT-50 solutions were assessed using a HAAKE Mars III rheometer (Thermo Scientific, United States). A parallel plate geometry with P20CSL plates and a spacing of 0.46 mm was utilized for the analysis. Amplitude sweep tests were performed over a strain range of 0.01% to 100% at a temperature of 25 °C to identify the linear viscoelastic region (LVR). The samples were subjected to shear rate variations from 0.01 to 100 s^{-1}.

6.4.4. Differential scanning calorimetry (DSC)

Differential scanning calorimetry (DSC) analysis was performed using DSC equipment (Discovery 2500, TA Instruments, DE, USA). The samples weighing 7 mg each were heated

from 26 to 260 °C at a rate of 10 °C/min under a nitrogen atmosphere at a flow rate of 50 mL min^{1}. These temperatures were used to assess the thermal stability and phase transitions of the mats, providing insights into their structural integrity. To ensure accuracy, each sample was tested using at least three replicates at 25 °C.

6.4.5. Mechanical properties

The mechanical properties of the samples were assessed using a Mandel-Shimadzu (AGS-X) tensile testing unit 0.5 kN load cell (Kyoto, Japan). The speed was set to 1 mm/min, and the gauge length was maintained at 15 mm for each sample. Five test specimens were cut from each of the PVA-Zein, PZT-15, PZT-30, and PZT-50 fiber mats for testing. The ultimate tensile strength, elongation at break, and Young's modulus of each sample were determined.

6.4.6. Degradation behavior of PVA/Zein-Toc mats

The short-term degradation of PVA/Zein-Toc mats was studied under simulated physiological conditions over 24 hours. Mats were fabricated using the solution blow spinning technique and subsequently immersed in phosphate-buffered saline (PBS) at pH 7.4 and 37°C to mimic physiological environments. Uniformly cut pieces of the mats were weighed to determine their initial mass. The samples were then immersed in PBS and collected at predetermined time intervals of 0, 0.5, 1, 2,4, 8, and 24 hours. To assess degradation, weight loss was calculated as a percentage of the initial mass (equation 6.3). Additionally, Fourier-transform infrared spectroscopy (FTIR) analysis was conducted on the dried samples at each time point to identify any chemical changes in key functional groups. The analysis focused on hydroxyl (–OH) and acetate (C=O) groups associated with PVA, as well as amide I (C=O stretch) and amide II (N-H bend) bands for zein, and characteristic peaks of α-tocopherol. This approach allowed for the detailed evaluation of the degradation profile and structural integrity of the mats over time.

$$WL(\%) = \frac{W_0 - W_1}{W_0} \times 100 \qquad (6.3)$$

where: W_0 is the initial weight of the fiber sample and W_1 is the weight of the fiber sample after immersion at different time intervals.

6.5. *In vitro* drug release kinetics

The release kinetics of α-tocopherol from PVA-Zein, PZT-15, PZT-30, and PZT-50 fiber mats were analyzed using UV-visible spectroscopy. Samples (2 mg, 10 mm × 10 mm) were affixed to an adhesive polyimide film and placed in test tubes containing 2 mL of 0.01 M phosphate-buffered saline (PBS) (pH 7.4).The test tubes were then stored in an incubation shaker at 37 °C and 100 rpm to simulate wound dressing conditions on the skin. At predetermined intervals within 24 h, 3 mL of PBS was removed and replaced with an equal volume of fresh PBS. The absorbance of the withdrawn samples was measured at the characteristic peak of α-tocopherol (292 nm) using a Cary 300 Bio UV-visible spectrophotometer.

The total amount of α-tocopherol released into PBS was determined by comparing the absorbance values to a pre-established calibration curve **Figure D1**. Three replicates of each sample were analyzed to determine drug release, and the results were expressed in terms of cumulative release as a function of time, as per equation (6.4):

$$Release(\%) = \frac{Amount\ of\ \alpha - \text{Toc}\ released}{Total\ amout\ of\ \alpha - \text{Toc loaded into the nanofiber}} \times 100 \qquad (6.4)$$

6.6.Mathematical models for drug release kinetics

The mechanism of α-tocopherol release was analyzed using several kinetic models, including zero-order, first-order, Higuchi diffusion, and Korsmeyer-Peppas models. These models were employed to determine the diffusion exponent (n) and understand the release mechanisms. The release data were fitted to each model, and the one with the highest correlation coefficient (R^2) was used to calculate the release kinetics of α-tocopherol [258]. The equations used for these models are as follows.

$$Q_t = Q_0 + K_0 t \quad (6.5)$$

$$\ln(Q_t - Q_t) = lnQ_0 - K_1 t \quad (6.6)$$

$$Q_t = K_H \sqrt{t} \quad (6.7)$$

$$\frac{Q_t}{Q_\infty} = K_k t^n \quad (6.8)$$

Where Ko, K_1, K_H, and K_{KK} are the zero-order release, first-order release, Higuchi, and Korsmeyer constants, respectively. Qo and n are the initial release amount (mg/mL) and diffusion or release exponent, respectively.

6.7. Cell culture studies

NIH3T3 mouse fibroblast cells (ATCC, US) were cultured according to the supplier's recommendations at 37 °C and 5% CO_2 in maintenance media comprising DMEM, 10% FBS, and 1% PS. Cell suspensions in the maintenance media were seeded into 24-well plates and incubated for 24 h at 37°C in a humidified atmosphere containing 5% CO_2 to achieve a monolayer cell culture. NIH3T3 cells at 28-30 passages were used for the experiments, and the seeding density was 10,000 cells/cm² unless otherwise specified.

6.7.1. Cell viability and cytotoxicity test

The PVA-Zein, PZT-15, PZT-30, and PZT-50 samples were cut into disc shapes (1 cm²) and UV-sterilized for 30 minutes inside a biosafety cabinet. Subsequently, the samples were incubated in serum-free media of DMEM with 1% PS for 24 h at 37°C. After 24 h, 500 µL of the sample extract were added to each experimental well containing a cell monolayer, and 500 µL of fresh culture media was added to the positive control tissue culture polystyrene (TCPS) well. Before addition to the cell monolayer, 10% FBS was added to the extracts. The plates were incubated for 24 h at 37°C in a humidified atmosphere with 5% CO_2.

Cell viability was assessed using Live/Dead staining with 0.25 µL of 4 mM eBioscience Calcein AM Viability Dye (65-0853-39 Invitrogen) and 1 µL of 2 µM ethidium homodimer-1 (E1169 Invitrogen) diluted with DMEM for each well (with two experimental replicas). After 24 h, extracts were withdrawn from each well, and the experimental replicas were incubated with the Live/Dead staining solution in the dark at room temperature for 30 minutes. NIH3T3 cells cultured in TCPS well plates served as the positive control, and the ethanol-treated NIH3T3s served as the negative control. Stained cells were imaged with a Zeiss fluorescence microscope (Axio Observer Z1) and analyzed using Fiji.

The cytotoxicity of samples was evaluated by an alamarBlue cell viability assay according to the manufacturer's recommendation. Briefly, NIH3T3 cells were seeded onto a 24-well plate with three experimental replicates and allowed to form a monolayer over 24 h. Cultured cells were exposed to the extract solution at 37 °C and 5% CO_2 for 24 h. After this incubation period, the extracts were replaced with 10% (v/v) alamarBlue™ Cell Viability Reagent (Thermo Fischer Scientific, USA) in maintenance media and incubated at 37°C for 1 h. The fluorescence intensities for each sample of the biological replicates were recorded at an excitation wavelength of 560 nm and emission wavelength of 590 nm using a microplate reader (BioTek Citation 5, USA). NIH3T3 cells cultured directly in TCPS well plates served as the positive control, and wells without cells served as the background. The cell viability % was determined by normalizing with the positive TCPS control.

6.8. Statistical analysis

All statistical analyses were performed using GraphPad Prism version 9. The mean ± standard deviation of all data is included in the results. The numbers of replicates are listed in the figure legends. To evaluate statistical significance, ordinary one-way ANOVA with Tukey's multiple comparison test was used.

6.9.Results and Discussion

6.9.1. Morphology analysis of tocopherol loaded PVA-Zein nonwoven fiber mats

The morphology of the fibrous mats was analyzed via scanning electron microscopy (SEM). As depicted in **Figure 6.1**, the mats displayed distinct morphologies based on α-tocopherol loading levels. As illustrated in **Figure 6.1a**, the control PVA-Zein Fibers exhibited a homogeneous structure with smooth, uninterrupted fibers covering the entire surface and no bead formation. The average fiber diameter was measured to be 587.7 nm using the ImageJ software after analyzing approximately 100 fibers, as shown in (**Figure 6.1e)**. The PZT-15 fibrous mat, as displayed in **Figure 6.1b**, exhibited a similar smooth morphology, with small particles distributed along the fibers, indicating the successful encapsulation of α-tocopherol within the zein matrix. The average diameter of these fibers increased to 796.4 nm, as shown in (**Figure 6.1f)**, suggesting that the addition of encapsulated α-tocopherol affects the fiber formation process, as expected [260,261]. The surface of the PZT-30 fibrous mat, as depicted in the **Figure 6.1c**, exhibited a more prominent particle distribution that was uniformly dispersed along the length of the fibers. This uniform distribution suggests the effective encapsulation and integration of α-tocopherol. The average fiber diameter noticeably decreased to 347.2 nm (**Figure 6.1g**), which was likely attributable to alterations in viscosity and surface tension resulting from increased α-tocopherol loading[262].

Furthermore, **Figure 6.1d** shows the PZT-50 nonwoven mat with the densest particle distribution on the fiber surface, indicating a high loading level. The average fiber diameter was measured to be 354.8 nm **(Figure 6.1h),** which is slightly greater than that of the PZT-30 fibers, but still significantly smaller than that of the control and PZT-15 fibers. These findings suggest that fiber diameter is inversely proportional to the concentration of α-tocopherol loaded in the samples, with higher concentrations resulting in smaller fiber diameters. The observed morphologies suggest that α-tocopherol significantly influences the fiber formation process,

possibly due to changes in the solution properties, such as viscosity and surface tension, during the solution blowing process [260,262,263].Smaller fiber diameters are associated with increased specific surface area and higher porosity, which leads to several potential benefits for wound healing. Literature indicates that fibers with smaller diameters enhance cell attachment and migration due to the larger surface area available for cell interaction, which promotes faster tissue regeneration[264]. Additionally, the smaller pore size associated with reduced fiber diameters can improve the controlled release of therapeutic agents, ensuring localized and sustained delivery of bioactive compounds like α-tocopherol to the wound [265]. Overall, SEM analysis showed the successful incorporation of encapsulated α-tocopherol nanoparticles into the PVA-zein fibers and the impact of tocopherol loading on the fiber morphology. These findings are crucial for wound dressing applications, where the fiber dimensions could affect the controlled tocopherol release, which provides therapeutic benefits, and the fiber matrix offers structural support.

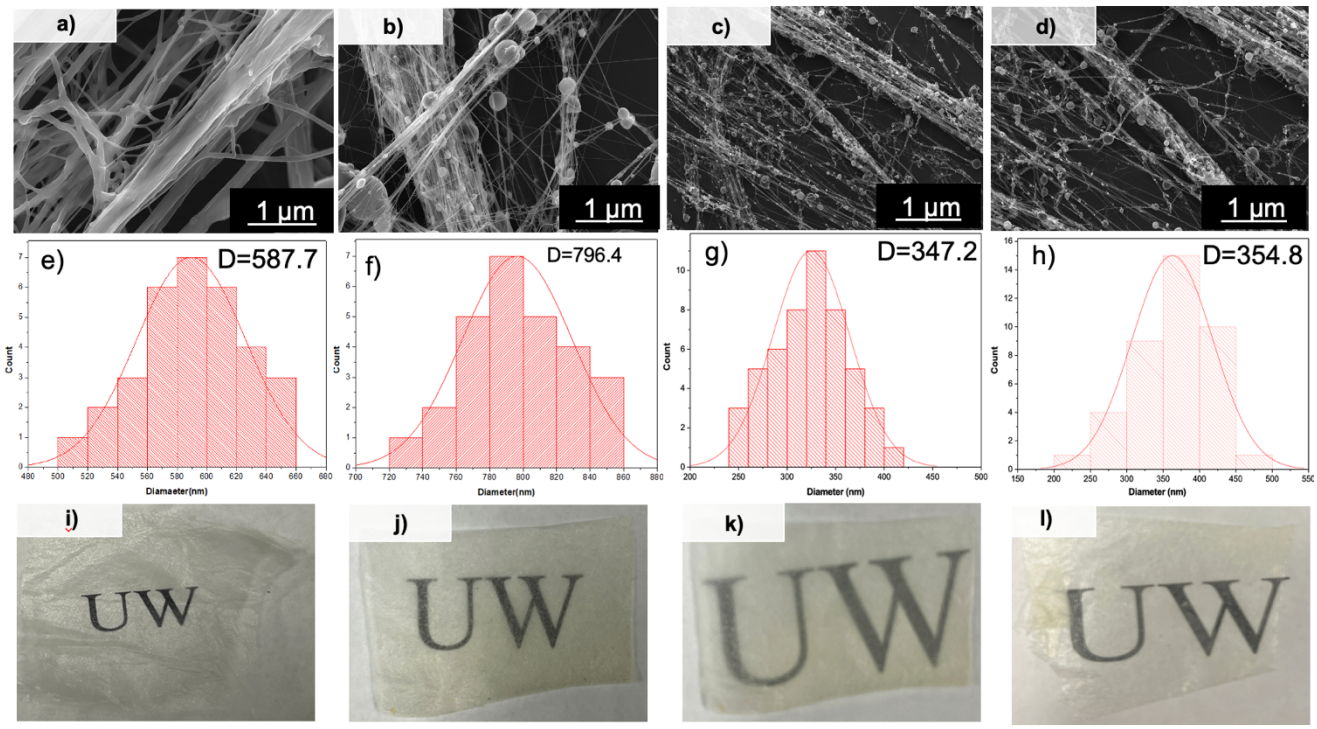


Figure 6.1 Demonstrates the morphology of the nanofibers, revealing uniform diameter distribution and smooth surface topography, which are critical for ensuring consistent drug release: (a) SEM image of control PVA-zein fibers without α-tocopherol; (b) SEM image of PZT-15 fibers with 15% α-tocopherol; (c) SEM image of PZT-30 fibers with 30% α-tocopherol showing a more pronounced and uniform distribution of particles on the fiber surface; and (d) SEM image of PZT-50 fibers loaded with 50% α-tocopherol, exhibiting the densest particle distribution, indicating a high loading level.**(e-h)** Fiber diameter distributions corresponding to images **(a-d),** respectively, with average diameters of 587.7 nm, 796.4 nm, 347.2 nm, and 354.8 nm. (**i-l**) depict pictures of fibrous mats.

6.9.2. ATR-FTIR and Rheology Analysis

ATR-FTIR was used to characterize the molecular interactions among the components in the nonwoven mat samples. The FTIR spectra of the PVA-Zein and α-tocopherol loaded fiber mats (**Figure 6.2a**) shows several peaks corresponding to the presence of zein: around 3300 cm^{-1} for OH/NH stretching vibrations, 1735 cm^{-1} for C=O stretching (amide I), and 1590 cm^{-1} for N-H bending (amide II) associated with the protein's aromatic ring [93,266]. These characteristic peaks confirm the presence of zein in the fibrous mats.

The spectra also reveal peaks indicative of the PVA component, such as the broad OH stretching band around 3300 cm^{-1}, which overlaps with the NH stretching of zein, and the peak at 1090

cm^{-1} corresponding to the C-O stretching vibrations[89,257]. Additionally, the spectra of the tα-tocopherol loaded samples (PZT-15, PZT-30, and PZT-50) display a peak at 1079 cm^{-1}, corresponding to the C-O-C stretching vibrations, and a peak around 690 cm^{-1}, which can be attributed to CH bending vibrations of the tocopherol molecule[61,205] that vary in intensity with their concentrations. These bands confirmed the successful incorporation of α-tocopherol into the fiber mats. Furthermore, the spectra showed that the intensity of the peaks varied with the concentration of α-tocopherol, indicating changes in the molecular interactions as a result of the concentrations within the fiber matrix. The characteristic bands of α-tocopherol were observed without significant shifts, suggesting that no new chemical bonds were formed between α-tocopherol and the PVA-Zein matrix during the solution blowing process. This observation indicates that the encapsulation process primarily involves physical entrapment rather than chemical interactions [202]. The presence of characteristic peaks from both α-tocopherol and the PVA-Zein matrix, along with the absence of significant peak shifts, suggests that the components retain their individual chemical structures, contributing to the overall functionality of the fibrous mats for wound dressing applications.

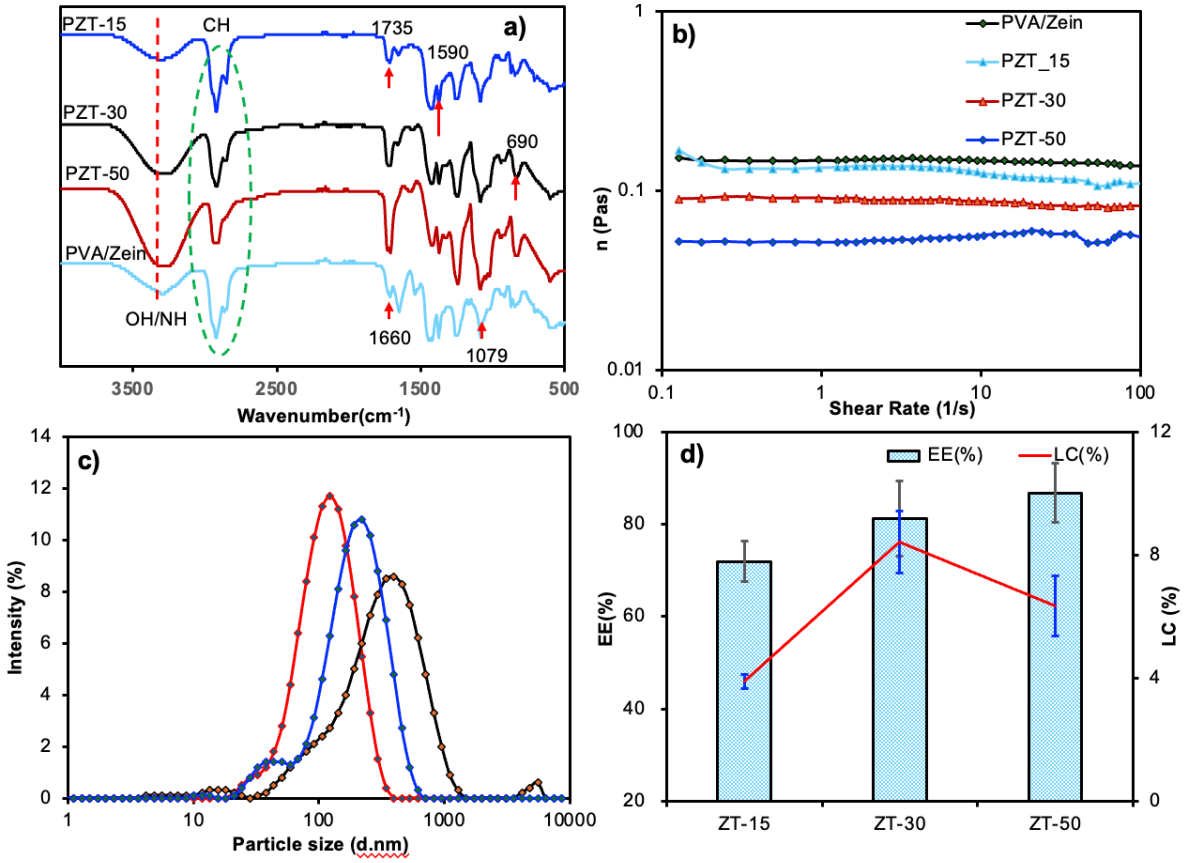


Figure 6.2*.ATR-FTIR and Rheological Analysis of PVA-Zein/α-tocopherol Fibrous Mats. (a) ATR-FTIR spectra of PVA-Zein and PVA-Zein/α-tocopherol fibrous mats with different α-tocopherol loadings (PZT-15, PZT-30, and PZT-50). The samples were analyzed over the wavenumber range of 500–4000 cm⁻¹ using an ATR-FTIR spectrometer (Thermo Nicolet 6700), and 64 scans were collected for each sample with a resolution of 4 cm⁻¹. Key peaks at 3300 cm⁻¹ (OH/NH stretching), 1735 cm⁻¹ (C=O stretching), and 1590 cm⁻¹ (N-H bending) are identified to confirm the presence of zein and PVA, while peaks at 1079 cm⁻¹ and 690 cm⁻¹ correspond to the C-O-C and CH bending vibrations of α-tocopherol.(b) Rheological profiles of PVA-Zein and PVA-Zein/α-tocopherol solutions (PZT-15, PZT-30, PZT-50) as a function of shear rate (0.01 to 100 s⁻¹), measured at 25 °C using a HAAKE Mars III rheometer with P20CSL parallel plates and a gap size of 0.46 mm. The solutions were prepared with 10 wt.% PVA in deionized water and varying concentrations of α-tocopherol-loaded zein nanoparticles (15%, 30%, and 50%).(c) Particle size distributions of α-tocopherol-loaded zein nanoparticles (ZT-15, ZT-30, ZT-50) showing unimodal distribution with increasing particle size at higher tocopherol concentrations.(d) Encapsulation efficiency (EE%) and Loading capacity (LC%) for α-tocopherol-loaded zein nanoparticles. ZT-50 exhibited the highest EE% (~92%) and LC%, with ZT-30 displaying (~10%) .*

The rheological properties of the PVA-Zein solutions loaded with varying concentrations of α-tocopherol (15%, 30%, and 50%) were analyzed to understand their behavior before the solution-blow spinning process. **Figure 6.2b** presents the rheological properties of (PZT-15, PZT-30, and PZT-50) solutions as a function of the shear rate. The viscosity measurements

indicate that all solutions display near-Newtonian behavior across the shear rate range of 0.1 to 100 s^{-1}, which is consistent with previous literature on consistent flow properties under varying shear conditions for most polymer solutions [267]. The control PVA-Zein solution showed the highest viscosity, whereas the addition of α-tocopherol resulted in a decrease in viscosity. Among the α-tocopherol-loaded solutions, the PZT-50 dispersion exhibited the lowest viscosity, followed by PZT-30 and PZT-15, which displayed relatively high viscosities. The observed reduction in viscosity with increasing tocopherol concentration can be attributed to the plasticizing effect of tocopherol, which enhances the mobility of polymer chains [259]. This behavior is beneficial for the solution blowing process, as it facilitates the formation of uniform and continuous fibers. Notably, the particle size distribution of tocopherol-loaded zein nanoparticles (ZT-15, ZT-30, and ZT-50) exhibited an unimodal distribution across all formulations, with the majority of particles clustered around the average particle size **(Figure 6.2c).** The particle size increased with increasing α-tocopherol content, indicating the influence of α-tocopherol on nanoparticle formation. This increase in size can be attributed to the variation in the precipitation efficiency of tocopherol during the fabrication process, resulting from the differences in its interaction with the zein matrix.

The encapsulation efficiency (EE%) and loading capacity (LC%) of α-tocopherol in the nanoparticles are shown in **(Figure 6.2d)**. ZT-50 exhibited the highest EE% at approximately 92%, while ZT-30 showed the highest LC% at around 10%. These results suggest that an intermediate α-tocopherol concentration provides optimal encapsulation efficiency and maximizes loading capacity [205,268].

6.9.3. Thermal properties, degradation behavior, and surface charge analysis of PVA-Zein/α-tocopherol nanofibrous mats

The thermal behavior of PVA-Zein/α-tocopherol fiber mats with different tocopherol contents (PZT-15, PZT-30, and PZT-50) is shown in **Figure 6.3a**. The DSC curve of the PVA-Zein

(control) matrix exhibited a broad endothermic transition at approximately 96 °C, which was associated with the glass transition temperature (Tg) of PVA and the release of absorbed water (due to the hygroscopic nature of PVA) [269]. This also suggests that the material is either amorphous or semi-crystalline [270]. The DSC curves for PZT-15, PZT-30, and PZT-50 showed progressively pronounced endothermic transitions toward lower temperatures with increasing tocopherol content, indicating stronger interactions and a plasticizing effect on the PVA matrix [271,272]. The DSC melting profiles are crucial for identifying the state of tocopherol and confirming that its incorporation into the fiber mats likely suppresses its crystallization, forming an amorphous complex with the polymer. This ensures sustained and controlled release of the drug, thus enhancing its therapeutic efficacy [273,274].

The physical state of an active pharmaceutical ingredient can significantly influence its bioavailability and stability, which is particularly relevant for fiber mats [258]. The absence of a sharp melting peak for tocopherol in the DSC profiles suggests that tocopherol existed in an amorphous or disordered crystalline phase within the polymer matrix. This amorphous state can be advantageous because it typically offers higher solubility and, consequently, better bioavailability in the wound area when used for wound healing applications [275]. **Figure 6.3b** shows the zeta potential measurements for zein nanoparticles, ZT-15, ZT-30, and ZT-50, which displayed approximately -31 mV, -27 mV, -24 mV, and -19 mV, respectively. The decrease in zeta potential was attributed to the deposition of α-tocopherol molecules on the surface of zein NPs. The deposited bioactive can prevent the adsorption of stabilizers, leading to electrostatic and hydrophobic interactions, and increasing the tendency of zein nanoparticles to aggregate [276]. Conversely, in this study, less α-tocopherol encapsulated in zein nanoparticles exhibited excellent colloidal stability, reducing the likelihood of nanoparticle aggregation within the PVA composite dispersion. Overall, the good stability of the nanoparticles ensured the formation of uniform fibrous mats and consistent bioactive release properties.

The weight loss profile (**Figure 6.3c**) and FTIR spectra (Figure 4d) highlight the degradation behavior of the PVA/Zein-α-tocopherol mats. Over a 24-hour period, PVA-Zein mats exhibited the highest weight loss, reaching 29%, indicating a faster degradation rate. In contrast, the α-tocopherol-loaded samples PZT-15, PZT-30, and PZT-50 showed lower weight loss percentages of 26%, 24%, and 19%, respectively. Among these, PZT-50 displayed the lowest degradation rate. The reduced weight loss in the PZT samples indicates that the incorporation of α-tocopherol enhances the structural stability of the mats, allowing for more controlled degradation. This property is beneficial for applications requiring sustained release of bioactive agents over time. The weight loss profiles observed in our study are consistent with the behavior reported for zein-based bio composites. For example, Wu et al., investigated the in vitro degradation of zein/PCL scaffolds in PBS. Their results showed that scaffolds containing higher zein content exhibited greater weight loss over time. After 28 days, zein/PCL scaffolds with 20% and 40% zein content exhibited 15% and 32% weight loss, respectively, highlighting that increased zein content accelerates degradation. This correlates with our findings, where the incorporation of α-tocopherol into PVA/Zein mats similarly modulated the degradation rates, indicating a controlled release mechanism [277].

The FTIR spectra **(Figure 6.3d)** further support this observation, highlighting the chemical structure changes over time. Characteristic peaks corresponding to hydroxyl (–OH) stretching around 3200–3500 cm^{-1} and amide I (C=O stretch) and amide II (N-H bend) bands around 1600–1700 cm^{-1} show slight shifts and intensity changes, indicating polymer hydrolysis and matrix breakdown. The C–H stretching bands around 2800-2900 cm^{-1} were monitored to evaluate the integrity of the polymer backbone over time. Across all samples, (PZT-15, PZT-30, PZT-50) demonstrated minimal changes in peak intensity in this region compared to PVAZein, suggesting that the inclusion of α-tocopherol and PVA contributes to enhanced structural stability and slower degradation of the aliphatic chains. Notably, PZT-50 retains more

of its characteristic peaks over time compared to PVA-Zein, correlating with its slower degradation rate observed in the weight loss data. These results confirm that the PZT samples undergo controlled and sustained degradation, making them effective candidates for wound healing applications with prolonged bioactive release.

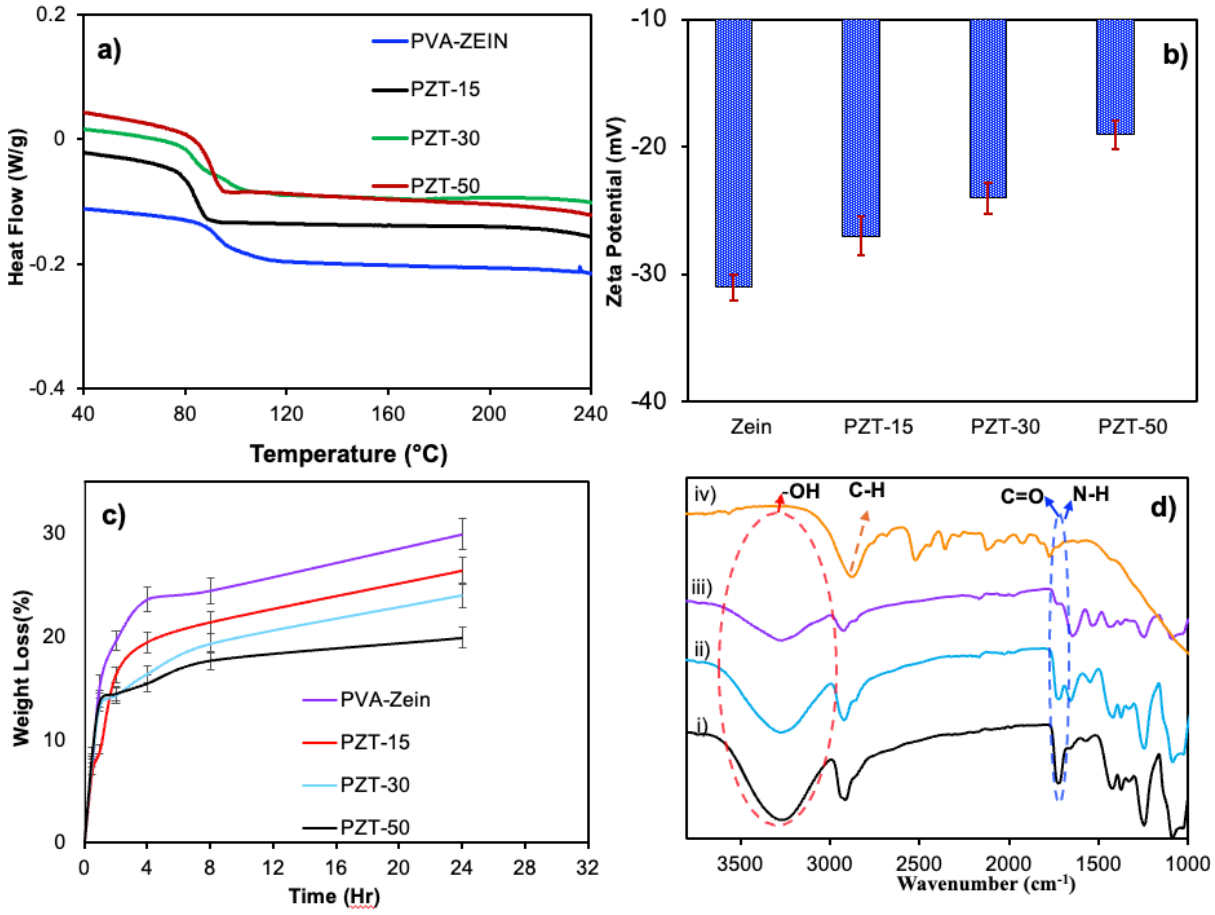


Figure 6.3. *Structural Characterization and Degradation Behavior of PVA/Zein-Tocopherol Nanofibrous Mats:(a) DSC Thermograms of PVA-Zein (control) and PZT-15, PZT-30, and PZT-50 fibrous mats were recorded using DSC (Discovery 2500, TA Instruments) over a temperature range of 26 to 260 °C at a heating rate of 10 °C/min under nitrogen atmosphere (50 mL/min). The thermograms depict the endothermic transitions corresponding to the glass transition temperature and thermal degradation.(b) Zeta Potential Measurements of zein nanoparticles and α-tocopherol-loaded samples (ZT-15, ZT-30, ZT-50) were determined in PBS solution (pH 7.4) at 25 °C using a Zetasizer Nano (Malvern Panalytical). The zeta potential values indicate surface charge changes with increasing α-tocopherol loading.(c) Weight Loss Profiles of PVA-Zein and PZT samples during immersion in PBS at pH 7.4 and 37 °C over 24 hours. Fiber mats were weighed at intervals of 0, 0.5, 1, 2, 4, 8, and 24 hours, and weight loss was calculated as a percentage of the initial mass.(d) FTIR Spectral Analysis of PVA-Zein, PZT-15, PZT-30, and PZT-50 over 24 hours of degradation in PBS. Key peaks were monitored for hydroxyl (–OH) stretching at 3200–3500 cm^{-1}, amide I (C=O stretching) and amide II (N-H bending) at 1600–1700 cm^{-1}, and C-H stretching bands at 2800–2900 cm^{-1} to evaluate chemical changes in the polymer backbone during degradation.*

6.9.4. Mechanical properties of nonwoven fibrous mats

The mechanical properties of the nonwoven fibrous mats were assessed via tensile testing, which revealed the stress-strain behavior of the mats (**Figure 6.4a)**. The mechanical properties of the control PVA-Zein fibers were found to be the lowest in terms of tensile strength and elongation at break, suggesting a limited performance. However, increasing the concentration of encapsulated α-tocopherol resulted in significant improvements in mechanical properties, particularly at higher concentrations of α-tocopherol. The tensile strength **(Figure 6.4b)** of the mats increased proportionally with the addition of the encapsulated α-tocopherol. The control PVA-Zein fibers displayed a tensile strength of approximately 0.74 MPa. In contrast, the tensile strength increased to 1.01 MPa, 1.24 MPa, and 1.57 MPa for fibrous mats with 15%, 30%, and 50% α-tocopherol, respectively. This trend indicates that encapsulated tocopherol with relatively rigid zein chains acts as a reinforcing filler, enhancing the load-bearing capacity of the fiber [261]. It is likely that the encapsulated tocopherol nanoparticles, which manifested as nano-beads in the fibers, could also have enhanced the fiber entanglements in the nonwoven mats, resulting in improved tensile properties. The tensile strength and elongation of the PVA-zein mats are comparable to those of synthetic wound dressings, indicating that our mats can provide the necessary mechanical support for wound sites [257].

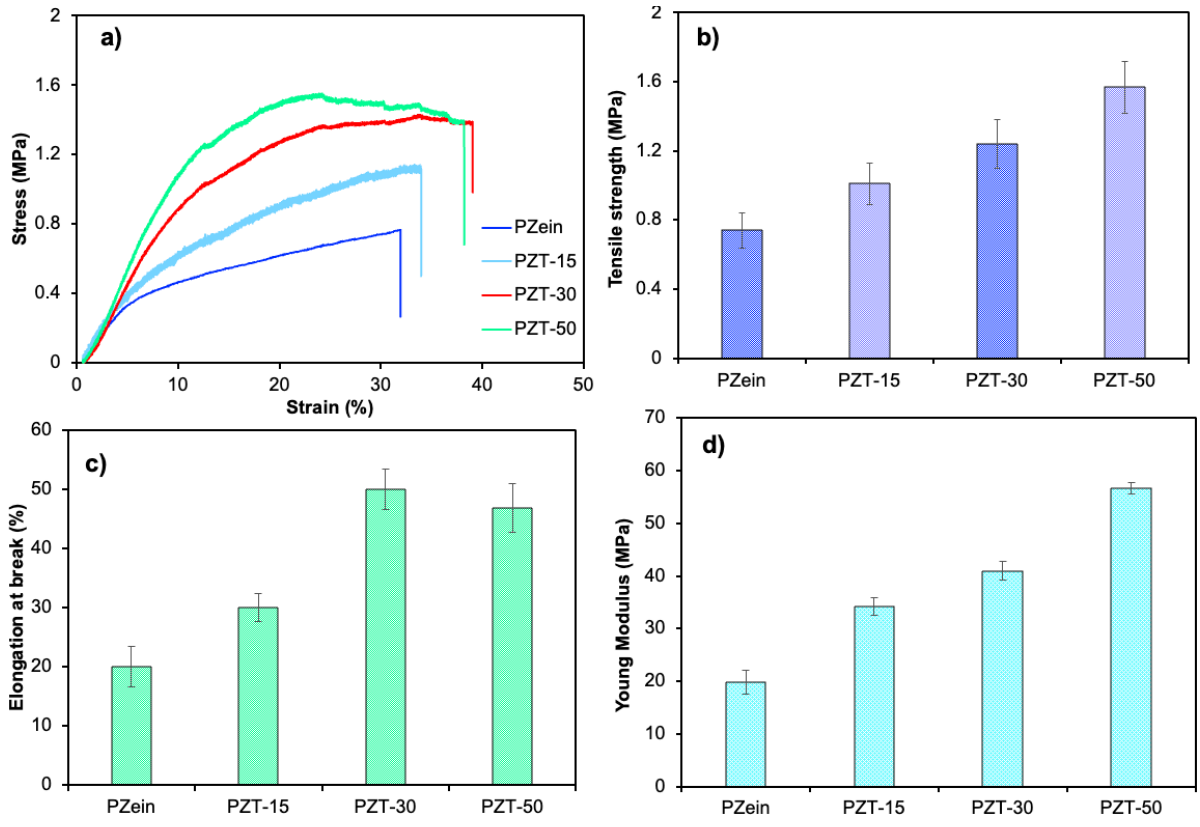


Figure 6.4. *Mechanical properties of nonwoven fiber mats from PVA-Zein loaded with α-tocopherol:(a) Stress-strain curves of PVA-Zein (control), PZT-15, PZT-30, and PZT-50 fiber mats, obtained through tensile testing using a Mandel-Shimadzu (AGS-X) tensile tester with a 0.5 kN load cell. The gauge length was set to 15 mm, and the test speed was 1 mm/min. (b) Tensile strength of the nonwoven fiber mats measured under the same conditions. Five samples were tested per group, and the mean values are presented with standard deviations.(c) Elongation at break, calculated as the percentage of elongation relative to the original length of the mats under tensile loading.(d) Young's modulus, which represents the stiffness of the fiber mats, was calculated as the slope of the linear portion of the stress-strain curve for each sample. PZT-15, PZT-30, and PZT-50 indicate fibers loaded with 15%, 30%, and 50% α-tocopherol, respectively.*

Similarly, elongation at break **(Figure 6. 4c)** was positively correlated with the α-tocopherol content. The control PVA-Zein fibers had an elongation at break of approximately 20%, whereas the PZT-15, PZT-30, and PZT-50 fibers had elongations of 30, 50, and 47%, respectively. This increase in flexibility in conjunction with improvement in tensile strength is indicative of enhancement in toughness, which is beneficial for wound dressing applications [278]. Additionally, Young's modulus **(Figure 6.4d)** values increased with increasing α-tocopherol content. The control PVA-Zein fibers had a Young's modulus of approximately

19.82 MPa. With the addition of 15, 30, and 50% α-tocopherol, the Young's modulus increased to 34, 41, and 57 MPa, respectively. This suggests that zein not only enhances the encapsulation efficiency of α-tocopherol but also increases the rigidity of the baseline fibers [61,92].

6.9.5. Tocopherol release kinetics from nonwoven fibrous mats

The cumulative release kinetics of α-tocopherol from nonwoven fibrous mats composed of PVA-Zein loaded with different concentrations of α-tocopherol (PZT-15, PZT-30, and PZT-50) were evaluated for 24 h, as shown in **Figure 6. 5a.** All formulations exhibited substantial release of the encapsulated substance within the initial 2 h, amounting to approximately 40% of the tocopherol bioactive molecules, which typically accumulate on the fiber surface during the solution blow process. This initial burst is crucial because it is essential to eliminate interfering bacteria before they proliferate to enhance wound healing, as tocopherol has antimicrobial properties [279]. Subsequently, progressively steady, and stable release was observed over the following 24 h for all samples (PZT-15, PZT-30, and PZT-50), amounting to approximately 70%, 76%, and 84%, respectively, for up to 24 h. The sustained and continuous release characteristics of α-tocopherol-loaded PVA-Zein fibrous mats are consistent with the advantages of zein encapsulation efficiency and lower hydrophilicity, which enable prolonged and sustained release, resulting in improved therapeutic effects of α-tocopherol [271]. Furthermore, the sustained release of α-tocopherol over time implies potential benefits in managing oxidative stress in chronic wounds, contributing to accelerated wound healing and reduced inflammation.

Additionally, the release mechanism of α-tocopherol from PVA-zein fibrous mats was studied using four kinetic models **Figure 6.5(b-d)**. This was performed to understand the underlying processes involved in the release of bioactive compounds from fibrous mats [280].

The release kinetics of the PZT-15, PZT-30, and PZT-50 samples were most effectively represented by the Korsmeyer-Peppas model and Higuchi models that provided a suitable fit,

suggesting a sustained release, which indicated a combination of diffusion and polymer relaxation mechanisms. In contrast, the release kinetics of PZT-15, PZT-30, and PZT-50 did not adhere to zero-order and first-order release dynamics. A more accurate explanation for the observed release behavior was provided by the Higuchi and Korsmeyer-Peppas models, as their plots exhibited a high degree of linearity [257]. The Higuchi model appeared to provide the best fit. The faster release rate of α-tocopherol in the PZT-15 mats compared to the PZT-30 and PZT-50 mats can be attributed to their smaller fiber diameter and increased surface area, facilitating greater diffusion of the encapsulated bioactive compound. The release mechanism was mathematically represented as a function of the diffusion exponent (n), and the release of α-tocopherol followed the Fickian diffusion (n = 0.4) with good accuracy. This observation highlights that the PVA-zein fibrous mats containing α-tocopherol demonstrate a controlled release pattern, making them suitable for use in wound dressings where sustained release of bioactive agents is beneficial. Research indicates that the size of drug-loaded nanoparticles significantly influences their release kinetics and therapeutic efficacy in wound healing. Nanoparticles of smaller dimensions exhibit a higher surface area-to-volume ratio, resulting in accelerated initial drug release and enhanced cellular uptake, which is advantageous for immediate treatment [281]. In contrast, larger nanoparticles (>100 nm) provide a more sustained release, ideal for prolonged delivery[282]. In our study, the α-tocopherol-loaded zein nanoparticles (average size 347 nm) exhibited a biphasic release: an initial burst followed by sustained release. Overall, the controlled release of α-tocopherol from the PVA-zein nonwoven mats is facilitated by the structural properties of the zein nanoparticles and their incorporation within the PVA matrix. Zein, a hydrophobic prolamin protein, encapsulates α-tocopherol, creating a barrier that controls the diffusion rate of the drug. The PVA matrix modulates the release by providing an additional layer of control over the swelling and degradation properties of the mats. This combined system enables a biphasic release profile an initial burst for

immediate therapeutic effects followed by sustained release for prolonged wound healing [19]. The relevant parameters calculated for tocopherol release are summarized in **Table D1**, and the calibration curve is shown in the supporting **Figure D1**.

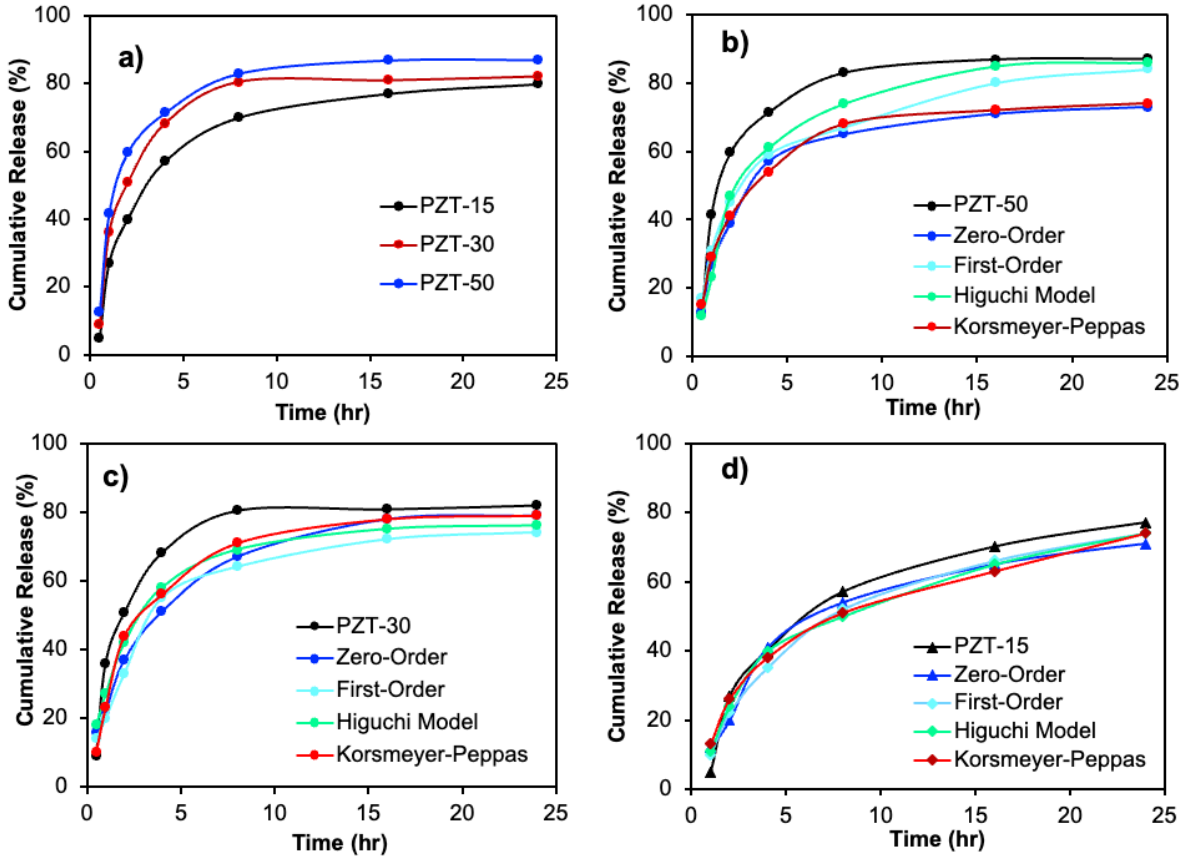


Figure 6.5. *Release Kinetics of α-tocopherol from PVA-Zein/α-tocopherol Fibrous Mats: (a) Cumulative release profiles of α-tocopherol from PZT-15, PZT-30, and PZT-50 fibrous mats over 24 hours. Samples were incubated in 2 mL of phosphate-buffered saline (0.01 M PBS) (pH 7.4) at 37°C with constant agitation (100 rpm) section 2.6. Tocopherol release was quantified using UV-visible spectrophotometry at 292 nm. Three replicates were analyzed for each sample, and the cumulative release was calculated as a percentage of the total tocopherol loaded in the mats. (b) Release kinetics of PZT-50 fitted to zero-order, first-order, Higuchi, and Korsmeyer-Peppas models. (c) Release kinetics of PZT-30 analyzed using the same models as in (b).(d) Release kinetics of PZT-15, also fitted to zero-order, first-order, Higuchi, and Korsmeyer-Peppas models. The best-fit model for each formulation was selected based on the highest correlation coefficient (R^2). The release was driven primarily by Fickian diffusion and polymer relaxation, with initial burst release followed by sustained release. This data supports the potential for controlled therapeutic delivery in wound healing applications.*

6.9.6. Cell Viability and Cytotoxicity Study

A comparative analysis of cell viability on cells cultured with sample extracts of PVA-Zein, PZT-15, PZT-30, and PZT-50 revealed that most cells on the well plate remained viable after 24 h of culture in the sample extract solution **(Figure 6.6a).** No significant cell death was observed in cell populations incubated with the three different ratios of PZT sample extracts (95.95%, 94.8%, and 96.65% live cell population in PZT-15, PZT-30, and PZT-50, respectively), when compared with the live cell population of the positive controls of cells incubated with fresh culture media (97.8%) and PVA-Zein sample extract (95.95%) (**Figure 6.6c**). Notably, the majority of cells maintained fibroblast morphology and were well spread on PZT-15, PZT-30, and PZT-50 sample extracts when compared to TCPS and PVA-Zein **Figure 6. 6 (a-b**).

Zein a plant-derived corn protein, has been studied for its ability to mimic the structure and function of natural extracellular matrix (ECM) proteins by promoting cell-substrate interactions, modulating intracellular signaling cascades involved in cell spreading and migration, and exhibiting antimicrobial properties [26,283]. In contrast, α-tocopherol, a potent antioxidant known for its protective effects against oxidative stress, can modulate signaling pathways involved in cell proliferation, adhesion, and immune response processes and has an anti-inflammatory effect [284–286]. As a result, the presence of zein can stimulate fibroblasts to produce ECM components essential for tissue repair and regeneration, whereas α-tocopherol can support the stability of newly synthesized ECM components by protecting them from oxidative degradation. Moreover, the biocompatible zein protein provides a conducive environment for cell adhesion[6] while α-tocopherol helps maintain cellular integrity and function [287], by promoting cell spreading and the formation of a stable cell layer. Therefore, the combined presence of α-tocopherol and zein protein can elicit synergistic effects on cellular

responses, offering benefits for wound healing such as enhanced cell migration, spreading, proliferation, modulation of the inflammatory response, and tissue regeneration.

The cytotoxicity was determined using the alamarBlue cell viability assay at 24 h (**Figure 6. 6d**). The normalized cell viability % of NIH3T3 cultured with extracts of PVA-Zein, PZT-15, PZT-30, and PZT-50 were 100.3 ± 2.7%, 90 ± 6%, 103.3 ± 6% and 106 ± 7%, respectively at 24 h. These results align with the ISO 10993-5:2009 standards for the biological evaluation of medical devices and materials, which suggest that cell viability exceeding 70% can be considered noncytotoxic [288]. All three PZT samples appeared to be promising and safe materials for wound healing studies. Compared to conventional wound dressings like gauze and hydrocolloids, our PVA-zein/α-tocopherol fiber mats demonstrate enhanced functionality through sustained drug release and biocompatibility. While synthetic polymer dressings such as PLGA have certain advantages, the unique antioxidant release profile and scalability of our mats provide a novel approach to wound care.

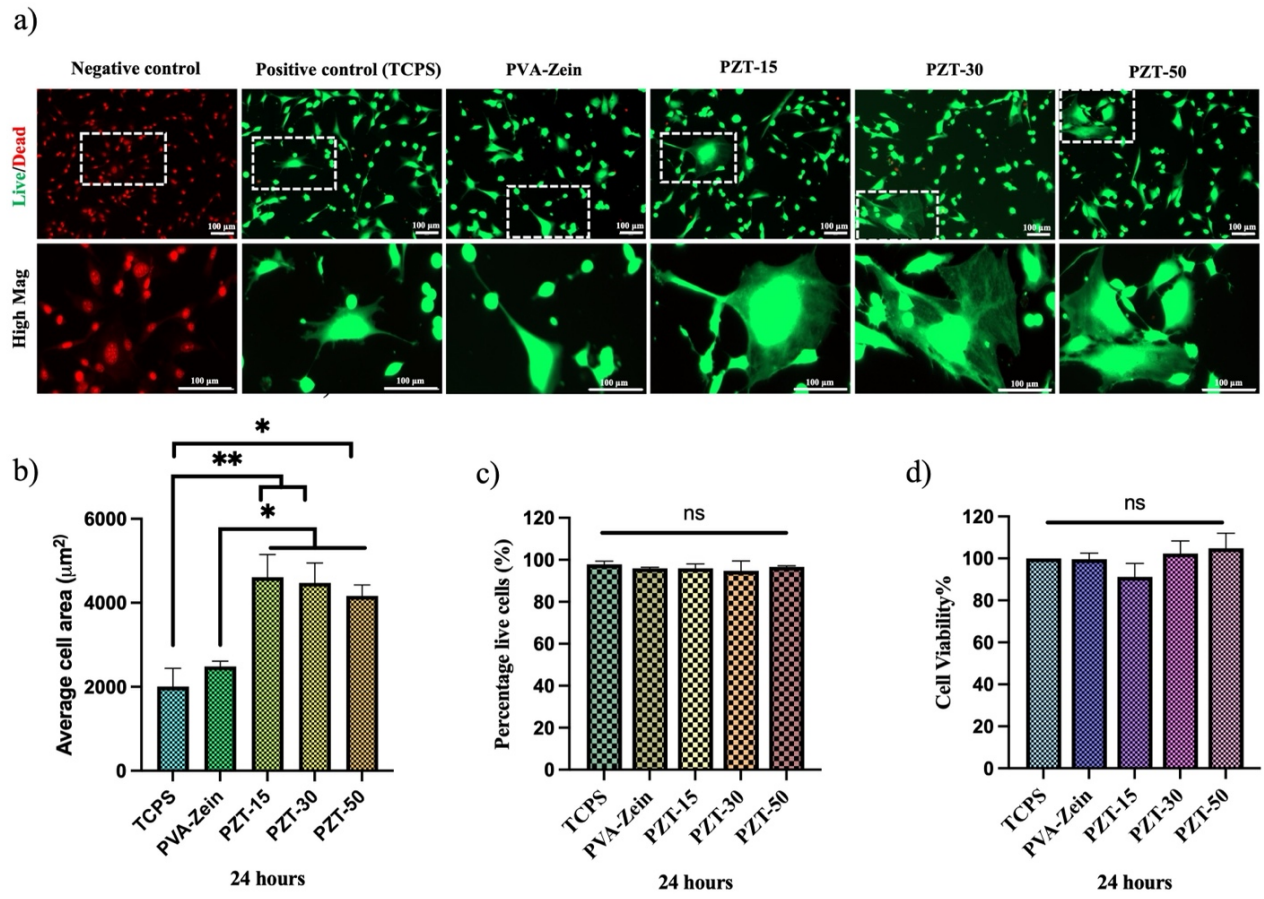


Figure 6 .6. Cell Viability and Cytotoxicity Studies (a) Representative fluorescence microscopy images of Live/Dead staining of NIH3T3 cells cultured with extracts from PVA-Zein, PZT-15, PZT-30, and PZT-50 at 24 h. Ethanol-treated cells served as a negative control and cells on tissue culture polystyrene (TCPS) with culture media served as a positive control. Cells were stained with calcein-AM for live cells (green fluorescence) and ethidium homodimer-1 for dead cells (red fluorescence). Scale bar = 100 µm. (b) Average cell area (20 cells from 2 samples were counted for each group). n = 2, * and ** indicate a significant difference using one-way ANOVA with $p < 0.05$ and $p < 0.01$, respectively. Scale bar = 100 µm. (c) Percentage of live cells after 24 h (n = 2). (d) Percentage of cell viability at 24 h in cells treated with extracts from PZ, PZT-15, PZT-30, and PZT-50 samples and cells cultured on TCPS (positive control) with culture media (cell viability % of all the samples at 24 h were normalized to TCPS positive control). n = 3, 'ns' indicates no significant difference using ordinary one-way ANOVA with Tukey's multiple comparison test.

6.10. Concluding Remarks

The present study aimed to develop biocompatible bioactive carriers in the form of nonwoven PVA-zein/α-tocopherol fiber mats suitable for wound dressing applications. The use of PVA-zein as a carrier of α-tocopherol offers unique advantages. Zein, a plant-derived protein, mimics the structure and function of natural extracellular matrix (ECM) proteins, promoting cell-substrate interactions and supporting cell spreading and migration. The amphiphilic nature of zein aids the uniform dispersion of α-tocopherol, enhancing its stability and bioavailability. Solution blowing was chosen because of its ability to rapidly produce uniform, high-quality nonwovens on an industrial scale. α-Tocopherol was used as the model bioactive compound, known for its potent antioxidant properties and ability to enhance wound healing. The fibrous mats exhibited a uniform morphology, improved thermal and mechanical properties, with a higher α-tocopherol content. These fibrous mats demonstrated a controlled release profile, characterized by an initial burst followed by a sustained release of α-tocopherol over 24 hours, ensures an immediate therapeutic effect followed by a sustained presence of the bioactive compound, supporting continuous healing. Cytotoxicity assays confirmed high cell viability (>90%) and enhanced cell spreading, highlighting the excellent biocompatibility of mats. The novel PVA-zein/α-tocopherol nonwoven fibrous mats developed in this study hold great promise for use in various single-use biomedical products, including wound dressings. Overall, while this study highlight the potential these fibrous mats potential in wound healing applications. Future work could focus on optimizing fiber composition to further enhance antimicrobial properties. Additionally, in vivo studies will be essential to confirm the clinical efficacy of the α-tocopherol release and its impact on wound healing.

Chapter 7. Conclusions and Future Work

7.1. Conclusions

This dissertation explored the modification, blending, and application of zein-based biopolymers to address sustainability challenges in packaging and biomedical applications. The inherent limitations of zein, including poor processability, weak mechanical properties, and low thermal stability, were systematically addressed through chemical modifications, polymer blending, and development of bioactive delivery systems.

Initially, zein was chemically modified via esterification using fatty acids of varying chain lengths (C6, C10, and C16), aiming to enhance processability, mechanical properties, and hydrophobicity. The surface properties, rheology, and chemical structure were extensively characterized using FTIR and 13C-NMR spectroscopy. Modified zein exhibited improved melt-processability and increased tensile strength, particularly with decanoic acid, which also decreased water absorption, making it viable for sustainable packaging applications. The fatty acid chains acted as internal plasticizers, improving film flexibility and durability.

The second focus was on creating zein-based blends with poly(butylene adipate-co-terephthalate) (PBAT) to develop biodegradable films. Melt extrusion facilitated the fabrication of mZein/PBAT films with varying compositions, where optimal properties were observed in a blend containing 30 wt% mZein and 70 wt% PBAT. This composition achieved tensile strength of 10.88 MPa, elongation at break of 561.41%, and an elastic modulus of 105.63 MPa. The enhanced oxygen and moisture barrier properties, alongside improved disintegration, indicate that these blends can serve as effective biodegradable packaging materials, reducing reliance on conventional plastics.

The third investigation involved zein nanoparticles (ZNPs) synthesized through an antisolvent co-precipitation method using green solvents (water and ethanol). These nanoparticles co-

encapsulated quercetin and α-tocopherol, achieving high encapsulation efficiency (up to 96%) and controlled particle sizes (50-320 nm). The ZNPs provided sustained release of quercetin (79.7%) and α-tocopherol (60.4%) over 8 hours, highlighting their potential as bioactive delivery systems for pharmaceuticals, nutraceuticals, and functional food applications. Molecular interactions, including hydrogen bonding and hydrophobic forces, contributed to the stability and controlled release of the bioactive compounds.

Lastly, the fabrication of α-tocopherol-encapsulated nonwoven fiber mats composed of poly(vinyl alcohol) (PVA) and zein was achieved using solution blow spinning. The fiber mats displayed uniform morphology (350-796 nm in diameter), improved tensile strength, and sustained α-tocopherol release over 24 hours. Cytotoxicity studies demonstrated high cell viability (>90%), confirming their biocompatibility and potential as wound dressings for therapeutic delivery.

The results collectively enhance the functional properties and expand the application potential of zein as a sustainable biopolymer. This work provides a new framework for zein functionalization through chemical modifications, blending, and scalable production, enabling applications in sustainable packaging and bioactive delivery in pharmaceuticals and biomedical devices.

7.2. Recommendations and Future Work

The following future work is recommended to further enhance the functional properties of zein-based biopolymers and expand their applications across packaging, pharmaceutical delivery, and biomedical sectors.

In chapter 3, further exploration into alternative chemical modification techniques, such as cross-linking and graft copolymerization, could enhance the mechanical, thermal, and barrier properties of zein, broadening its applicability. These additional modification routes could be systematically compared to the esterification process discussed in this thesis, providing insight into the most effective methods for optimizing zein's performance for targeted applications.

In Chapter 4, it was found that mZein/PBAT blends demonstrated improved mechanical and barrier properties suitable for sustainable packaging. However, further work can be done: One critical area for future work is the scalable production of these zein-based blends. Research should focus on optimizing processing parameters during extrusion, including temperature profiles, shear rates, and screw configurations. These optimizations will enhance blend homogeneity and interfacial adhesion, potentially increasing mechanical strength and film uniformity. Beyond PBAT, the blending of modified zein (mZein) with other biodegradable polymers such as polylactic acid (PLA), polycaprolactone (PCL), or poly(3-hydroxybutyrate) (PHB) should be explored. PHB, in particular, offers promising biodegradability and thermal stability, making it an ideal candidate for improving the material properties and expanding the range of applications of mZein-based blends. Future studies should investigate the compatibility, mechanical properties, and degradation behavior of these blends to optimize their performance for practical applications. This will allow a comprehensive understanding of blend compatibility and structure-property relationships, potentially leading to biodegradable composites with tailored mechanical and barrier properties suitable for a wide range of packaging and agricultural applications. Given the global focus on sustainability,

understanding the end-of-life behavior of these mZein blends is crucial. Future research should conduct biodegradability studies under different environmental conditions (e.g., soil, marine, compost) to establish their ecological impact. Such studies will confirm the potential of these blends as sustainable alternatives to traditional plastic films.

Chapter 5 explored the use of zein nanoparticles (ZNPs) for the co-encapsulation and controlled release of bioactive compounds. To maximize their therapeutic potential and expand their applications. Further work is needed to enhance the functionality of ZNPs by exploring surface modifications, such as PEGylation or conjugation with targeting ligands. Such modifications would improve the stability of the nanoparticles in physiological environments and enable site-specific delivery for pharmaceutical and nutraceutical applications. The encapsulation efficiency, particle size control, and release kinetics of ZNPs should be studied for a broader range of bioactive molecules, including hydrophilic compounds, proteins, and peptides. This will help tailor the nanoparticles for applications in different fields, such as drug delivery, functional foods, and active packaging, providing a wider scope of potential commercial uses. Stability of ZNPs during storage and in various environmental conditions (e.g., temperature, pH, light exposure) must be rigorously assessed. Stability testing will ensure that encapsulated bioactives retain their potency and that release profiles remain controlled and predictable for potential commercial and pharmaceutical products.

Chapter 6 provided insights into the fabrication of nonwoven fiber mats comprising PVA and zein encapsulated with α-tocopherol. To enhance the biomedical utility of these materials, several key areas should be explored. To further improve the mats' mechanical robustness and flexibility, future work should explore different solution blow spinning parameters, such as polymer concentration, airflow rate, and nozzle configurations. Alternative spinning techniques, like electrospinning, may allow better control over fiber diameter and distribution, leading to fibers with uniform morphology and enhanced mechanical strength[131].

Expanding the encapsulation capability of the mats to include multiple bioactive compounds (e.g., antimicrobial agents, anti-inflammatory drugs) will enhance their multifunctionality and therapeutic potential for wound healing.

The controlled release kinetics of these agents should be carefully optimized to match the requirements of different wound healing stages, enabling comprehensive and sustained therapeutic effects. While in-vitro cytotoxicity tests indicated the biocompatibility of the mats, in-vivo studies on animal models are critical for validating their wound healing efficacy, biocompatibility, and regenerative properties. These studies will help assess tissue integration, wound closure rates, and potential immune responses, providing essential data for translating the mats into clinical use.

References

1. Cózar, A.; Echevarría, F.; González-Gordillo, J.I.; Irigoien, X.; Úbeda, B.; Hernández-León, S.; Palma, Á.T.; Navarro, S.; García-de-Lomas, J.; Ruiz, A.; et al. Plastic Debris in the Open Ocean. *Proc Natl Acad Sci U S A* **2014**, *111*, 10239–10244, doi:10.1073/pnas.1314705111.
2. Macleod, M.; Peter, H.; Arp, H.; Tekman, M.B.; Jahnke, A. *The Global Threat from Plastic Pollution*;
3. Wu, F.; Misra, M.; Mohanty, A.K. Challenges and New Opportunities on Barrier Performance of Biodegradable Polymers for Sustainable Packaging. *Prog Polym Sci* 2021, *117*.
4. Yuan, Z.; Nag, R.; Cummins, E. Human Health Concerns Regarding Microplastics in the Aquatic Environment - From Marine to Food Systems. *Science of the Total Environment* 2022, *823*.
5. Laycock, B.; Nikolić, M.; Colwell, J.M.; Gauthier, E.; Halley, P.; Bottle, S.; George, G. Lifetime Prediction of Biodegradable Polymers. *Prog Polym Sci* 2017, *71*.
6. da Silva, A.C.; Córdoba de Torresi, S.I. Advances in Conducting, Biodegradable and Biocompatible Copolymers for Biomedical Applications. *Front Mater* 2019, *6*.
7. Corradini, E.; Curti, P.S.; Meniqueti, A.B.; Martins, A.F.; Rubira, A.F.; Muniz, E.C. Recent Advances in Food-Packing, Pharmaceutical and Biomedical Applications of Zein and Zein-Based Materials. *Int J Mol Sci* 2014, *15*, 22438–22470.
8. Xiuli, W.; Yurong, Z.; Yuzhong, W. Recent Progress in Starch-Based Polymeric Materials. *Acta Polymerica Sinica* **2011**, doi:10.3724/SP.J.1105.2011.10249.
9. Ojogbo, E.; Ogunsona, E.O.; Mekonnen, T.H. Chemical and Physical Modifications of Starch for Renewable Polymeric Materials. *Materials Today Sustainability* 2020, *7–8*.
10. Mekonnen, T.; Mussone, P.; Khalil, H.; Bressler, D. Progress in Bio-Based Plastics and Plasticizing Modifications. *J Mater Chem A Mater* **2013**, *1*, doi:10.1039/c3ta12555f.
11. Anderson, T.J.; Lamsa, B.P. Zein Extraction from Corn, Corn Products, and Coproducts and Modifications for Various Applications: A Review. *Cereal Chem* 2011, *88*.
12. Shi, K.E.; Huang, Y.; Yu, H.; Lee, T.-C.; Huang, Q. Reducing the Brittleness of Zein Films through Chemical Modification. *J. Agric. Food Chem* **2011**, *59*, 56–61, doi:10.1021/jf103164r.
13. Wu, Q.; Yoshino, T.; Sakabe, H.; Zhang, H.; Isobe, S. Chemical Modification of Zein by Bifunctional Polycaprolactone (PCL). *Polymer (Guildf)* **2003**, *44*, doi:10.1016/S0032-3861(03)00314-8.
14. Wei, B.; Zhao, Y.; Wei, Y.; Yao, J.; Chen, X.; Shao, Z. Morphology and Properties of a New Biodegradable Material Prepared from Zein and Poly(Butylene Adipate-Terephthalate) by Reactive Blending. *ACS Omega* **2019**, *4*, 5609–5616, doi:10.1021/acsomega.9b00210.
15. Zhang, L.; Liu, Z.; Wang, X.; Dong, S.; Sun, Y.; Zhao, Z. The Properties of Chitosan/Zein Blend Film and Effect of Film on Quality of Mushroom (Agaricus Bisporus). *Postharvest Biol Technol* **2019**, *155*, doi:10.1016/j.postharvbio.2019.05.013.

16. Corradini, E.; Curti, P.S.; Meniqueti, A.B.; Martins, A.F.; Rubira, A.F.; Muniz, E.C. Recent Advances in Food-Packing, Pharmaceutical and Biomedical Applications of Zein and Zein-Based Materials. *Int J Mol Sci* 2014, *15*, 22438–22470.
17. Yan, X.; Li, M.; Xu, X.; Liu, X.; Liu, F. Zein-Based Nano-Delivery Systems for Encapsulation and Protection of Hydrophobic Bioactives: A Review. *Front Nutr* 2022, *9*.
18. Rodríguez-Félix, F.; Del-Toro-Sánchez, C.L.; Javier Cinco-Moroyoqui, F.; Juárez, J.; Ruiz-Cruz, S.; López-Ahumada, G.A.; Carvajal-Millan, E.; Castro-Enríquez, D.D.; Barreras-Urbina, C.G.; Tapia-Hernández, J.A. Preparation and Characterization of Quercetin-Loaded Zein Nanoparticles by Electrospraying and Study of In Vitro Bioavailability. *J Food Sci* **2019**, *84*, doi:10.1111/1750-3841.14803.
19. Bonferoni, M.C.; Riva, F.; Invernizzi, A.; Dellera, E.; Sandri, G.; Rossi, S.; Marrubini, G.; Bruni, G.; Vigani, B.; Caramella, C.; et al. Alpha Tocopherol Loaded Chitosan Oleate Nanoemulsions for Wound Healing. Evaluation on Cell Lines and Ex Vivo Human Biopsies, and Stabilization in Spray Dried Trojan Microparticles. *European Journal of Pharmaceutics and Biopharmaceutics* **2018**, *123*, doi:10.1016/j.ejpb.2017.11.008.
20. Guo, Y.; Liu, Z.; An, H.; Li, M.; Hu, J. Nano-Structure and Properties of Maize Zein Studied by Atomic Force Microscopy. *J Cereal Sci* **2005**, *41*, doi:10.1016/j.jcs.2004.12.005.
21. Wang, M.; Li, D.; Li, J.; Li, S.; Chen, Z.; Yu, D.G.; Liu, Z.; Guo, J.Z. Electrospun Janus Zein–PVP Nanofibers Provide a Two-Stage Controlled Release of Poorly Water-Soluble Drugs. *Mater Des* **2020**, *196*, doi:10.1016/j.matdes.2020.109075.
22. Amjadi, S.; Gholizadeh, S.; Ebrahimi, A.; Almasi, H.; Hamishehkar, H.; Taheri, R.A. Development and Characterization of the Carvone-Loaded Zein/Pullulan Hybrid Electrospun Nanofibers for Food and Medical Applications. *Ind Crops Prod* **2022**, *183*, doi:10.1016/j.indcrop.2022.114964.
23. Rees, E.D.; Singer, S.J. A Preliminary Study of the Properties of Proteins in Some Nonaqueous Solvents. *Arch Biochem Biophys* **1956**, *63*, doi:10.1016/0003-9861(56)90018-2.
24. Shukla, R.; Cheryan, M. Zein: The Industrial Protein from Corn. *Ind Crops Prod* **2001**, *13*, doi:10.1016/S0926-6690(00)00064-9.
25. Kriz, A.L.; Larkins, B.A.; Fraley, R.T.; Jones, T.J. *Molecular Genetic Approaches to Maize Improvement*; 2008;
26. Shi, W.; Dumont, M.J. Review: Bio-Based Films from Zein, Keratin, Pea, and Rapeseed Protein Feedstocks. *J Mater Sci* 2014, *49*.
27. Dong, S.; Guo, P.; Chen, Y.; Chen, G. yun; Ji, H.; Ran, Y.; Li, S. hong; Chen, Y. Surface Modification via Atmospheric Cold Plasma (ACP): Improved Functional Properties and Characterization of Zein Film. *Ind Crops Prod* **2018**, *115*, doi:10.1016/j.indcrop.2018.01.080.
28. Gagliardi, A.; Voci, S.; Paolino, D.; Fresta, M.; Cosco, D. Influence of Various Model Compounds on the Rheological Properties of Zein-Based Gels. *Molecules* **2020**, *25*, doi:10.3390/molecules25143174.
29. Xu, Y.; Wei, Z.; Xue, C.; Huang, Q. Assembly of Zein–Polyphenol Conjugates via Carbodiimide Method: Evaluation of Physicochemical and Functional Properties. *LWT* **2022**, *154*, doi:10.1016/j.lwt.2021.112708.

30. Raza, A.; Hayat, U.; Bilal, M.; Iqbal, H.M.N.; Wang, J.Y. Zein-Based Micro- and Nano-Constructs and Biologically Therapeutic Cues with Multi-Functionalities for Oral Drug Delivery Systems. *J Drug Deliv Sci Technol* 2020, *58*.
31. Sun, Y.; Wei, Z.; Xue, C. Development of Zein-Based Nutraceutical Delivery Systems: A Systematic Overview Based on Recent Researches. *Food Hydrocoll* 2023, *137*.
32. Wei, Y.; Hu, L.; Yao, J.; Shao, Z.; Chen, X. Facile Dissolution of Zein Using a Common Solvent Dimethyl Sulfoxide. **2019**, doi:10.1021/acs.langmuir.9b00670.
33. Matsushima, N.; Danno, G.I.; Takezawa, H.; Izumi, Y. Three-Dimensional Structure of Maize α-Zein Proteins Studied by Small-Angle X-Ray Scattering. *Biochimica et Biophysica Acta (BBA) - Protein Structure and Molecular Enzymology* **1997**, *1339*, 14–22, doi:10.1016/S0167-4838(96)00212-9.
34. Giteru, S.G.; Ali, M.A.; Oey, I. Recent Progress in Understanding Fundamental Interactions and Applications of Zein. *Food Hydrocoll* 2021, *120*.
35. Momany, F.A.; Sessa, D.J.; Lawton, J.W.; Selling, G.W.; Hamaker, S.A.H.; Willett, J.L. Structural Characterization of α-Zein. *J Agric Food Chem* **2006**, *54*, doi:10.1021/jf058135h.
36. Zhang, X.; Dong, C.; Hu, Y.; Gao, M.; Luan, G. Zein as a Structural Protein in Gluten-Free Systems: An Overview. *Food Science and Human Wellness* 2021, *10*.
37. Wang, Y.; Padua, G.W. Formation of Zein Microphases in Ethanol-Water. *Langmuir* **2010**, *26*, doi:10.1021/la101688v.
38. Tapia-Hernández, J.A.; Rodríguez-Felix, F.; Juárez-Onofre, J.E.; Ruiz-Cruz, S.; Robles-García, M.A.; Borboa-Flores, J.; Wong-Corral, F.J.; Cinco-Moroyoqui, F.J.; Castro-Enríquez, D.D.; Del-Toro-Sánchez, C.L. Zein-Polysaccharide Nanoparticles as Matrices for Antioxidant Compounds: A Strategy for Prevention of Chronic Degenerative Diseases. *Food Research International* 2018, *111*, 451–471.
39. Chawda, P.J.; Shi, J.; Xue, S.; Young Quek, S. Co-Encapsulation of Bioactives for Food Applications. *Food Quality and Safety* 2017, *1*.
40. Liu, K.; Chen, Y.Y.; Pan, L.H.; Li, Q.M.; Luo, J.P.; Zha, X.Q. Co-Encapsulation Systems for Delivery of Bioactive Ingredients. *Food Research International* 2022, *155*.
41. Chen, S.; Sun, C.; Wang, Y.; Han, Y.; Dai, L.; Abliz, A.; Gao, Y. Quercetagetin-Loaded Composite Nanoparticles Based on Zein and Hyaluronic Acid: Formation, Characterization, and Physicochemical Stability. *J Agric Food Chem* **2018**, *66*, 7441–7450, doi:10.1021/acs.jafc.8b01046.
42. Huang, M.; Liang, C.; Tan, C.; Huang, S.; Ying, R.; Wang, Y.; Wang, Z.; Zhang, Y. Liposome Co-Encapsulation as a Strategy for the Delivery of Curcumin and Resveratrol. *Food Funct* **2019**, *10*, doi:10.1039/c9fo01338e.
43. Huang, H.; Belwal, T.; Liu, S.; Duan, Z.; Luo, Z. Novel Multi-Phase Nano-Emulsion Preparation for Co-Loading Hydrophilic Arbutin and Hydrophobic Coumaric Acid Using Hydrocolloids. *Food Hydrocoll* **2019**, *93*, doi:10.1016/j.foodhyd.2019.02.023.
44. Tadele, D.T.; David, D.; Yim, E.; Mekonnen, T.H. Development and Characterization of PVA-Zein/α-Tocopherol Nonwoven Mats for Functional Wound Dressing Applications. *Colloids Surf B Biointerfaces* **2024**, 114355, doi:https://doi.org/10.1016/j.colsurfb.2024.114355.

45. Santos, M.G.; Carpinteiro, D.A.; Thomazini, M.; Rocha-Selmi, G.A.; da Cruz, A.G.; Rodrigues, C.E.C.; Favaro-Trindade, C.S. Coencapsulation of Xylitol and Menthol by Double Emulsion Followed by Complex Coacervation and Microcapsule Application in Chewing Gum. *Food Research International* **2014**, *66*, doi:10.1016/j.foodres.2014.10.010.
46. Huang, E.; Quek, S.Y.; Fu, N.; Wu, W.D.; Chen, X.D. Co-Encapsulation of Coenzyme Q10 and Vitamin E: A Study of Microcapsule Formation and Its Relation to Structure and Functionalities Using Single Droplet Drying and Micro-Fluidic-Jet Spray Drying. *J Food Eng* **2019**, *247*, doi:10.1016/j.jfoodeng.2018.11.017.
47. Ahmadi, S.S.; Aminzare, M.; Hassanzad Azar, H.; Nikfarjam, N.; Roohinejad, S.; Greiner, R.; Tahergorabi, R. Application of Electrospun Zein/Polyvinyl Alcohol Nanofibers Incorporating Thymoquinone and Electrosprayed Resveratrol Nanoparticles on the Shelf Life of Fresh Rainbow Trout Fillet and Inoculated Escherichia Coli O157:H7. *Food Control* **2024**, *155*, doi:10.1016/j.foodcont.2023.110089.
48. Yan, X.; Zhang, X.; McClements, D.J.; Zou, L.; Liu, X.; Liu, F. Co-Encapsulation of Epigallocatechin Gallate (EGCG) and Curcumin by Two Proteins-Based Nanoparticles: Role of EGCG. *J Agric Food Chem* **2019**, *67*, doi:10.1021/acs.jafc.9b04415.
49. Chen, S.; Han, Y.; Huang, J.; Dai, L.; Du, J.; McClements, D.J.; Mao, L.; Liu, J.; Gao, Y. Fabrication and Characterization of Layer-by-Layer Composite Nanoparticles Based on Zein and Hyaluronic Acid for Codelivery of Curcumin and Quercetagetin. *ACS Appl Mater Interfaces* **2019**, *11*, doi:10.1021/acsami.9b02529.
50. Wang, M.; Fu, Y.; Chen, G.; Shi, Y.; Li, X.; Zhang, H.; Shen, Y. Fabrication and Characterization of Carboxymethyl Chitosan and Tea Polyphenols Coating on Zein Nanoparticles to Encapsulate β-Carotene by Anti-Solvent Precipitation Method. *Food Hydrocoll* **2018**, *77*, doi:10.1016/j.foodhyd.2017.10.036.
51. Wei, Y.; Wang, C.; Liu, X.; Mackie, A.; Zhang, M.; Dai, L.; Liu, J.; Mao, L.; Yuan, F.; Gao, Y. Co-Encapsulation of Curcumin and β-Carotene in Pickering Emulsions Stabilized by Complex Nanoparticles: Effects of Microfluidization and Thermal Treatment. *Food Hydrocoll* **2022**, *122*, doi:10.1016/j.foodhyd.2021.107064.
52. Chen, H.; Zhang, Y.; Zhong, Q. Physical and Antimicrobial Properties of Spray-Dried Zein-Casein Nanocapsules with Co-Encapsulated Eugenol and Thymol. *J Food Eng* **2014**, *144*, doi:10.1016/j.jfoodeng.2014.07.021.
53. Ji, C.; Khan, M.A.; Chen, K.; Liang, L. Coating of DNA and DNA Complexes on Zein Particles for the Encapsulation and Protection of Kaempferol and α-Tocopherol. *J Food Eng* **2023**, *352*, doi:10.1016/j.jfoodeng.2023.111520.
54. Baspinar, Y.; Üstündas, M.; Bayraktar, O.; Sezgin, C. Curcumin and Piperine Loaded Zein-Chitosan Nanoparticles: Development and in-Vitro Characterisation. *Saudi Pharmaceutical Journal* **2018**, *26*, doi:10.1016/j.jsps.2018.01.010.
55. Leena, M.M.; Anukiruthika, T.; Moses, J.A.; Anandharamakrishnan, C. Co-Delivery of Curcumin and Resveratrol through Electrosprayed Core-Shell Nanoparticles in 3D Printed Hydrogel. *Food Hydrocoll* **2022**, *124*, doi:10.1016/j.foodhyd.2021.107200.

56. Wei, Y.; Yang, S.; Zhang, L.; Dai, L.; Tai, K.; Liu, J.; Mao, L.; Yuan, F.; Gao, Y.; Mackie, A. Fabrication, Characterization and in Vitro Digestion of Food Grade Complex Nanoparticles for Co-Delivery of Resveratrol and Coenzyme Q10. *Food Hydrocoll* **2020**, *105*, doi:10.1016/j.foodhyd.2020.105791.
57. Khan, M.S.; Fatima, M.; Gupta, G.; Md, S.; Kesharwani, P. Recent Progress in Zein Nanoparticles: A Promising Approach for Advancing Cancer Therapy. *J Drug Deliv Sci Technol* **2024**, *97*, 105770, doi:https://doi.org/10.1016/j.jddst.2024.105770.
58. Liu, G.; An, D.; Li, J.; Deng, S. Zein-Based Nanoparticles: Preparation, Characterization, and Pharmaceutical Application. *Front Pharmacol* 2023, *14*.
59. Bao, X.; Rong, S.; Fu, Q.; Liu, H.; Han, Y.; Liu, F.; Ye, Z.; Chen, S. Zein-Yeast Carboxymethyl Glucan Particles Formed by Anti-Solvent Precipitation for Encapsulating Resveratrol. *Int J Biol Macromol* **2023**, *253*, 127557, doi:10.1016/j.ijbiomac.2023.127557.
60. Huang, X.; Dai, Y.; Cai, J.; Zhong, N.; Xiao, H.; McClements, D.J.; Hu, K. Resveratrol Encapsulation in Core-Shell Biopolymer Nanoparticles: Impact on Antioxidant and Anticancer Activities. *Food Hydrocoll* **2017**, *64*, 157–165, doi:10.1016/j.foodhyd.2016.10.029.
61. T. Tadele, D.; H. Mekonnen, T. Co-Encapsulation of Quercetin and α-Tocopherol Bioactives in Zein Nanoparticles: Synergistic Interactions, Stability, and Controlled Release. *ACS Appl Polym Mater* **2024**, *0*, doi:10.1021/acsapm.3c03000.
62. Ma, L.; Su, C.R.; Li, S.Y.; He, S.; Nag, A.; Yuan, Y. Co-Delivery of Curcumin and Quercetin in the Bilayer Structure Based on Complex Coacervation. *Food Hydrocoll* **2023**, *144*, doi:10.1016/j.foodhyd.2023.108907.
63. Karthikeyan, K.; Lakra, R.; Rajaram, R.; Korrapati, P.S. Development and Characterization of Zein-Based Micro Carrier System for Sustained Delivery of Aceclofenac Sodium. *AAPS PharmSciTech* **2012**, *13*, doi:10.1208/s12249-011-9731-x.
64. Wei, Y.; Guo, A.; Liu, Z.; Zhang, L.; Liao, W.; Liu, J.; Mao, L.; Yuan, F.; Gao, Y. Development of Curcumin Loaded Core-Shell Zein Microparticles Stabilized by Cellulose Nanocrystals and Whey Protein Microgels through Interparticle Interactions. *Food Funct* **2021**, *12*, doi:10.1039/d1fo00959a.
65. Zheng, H.; Wang, J.; You, F.; Zhou, M.; Shi, S. Fabrication, Characterization, and Antimicrobial Activity of Carvacrol-Loaded Zein Nanoparticles Using the PH-Driven Method. *Int J Mol Sci* **2022**, *23*, doi:10.3390/ijms23169227.
66. Liu, G.; Wei, D.; Wang, H.; Hu, Y.; Jiang, Y. Self-Assembly of Zein Microspheres with Controllable Particle Size and Narrow Distribution Using a Novel Built-in Ultrasonic Dialysis Process. *Chemical Engineering Journal* **2016**, *284*, doi:10.1016/j.cej.2015.09.067.
67. Wang, H.; Zhang, X.; Zhu, W.; Jiang, Y.; Zhang, Z. Self-Assembly of Zein-Based Microcarrier System for Colon-Targeted Oral Drug Delivery. *Ind Eng Chem Res* **2018**, *57*, doi:10.1021/acs.iecr.8b02092.
68. Zhong, Q.; Jin, M. Zein Nanoparticles Produced by Liquid-Liquid Dispersion. *Food Hydrocoll* **2009**, *23*, 2380–2387, doi:10.1016/j.foodhyd.2009.06.015.
69. Mohammed, N.K.; Tan, C.P.; Manap, Y.A.; Muhialdin, B.J.; Hussin, A.S.M. Spray Drying for the Encapsulation of Oils—A Review. *Molecules* 2020, *25*.

70. Zhong, Q.; Jin, M.; Davidson, P.M.; Zivanovic, S. Sustained Release of Lysozyme from Zein Microcapsules Produced by a Supercritical Anti-Solvent Process. *Food Chem* **2009**, *115*, doi:10.1016/j.foodchem.2008.12.063.
71. Franco, P.; Reverchon, E.; De Marco, I. Zein/Diclofenac Sodium Coprecipitation at Micrometric and Nanometric Range by Supercritical Antisolvent Processing. *Journal of CO2 Utilization* **2018**, *27*, doi:10.1016/j.jcou.2018.08.015.
72. Malik, S.; Subramanian, S.; Hussain, T.; Nazir, A.; Ramakrishna, S. Electrosprayed Nanoparticles as Drug Delivery Systems for Biomedical Applications. *Curr Pharm Des* **2021**, *28*, doi:10.2174/1381612827666210929114621.
73. Mahalakshmi, L.; Leena, M.M.; Moses, J.A.; Anandharamakrishnan, C. Micro- and Nano-Encapsulation of β-Carotene in Zein Protein: Size-Dependent Release and Absorption Behavior. *Food Funct* **2020**, *11*, doi:10.1039/c9fo02088h.
74. Hu, M.X.; Chen, X.L.; Song, L.J.; He, F. Arachidonic Acid-Encapsulated Microcapsules with Core-Shell Structure Prepared by Coaxial Electrospray. *J Appl Polym Sci* **2021**, *138*, doi:10.1002/app.50403.
75. Xing, M.; Zhao, H.; Ahmed, R.; Wang, X.; Liu, J.; Wang, J.; Guo, A.; Wang, M. Fabrication of Resveratrol-Loaded Zein Nanoparticles Based on Flash Nanoprecipitation. *Colloids Surf A Physicochem Eng Asp* **2022**, *654*, doi:10.1016/j.colsurfa.2022.129829.
76. van Ballegooie, C.; Man, A.; Andreu, I.; Gates, B.D.; Yapp, D. Using a Microfluidics System to Reproducibly Synthesize Protein Nanoparticles: Factors Contributing to Size, Homogeneity, and Stability. *Processes* **2019**, *7*, doi:10.3390/pr7050290.
77. Jeevanandam, J.; Barhoum, A.; Chan, Y.S.; Dufresne, A.; Danquah, M.K. Review on Nanoparticles and Nanostructured Materials: History, Sources, Toxicity and Regulations. *Beilstein Journal of Nanotechnology* 2018, *9*.
78. Couto, A.F.; Favretto, M.; Paquis, R.; Estevinho, B.N. Co-Encapsulation of Epigallocatechin-3-Gallate and Vitamin B12 in Zein Microstructures by Electrospinning/Electrospraying Technique. *Molecules* **2023**, *28*, doi:10.3390/molecules28062544.
79. Dolgin, J.; Hanumantharao, S.N.; Farias, S.; Simon, C.G.; Rao, S. Mechanical Properties and Morphological Alterations in Fiber-Based Scaffolds Affecting Tissue Engineering Outcomes. *Fibers* 2023, *11*.
80. Altan, A.; Çayır, Ö. Encapsulation of Carvacrol into Ultrafine Fibrous Zein Films via Electrospinning for Active Packaging. *Food Packag Shelf Life* **2020**, *26*, doi:10.1016/j.fpsl.2020.100581.
81. Rahman, M.; Dip, T.M.; Haase, T.; Truong, Y.B.; Le, T.C.; Houshyar, S. Fabrication of Zein-Based Fibrous Scaffolds for Biomedical Applications—A Review. *Macromol Mater Eng* 2023, *308*.
82. Huang, W.; Zou, T.; Li, S.; Jing, J.; Xia, X.; Liu, X. Drug-Loaded Zein Nanofibers Prepared Using a Modified Coaxial Electrospinning Process. *AAPS PharmSciTech* **2013**, *14*, doi:10.1208/s12249-013-9953-1.
83. Horuz, T.İ.; Belibağlı, K.B. Nanoencapsulation of Carotenoids Extracted from Tomato Peels into Zein Fibers by Electrospinning. *J Sci Food Agric* **2019**, *99*, doi:10.1002/jsfa.9244.
84. Lu, H.; Qiu, Y.; Wang, Q.; Li, G.; Wei, Q. Nanocomposites Prepared by Electrohydrodynamics and Their Drug Release Properties. *Materials Science and Engineering C* **2018**, *91*, doi:10.1016/j.msec.2018.05.024.

85. Wang, L.; Xue, J.; Zhang, Y. Preparation and Characterization of Curcumin Loaded Caseinate/Zein Nanocomposite Film Using PH-Driven Method. *Ind Crops Prod* **2019**, *130*, doi:10.1016/j.indcrop.2018.12.072.
86. Daristotle, J.L.; Behrens, A.M.; Sandler, A.D.; Kofinas, P. A Review of the Fundamental Principles and Applications of Solution Blow Spinning. *ACS Appl Mater Interfaces* **2016**, *8*, doi:10.1021/acsami.6b12994.
87. Medeiros, E.S.; Glenn, G.M.; Klamczynski, A.P.; Orts, W.J.; Mattoso, L.H.C. Solution Blow Spinning: A New Method to Produce Micro- and Nanofibers from Polymer Solutions. *J Appl Polym Sci* **2009**, *113*, doi:10.1002/app.30275.
88. Liu, F.; Avena-Bustillos, R.J.; Woods, R.; Chiou, B. Sen; Williams, T.G.; Wood, D.F.; Bilbao-Sainz, C.; Yokoyama, W.; Glenn, G.M.; McHugh, T.H.; et al. Preparation of Zein Fibers Using Solution Blow Spinning Method. *J Food Sci* **2016**, *81*, N3015–N3025, doi:10.1111/1750-3841.13537.
89. Natarelli, C.V.L.; de Barros, H.E.A.; Freitas, H.R.; Bufalo, T.C. e.; Dias, E.S.; de Oliveira, J.E.; Marconcini, J.M. PVA/Zein Nanofibers Obtained by Solution Blow Spinning. *J Mater Sci* **2023**, *58*, doi:10.1007/s10853-023-08861-1.
90. Li, R.; Ma, Y.; Zhang, Y.; Zhang, M.; Sun, D. Potential of RhBMP-2 and Dexamethasone-Loaded Zein/PLLA Scaffolds for Enhanced in Vitro Osteogenesis of Mesenchymal Stem Cells. *Colloids Surf B Biointerfaces* **2018**, *169*, doi:10.1016/j.colsurfb.2018.05.039.
91. Tadele, D.T.; Shorey, R.; Mekonnen, T.H. Fatty Acid Modified Zein Films: Effect of Fatty Acid Chain Length on the Processability and Thermomechanical Properties of Modified Zein Films. *Ind Crops Prod* **2023**, *192*, doi:10.1016/j.indcrop.2022.116028.
92. Tadele, D.T.; Trinh, B.M.; Mekonnen, T.H. PBAT/Corn Zein Ester Blends: Rheology, Morphology, and Physicochemical Properties. *Polymer (Guildf)* **2023**, *283*, doi:10.1016/j.polymer.2023.126258.
93. Tadele, D.T.; Shorey, R.; Mekonnen, T.H. Fatty Acid Modified Zein Films: Effect of Fatty Acid Chain Length on the Processability and Thermomechanical Properties of Modified Zein Films. *Ind Crops Prod* **2023**, *192*, doi:10.1016/j.indcrop.2022.116028.
94. Li, H.; Wang, D.; Liu, C.; Zhu, J.; Fan, M.; Sun, X.; Wang, T.; Xu, Y.; Cao, Y. Fabrication of Stable Zein Nanoparticles Coated with Soluble Soybean Polysaccharide for Encapsulation of Quercetin. *Food Hydrocoll* **2019**, *87*, 342–351, doi:10.1016/j.foodhyd.2018.08.002.
95. Huang, X.; Ge, X.; Zhou, L.; Wang, Y. Eugenol Embedded Zein and Poly(Lactic Acid) Film as Active Food Packaging: Formation, Characterization, and Antimicrobial Effects. *Food Chem* **2022**, *384*, doi:10.1016/j.foodchem.2022.132482.
96. Liu, J.; Zhang, Y.; He, S.; Zhou, A.; Gao, B.; Yan, M.; Yu, L. (Lucy) Microbial Transglutaminase-Induced Cross-Linking of Sodium Caseinate as the Coating Stabilizer of Zein Nanoparticles. *LWT* **2021**, *138*, doi:10.1016/j.lwt.2020.110624.
97. Hao, L.; Lin, G.; Chen, C.; Zhou, H.; Chen, H.; Zhou, X. Phosphorylated Zein as Biodegradable and Aqueous Nanocarriers for Pesticides with Sustained-Release and Anti-UV Properties. *J Agric Food Chem* **2019**, *67*, doi:10.1021/acs.jafc.9b03060.

98. Chen, L.; Lin, Y.; Zhou, H.; Hao, L.; Chen, H.; Zhou, X. A Stable Polyamine-Modified Zein-Based Nanoformulation with High Foliar Affinity and Lowered Toxicity for Sustained Avermectin Release. *Pest Manag Sci* **2021**, *77*, doi:10.1002/ps.6374.
99. Li, Y.; Bai, Y.; Huang, J.; Yuan, C.; Ding, T.; Liu, D.; Hu, Y. Airglow Discharge Plasma Treatment Affects the Surface Structure and Physical Properties of Zein Films. *J Food Eng* **2020**, *273*, doi:10.1016/j.jfoodeng.2019.109813.
100. Sun, C.; Yang, J.; Liu, F.; Yang, W.; Yuan, F.; Gao, Y. Effects of Dynamic High-Pressure Microfluidization Treatment and the Presence of Quercetagetin on the Physical, Structural, Thermal, and Morphological Characteristics of Zein Nanoparticles. *Food Bioproc Tech* **2016**, *9*, doi:10.1007/s11947-015-1627-4.
101. He, W.; Tian, L.; Fang, F.; Pan, S.; Jones, O.G. Heat-Induced Glycosylation with Dextran to Enhance Solubility and Interfacial Properties of Enzymatically Hydrolyzed Zein. *J Food Eng* **2022**, *321*, doi:10.1016/j.jfoodeng.2022.110946.
102. He, W.; Tian, L.; Fang, F.; Chen, D.; Federici, E.; Pan, S.; Jones, O.G. Limited Hydrolysis and Conjugation of Zein with Chitosan Oligosaccharide by Enzymatic Reaction to Improve Functional Properties. *Food Chem* **2021**, *348*, doi:10.1016/j.foodchem.2021.129035.
103. Zhang, Z.; Zhou, R.; Ke, L.; Li, J.; Jayan, H.; El-Seedi, H.R.; Zou, X.; Guo, Z. Development of Multifunctional Metal-Organic Frameworks (MOFs)-Based Nanofiller Materials in Food Packaging: A Comprehensive Review. *Trends Food Sci Technol* **2024**, *154*, 104771, doi:https://doi.org/10.1016/j.tifs.2024.104771.
104. Safdar Ali, R.; Meng, H.; Li, Z. Zinc-Based Metal-Organic Frameworks in Drug Delivery, Cell Imaging, and Sensing. *Molecules* 2021, *27*.
105. Lv, Y.; Ding, D.; Zhuang, Y.; Feng, Y.; Shi, J.; Zhang, H.; Zhou, T.L.; Chen, H.; Xie, R.J. Chromium-Doped Zinc Gallogermanate@Zeolitic Imidazolate Framework-8: A Multifunctional Nanoplatform for Rechargeable in Vivo Persistent Luminescence Imaging and PH-Responsive Drug Release. *ACS Appl Mater Interfaces* **2019**, *11*, doi:10.1021/acsami.8b19172.
106. Kasaai, M.R. Zein and Zein -Based Nano-Materials for Food and Nutrition Applications: A Review. *Trends Food Sci Technol* 2018, *79*.
107. Hu, K.; McClements, D.J. Fabrication of Biopolymer Nanoparticles by Antisolvent Precipitation and Electrostatic Deposition: Zein-Alginate Core/Shell Nanoparticles. *Food Hydrocoll* **2015**, *44*, doi:10.1016/j.foodhyd.2014.09.015.
108. Oleandro, E.; Stanzione, M.; Buonocore, G.G.; Lavorgna, M. Zein-Based Nanoparticles as Active Platforms for Sustainable Applications: Recent Advances and Perspectives. *Nanomaterials* **2024**, *14*, doi:10.3390/nano14050414.
109. Chen, J.; Guo, Y.; Zhang, X.; Liu, J.; Gong, P.; Su, Z.; Fan, L.; Li, G. Emerging Nanoparticles in Food: Sources, Application, and Safety. *J Agric Food Chem* 2023, *71*.
110. Wang, D.; Sun, J.; Li, J.; Sun, Z.; Liu, F.; Du, L.; Wang, D. Preparation and Characterization of Gelatin/Zein Nanofiber Films Loaded with Perillaldehyde, Thymol, or ε-Polylysine and Evaluation of Their Effects on the Preservation of Chilled Chicken Breast. *Food Chem* **2022**, *373*, doi:10.1016/j.foodchem.2021.131439.

111. Zhang, Z.; Li, R.; Tang, H.; Li, J.X. Interactions and Characterization of Zein-BSA Nanoparticles: Multi-Spectral Analysis and Molecular Simulations. *J Mol Liq* **2023**, *391*, doi:10.1016/j.molliq.2023.123293.
112. Jiao, Y.; Zheng, X.; Chang, Y.; Li, D.; Sun, X.; Liu, X. Zein-Derived Peptides as Nanocarriers to Increase the Water Solubility and Stability of Lutein. In Proceedings of the Food and Function; 2018; Vol. 9.
113. Ma, L.; Su, C.; Li, X.; Wang, H.; Luo, M.; Chen, Z.; Zhang, B.; Zhu, J.; Yuan, Y. Preparation and Characterization of Bilayered Microencapsulation for Co-Delivery Lactobacillus Casei and Polyphenols via Zein-Chitosan Complex Coacervation. *Food Hydrocoll* **2024**, *148*, doi:10.1016/j.foodhyd.2023.109410.
114. Afroz Ali, S.M.; Niaz, T.; Munir, A.; Shahid, R.; Shabbir, S.; Noor, T.; Imran, M. Potential of Pectin-Chitosan Based Composite Films Embedded with Quercetin-Loaded Nanofillers to Control Meat Associated Spoilage Bacteria. *Food Biosci* **2023**, *53*, doi:10.1016/j.fbio.2023.102547.
115. Rahman, M.; Dip, T.M.; Haase, T.; Truong, Y.B.; Le, T.C.; Houshyar, S. Fabrication of Zein-Based Fibrous Scaffolds for Biomedical Applications—A Review. *Macromol Mater Eng* 2023, *308*.
116. Zhang, Y.; Cui, L.; Li, F.; Shi, N.; Li, C.; Yu, X.; Chen, Y.; Kong, W. Design, Fabrication and Biomedical Applications of Zein-Based Nano/Micro-Carrier Systems. *Int J Pharm* 2016, *513*, 191–210.
117. Tortorella, S.; Mirko Maturi, ab; Vetri Buratti, V.; Vozzolo, G.; Locatelli, E.; Sambri, L.; Comes Franchini, M. Zein as a Versatile Biopolymer: Different Shapes for Different Biomedical Applications. **2021**, doi:10.1039/d1ra07424e.
118. Ahmed, Y.; Yasir, M.; Ur Rehman, M.A. Fabrication and Characterization of Zein/Hydroxyapatite Composite Coatings for Biomedical Applications. *Surfaces* **2020**, *3*, doi:10.3390/surfaces3020018.
119. Babitha, S.; Korrapati, P.S. Biodegradable Zein-Polydopamine Polymeric Scaffold Impregnated with TiO2 Nanoparticles for Skin Tissue Engineering. *Biomedical Materials (Bristol)* **2017**, *12*, doi:10.1088/1748-605X/aa7d5a.
120. Kakadellis, S.; Rosetto, G. Achieving a Circular Bioeconomy for Plastics. **2021**, doi:10.1126/science.abj1003.
121. Ojogbo, E.; Blanchard, R.; Mekonnen, T. Hydrophobic and Melt Processable Starch-Laurate Esters: Synthesis, Structure-Property Correlations. *J. Polym. Sci., Part A: Polym. Chem* **2018**, *56*, 2611–2622, doi:10.1002/pola.29237.
122. Akharume, F.U.; Aluko, R.E.; Adedeji, A.A. Modification of Plant Proteins for Improved Functionality: A Review. *Compr Rev Food Sci Food Saf* 2021, *20*, 198–224.
123. Mekonnen, T.; Mussone, P.; Bressler, D. Valorization of Rendering Industry Wastes and Co-Products for Industrial Chemicals, Materials and Energy: Review. *Crit Rev Biotechnol* 2016, *36*.
124. Mekonnen T, M.M.M.A. Fermented Soymeals and Their Reactive Blends with Poly (Butylene Adipate-Co-Terephthalate) in Engineering Biodegradable Cast Films for Sustainable Packaging. *ACS Sustain Chem Eng* **2016**, 782–793.
125. Lásztity, R. *The Chemistry of Cereal Proteins, Second Edition*; 2017;
126. Rouf, T.B.; Schmidt, G.; Kokini, J.L. Correction to: Zein–Laponite® Nanocomposites with Improved Mechanical, Thermal and Barrier Properties. *J Mater Sci* **2018**, *53*, doi:10.1007/s10853-018-2600-1.

127. Weissmueller, N.T.; Lu, H.D.; Hurley, A.; Prud'Homme, R.K. Nanocarriers from GRAS Zein Proteins to Encapsulate Hydrophobic Actives. *Biomacromolecules* **2016**, *17*, 3828–3837, doi:10.1021/acs.biomac.6b01440.
128. Padua, G.W.; Guardiola, L. V. Microcapsules Produced from Zein. In *Microencapsulation and Microspheres for Food Applications*; 2015.
129. Uchtmann, D.L. Starlink a Case Study of Agricultural Biotechnology Regulation. *Drake Journal of Agricultural Law* **2002**, *7*.
130. Saithongdee, A.; Praphairaksit, N.; Imyim, A. Electrospun Curcumin-Loaded Zein Membrane for Iron(III) Ions Sensing. *Sens Actuators B Chem* **2014**, *202*, doi:10.1016/j.snb.2014.06.036.
131. Tadele, D.T.; Islam, M.S.; Mekonnen, T.H. Zein-Based Nanoparticles and Nanofibers: Co-Encapsulation, Characterization, and Application in Food and Biomedicine. *Trends Food Sci Technol* **2025**, *155*, 104809, doi:https://doi.org/10.1016/j.tifs.2024.104809.
132. Masamba, K.; Li, Y.; Hategekimana, J.; Liu, F.; Ma, J.; Zhong, F. Effect of Type of Plasticizers on Mechanical and Water Barrier Properties of Transglutaminase Cross-Linked Zein-Oleic Acid Composite Films. *International Journal of Food Engineering* **2016**, *12*, doi:10.1515/ijfe-2015-0289.
133. Lai, H.M.; Padua, G.W.; Wei, L.S. Properties and Microstructure of Zein Sheets Plasticized with Palmitic and Stearic Acids. *Cereal Chem* **1997**, *74*, doi:10.1094/CCHEM.1997.74.1.83.
134. Mekonnen, T.H.; Misra, M.; Mohanty, A.K. Processing, Performance, and Applications of Plant and Animal Protein-Based Blends and Their Biocomposites. In *Biocomposites: Design and Mechanical Performance*; 2015.
135. Gezer, P.G.; Brodsky, S.; Hsiao, A.; Liu, G.L.; Kokini, J.L. Modification of the Hydrophilic/Hydrophobic Characteristic of Zein Film Surfaces by Contact with Oxygen Plasma Treated PDMS and Oleic Acid Content. *Colloids Surf B Biointerfaces* **2015**, *135*, doi:10.1016/j.colsurfb.2015.07.006.
136. Lai, H.M.; Geil, P.H.; Padua, G.W. X-Ray Diffraction Characterization of the Structure of Zein-Oleic Acid Films. *J Appl Polym Sci* **1999**, *71*, doi:10.1002/(SICI)1097-4628(19990222)71:8<1267::AID-APP7>3.0.CO;2-O.
137. Wang, Q.; Geil, P.; Padua, G. Role of Hydrophilic and Hydrophobic Interactions in Structure Development of Zein Films. *J Polym Environ* **2004**, *12*, doi:10.1023/B:JOOE.0000038552.88467.fc.
138. Li, Y.; Xia, Q.; Shi, K.; Huang, Q. Scaling Behaviors of R-Zein in Acetic Acid Solutions. *J. Phys. Chem. B* **2011**, *115*, 9695–9702, doi:10.1021/jp203476m.
139. Wang, Q.; Yang, Y.; Chen, X.; Shao, Z. Investigation of Rheological Properties and Conformation of Silk Fibroin in the Solution of AmimCl. **2012**, doi:10.1021/bm300387z.
140. Ji, Y.; Yang, X.; Ji, Z.; Zhu, L.; Ma, N.; Chen, D.; Jia, X.; Tang, J.; Cao, Y. DFT-Calculated IR Spectrum Amide I, II, and III Band Contributions of N-Methylacetamide Fine Components. *ACS Omega* **2020**, *5*, 8572–8578, doi:10.1021/ACSOMEGA.9B04421/SUPPL_FILE/AO9B04421_SI_001.PDF.
141. Arcan, I.; Yemenicioğlu, A. Development of Flexible Zein-Wax Composite and Zein-Fatty Acid Blend Films for Controlled Release of Lysozyme. *Food Research International* **2013**, *51*, doi:10.1016/j.foodres.2012.12.011.

142. Shorey, R.; Gupta, A.; Mekonnen, T.H. Hydrophobic Modification of Lignin for Rubber Composites. *Ind Crops Prod* **2021**, *174*, doi:10.1016/j.indcrop.2021.114189.
143. Prakash, G.K.; Mahadevan, K.M. Enhancing the Properties of Wood through Chemical Modification with Palmitoyl Chloride. *Appl Surf Sci* **2008**, *254*, doi:10.1016/j.apsusc.2007.07.137.
144. Shorey, R.; Mekonnen, T.H. Sustainable Paper Coating with Enhanced Barrier Properties Based on Esterified Lignin and PBAT Blend. *Int J Biol Macromol* **2022**, *209*, 472–484, doi:10.1016/j.ijbiomac.2022.04.037.
145. Arcan, I.; Yemenicioğlu, A. Controlled Release Properties of Zein-Fatty Acid Blend Films for Multiple Bioactive Compounds. *J Agric Food Chem* **2014**, *62*, doi:10.1021/jf500666w.
146. Forato, L.A.; Colnago, L.A.; Garratt, R.C.; Lopes, M.A. Identification of Free Fatty Acids in Maize Protein Bodies and Purified α Zeins by 13C and 1H Nuclear Magnetic Resonance. *Biochimica et Biophysica Acta - Protein Structure and Molecular Enzymology* **2000**, *1543*, doi:10.1016/S0167-4838(00)00190-4.
147. Alcântara, A.C.S.; Darder, M.; Aranda, P.; Ruiz-Hitzky, E. Zein-Fibrous Clays Biohybrid Materials. *Eur J Inorg Chem* **2012**, doi:10.1002/ejic.201200582.
148. Neo, Y.P.; Perera, C.O.; Nieuwoudt, M.K.; Zujovic, Z.; Jin, J.; Ray, S.; Gizdavic-Nikolaidis, M. Influence of Heat Curing on Structure and Physicochemical Properties of Phenolic Acid Loaded Proteinaceous Electrospun Fibers. *J Agric Food Chem* **2014**, *62*, doi:10.1021/jf500841m.
149. Li, Y.; Li, J.; Xia, Q.; Zhang, B.; Wang, Q.; Huang, Q. Understanding the Dissolution of α-Zein in Aqueous Ethanol and Acetic Acid Solutions. *Journal of Physical Chemistry B* **2012**, *116*, doi:10.1021/jp305709y.
150. Gao, Y.; Zheng, H.; Wang, J.; Wu, J.; Li, X.; Liu, · Gang Physicochemical Properties of Zein Films Cross-Linked with Glutaraldehyde. *Polymer Bulletin* **123AD**, doi:10.1007/s00289-021-03723-9.
151. Ojogbo, E.; Jardin, J.; Mekonnen, T.H. Robust and Sustainable Starch Ester Nanocomposite Films for Packaging Applications. *Ind Crops Prod* **2021**, *160*, doi:10.1016/j.indcrop.2020.113153.
152. Nonthanum, P.; Lee, Y.; Padua, G.W. Effect of γ-Zein on the Rheological Behavior of Concentrated Zein Solutions. *J Agric Food Chem* **2012**, *60*, doi:10.1021/jf2035302.
153. Ghanbarzadeh, B.; Oromiehie, A.; Musavi, M. Effect of Polyolic Plasticizers on Rheological. *Polym J* **2006**, *15*.
154. Smith, P.T.; Basu, A.; Saha, A.; Nelson, A. Chemical Modification and Printability of Shear-Thinning Hydrogel Inks for Direct-Write 3D Printing. *Polymer (Guildf)* **2018**, *152*, doi:10.1016/j.polymer.2018.01.070.
155. Lai, H.M.; Padua, G.W. Properties and Microstructure of Plasticized Zein Films. *Cereal Chem* **1997**, *74*, doi:10.1094/CCHEM.1997.74.6.771.
156. Chen, Y.; Ye, R.; Liu, J. Effects of Different Concentrations of Ethanol and Isopropanol on Physicochemical Properties of Zein-Based Films. *Ind Crops Prod* **2014**, *53*, doi:10.1016/j.indcrop.2013.12.034.
157. Mekonnen, T.; Mussone, P.; Khalil, H.; Bressler, D. Progress in Bio-Based Plastics and Plasticizing Modifications. *J Mater Chem A Mater* **2013**, *1*, doi:10.1039/c3ta12555f.

158. Giacovelli, C. *Single-Use Plastic: A Roadmap for Sustainability*; 2018;
159. Herberz, T.; Barlow, C.Y.; Finkbeiner, M. Sustainability Assessment of a Single-Use Plastics Ban. *Sustainability (Switzerland)* **2020**, *12*, doi:10.3390/su12093746.
160. Muthuraj, R.; Misra, M.; Mohanty, A.K. Biodegradable Poly(Butylene Succinate) and Poly(Butylene Adipate-Co-Terephthalate) Blends: Reactive Extrusion and Performance Evaluation. *J Polym Environ* **2014**, *22*, doi:10.1007/s10924-013-0636-5.
161. Dammak, M.; Fourati, Y.; Tarrés, Q.; Delgado-Aguilar, M.; Mutjé, P.; Boufi, S. Blends of PBAT with Plasticized Starch for Packaging Applications: Mechanical Properties, Rheological Behaviour and Biodegradability. *Ind Crops Prod* **2020**, *144*, doi:10.1016/j.indcrop.2019.112061.
162. Huang, F.; Wu, L.; Li, B.G. Sulfonated Biodegradable PBAT Copolyesters with Improved Gas Barrier Properties and Excellent Water Dispersibility: From Synthesis to Structure-Property. *Polym Degrad Stab* **2020**, *182*, doi:10.1016/j.polymdegradstab.2020.109391.
163. Li, J.; Lai, L.; Wu, L.; Severtson, S.J.; Wang, W.J. Enhancement of Water Vapor Barrier Properties of Biodegradable Poly(Butylene Adipate- Co-Terephthalate) Films with Highly Oriented Organomontmorillonite. *ACS Sustain Chem Eng* **2018**, *6*, doi:10.1021/acssuschemeng.8b00430.
164. Reddy, M.M.; Misra, M.; Mohanty, A.K. Biodegradable Blends from Corn Gluten Meal and Poly(Butylene Adipate-Co-Terephthalate) (PBAT): Studies on the Influence of Plasticization and Destructurization on Rheology, Tensile Properties and Interfacial Interactions. *J Polym Environ* **2014**, *22*, doi:10.1007/s10924-014-0640-4.
165. John, J.; Mani, R.; Bhattacharya, M. Evaluation of Compatibility and Properties of Biodegradable Polyester Blends. *J Polym Sci A Polym Chem* **2002**, *40*, doi:10.1002/pola.10297.
166. Huang, P.; Zhong, Z.; Zheng, S.; Zhu, W.; Guo, Q. Miscibility and Interchange Reactions in Blends of Bisphenol-A-Type Epoxy Resin and Poly(Ethylene Terephthalate). *J Appl Polym Sci* **1999**, *73*, doi:10.1002/(SICI)1097-4628(19990801)73:5<639::AID-APP4>3.0.CO;2-F.
167. Zhou, X.; Mohanty, A.; Misra, M. A New Biodegradable Injection Moulded Bioplastic from Modified Soy Meal and Poly (Butylene Adipate-Co-Terephthalate): Effect of Plasticizer and Denaturant. *J Polym Environ* **2013**, *21*, doi:10.1007/s10924-013-0578-y.
168. Brandelero, R.P.H.; Yamashita, F.; Grossmann, M.V.E. The Effect of Surfactant Tween 80 on the Hydrophilicity, Water Vapor Permeation, and the Mechanical Properties of Cassava Starch and Poly(Butylene Adipate-Co-Terephthalate) (PBAT) Blend Films. *Carbohydr Polym* **2010**, *82*, doi:10.1016/j.carbpol.2010.06.034.
169. Ghanbarzadeh, B.; Oromiehi, A.R. Biodegradable Biocomposite Films Based on Whey Protein and Zein: Barrier, Mechanical Properties and AFM Analysis. *Int J Biol Macromol* **2008**, *43*, 209–215, doi:10.1016/j.ijbiomac.2008.05.006.
170. Lawton, J.W. Plasticizers for Zein: Their Effect on Tensile Properties and Water Absorption of Zein Films. *Cereal Chem* **2004**, *81*, doi:10.1094/CCHEM.2004.81.1.1.
171. Kyu Kim, S.; Wook Jung, H.; Son, D.; Hyeok Han, J.; Kang, D.; In Kang, S.; Lee, J.; Kie Shim, J. In Situ Reactive Compatibilization of Thermoplastic

Starch/Poly(Butylene Adipate-Co-Terephthalate) Blends with Robust Water Resistance Performance. *ACS Appl Polym Mater* **2023**, *0*, doi:10.1021/acsapm.3c00774.
172. Charfeddine, I.; Majesté, J.C.; Carrot, C.; Lhost, O. Surface Tension and Interfacial Tension of Polyolefins and Polyolefin Blends. *J Appl Polym Sci* **2022**, *139*, doi:10.1002/app.51885.
173. Zhou, X.; Mohanty, A.; Misra, M. A New Biodegradable Injection Moulded Bioplastic from Modified Soy Meal and Poly (Butylene Adipate-Co-Terephthalate): Effect of Plasticizer and Denaturant. *J Polym Environ* **2013**, *21*, doi:10.1007/s10924-013-0578-y.
174. Samuel, C.; Parpaite, T.; Lacrampe, M.F.; Soulestin, J.; Lhost, O. Melt Compatibility between Polyolefins: Evaluation and Reliability of Interfacial/Surface Tensions Obtained by Various Techniques. *Polym Test* **2019**, *78*, doi:10.1016/j.polymertesting.2019.105995.
175. Chen, G.; Chen, Y.; Jin, N.; Li, J.; Dong, S.; Li, S.; Zhang, Z.; Chen, Y. Zein Films with Porous Polylactic Acid Coatings via Cold Plasma Pre-Treatment. *Ind Crops Prod* **2020**, *150*, doi:10.1016/j.indcrop.2020.112382.
176. Koh, J.J.; Zhang, X.; He, C. Fully Biodegradable Poly(Lactic Acid)/Starch Blends: A Review of Toughening Strategies. *Int J Biol Macromol* 2018, *109*.
177. Tavares, L.B.; Ito, N.M.; Salvadori, M.C.; dos Santos, D.J.; Rosa, D.S. PBAT/Kraft Lignin Blend in Flexible Laminated Food Packaging: Peeling Resistance and Thermal Degradability. *Polym Test* **2018**, *67*, doi:10.1016/j.polymertesting.2018.03.004.
178. Stein, G.E.; Laws, T.S.; Verduzco, R. Tailoring the Attraction of Polymers toward Surfaces. *Macromolecules* **2019**, *52*, doi:10.1021/acs.macromol.9b00492.
179. Gu, L.; Macosko, C.W. Evaluating PE/PLA Interfacial Tension Using Ternary Immiscible Polymer Blends. *J Appl Polym Sci* **2021**, *138*, doi:10.1002/app.50623.
180. Gong, P.; Zhao, Y.; Li, K.; Tian, H.; Li, C. Effect of Plasticizer Content on the Structure and Properties of SPI/MA-g-PBAT Blend Films. *J Polym Environ* **2022**, *30*, doi:10.1007/s10924-021-02223-1.
181. Fourati, Y.; Tarrés, Q.; Mutjé, P.; Boufi, S. PBAT/Thermoplastic Starch Blends: Effect of Compatibilizers on the Rheological, Mechanical and Morphological Properties. *Carbohydr Polym* **2018**, *199*, doi:10.1016/j.carbpol.2018.07.008.
182. Vieira, M.G.A.; Da Silva, M.A.; Dos Santos, L.O.; Beppu, M.M. Natural-Based Plasticizers and Biopolymer Films: A Review. *Eur Polym J* 2011, *47*.
183. Guo, G.; Zhang, C.; Du, Z.; Zou, W.; Tian, H.; Xiang, A.; Li, H. Structure and Property of Biodegradable Soy Protein Isolate/PBAT Blends. *Ind Crops Prod* **2015**, *74*, doi:10.1016/j.indcrop.2015.06.009.
184. Arruda, L.C.; Magaton, M.; Bretas, R.E.S.; Ueki, M.M. Influence of Chain Extender on Mechanical, Thermal and Morphological Properties of Blown Films of PLA/PBAT Blends. *Polym Test* **2015**, *43*, doi:10.1016/j.polymertesting.2015.02.005.
185. Saikrishnan, S.; Jubinville, D.; Tzoganakis, C.; Mekonnen, T.H. Thermo-Mechanical Degradation of Polypropylene (PP) and Low-Density Polyethylene (LDPE) Blends Exposed to Simulated Recycling. *Polym Degrad Stab* **2020**, *182*, doi:10.1016/j.polymdegradstab.2020.109390.

186. Sochi, T. Analytical Solutions for the Flow of Carreau and Cross Fluids in Circular Pipes and Thin Slits. *Rheol Acta* **2015**, *54*, doi:10.1007/s00397-015-0863-x.
187. Sochi, T. Further Validation to the Variational Method to Obtain Flow Relations for Generalized Newtonian Fluids. *Korea Australia Rheology Journal* **2015**, *27*, doi:10.1007/s13367-015-0012-1.
188. Lendvai, L.; Apostolov, A.; Karger-Kocsis, J. Characterization of Layered Silicate-Reinforced Blends of Thermoplastic Starch (TPS) and Poly(Butylene Adipate-Co-Terephthalate). *Carbohydr Polym* **2017**, *173*, doi:10.1016/j.carbpol.2017.05.100.
189. Wang, Y.; Li, D.; Wang, L.J.; Yang, L.; Özkan, N. Dynamic Mechanical Properties of Flaxseed Gum Based Edible Films. *Carbohydr Polym* **2011**, *86*, doi:10.1016/j.carbpol.2011.04.079.
190. Zhang, S.; He, Y.; Lin, Z.; Li, J.; Jiang, G. Effects of Tartaric Acid Contents on Phase Homogeneity, Morphology and Properties of Poly (Butyleneadipate-Co-Terephthalate)/Thermoplastic Starch Bio-Composities. *Polym Test* **2019**, *76*, doi:10.1016/j.polymertesting.2019.04.005.
191. Winkler, H.; Vorwerg, W.; Schmid, M. Synthesis of Hydrophobic Whey Protein Isolate by Acylation with Fatty Acids. *Eur Polym J* **2015**, *62*, doi:10.1016/j.eurpolymj.2014.10.014.
192. De Boer, F.Y.; Van Dijk-Moes, R.J.A.; Imhof, A.; Velikov, K.P. Characterization of the Scattering and Absorption of Colored Zein Colloids in Optically Dense Dispersions. *Langmuir* **2019**, *35*, doi:10.1021/acs.langmuir.9b01357.
193. Costa, F.A.T. da; Bardi, M.A.G. AVALIAÇÃO DA BIODEGRADAÇÃO E ENVELHECIMENTO ACELERADO POR RADIAÇÃO ULTRAVIOLETA NA BLENDA PBAT/TPS. In *Engenharia Moderna: Soluções para Problemas da Sociedade e da Indústria*; 2020.
194. Siracusa, V.; Lotti, N.; Munari, A.; Dalla Rosa, M. Poly(Butylene Succinate) and Poly(Butylene Succinate-Co-Adipate) for Food Packaging Applications: Gas Barrier Properties after Stressed Treatments. *Polym Degrad Stab* **2015**, *119*, doi:10.1016/j.polymdegradstab.2015.04.026.
195. Ren, P.G.; Liu, X.H.; Ren, F.; Zhong, G.J.; Ji, X.; Xu, L. Biodegradable Graphene Oxide Nanosheets/Poly-(Butylene Adipate-Co-Terephthalate) Nanocomposite Film with Enhanced Gas and Water Vapor Barrier Properties. *Polym Test* **2017**, *58*, doi:10.1016/j.polymertesting.2016.12.022.
196. Muthuraj, R.; Misra, M.; Mohanty, A.K. Biodegradable Compatibilized Polymer Blends for Packaging Applications: A Literature Review. *J Appl Polym Sci* 2018, *135*.
197.
198. Daliu, P.; Santini, A.; Novellino, E. From Pharmaceuticals to Nutraceuticals: Bridging Disease Prevention and Management. *Expert Rev Clin Pharmacol* **2019**, *12*, doi:10.1080/17512433.2019.1552135.
199. Bergamin, A.; Mantzioris, E.; Cross, G.; Deo, P.; Garg, S.; Hill, A.M. Nutraceuticals: Reviewing Their Role in Chronic Disease Prevention and Management. *Pharmaceut Med* 2019, *33*.
200. Roy, S.; Ezati, P.; Khan, A.; Rhim, J.W. New Opportunities and Advances in Quercetin-Added Functional Packaging Films for Sustainable Packaging Applications: A Mini-Review. *Crit Rev Food Sci Nutr* 2023.

201. Zhang, F.; Khan, M.A.; Cheng, H.; Liang, L. Co-Encapsulation of α-Tocopherol and Resveratrol within Zein Nanoparticles: Impact on Antioxidant Activity and Stability. *J Food Eng* **2019**, *247*, 9–18, doi:10.1016/j.jfoodeng.2018.11.021.
202. Zhang, L.; Liu, Z.; Sun, Y.; Wang, X.; Li, L. Effect of α-Tocopherol Antioxidant on Rheological and Physicochemical Properties of Chitosan/Zein Edible Films. *LWT* **2020**, *118*, doi:10.1016/j.lwt.2019.108799.
203. Ye, F.; Astete, C.E.; Sabliov, C.M. Entrapment and Delivery of α-Tocopherol by a Self-Assembled, Alginate-Conjugated Prodrug Nanostructure. *Food Hydrocoll* **2017**, *72*, 62–72, doi:10.1016/j.foodhyd.2017.05.032.
204. Zhang, Z.; Hu, Y.; Ji, H.; Lin, Q.; Li, X.; Sang, S.; Julian McClements, D.; Chen, L.; Long, J.; Jiao, A.; et al. Physicochemical Stability, Antioxidant Activity, and Antimicrobial Activity of Quercetin-Loaded Zein Nanoparticles Coated with Dextrin-Modified Anionic Polysaccharides. *Food Chem* **2023**, *415*, doi:10.1016/j.foodchem.2023.135736.
205. Zhang, F.; Khan, M.A.; Cheng, H.; Liang, L. Co-Encapsulation of α-Tocopherol and Resveratrol within Zein Nanoparticles: Impact on Antioxidant Activity and Stability. *J Food Eng* **2019**, *247*, 9–18, doi:10.1016/j.jfoodeng.2018.11.021.
206. Chen, S.; McClements, D.J.; Jian, L.; Han, Y.; Dai, L.; Mao, L.; Gao, Y. Core-Shell Biopolymer Nanoparticles for Co-Delivery of Curcumin and Piperine: Sequential Electrostatic Deposition of Hyaluronic Acid and Chitosan Shells on the Zein Core. *ACS Appl Mater Interfaces* **2019**, *11*, 38103–38115, doi:10.1021/acsami.9b11782.
207. Zou, L.; Zheng, B.; Zhang, R.; Zhang, Z.; Liu, W.; Liu, C.; Xiao, H.; McClements, D.J. Enhancing the Bioaccessibility of Hydrophobic Bioactive Agents Using Mixed Colloidal Dispersions: Curcumin-Loaded Zein Nanoparticles plus Digestible Lipid Nanoparticles. *Food Research International* **2016**, *81*, doi:10.1016/j.foodres.2015.12.035.
208. Weissmueller, N.T.; Lu, H.D.; Hurley, A.; Prud'Homme, R.K. Nanocarriers from GRAS Zein Proteins to Encapsulate Hydrophobic Actives. *Biomacromolecules* **2016**, *17*, 3828–3837, doi:10.1021/acs.biomac.6b01440.
209. Ghanbarzadeh, B.; Oromiehi, A.R. Biodegradable Biocomposite Films Based on Whey Protein and Zein: Barrier, Mechanical Properties and AFM Analysis. *Int J Biol Macromol* **2008**, *43*, 209–215, doi:10.1016/j.ijbiomac.2008.05.006.
210. Dai, L.; Wei, Y.; Sun, C.; Mao, L.; McClements, D.J.; Gao, Y. Development of Protein-Polysaccharide-Surfactant Ternary Complex Particles as Delivery Vehicles for Curcumin. *Food Hydrocoll* **2018**, *85*, 75–85, doi:10.1016/j.foodhyd.2018.06.052.
211. Davidov-Pardo, G.; Joye, I.J.; Espinal-Ruiz, M.; McClements, D.J. Effect of Maillard Conjugates on the Physical Stability of Zein Nanoparticles Prepared by Liquid Antisolvent Coprecipitation. *J Agric Food Chem* **2015**, *63*, 8510–8518, doi:10.1021/acs.jafc.5b02699.
212. Liang, H.; Zhou, B.; He, L.; An, Y.; Lin, L.; Li, Y.; Liu, S.; Chen, Y.; Li, B. Fabrication of Zein/Quaternized Chitosan Nanoparticles for the Encapsulation and Protection of Curcumin. *RSC Adv* **2015**, *5*, doi:10.1039/c4ra14270e.
213. Peng, S.; Li, Z.; Zou, L.; Liu, W.; Liu, C.; McClements, D.J. Enhancement of Curcumin Bioavailability by Encapsulation in Sophorolipid-Coated Nanoparticles: An in Vitro and in Vivo Study. *J Agric Food Chem* **2018**, *66*, doi:10.1021/acs.jafc.7b05478.

214. Zou, Y.; Qian, Y.; Rong, X.; Cao, K.; McClements, D.J.; Hu, K. Encapsulation of Quercetin in Biopolymer-Coated Zein Nanoparticles: Formation, Stability, Antioxidant Capacity, and Bioaccessibility. *Food Hydrocoll* **2021**, *120*, doi:10.1016/j.foodhyd.2021.106980.
215. Yin, Y.C.; Yin, S.W.; Yang, X.Q.; Tang, C.H.; Wen, S.H.; Chen, Z.; Xiao, B. jie; Wu, L.Y. Surface Modification of Sodium Caseinate Films by Zein Coatings. *Food Hydrocoll* **2014**, *36*, doi:10.1016/j.foodhyd.2013.08.027.
216. Wang, L.; Hao, L.; Hou, H.; Wang, L.; Liu, S.; Tang, R.; Mao, J.; Zhou, Q.; Deng, Q.; Yan, L.; et al. Carboxymethylpachymaran-Coated Zein Nanoparticles for Oral Delivery of Curcumin: Formation, Characterization, Physicochemical Stability, and Controlled Release Properties. *ACS Food Science and Technology* **2023**, *3*, 170–181, doi:10.1021/acsfoodscitech.2c00354.
217. Zheng, B.; Peng, S.; Zhang, X.; McClements, D.J. Impact of Delivery System Type on Curcumin Bioaccessibility: Comparison of Curcumin-Loaded Nanoemulsions with Commercial Curcumin Supplements. *J Agric Food Chem* **2018**, *66*, doi:10.1021/acs.jafc.8b03174.
218. Sánchez-López, E.; Ettcheto, M.; Egea, M.A.; Espina, M.; Cano, A.; Calpena, A.C.; Camins, A.; Carmona, N.; Silva, A.M.; Souto, E.B.; et al. Memantine Loaded PLGA PEGylated Nanoparticles for Alzheimer's Disease: In Vitro and in Vivo Characterization. *J Nanobiotechnology* **2018**, *16*, doi:10.1186/s12951-018-0356-z.
219. Sun, Y.; Zhong, M.; Kang, M.; Liao, Y.; Wang, Z.; Li, Y.; Qi, B. Novel Core-Shell Nanoparticles: Encapsulation and Delivery of Curcumin Using Guanidine Hydrochloride-Induced Oleosome Protein Self-Assembly. *LWT* **2023**, *173*, doi:10.1016/j.lwt.2022.114352.
220. Le, H. Van; Le Cerf, D.; Le, H. V; Le Cerf, D. 2204283 (1 of 26) Colloidal Polyelectrolyte Complexes from Hyaluronic Acid: Preparation and Biomedical Applications. **2022**, doi:10.1002/smll.202204283.
221. Wei, Y.; Guo, A.; Liu, Z.; Mao, L.; Yuan, F.; Gao, Y.; Mackie, A. Structural Design of Zein-Cellulose Nanocrystals Core–Shell Microparticles for Delivery of Curcumin. *Food Chem* **2021**, *357*, doi:10.1016/j.foodchem.2021.129849.
222. Liu, J.; Yu, H.; Kong, J.; Ge, X.; Sun, Y.; Mao, M.; Wang, D.Y.; Wang, Y. Preparation, Characterization, Stability, and Controlled Release of Chitosan-Coated Zein/Shellac Nanoparticles for the Delivery of Quercetin. *Food Chem* **2024**, *444*, 138634, doi:10.1016/J.FOODCHEM.2024.138634.
223. da Rosa, C.G.; de Oliveira Brisola Maciel, M.V.; de Carvalho, S.M.; de Melo, A.P.Z.; Jummes, B.; da Silva, T.; Martelli, S.M.; Villetti, M.A.; Bertoldi, F.C.; Barreto, P.L.M. Characterization and Evaluation of Physicochemical and Antimicrobial Properties of Zein Nanoparticles Loaded with Phenolics Monoterpenes. *Colloids Surf A Physicochem Eng Asp* **2015**, *481*, 337–344, doi:10.1016/j.colsurfa.2015.05.019.
224. Trivedi, D.; Venkata Satyanarayana Reddy Karri, V.; Spandana M, A.K.; Kuppusamy, G. Design of Experiments: Optimization and Applications in Pharmaceutical Nanotechnology. *Chem Sci Rev Lett* **2015**, *2015*.
225. Tavares Luiz, M.; Santos Rosa Viegas, J.; Palma Abriata, J.; Viegas, F.; Testa Moura de Carvalho Vicentini, F.; Lopes Badra Bentley, M.V.; Chorilli, M.; Maldonado Marchetti, J.; Tapia-Blácido, D.R. Design of Experiments (DoE) to Develop and to Optimize Nanoparticles as Drug Delivery Systems. *European Journal of*

Pharmaceutics and Biopharmaceutics **2021**, *165*, 127–148, doi:10.1016/j.ejpb.2021.05.011.
226. Rampado, R.; Peer, D. Design of Experiments in the Optimization of Nanoparticle-Based Drug Delivery Systems. *Journal of Controlled Release* **2023**, *358*, doi:10.1016/j.jconrel.2023.05.001.
227. Ellen MacArthur Foundation/World economic forum The New Plastics Economy: Catalysing Action. *World Economic Forum* **2017**.
228. Degli Esposti, M.; Morselli, D.; Fava, F.; Bertin, L.; Cavani, F.; Viaggi, D.; Fabbri, P. The Role of Biotechnology in the Transition from Plastics to Bioplastics: An Opportunity to Reconnect Global Growth with Sustainability. *FEBS Open Bio* 2021, *11*.
229. Phiri, R.; Mavinkere Rangappa, S.; Siengchin, S.; Oladijo, O.P.; Dhakal, H.N. Development of Sustainable Biopolymer-Based Composites for Lightweight Applications from Agricultural Waste Biomass: A Review. *Advanced Industrial and Engineering Polymer Research* 2023, *6*.
230. Mooney, B.P. The Second Green Revolution? Production of Plant-Based Biodegradable Plastics. *Biochemical Journal* 2009, *418*.
231. Chang, B.P.; Trinh, B.M.; Tadele, D.T.; Bandara, N.; Mekonnen, T.H. Natural Antioxidant and Antimicrobial Agents and Processing Technologies for the Design of Active Food Packaging Polymers. *Polymer Reviews* **2023**, doi:10.1080/15583724.2023.2234464.
232. Baranwal, J.; Barse, B.; Fais, A.; Delogu, G.L.; Kumar, A. Biopolymer: A Sustainable Material for Food and Medical Applications. *Polymers (Basel)* 2022, *14*.
233. Dias, Y.J.; Kolbasov, A.; Sinha-Ray, S.; Pourdeyhimi, B.; Yarin, A.L. Theoretical and Experimental Study of Dissolution Mechanism of Cellulose. *J Mol Liq* **2020**, *312*, doi:10.1016/j.molliq.2020.113450.
234. Sreedevi, S.; Unni, K.N.; Sajith, S.; Priji, P.; Josh, M.S.; Benjamin, S. Bioplastics: Advances in Polyhydroxybutyrate Research. In; 2014.
235. Keskin, G.; Klzll, G.; Bechelany, M.; Pochat-Bohatier, C.; Öner, M. Potential of Polyhydroxyalkanoate (PHA) Polymers Family as Substitutes of Petroleum Based Polymers for Packaging Applications and Solutions Brought by Their Composites to Form Barrier Materials. In Proceedings of the Pure and Applied Chemistry; 2017; Vol. 89.
236. Frykberg, R.G.; Banks, J. Challenges in the Treatment of Chronic Wounds. *Adv Wound Care (New Rochelle)* **2015**, *4*, doi:10.1089/wound.2015.0635.
237. Hua, S.; de Matos, M.B.C.; Metselaar, J.M.; Storm, G. Current Trends and Challenges in the Clinical Translation of Nanoparticulate Nanomedicines: Pathways for Translational Development and Commercialization. *Front Pharmacol* 2018, *9*.
238. Preethi, G.U.; Unnikrishnan, B.S.; Sreekutty, J.; Archana, M.G.; Anupama, M.S.; Shiji, R.; Raveendran Pillai, K.; Joseph, M.M.; Syama, H.P.; Sreelekha, T.T. Semi-Interpenetrating Nanosilver Doped Polysaccharide Hydrogel Scaffolds for Cutaneous Wound Healing. *Int J Biol Macromol* **2020**, *142*, doi:10.1016/j.ijbiomac.2019.10.012.
239. Creţu, B.E.B.; Dodi, G.; Gardikiotis, I.; Balan, V.; Nacu, I.; Stoica, I.; Stoleru, E.; Rusu, A.G.; Ghilan, A.; Nita, L.E.; et al. Bioactive Composite Cryogels Based on

Poly (Vinyl Alcohol) and a Polymacrolactone as Tissue Engineering Scaffolds: In Vitro and In Vivo Studies. *Pharmaceutics* **2023**, *15*, doi:10.3390/pharmaceutics15122730.
240. Gherasim, O.; Puiu, R.A.; Bîrca, A.C.; Burduşel, A.C.; Grumezescu, A.M. An Updated Review on Silver Nanoparticles in Biomedicine. *Nanomaterials* 2020, *10*.
241. Mariia, K.; Arif, M.; Shi, J.; Song, F.; Chi, Z.; Liu, C. Novel Chitosan-Ulvan Hydrogel Reinforcement by Cellulose Nanocrystals with Epidermal Growth Factor for Enhanced Wound Healing: In Vitro and in Vivo Analysis. *Int J Biol Macromol* **2021**, *183*, doi:10.1016/j.ijbiomac.2021.04.156.
242. Tenchov, R.; Bird, R.; Curtze, A.E.; Zhou, Q. Lipid Nanoparticles from Liposomes to MRNA Vaccine Delivery, a Landscape of Research Diversity and Advancement. *ACS Nano* 2021, *15*.
243. Hamdan, S.; Pastar, I.; Drakulich, S.; Dikici, E.; Tomic-Canic, M.; Deo, S.; Daunert, S. Nanotechnology-Driven Therapeutic Interventions in Wound Healing: Potential Uses and Applications. *ACS Cent Sci* **2017**, *3*, doi:10.1021/acscentsci.6b00371.
244. Idrees, H.; Zaidi, S.Z.J.; Sabir, A.; Khan, R.U.; Zhang, X.; Hassan, S.U. A Review of Biodegradable Natural Polymer-Based Nanoparticles for Drug Delivery Applications. *Nanomaterials* 2020, *10*.
245. Singh, R.; Bellat, V.; Wang, M.; Schweitzer, M.E.; Wu, Y.L.; Tung, C.H.; Souweidane, M.M.; Law, B. Volume of Distribution and Clearance of Peptide-Based Nanofiber after Convection-Enhanced Delivery. *J Neurosurg* **2018**, *129*, doi:10.3171/2017.2.JNS162273.
246. Hu, X.; Liu, S.; Zhou, G.; Huang, Y.; Xie, Z.; Jing, X. Electrospinning of Polymeric Nanofibers for Drug Delivery Applications. *Journal of Controlled Release* 2014, *185*.
247. Luraghi, A.; Peri, F.; Moroni, L. Electrospinning for Drug Delivery Applications: A Review. *Journal of Controlled Release* 2021, *334*.
248. Dang, A.; Wang, Y.; Zhang, H.; Panatdasirisuk, W.; Xia, Y.; Wang, Z.; Jariwala, D.; Li, T.; Yang, S. Electrospun Gold Nanoprism/Poly(Vinyl Alcohol) Nanofibers for Flexible and Free-Standing Surface-Enhanced Raman Scattering Substrates. *ACS Appl Nano Mater* **2022**, *5*, doi:10.1021/acsanm.2c00689.
249. Haider, A.; Haider, S.; Kang, I.K. A Comprehensive Review Summarizing the Effect of Electrospinning Parameters and Potential Applications of Nanofibers in Biomedical and Biotechnology. *Arabian Journal of Chemistry* 2018, *11*.
250. Omer, S.; Forgách, L.; Zelkó, R.; Sebe, I. Scale-up of Electrospinning: Market Overview of Products and Devices for Pharmaceutical and Biomedical Purposes. *Pharmaceutics* 2021, *13*.
251. Pant, B.; Park, M.; Park, S.J. Drug Delivery Applications of Core-Sheath Nanofibers Prepared by Coaxial Electrospinning: A Review. *Pharmaceutics* 2019, *11*.
252. Kolbasov, A.; Sinha-Ray, S.; Joijode, A.; Hassan, M.A.; Brown, D.; Maze, B.; Pourdeyhimi, B.; Yarin, A.L. Industrial-Scale Solution Blowing of Soy Protein Nanofibers. *Ind Eng Chem Res* **2016**, *55*, doi:10.1021/acs.iecr.5b04277.
253. Dias, Y.J.; Robles, J.R.; Sinha-Ray, S.; Abiade, J.; Pourdeyhimi, B.; Niemczyk-Soczynska, B.; Kolbuk, D.; Sajkiewicz, P.; Yarin, A.L. Solution-Blown Poly(Hydroxybutyrate) and ϵ-Poly- l -Lysine Submicro- And Microfiber-Based Sustainable Nonwovens with Antimicrobial Activity for Single-Use Applications. *ACS Biomater Sci Eng* **2021**, *7*, doi:10.1021/acsbiomaterials.1c00594.

254. Rawlins, J.; Kang, J. Fine Liquid Blowing: A High Reynolds Number, High Production Rate Nanofiber Manufacturing Technique. *J Appl Polym Sci* **2019**, *136*, doi:10.1002/app.47384.
255. Cui, J.; Qiu, L.; Qiu, Y.; Wang, Q.; Wei, Q. Co-Electrospun Nanofibers of PVA-SbQ and Zein for Wound Healing. *J Appl Polym Sci* **2015**, *132*, doi:10.1002/app.42565.
256. Mary, A.S.; Raghavan, V.S.; Kagula, S.; Krishnakumar, V.; Kannan, M.; Gorthi, S.S.; Rajaram, K. Enhanced in Vitro Wound Healing Using PVA/B-PEI Nanofiber Mats: A Promising Wound Therapeutic Agent against ESKAPE and Opportunistic Pathogens. *ACS Appl Bio Mater* **2021**, *4*, doi:10.1021/acsabm.1c00985.
257. Kan, Y.; Bondareva, J. V.; Statnik, E.S.; Cvjetinovic, J.; Lipovskikh, S.; Abdurashitov, A.S.; Kirsanova, M.A.; Sukhorukhov, G.B.; Evlashin, S.A.; Salimon, A.I.; et al. Effect of Graphene Oxide and Nanosilica Modifications on Electrospun Core-Shell PVA–PEG–SiO2@PVA–GO Fiber Mats. *Nanomaterials* **2022**, *12*, doi:10.3390/nano12060998.
258. Ghalei, S.; Asadi, H.; Ghalei, B. Zein Nanoparticle-Embedded Electrospun PVA Nanofibers as Wound Dressing for Topical Delivery of Anti-Inflammatory Diclofenac. *J Appl Polym Sci* **2018**, *135*, doi:10.1002/app.46643.
259. Oral, E.; Rowell, S.L.; Muratoglu, O.K. The Effect of α-Tocopherol on the Oxidation and Free Radical Decay in Irradiated UHMWPE. *Biomaterials* **2006**, *27*, doi:10.1016/j.biomaterials.2006.07.017.
260. Wen, P.; Wen, Y.; Zong, M.H.; Linhardt, R.J.; Wu, H. Encapsulation of Bioactive Compound in Electrospun Fibers and Its Potential Application. *J Agric Food Chem* 2017, *65*.
261. Wongsasulak, S.; Pathumban, S.; Yoovidhya, T. Effect of Entrapped α-Tocopherol on Mucoadhesivity and Evaluation of the Release, Degradation, and Swelling Characteristics of Zein-Chitosan Composite Electrospun Fibers. *J Food Eng* **2014**, *120*, doi:10.1016/j.jfoodeng.2013.07.028.
262. De Oliveira Mori, C.L.S.; Dos Passos, N.A.; Oliveira, J.E.; Mattoso, L.H.C.; Mori, F.A.; Carvalho, A.G.; De Souza Fonseca, A.; Tonoli, G.H.D. Electrospinning of Zein/Tannin Bio-Nanofibers. *Ind Crops Prod* **2014**, *52*, doi:10.1016/j.indcrop.2013.10.047.
263. Liu, Y.; He, J.H.; Yu, J.Y.; Zeng, H.M. Controlling Numbers and Sizes of Beads in Electrospun Nanofibers. *Polym Int* **2008**, *57*, doi:10.1002/pi.2387.
264. Cui, S.; Sun, X.; Li, K.; Gou, D.; Zhou, Y.; Hu, J.; Liu, Y. Polylactide Nanofibers Delivering Doxycycline for Chronic Wound Treatment. *Materials Science and Engineering C* **2019**, *104*, doi:10.1016/j.msec.2019.109745.
265. Azimi, B.; Maleki, H.; Zavagna, L.; de la Ossa, J.G.; Linari, S.; Lazzeri, A.; Danti, S. Bio-Based Electrospun Fibers for Wound Healing. *J Funct Biomater* 2020, *11*.
266. Gillgren, T.; Barker, S.A.; Belton, P.S.; Georget, D.M.R.; Stading, M. Plasticization of Zein: A Thermomechanical, FTIR, and Dielectric Study. *Biomacromolecules* **2009**, *10*, doi:10.1021/bm801374q.
267. Santos, A.M.C.; Medeiros, E.L.G.; Blaker, J.J.; Medeiros, E.S. Aqueous Solution Blow Spinning of Poly(Vinyl Alcohol) Micro- and Nanofibers. *Mater Lett* **2016**, *176*, doi:10.1016/j.matlet.2016.04.101.
268. Tadele, D.T.; Mekonnen, T.H. Co-Encapsulation of Quercetin and α-Tocopherol Bioactives in Zein Nanoparticles: Synergistic Interactions, Stability, and Controlled Release., doi:10.1021/acsapm.3c03000.

269. Jeong, J.P.; Kim, K.; Kim, J.; Kim, Y.; Jung, S. New Polyvinyl Alcohol/Succinoglycan-Based Hydrogels for PH-Responsive Drug Delivery. *Polymers (Basel)* **2023**, *15*, doi:10.3390/polym15143009.
270. Rathna, G.V.N.; Jog, J.P.; Gaikwad, A.B. Development of Non-Woven Nanofibers of Egg Albumen-Poly (Vinyl Alcohol) Blends: Influence of Solution Properties on Morphology of Nanofibers. *Polym J* **2011**, *43*, doi:10.1038/pj.2011.34.
271. Dos Santos, D.M.; De Annunzio, S.R.; Carmello, J.C.; Pavarina, A.C.; Fontana, C.R.; Correa, D.S. Combining Coaxial Electrospinning and 3D Printing: Design of Biodegradable Bilayered Membranes with Dual Drug Delivery Capability for Periodontitis Treatment. *ACS Appl Bio Mater* **2022**, *5*, doi:10.1021/acsabm.1c01019.
272. Cheng, J.; Wang, J.; Cui, L. Incorporation of α-Tocopherol into Pea Protein Edible Film Using PH-Shifting and Nanoemulsion Treatments: Enhancing Its Antioxidant Activity without Negative Impacts on Mechanical Properties. *Foods* **2023**, *12*, doi:10.3390/foods12102022.
273. Li, K.K.; Yin, S.W.; Yin, Y.C.; Tang, C.H.; Yang, X.Q.; Wen, S.H. Preparation of Water-Soluble Antimicrobial Zein Nanoparticles by a Modified Antisolvent Approach and Their Characterization. *J Food Eng* **2013**, *119*, doi:10.1016/j.jfoodeng.2013.05.038.
274. Patel, A.; Hu, Y.; Tiwari, J.K.; Velikov, K.P. Synthesis and Characterisation of Zein-Curcumin Colloidal Particles. *Soft Matter* **2010**, *6*, doi:10.1039/c0sm00800a.
275. Murdande, S.B.; Pikal, M.J.; Shanker, R.M.; Bogner, R.H. Aqueous Solubility of Crystalline and Amorphous Drugs: Challenges in Measurement. *Pharm Dev Technol* 2011, *16*.
276. Zhang, Y.; Niu, Y.; Luo, Y.; Ge, M.; Yang, T.; Yu, L.; Wang, Q. Fabrication, Characterization and Antimicrobial Activities of Thymolloaded Zein Nanoparticles Stabilized by Sodium Caseinate-Chitosan Hydrochloride Double Layers. *Food Chem* **2014**, *142*, doi:10.1016/j.foodchem.2013.07.058.
277. Wu, F.; Wei, J.; Liu, C.; O'Neill, B.; Ngothai, Y. Fabrication and Properties of Porous Scaffold of Zein/PCL Biocomposite for Bone Tissue Engineering. *Compos B Eng* **2012**, *43*, doi:10.1016/j.compositesb.2012.02.040.
278. Feng, Y.; Li, X.; Zhang, Q.; Yan, S.; Guo, Y.; Li, M.; You, R. Mechanically Robust and Flexible Silk Protein/Polysaccharide Composite Sponges for Wound Dressing. *Carbohydr Polym* **2019**, *216*, doi:10.1016/j.carbpol.2019.04.008.
279. Karataş, A.; Hilal Algan, A.; Pekel-Bayramgil, N.; Turhan, F.; Altanlar, N. Ofloxacin Loaded Electrospun Fibers for Ocular Drug Delivery: Effect of Formulation Variables on Fiber Morphology and Drug Release. *Curr Drug Deliv* **2016**, *13*, doi:10.2174/1567201812666151030162258.
280. Sharma, D.; Satapathy, B.K. Understanding Release Kinetics and Collapse Proof Suture Retention Response of Curcumin Loaded Electrospun Mats Based on Aliphatic Polyesters and Their Blends. *J Mech Behav Biomed Mater* **2021**, *120*, doi:10.1016/j.jmbbm.2021.104556.
281. Mitchell, M.J.; Billingsley, M.M.; Haley, R.M.; Wechsler, M.E.; Peppas, N.A.; Langer, R. Engineering Precision Nanoparticles for Drug Delivery. *Nat Rev Drug Discov* 2021, *20*.
282. Rizvi, S.A.A.; Saleh, A.M. Applications of Nanoparticle Systems in Drug Delivery Technology. *Saudi Pharmaceutical Journal* 2018, *26*.

283. Limaye, A.; Perumal, V.; Karner, C.M.; Livingston Arinzeh, T. Plant-Derived Zein as an Alternative to Animal-Derived Gelatin for Use as a Tissue Engineering Scaffold. *Adv Nanobiomed Res* **2024**, *4*, doi:10.1002/anbr.202300104.
284. Górnicka, M.; Ciecierska, A.; Hamulka, J.; Drywień, M.E.; Frackiewicz, J.; Górnicki, K.; Wawrzyniak, A. α-Tocopherol Protects the Heart, Muscles, and Testes from Lipid Peroxidation in Growing Male Rats Subjected to Physical Efforts. *Oxid Med Cell Longev* **2019**, *2019*, doi:10.1155/2019/8431057.
285. Zakharova, I.O.; Sokolova, T. V.; Vlasova, Y.A.; Bayunova, L. V.; Rychkova, M.P.; Avrova, N.F. α-Tocopherol at Nanomolar Concentration Protects Cortical Neurons against Oxidative Stress. *Int J Mol Sci* **2017**, *18*, doi:10.3390/ijms18010216.
286. Garcia, J.; Felix, M.; Cordobés, F.; Guerrero, A. Effect of Solvent and Additives on the Electrospinnability of BSA Solutions. *Colloids Surf B Biointerfaces* **2022**, *217*, doi:10.1016/j.colsurfb.2022.112683.
287. Camillo, L.; Grossini, E.; Farruggio, S.; Marotta, P.; Gironi, L.C.; Zavattaro, E.; Savoia, P. Alpha-Tocopherol Protects Human Dermal Fibroblasts by Modulating Nitric Oxide Release, Mitochondrial Function, Redox Status, and Inflammation. *Skin Pharmacol Physiol* **2022**, *35*, doi:10.1159/000517204.
288. Schneider, K.H.; Oberoi, G.; Unger, E.; Janjic, K.; Rohringer, S.; Heber, S.; Agis, H.; Schedle, A.; Kiss, H.; Podesser, B.K.; et al. Medical 3D Printing with Polyjet Technology: Effect of Material Type and Printing Orientation on Printability, Surface Structure and Cytotoxicity. *3D Print Med* **2023**, *9*, doi:10.1186/s41205-023-00190-y.
289. Chen, Y.; Xu, C.; Cao, L.; Cao, X. Highly Toughened Polypropylene/Ethylene-Propylene-Diene Monomer/Zinc Dimethacrylate Ternary Blends Prepared via Peroxide-Induced Dynamic Vulcanization. *Mater Chem Phys* **2013**, *138*, doi:10.1016/j.matchemphys.2012.10.034.

Appendix A

Supporting Information from Chapter 3

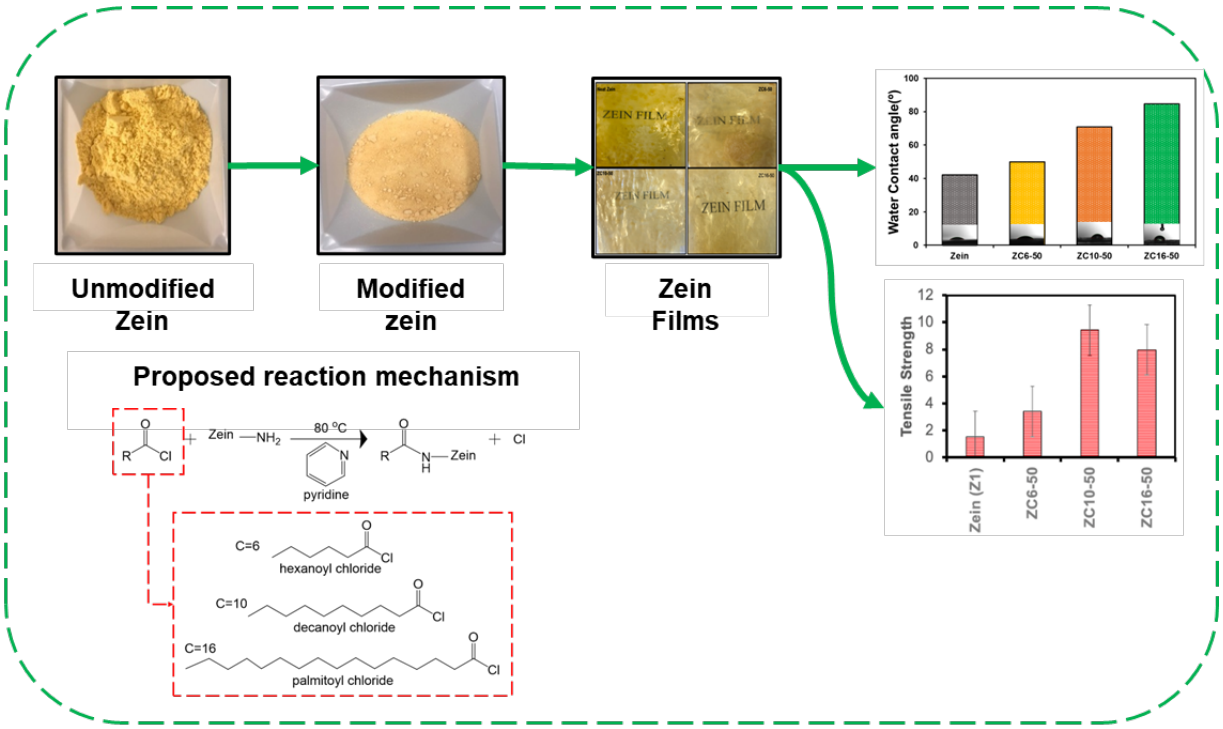


Figure A. Graphical abstract

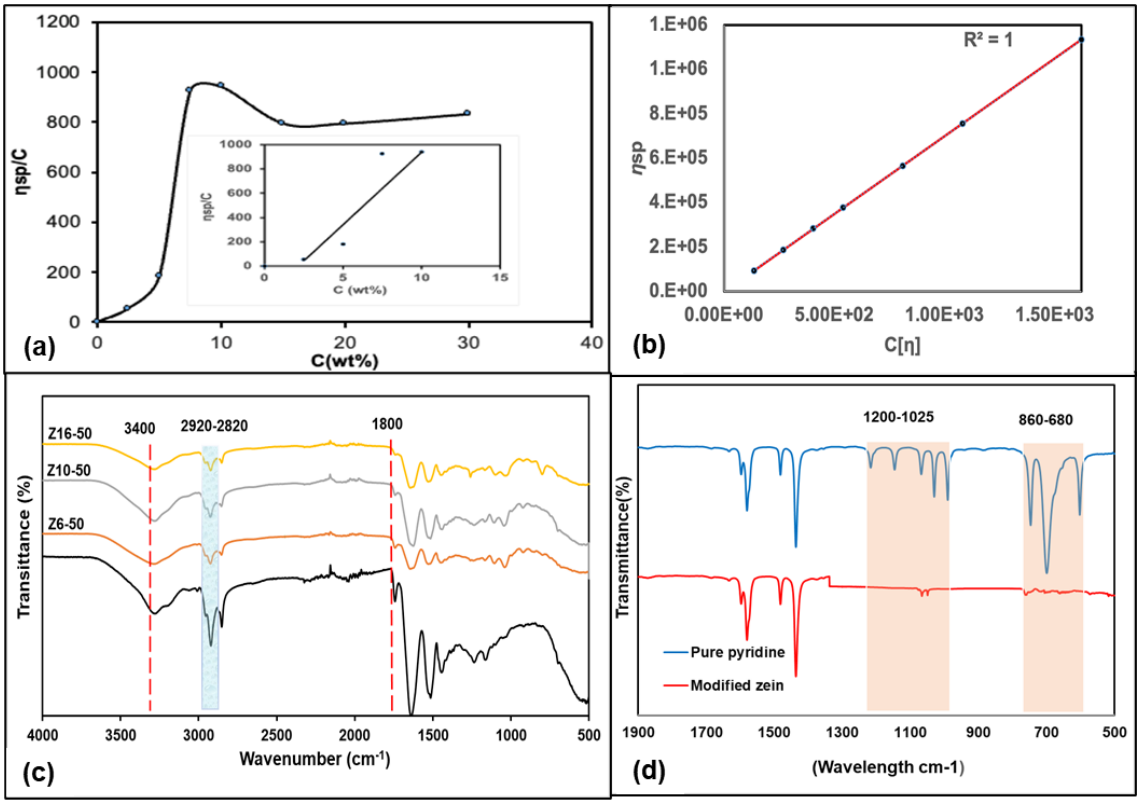


Figure A1. a) A plot between zero shear viscosity and average zein concentration at 25 °C, b) Specific viscosity, as a function of C[η], c) ATR-FTIR spectra of unmodified and modified zein films, and d) ATR-FTIR spectra of modified zein film and pure pyridine.

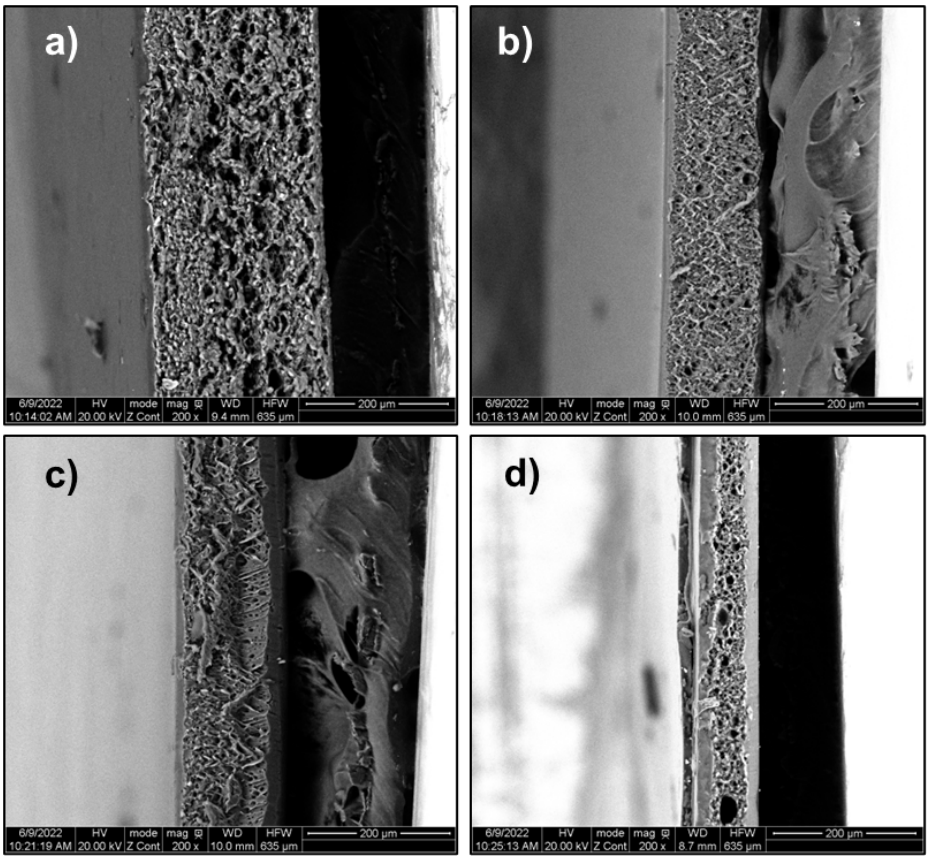


Figure A2. SEM surface images for cross sections of zein films a) net zein b) zein/hexanoyl acid (ZC6-50) c) zein/decanoyl acid (ZC10-50), d) zein/palmitic acid (ZC16-50)

Table A 1 Summary of mechanical properties for zein films

Sample	Tensile strength **(TS, MPa)**	Elongation at break **(ETB %)**	Young's Modulus **(MPa)**	Toughness **(MJ/m^3)**
Z1	1.70 ± 0.23^a	38.41 ± 4.56^a	154.42 ± 3.45^a	0.017 ± 0.001^a
ZC6-50	3.25 ± 0.86^b	48.22 ± 3.03^b	219.15 ± 1.60^b	0.526 ± 0.050^b
ZC10-50	8.27 ± 0.76^c	66.00 ± 4.91^c	173.13 ± 11.5^c	0.706 ± 0.230^{ab}
ZC16-50	6.61 ± 0.94^c	68.00 ± 3.70^c	154.05 ± 29.0^d	0.994 ± 0.100^c

*(a-d) denotes significant differences within each property for $\alpha < 0.05$). Results are average ± standard deviation from five sample specimen.

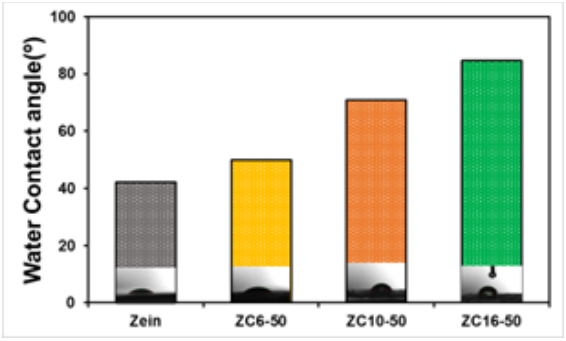


Figure A3. Water contact angle measurements.

Appendix B

Supporting Information from Chapter 4

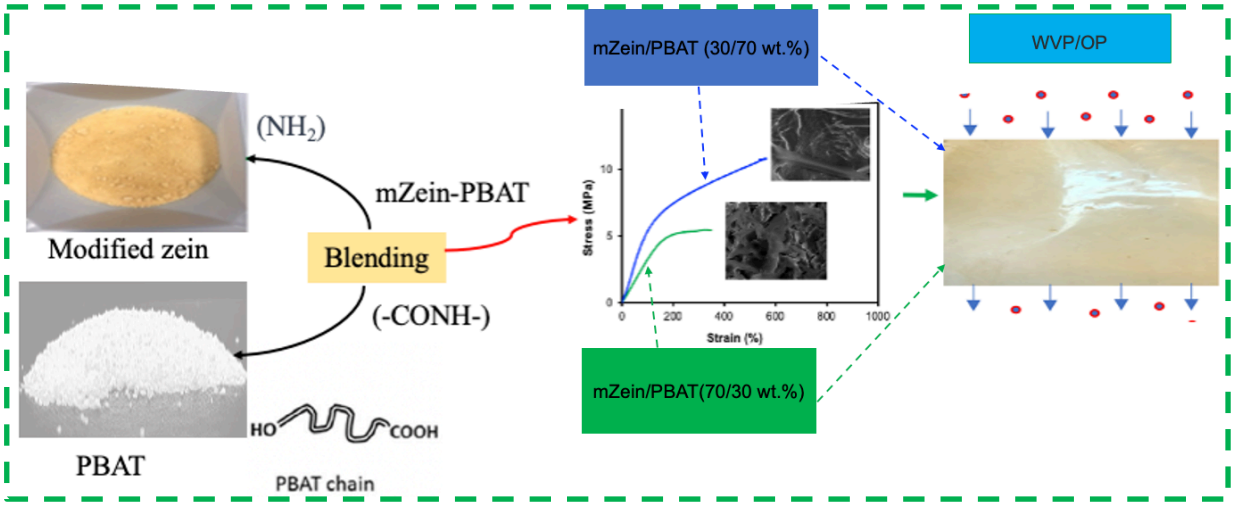


Figure B. Graphical abstract

The water contact angle, surface energy, and interfacial tension of the blend provide valuable information about the degree of interaction between the blends[172]. A higher water contact angle and lower surface energy indicate a more hydrophobic surface, while a lower interfacial tension suggests better compatibility between the two components. These parameters play a crucial role in determining the wettability, adhesion, and compatibility properties of the blend [288].

In comparison, unmodified zein generally exhibits a higher surface energy compared to the modified zein and PBAT blend as shown **Figure B1.** This higher surface energy indicates a more hydrophilic surface, which may impact the blend's wettability and adhesion properties. Additionally, the interfacial tension of unmodified zein and PBAT blend exhibit higher values compared to the modified zein and PBAT blend. Overall, understanding the surface properties

of these blends is crucial for their application in various industries, such as food packaging and biomedical engineering.

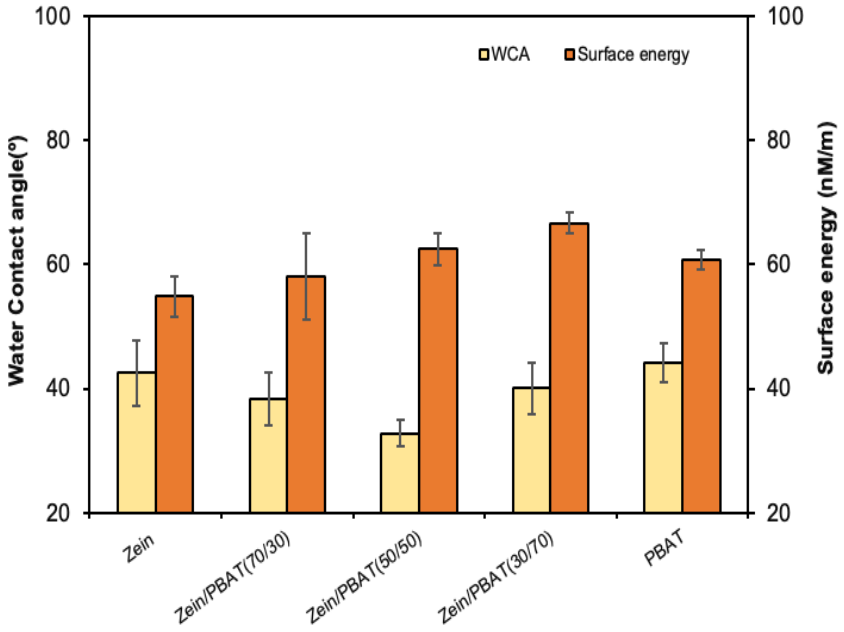


Figure B1. Water contact angle and surface energy for unmodified Zein/PBAT blend films.

Table B1 presents a summary of the key parameters and properties of both non-modified zein and the modified zein-PBAT blend, along with the corresponding values from previous studies. Additionally, our results reveal that the modified zein-PBAT blend outperforms non-modified zein in terms of oxygen and moisture barrier properties, optical properties, and disintegration behavior in a composting environment. These findings are in line with previous studies that have reported the advantageous characteristics of modified zein films.

Table B 1. Comparison of properties of mZein/PBAT blends with different studies on bio-based polymeric blends

Blend composition	**Modification/Compatibilizer**	**Properties**	**Value**	**Reference**
mZein/PBAT (30/70)	Decanoic acid	(WVP) (%)	68.00	This study
		(OP) (%)	59.02	
		Tensile Strength (MPa)	10.88	
		Elongation at Break(%)	561.41	
		Disintegration in Composting (%)	75.05	
Zein/PBAT (30/70)	Poly(ethylene glycol diglycidyl ether	(WVP)	-	[14]
		(OP)	-	
		Tensile Strength (MPa)	18.20	
		Elongation at Break(%)	860.04	
		Disintegration in Composting (%)	53.10	
TPS/PBAT (50/50)	Styrene glycidyl methacrylate copolymer	(WVP) (%)	80.21	[171]
		(OP)	-	
		Tensile Strength (MPa)	24.60	

		Elongation at Break(%)	107.81	
		Disintegration in Composting	-	

Table B.2. Summary of mechanical properties for unmodified and modified zein/PBAT blend films

Blend Composition	Tensile strength (MPa)	Elongation at break (%)	Elastic modulus (MPa)	Study
Zein	1.71 ± 0.51	50.12 ± 4.10	161.56± 11	This study
Zein/PBAT (70/30)	2.20± 1.11	46.67± 2.41	145.94± 16	
Zein/PBAT (50/50)	3.60± 1.71	72.48± 7.60	120.31± 23	
Zein/PBAT (30/70)	5.88± 0.20	102.61± 5.70	91.65± 12	
mZein/PBAT (70/30)	3.25± 0.46	87.31 ± 17	218.41 ± 1.77	
mZein/PBAT (50/50)	5.39 ± 0.76	152.35 ± 10.23	182.78 ± 1.57	
mZein/PBAT (30/70)	10.88 ± 1.15	561.41 ± 10.23	105.63 ± 8.19	
PBAT	13.61± 0.91	791.83± 20.10	72.23± 17	

Appendix C

Supporting Information from Chapter 5

The quantification of adsorbed and encapsulated materials in zein nanoparticles can be achieved through standard curve analysis. Design of Experiments (DOE) is provided, including factors and levels using a Box-Behnken design matrix for zein/quercetin/tocopherol nanoparticle formulation. Normal Probability Plot analysis is employed to analyze residuals in the study of zein/quercetin/tocopherol nanoparticles. Optimized Response Surfaces plots are presented to illustrate the optimization process for zein/quercetin/tocopherol nanoparticle formulations based on specific parameters.

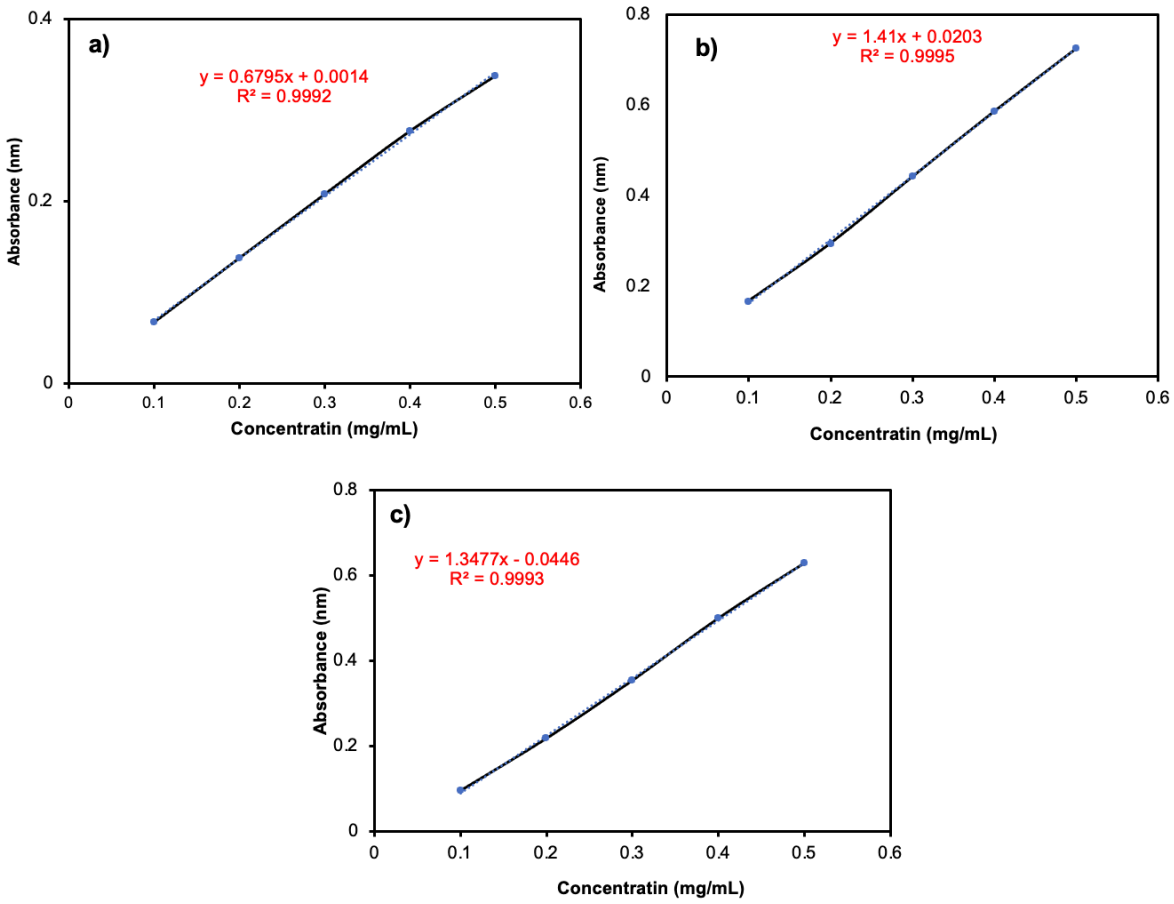


Figure C1. The calibration standards for quercetin and α-tocopherol were established at 369 nm and 295 nm, respectively, for the Zein/Que/Toc nanoparticles.

***Table C.1**. Experiment Factors and Levels*

Factors	**Level (−1)**	**Level (0)**	**Level (+1)**
Zein/Que/Toc (mg/mL), X_1	1	1.5	2
Tween 80 (mg), X_2	1.5	2.5	3.5
pH, X_3	4	6	8

Table C.2. Box-Behnken Design Matrix

Run	Zein/Que/Toc (X_1)	Tween 80 (X_2)	pH (X_3)	ZAv (nm)	PDI	ZP (mV)	EE(%)
1	1.5	3.5	8	229.1	0.327	-18.32	65.78
2	2	2.5	4	244.5	0.278	-25	70.24
3	1.5	2.5	6	256.4	0.266	-20.01	73.12
4	1	3.5	6	151.7	0.083	-32.16	79.89
5	1.5	2.5	6	201.45	0.243	-24.42	84.72
6	1.5	3.5	4	172.5	0.109	-37.71	94.85
7	1	1.5	6	145.9	0.112	-33.6	83.26
8	2	2.5	8	267.8	0.357	-30.52	91.49
9	1.5	1.5	8	238.7	0.122	-37.9	94.78
10	1	2.5	4	132.4	0.134	-40.42	84.54
11	2	1.5	6	211.6	0.27	-30.4	86.25
12	1.5	2.5	6	220.4	0.265	-28.7	82.05
13	1	2.5	8	149.6	0.102	-32.4	81.78
14	1.5	1.5	4	219.31	0.249	-23.34	87.9
15	2	3.5	6	163.82	0.114	-15.45	87.78

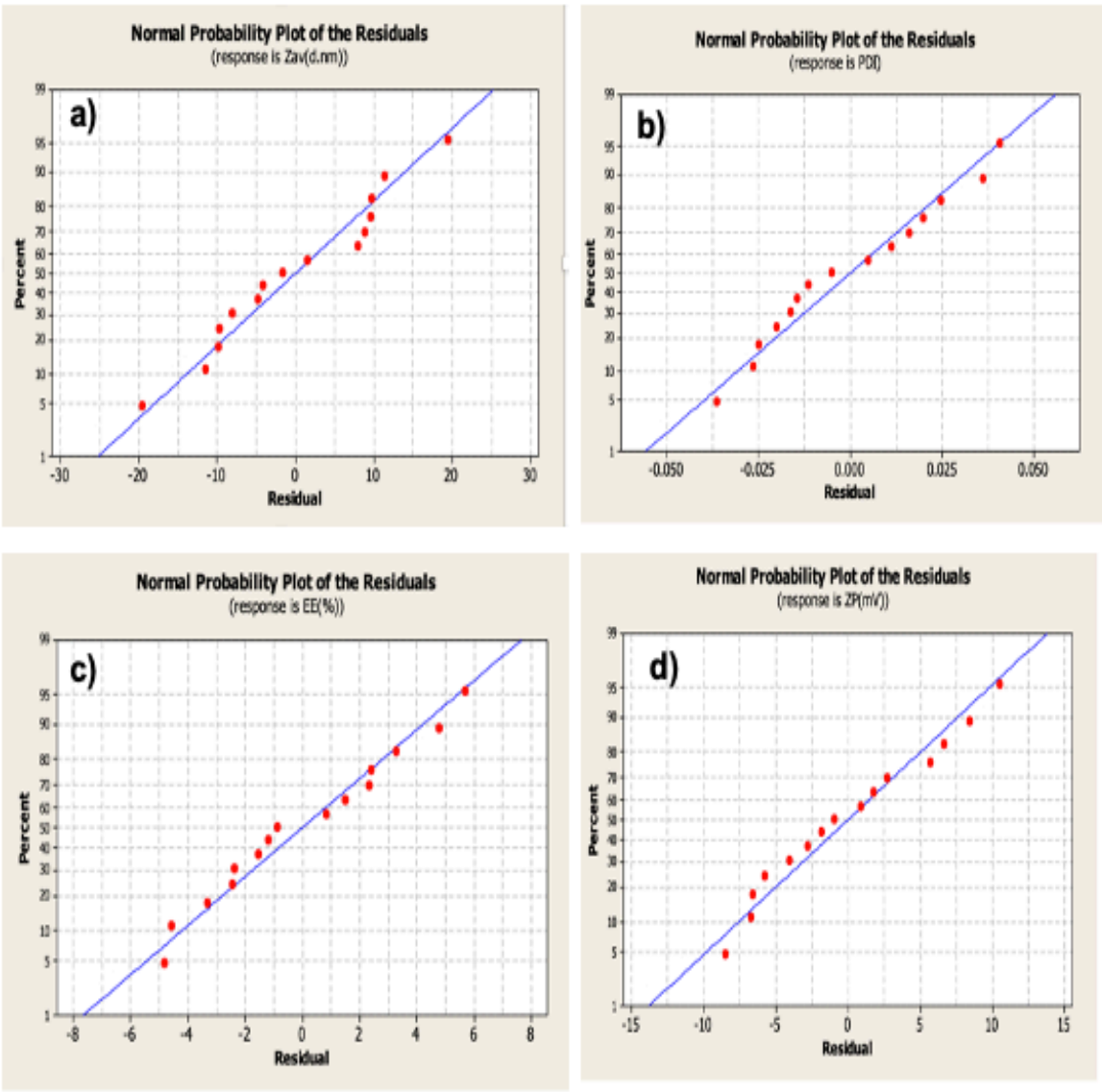


Figure C2. Normal probability plot of the average particle size, PDI, EE (%), and zeta potential of Zein/Que/Toc nanoparticles

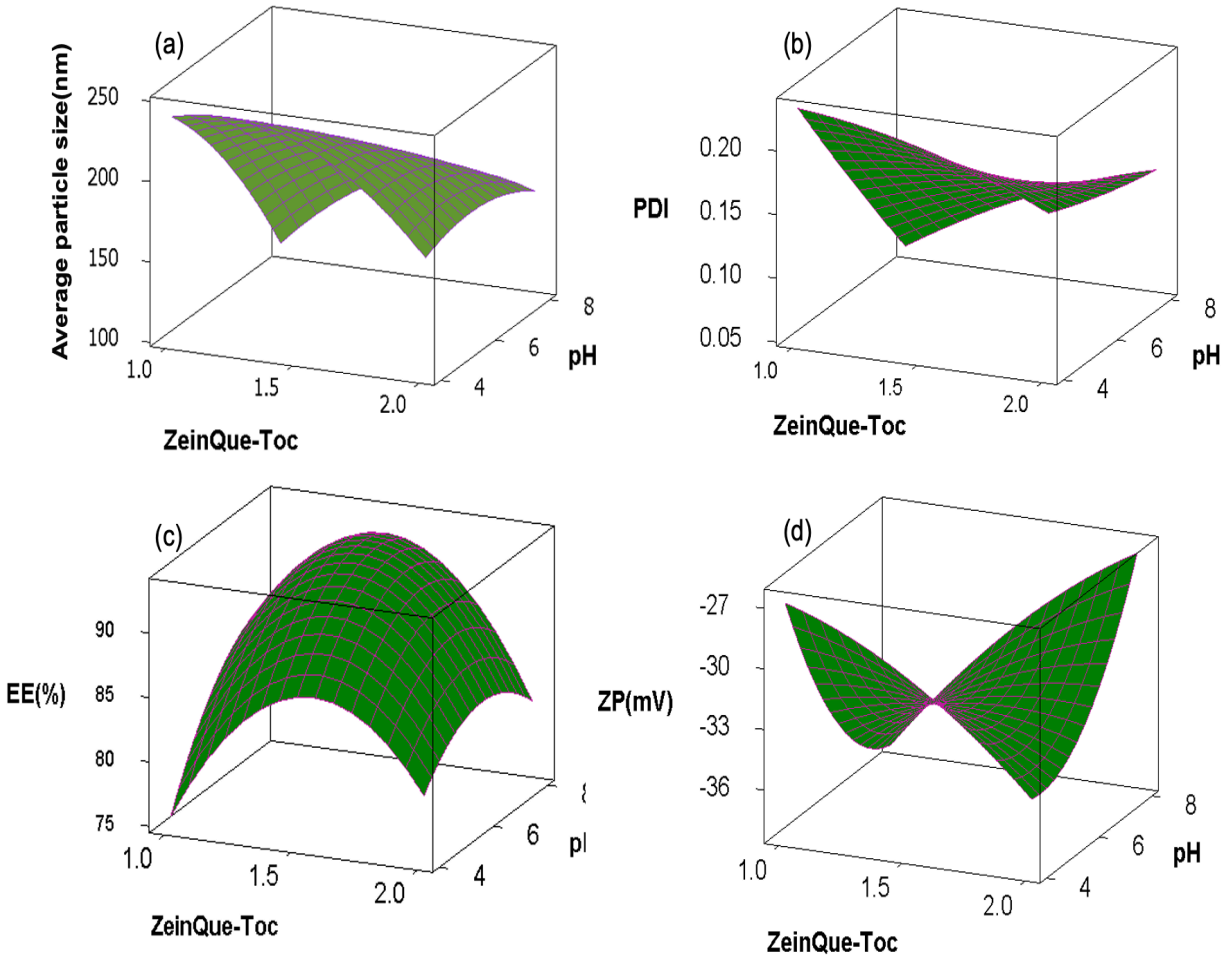


Figure C3. Response surfaces of the optimized zein/quercetin/tocopherol: a) average particle size, b) PDI, c) EE (%), and d) zeta potential of Zein/Que/Toc nanoparticles.

Appendix D

Supporting Information from Chapter 6

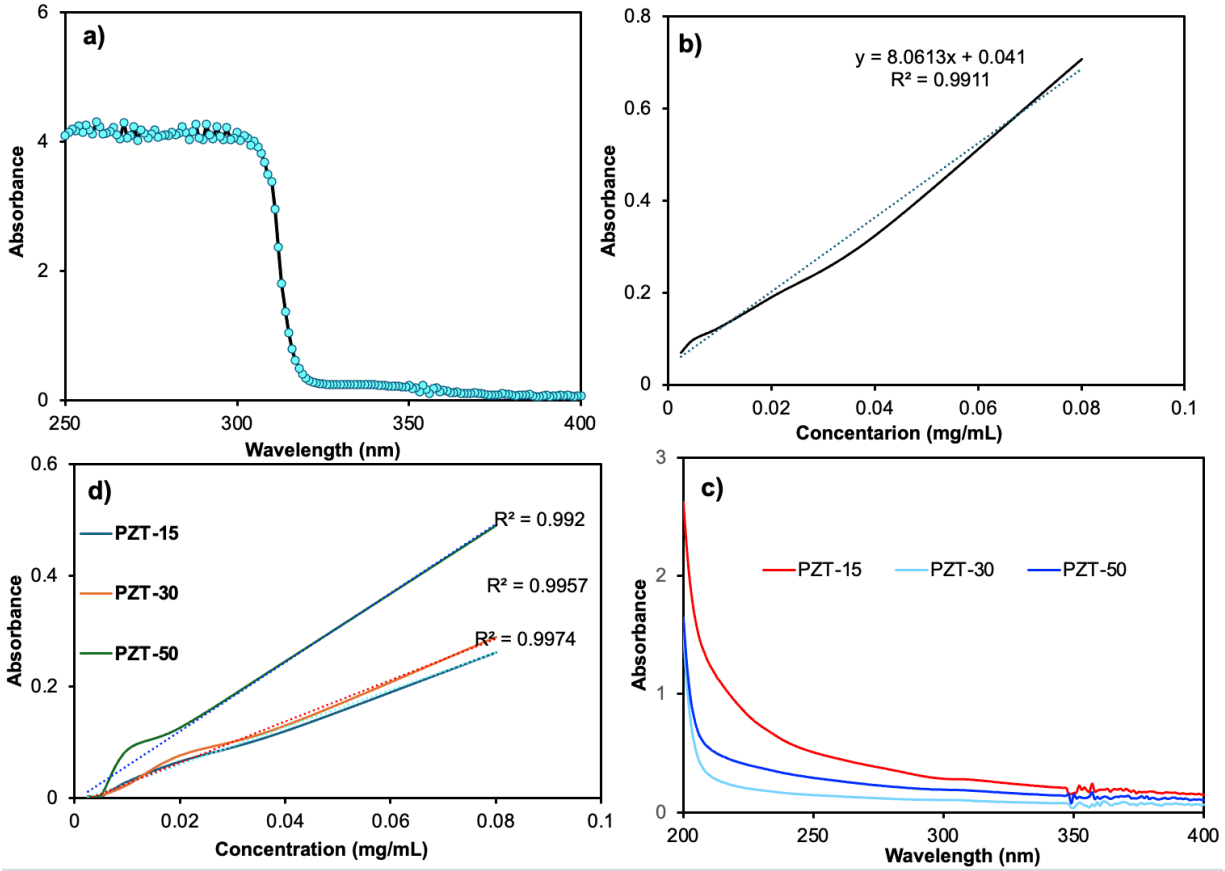


Figure D1: a) absorbance spectrum of pure tocopherol, b) calibration curve for determining EE% and LC%, c) calibration curve for determining tocopherol released from PVA-Zein fibrous mats, and d) absorbance spectra of PVA-Zein fibrous mats loaded with alpha tocopherol at 15%, 30%, and 50%.

Table D 1 . Release kinetics of nonwoven fibrous mats from PVA-zein-loaded α-tocopherol.

Model	Parameter	Tocopherol	PZT-15	PZT-30	PZT-50
Zero -Order	R^2	0.918	0.855	0.823	0.992
	K_0	2.123	0.567	0.822	1.342
	Q_0	0.254	0.479	0.324	0.672
First -Order	R^2	0.872	0.821	0.843	0.856
	K_1	2.067	1.896	2.342	2.053
	Q_0	1.562	0.785	1.871	1.321
Higuchi	R^2	0.974	0.987	0.991	0.998
	K_H	2.298	2.465	2.732	3.041
	Q_0	0.076	0.309	2.140	2.317
Korsmeyer-Peppas	R^2	0.995	0.999	0.996	0.992
	n	0.459	0.521	0.483	0.490
	K_{KP}	0.178	0.421	1.132	1.520

R^2 refers to the correlation coefficient, whereas Ko, K_1, K_H, and K_{KP} denote the zero-order release, first-order release, Higuchi, and Korsmeyer constants, respectively. Q_o and n represent the initial release amount and exponent, respectively.